



HAL
open science

Modeling of the flood regimes in coupled stream-aquifer systems

Serdar Korkmaz

► **To cite this version:**

Serdar Korkmaz. Modeling of the flood regimes in coupled stream-aquifer systems. Sciences of the Universe [physics]. École Nationale Supérieure des Mines de Paris, 2007. English. NNT : 2007ENMP1495 . pastel-00003360

HAL Id: pastel-00003360

<https://pastel.hal.science/pastel-00003360>

Submitted on 21 Feb 2008

HAL is a multi-disciplinary open access archive for the deposit and dissemination of scientific research documents, whether they are published or not. The documents may come from teaching and research institutions in France or abroad, or from public or private research centers.

L'archive ouverte pluridisciplinaire **HAL**, est destinée au dépôt et à la diffusion de documents scientifiques de niveau recherche, publiés ou non, émanant des établissements d'enseignement et de recherche français ou étrangers, des laboratoires publics ou privés.

MODELING OF THE FLOOD REGIMES IN COUPLED
STREAM-AQUIFER SYSTEMS

A THESIS SUBMITTED TO

ECOLE DOCTORALE GEOSCIENCES ET RESSOURCES NATURELLES PARIS
OF
ECOLE DES MINES DE PARIS

AND

THE GRADUATE SCHOOL OF NATURAL AND APPLIED SCIENCES
OF
MIDDLE EAST TECHNICAL UNIVERSITY

BY

SERDAR KORKMAZ

IN PARTIAL FULFILLMENT OF THE REQUIREMENTS FOR

THE DEGREE OF DOCTEUR
IN
HYDROLOGIE ET HYDROGEOLOGIE QUANTITATIVES

AND

THE DEGREE OF DOCTOR OF PHILOSOPHY
IN
CIVIL ENGINEERING

DECEMBER 2007

Approval of the thesis:

**MODELING OF THE FLOOD REGIMES IN COUPLED
STREAM-AQUIFER SYSTEMS**

submitted by **SERDAR KORKMAZ** in partial fulfillment of the requirements for the degree of **Docteur in Hydrologie et Hydrogéologie Quantitatives, Ecole des Mines de Paris** and **Doctor of Philosophy in Civil Engineering Department, Middle East Technical University** by,

Prof. Dr. Canan Özgen
Dean, Graduate School of **Natural and Applied Sciences**

Prof. Dr. Güney Özcebe
Head of Department, **Civil Engineering**

Prof. Dr. Halil Önder
Supervisor, **Civil Engineering Dept., METU**

Dr. Emmanuel Ledoux
Supervisor, **Centre de Géosciences, ENSMP**

Examining Committee Members:

Prof. Dr. Pierre Ribstein (France)
Université Paris 6

Prof. Dr. Halil Önder
Civil Engineering Dept., METU

Dr. Emmanuel Ledoux (France)
Centre de Géosciences, Ecole des Mines de Paris

Prof. Dr. Turgut Tokdemir
Engineering Sciences Dept., METU

Assoc. Prof. Dr. İsmail Aydın
Civil Engineering Dept., METU

Dr. Eric Martin (France)
Météo-France

Dr. Thierry Pointet (France)
Bureau de Recherches Géologiques et Minières

Date: December 18, 2007

I hereby declare that all information in this document has been obtained and presented in accordance with academic rules and ethical conduct. I also declare that, as required by these rules and conduct, I have fully cited and referenced all material and results that are not original to this work.

Name, Last name : Serdar Korkmaz

Signature :

ABSTRACT

MODELING OF THE FLOOD REGIMES IN COUPLED STREAM-AQUIFER SYSTEMS

Korkmaz, Serdar

Ph.D., Department of Civil Engineering (METU)

Ph.D., Centre de Géosciences (ENSMP)

Supervisor : Prof. Dr. Halil Önder

Supervisor : Dr. Emmanuel Ledoux

December 2007, 166 pages

In this study, hydrogeological modeling of the Somme river basin situated in the north of France was made with special emphasis on the stream-aquifer interaction. The coupled model developed at Ecole des Mines de Paris was used. Geographic Information Systems (GIS) tools were incorporated during all the stages of modeling process for both preparation of input data and visualization of the results of simulations. Initially, the process began with Digital Elevation Model (DEM) analysis. Afterwards, the surface and aquifer grids were generated by using nested grid generators and refinement was made on the stream network and subcatchment boundaries in order to increase the accuracy of numerical solution. In order to run the surface model, meteorological forcing, land use and soil type data were acquired. Surface model was used to partition the precipitation into evapotranspiration, infiltration and surface runoff components. A steady-state piezometric head distribution was computed by the groundwater model to serve as an initial condition to the coupled model. The flow in the unsaturated zone was simulated by using Nash cascade model. The unsteady groundwater and surface flow simulations were performed by taking into consideration the stream-aquifer interaction on a daily time step. The calibration and validation were realized by using the streamflow and piezometric head measurements distributed around the basin. The strong groundwater influence on the

hydrology of the basin is well represented by the model. Comparisons of predicted flooded areas in year 2001 were made with other models and a satellite derived image. In the end, several sensitivity analyses were performed for several parameters concerning the groundwater flow.

Keywords: hydrology, hydrogeology, coupled model, flood, stream-aquifer interaction, GIS, DEM, sensitivity analysis.

RESUME

MODÉLISATION DES RÉGIMES DE CRUE DES SYSTÈMES COUPLÉS AQUIFÈRES-RIVIÈRES

Korkmaz, Serdar

Ph.D., Department of Civil Engineering (METU)

Ph.D., Centre de Géosciences (ENSMP)

Directeur de thèse: Prof. Dr. Halil Önder

Directeur de thèse: Dr. Emmanuel Ledoux

Décembre 2007, 166 pages

Dans ce travail, une modélisation hydrogéologique du bassin-versant de la Somme dans le nord de la France a été menée avec une attention particulière sur l'interaction rivière-aquifère. Le modèle couplé développé à l'Ecole des Mines de Paris a été utilisé. Un Système d'Information Géographique a été incorporé à toutes les étapes du processus de modélisation pour la préparation des données d'entrée et la visualisation des résultats des simulations. Le processus commence tout d'abord par l'analyse du Modèle Numérique de Terrain (MNT). Ensuite, les maillages de surface et de l'aquifère ont été créés avec un maillage plus fin. Une discrétisation plus fine a été effectuée sur le réseau des rivières et les limites des sous-bassins dans le but d'augmenter la précision de la solution numérique. Pour faire tourner le modèle de surface, des données météorologiques, d'occupation du sol et de type de sol ont été acquises. Le modèle de surface permet de répartir les précipitations en évapotranspiration, infiltration et ruissellement de surface. Des niveaux piézométriques en régime permanent sont calculés par le modèle de nappe et constituent les conditions initiales du modèle couplé. L'écoulement dans la zone non saturée a été simulé par un modèle utilisant la cascade de Nash. Les simulations d'écoulement transitoire souterrain et de surface ont été réalisées en prenant en compte les interactions nappe-rivière sur un pas de temps journalier. La calibration et la

validation des résultats ont été faites en utilisant les mesures des débits et des niveaux piézométriques dans le bassin. La forte influence de la nappe sur le régime hydrologique du bassin est bien représentée par le modèle. Des comparaisons de prédiction des zones inondées en 2001 ont été effectuées avec d'autres modèles et une image satellitaire. Enfin, des analyses de sensibilité pour plusieurs paramètres d'écoulement souterrain ont été réalisées.

Mots-clés: hydrologie, hydrogéologie, modèle couplé, inondation, interaction nappe-rivière, SIG, MNT, analyse de sensibilité.

ÖZ

BİRLEŞİK NEHİR-AKİFER SİSTEMLERİNDE TAŞKIN REJİMLERİNİN MODELLENMESİ

Korkmaz, Serdar

Doktora, İnşaat Mühendisliği Bölümü (ODTÜ)

Doktora, Centre de Géosciences (ENSMP)

Tez Yöneticisi : Prof. Dr. Halil Önder

Tez Yöneticisi : Dr. Emmanuel Ledoux

Aralık 2007, 166 sayfa

Bu çalışmada Fransa'nın kuzeyinde yer alan Somme nehir havzasının hidrojeolojik modeli nehir-akifer etkileşimi göz önünde bulundurularak yapılmıştır. Bunun için Ecole des Mines de Paris'te geliştirilen birleşik model kullanılmıştır. Coğrafi Bilgi Sistemleri (CBS) araçları modellemenin bütün aşamalarında girdi verilerinin hazırlanması ve simülasyon sonuçlarının görsellenmesi amacıyla kullanılmıştır. İlk aşamada, Sayısal Yükseklik Modeli (SYM) analizi yapılmış ve havza ile ilgili alansal bilgi çıkartılmıştır. Daha sonra yüzey ve akifer için çözüm ağları oluşturulmuş ve nehirler ile alt havza sınırlarında sayısal çözümün kesinliğini artırmak amacıyla sıklaştırma yapılmıştır. Yüzey modelini kullanabilmek için meteorolojik veriler, arazi kullanımı ve toprak çeşidiyle ilgili veriler elde edilmiştir. Yüzey modeli düşen yağışın buharlaşma, sızma ve yüzey akımı olarak bölümlenmesinde kullanılmıştır. Yeraltı suyu modeli ile birleşik modele başlangıç koşulu oluşturması için sabit bir yeraltı suyu seviyesi hesaplanmıştır. Doymamış bölgedeki akım ise Nash çağlayan modeli ile hesaplanmıştır. Değişken yeraltı ve yüzey suyu akımlarının hesapları günlük zaman dilimleriyle ve de nehir-akifer etkileşimi hesaba katılarak yapılmıştır. Modelin kalibrasyonu ve doğrulanması havza üzerinde bulunan debi ve yeraltı suyu seviyesi ölçümleri ile gerçekleştirilmiştir. Yeraltı suyunun havzanın hidrolojik rejimi üzerindeki güçlü etkisi model tarafından başarıyla temsil edilmiştir.

Diğer modellerle debi ve 2001 yılı taşkın alanları karşılaştırmaları yapılmıştır. Son olarak da yeraltı suyu akımını etkileyen parametrelerle ilgili ilerde veri toplamayı yönlendirmesi amacıyla bir hassasiyet analizi sunulmuştur.

Anahtar Kelimeler: hidroloji, hidrojeoloji, birleşik model, taşkın, nehir-akifer etkileşimi, CBS, SYM, hassasiyet analizi.

To my parents and my brother

ACKNOWLEDGEMENTS

I wish to express my deepest gratitude to my supervisors Prof. Dr. Halil Önder and Dr. Emmanuel Ledoux for their guidance, advice, criticism, encouragements and insight throughout the research.

I also wish to thank Zouheir Hamrouni and the French Embassy staff in Turkey for their help in establishing this Joint PhD program and for the scholarship provided by the French Government during 15 months of my study.

I would like to thank Florence Habets from UMR Sisyphe at Ecole des Mines de Paris, who was responsible of a scientific program on the Somme river basin funded by the Centre National de la Recherche Scientifique (CNRS). Her constant and patient help providing advices all along this study was essential. I would also like to thank the members of the scientific committee of the project who gave me the opportunity of fruitful discussions. My acknowledgments are especially expressed to Dominique Thiéry from BRGM who provided quantity of data about the Somme aquifer system.

From Ecole des Mines, my thanks go to Nicolas Flipo, Pascal Viennot, André Levassor, Christelle Martin, Drissa Diarrassouba, Mounir Salim and all of the professors at Centre de Géosciences for sharing their lunchtimes, giving suggestions, and most of all, for their friendly attitude.

From Middle East Technical University, I would like to thank Mehmet Ata Bodur, Celal Soyarslan and Prof. Dr. Eyüp Özveren for sharing lunchtimes, making funny chats and keeping in touch while I was away.

I would like to acknowledge the assistance provided by the administrative staff of both institutes; in particular, my thanks go to Dominique Vassiliadis, Cahide Gökdemir and Sebay Durul.

I am very grateful to Serdar Ekinci, Hasan Sevinç, Selim Tezcan and Ahmet Düzce for their everlasting friendship and invaluable support during every moment of this long journey.

Finally, I would like to express my eternal gratitude to my parents Günay and Mümtaz, and to my brother Kerem. This PhD thesis would never have become reality without you.

SUMMARY OF THESIS IN FRENCH

Revue bibliographique :

Les interactions entre les eaux superficielles et les eaux souterraines ont fait l'objet d'une attention particulière de la part de nombreux chercheurs. Le phénomène d'interaction nappe-rivière est en effet important pour étudier les événements dangereux de crue et pour optimiser l'exploitation des ressources en eaux de surface et souterraines ; il a aussi des implications majeures sur le plan écologique (Hantush et al. 2002). Selon Sophocleous (2002), la nappe et les eaux de surface ne sont pas les composants isolés d'un système hydrologique, mais interagissent dans une variété de contextes physiographiques et climatiques. Donc, le développement de l'un des aspects concerne habituellement l'autre.

Selon leur position relative dans l'espace, Toth (1963) définit trois types différents de systèmes d'écoulement : local, intermédiaire et régional, qui s'expriment de manière emboîtée sur un bassin versant. Dans un système d'écoulement local, l'eau s'écoule vers un exutoire proche comme un étang ou une rivière. Dans un système d'écoulement régional, elle voyage sur une distance plus grande jusqu'aux rivières majeures, aux grands lacs ou aux océans. Le système d'écoulement intermédiaire concerne un domaine situé entre un affluent et un exutoire, mais, contrairement à un système d'écoulement régional, il ne contient ni la tête, ni l'aval du bassin.

La vidange d'une nappe n'est pas seulement localisée le long d'un cours d'eau mais elle se développe aussi à travers la zone de décharge en aval d'une ligne séparant les sous-bassins versants. Il en résulte que, si l'on utilise le débit de base comme indicateur de la recharge moyenne d'un domaine hydrologique, une erreur importante peut être introduite, car le débit de base peut ne représenter qu'une petite partie de la décharge totale provenant de ce domaine (Sophocleous 2002).

Larkin et Sharp (1992) classent les systèmes nappe-rivière suivant trois catégories (1) les systèmes dominés par l'inferoflux (le flux de la nappe s'écoule parallèlement à la rivière et dans la même direction qu'elle) ; (2) les systèmes dominés par le débit de base (le flux

de la nappe s'écoule perpendiculairement à la rivière, dans un sens ou dans l'autre selon que la rivière draine ou alimente) ; (3) les systèmes composites ; le mode d'écoulement dominant peut être déduit des données géomorphologiques tels que la pente du cours d'eau, la sinuosité de la rivière, le degré d'incision au sein des alluvions, le rapport largeur sur profondeur de chenal et la nature des dépôts fluviaux.

Sophocleous (2002) définit le débit de base comme l'eau qui parvient à une rivière sous l'effet d'une alimentation persistante, lentement variable, et qui soutient l'écoulement de la rivière entre les événements de crue. L'écoulement souterrain peut cependant aussi alimenter les rivières assez rapidement pour contribuer à la génération d'événements de forts régimes hydrodynamiques.

Certains chercheurs ont souligné l'influence du domaine souterrain sur les bassins hydrologiques. Par exemple, Beven (2000) indique que l'un des problèmes intervenant dans la compréhension complète des systèmes hydrologiques est que, lorsque la majorité de l'écoulement est de nature souterraine, notre capacité de mesurer et évaluer les processus d'écoulement souterrain est limitée.

Les considérations qui précèdent illustrent l'intérêt, sinon la nécessité, d'être capable de modéliser conjointement les écoulements de surface et les écoulements souterrains pour de nombreux cas de systèmes hydrologiques.

Objectifs :

Le bassin versant de la Somme dans le nord de la France a été concerné par une très forte crue pendant l'année 2001 durant laquelle les eaux ont atteint des cotes exceptionnelles et causé un dommage majeur à l'environnement. Cet événement a souligné la contribution des aquifères à l'hydrologie du bassin. Selon une estimation du BRGM (Bureau de Recherches Géologiques et Minières), près de 75% du volume de crue a été provoqué par l'exfiltration de la nappe à la surface du sol et par l'échange direct entre la nappe et la rivière. Le même événement a, par la suite, joué un rôle important dans le soutien des débits et il a atténué les conséquences de saisons sèches ultérieures telles que rencontrées au cours du printemps et de l'été 2003. En conséquence, dans ce travail de recherche, une modélisation hydrogéologique complète du bassin versant de la Somme a été menée avec une attention particulière portant sur l'interaction rivière-aquifère.

Résumé de la recherche :

Dans ce travail, un modèle hydrologique couplée du bassin versant de la Somme dans le nord de la France a été construit avec une attention particulière sur l'interaction rivière-aquifère. La modélisation a été basée sur le modèle couplé (MODCOU) développé à l'Ecole des Mines de Paris. Les outils SIG ont été utilisés pendant toutes les étapes de modélisation pour la préparation des données d'entrée puis la visualisation et l'exploitation des résultats de simulation.

Le processus de construction du modèle commence tout d'abord par l'extraction d'informations spatiales sur le bassin en s'appuyant sur l'analyse du Modèle Numérique de Terrain (MNT). Basée sur une image « raster » de la topographie avec une taille de pixel de 125 m, cette analyse a consisté à déterminer les directions de drainage, les surfaces drainées, à construire le réseau hydrographique, puis à partitionner le bassin en sous-bassins versants. Ces analyses ont été faites au moyen du programme HYDRODEM mis à disposition dans le cadre d'un partenariat avec le Cemagref de Lyon.

Après l'acquisition des données spatiales, une discrétisation du domaine de surface en mailles carrées emboîtées a été créé par le program SIGMOD. Une discrétisation plus fine a été employée sur le réseau des rivières et les limites des sous-bassins dans le but d'augmenter la précision de la solution numérique dans ces secteurs importants sur le plan hydrologique. Le maillage le plus approprié a été obtenu par tâtonnement. Plusieurs maillages ont ainsi été créés selon les réseaux de rivière retenus pour des seuils différents de la surface drainée par le réseau hydrographiques. Les petits sous-bassins versants ont été regroupés, lorsque cela était possible, pour éviter les raffinements inutiles. Les limites du domaine ont été étendues jusqu'aux plus proches limites naturelles telles que les rivières principales des bassins voisins, de manière à atteindre des conditions aux limites de piézométrie imposée pour l'aquifère. Cette démarche était nécessaire, car, dans le cas de la Somme, l'aquifère présente une extension régionale qui dépasse les limites du bassin versant superficiel. Ensuite, le maillage de l'aquifère a été créé au moyen du programme SIGSOU exactement sur la même géométrie spatiale que la couche de surface pour permettre la représentation de l'interaction surface-souterrain en chaque point du bassin. La procédure de regroupement des mailles intégrée aux programmes de maillage a été mise en œuvre pour réduire le nombre de mailles du modèle sur les pentes des sous-bassins versants loin des lignes de partage des eaux ; cependant, la discrétisation fine a été conservée au niveau des mailles rivières pour maintenir la précision dans l'interaction

nappe-rivière. Après la création des maillages, 71653 mailles pour la couche de surface et 63226 mailles pour la couche aquifère ont été retenues, les tailles des mailles se répartissant entre 125, 250, 500 et 1000 m.

Le modèle couplé se compose de 4 modules principaux, à savoir, MODSUR, NEWSAM, NONSAT and MODCOU. Pour exécuter le modèle de surface, MODSUR, les forçages météorologiques, les données d'occupation de sol et de type de sol sont requises. Le forçage météorologique (précipitation et évapotranspiration potentielle) a été fourni par Météo-France selon la procédure Safran sur un maillage couvrant la surface de bassin avec des mailles ayant une taille de 8 km, sur la période allant du 1/8/1985 au 31/7/2003 avec un pas de temps journalier. Les données d'occupation de sol proviennent de la base de données CORINE Land Cover et celles portant sur les types de sol de la base de données INRA au 1/1000000. Les données d'occupation de sol et de type de sol ont ensuite été croisées sous l'environnement SIG ArcGIS dans le but de construire les zones de production permettant la spatialisation du bilan hydrique en surface du bassin. Le programme MODSUR utilise une fonction production qui partage la précipitation entre ruissellement, infiltration et évapotranspiration réelle selon ces zones de production. Le programme calcule ensuite le volume de l'eau s'infiltrant sur chaque maille de surface, puis le volume d'eau arrivant dans chaque maille rivière à chaque pas de temps. La mise en œuvre de la fonction production de MODSUR nécessite la définition d'un jeu de paramètres propre à chaque zone de production. Pour identifier les valeurs optimales de ces paramètres une procédure de calibration a été suivie sur la période 1/8/1995-31/7/2003. L'effet de chaque paramètre sur l'hydrogramme de la Somme à Abbeville (5560 km²) a été analysé et décrit en détail. En fin de calibration, un contrôle de validité du modèle a été fait sur la période 1/8/1985-31/7/1995. Les critères statistiques obtenus à l'issue du calage ont été assez satisfaisants, conduisant par exemple à un coefficient de Nash-Sutcliffe de 0,93 sur la période de calibration, de 0,72 sur celle de validation et de 0,86 pour la période globale.

Le module logiciel intervenant en second lieu est NEWSAM qui simule l'écoulement en aquifère. Dans ce travail, il a été utilisé en régime permanent pour obtenir un niveau piézométrique initial. Pour ce faire, la moyenne des valeurs d'infiltration calculée sur la période de calage de MODSUR a été introduite en entrée du modèle souterrain. Une première estimation des paramètres hydrodynamiques (perméabilité et coefficient d'emmagasinement) a été fournie par le BRGM. En fonction de la disponibilité de ces

données, les perméabilités ont été définies sur 5 zones et transférées sur le maillage grâce au SIG. Comme le modèle utilise la transmissivité pour simuler l'écoulement, cette grandeur a été obtenue à partir des valeurs de perméabilité et de l'épaisseur moyenne de la nappe également fournie par le BRGM.

Les simulations en régime transitoire de l'écoulement de surface et de l'écoulement en nappe ont été effectuées avec le programme MODCOU. Ce programme simule le transfert en rivière et l'écoulement souterrain en tenant compte de l'interaction rivière-nappe. Comme données d'entrée, il est nécessaire de fournir les valeurs journalières de ruissellement en chaque maille rivière (calculées par MODSUR), l'alimentation journalière de la nappe (calculée par NONSAT en sortie de MODSUR), un niveau initial de piézométrie, la transmissivité, le coefficient d'emménagement, les prélèvements en nappe et les paramètres caractérisant la relation nappe-rivière (niveau de drainage, coefficient de transfert, débit maximal réinfiltrable), issus de NEWSAM. MODCOU fournit en sortie les débits journaliers aux stations hydrométriques et à l'exutoire du bassin, les chroniques piézométriques journalières en 50 points du domaine et la carte piézométrique de l'aquifère en fin de chaque année. Une calibration élaborée a été faite et chaque étape en a été décrite en détail. Au départ, une première calibration en régime permanent a porté sur les transmissivités en recherchant une correspondance entre la structure des cartes piézométriques simulées et observées. Les résultats ont ensuite été affinés en régime transitoire en réglant le coefficient d'emménagement et, si nécessaire, à nouveau la transmissivité pour reproduire au mieux les chroniques piézométriques. Au cours de la démarche de calage, un problème de représentation topographique a été mis en évidence se manifestant sous la forme de maximum ou de minimum locaux dans le MNT, préjudiciables à une bonne simulation des échanges hydriques entre le domaine de surface et le domaine souterrain, les variations parasites de l'altitude causant des irrégularités sur l'exfiltration calculée. Un programme a été écrit en FORTRAN pour appliquer une procédure de lissage au MNT sur l'ensemble de la surface du domaine et plus spécifiquement le long des rivières, pour lesquelles la résolution assez moyenne (125 m) du MNT était notablement insuffisante. Après l'exécution de cette procédure, un réajustement moyen de 0,03 m a été appliqué sur la surface du bassin. Sur chaque branche de rivière, les élévations des mailles ont été ramenées sur la ligne de pente moyenne de façon à rétablir une décroissance continue de l'amont vers l'aval là où cela était nécessaire. Cette correction a apporté une amélioration significative au calcul de l'exfiltration le long de réseau hydrographique. Dans une seconde étape, les valeurs

initiales de coefficient d'emménagement et de la transmissivité ont été reprises pour affiner le calage piézométrique local du modèle ; une amélioration nette a été obtenue sur 43 parmi les 50 stations piézométriques disponibles. Les retouches les plus importantes des paramètres du modèle ont eu lieu sur les sous-bassins de l'Avre et de la Selle. La dernière étape de calibration a porté sur le coefficient de tarissement des mailles rivières qui contrôle le transfert de l'eau d'une maille rivière à l'autre et finalement d'un bief à l'autre. Sa calibration a eu une bonne influence sur les hydrogrammes de l'Avre, de la Selle et de l'Hallue, particulièrement, en réduisant les pics qui parasitaient les débits calculés.

La simulation de transfert de l'eau dans la zone non-saturée a été menée au moyen du programme NONSAT. NONSAT calcule l'alimentation de la nappe à partir de l'infiltration à la surface préalablement calculé par MODSUR. Ce programme est en réalité exécuté avant MODCOU ; cependant, comme sa calibration a été faite, dans notre étude, après MODCOU, son emploi est décrit en dernier lieu. L'exécution de NONSAT implique d'identifier la répartition spatiale de deux paramètres, soit, le nombre des réservoirs en cascade représentant la colonne de milieu non-saturé et la constante de temps de vidange caractérisant ces réservoirs. L'épaisseur de la zone non-saturée, obtenue par différence entre la cote au sol et la piézométrie moyenne fournie par le BRGM, a été divisée en couches régulières de 5 m, correspondant chacune à un réservoir de transfert. Au final, chaque maille de surface se voit attribuer, en fonction de sa position dans l'espace un nombre de réservoirs et une constante de temps, paramètres qui resteront invariants au cours de la simulation. La calibration de la constante de temps a été menée en deux étapes ; une première valeur de 5 jours a donné les meilleurs résultats globaux sur l'ensemble du domaine ; une calibration plus détaillée a été ensuite effectuée en cherchant à différencier les sous-bassins correspondant à des stations hydrométriques. Cette seconde calibration a amélioré tous les hydrogrammes, particulièrement lors des épisodes de tarissement.

Une fois la calibration effectuée, la validité du modèle a été éprouvée sur les deux chroniques de débit de la Somme disponibles à Hangest-Sur-Somme (4835 km²) et à Peronne (1294 km²) qui n'avaient pas été utilisées dans le processus de calage. Les coefficients de Nash-Sutcliffe pour les débits ont été les suivants : 0,87 à Abbeville (calibration), 0,84 à Hangest-Sur-Somme (validation) et 0,78 à Peronne (validation), ce qui indique une bonne performance du modèle, malgré le caractère plutôt sévère du test

réalisé. L'autre validation a été faite sur les affluents de la Somme, la Nièvre, l'Avre et l'Hallue. Pour l'Avre et l'Hallue des résultats satisfaisants ont également été obtenus, mais pour la Nièvre le résultat s'est révélé décevant. Le débit est, en effet, presque toujours sous-estimé. Cela pouvait être dû à une calibration insuffisante des paramètres de fonction production ou à une spatialisation incorrecte des paramètres de production sur ce sous-bassin.

Une comparaison de notre modèle avec un autre modèle nommé CaB a été faite et il a été observé que MODCOU présente une meilleure performance, ce qui est sans doute dû au fait que CaB est un modèle de surface, fondé sur l'approche TOPMODEL qui n'est pas adaptée aux bassins présentant un aquifère développé en profondeur.

Pour ce qui concerne l'épisode de crue de 2001, la localisation de la lame d'eau exfiltrée calculée à la surface a été comparée avec une image satellitaire représentant le pourcentage de surface inondée ; une correspondance satisfaisante entre ces deux types d'information a été notée. La lame d'eau exfiltrée a en outre été comparée avec celle produite par le modèle MARTHE du BRGM. Les similarités et les différences ont été analysées en détail.

Enfin, des analyses de sensibilité ont été réalisées pour trois paramètres, soit, transmissivité, coefficient d'emménagement et coefficient de transfert nappe-rivière.

Discussion :

Au cours de la démarche de modélisation quelques problèmes ont été rencontrés, dont une tentative de solution a fait l'objet de cette thèse. Ces problèmes ont été décrits ci-dessous.

La sélection du MNT et le choix de sa résolution sont des étapes importantes. Pour minimiser le problème de calage entre le réseau hydrographiques figurant sur les cartes et celui dérivé d'une analyse du MNT, une élaboration du MNT à partir de la digitalisation d'une carte en courbes de niveau au lieu d'une image satellitaire est conseillée, car cela permet de réduire les erreurs de déplacement verticaux et horizontaux. Par ailleurs, à cause des limitations de nature informatique, une résolution de 125 m a été adoptée pour notre MNT. Ceci est raisonnable pour représenter la topographie générale ; cela est cependant insuffisant pour définir correctement les mailles rivières, particulièrement dans

la partie aval du bassin où les pentes sont très faibles. Une discrétisation plus fine aurait donc été préférable malgré le surcroît de temps calcul qui en aurait résulté. Nous considérons également qu'il est absolument nécessaire d'appliquer le plus tôt possible la procédure de filtrage du MNT pour en supprimer les irrégularités qui compromettent gravement la représentativité du drainage le long des rivières.

Un autre problème résulte du grand nombre des paramètres nécessaires au modèle par rapport aux observations disponibles. Cela peut entraîner une indétermination du modèle, signifiant qu'il peut y avoir plusieurs structures ou jeux de paramètre qui conduisent à des résultats tout aussi acceptables (Beven and Freer 2001). Ce problème peut ainsi apparaître quand un modèle est calé par deux utilisateurs différents. Pour résoudre cette difficulté, le nombre des observations concernant l'aquifère ainsi que la surface doit être augmenté.

Le prochain problème concerne l'écoulement en rivière. Ni le modèle couplé ni MARTHE ne parviennent à simuler de manière satisfaisante le débit de la Nièvre, ce qui peut être la conséquence d'une mauvaise représentation des phénomènes hydrologiques en cause, d'une calibration insuffisante ou encore d'erreurs dans les données de terrain. Une étude plus poussée sur ce bassin particulier serait donc judicieuse.

A propos du transfert dans la zone non-saturé, nous avons vu que notre approche au moyen d'une cascade de réservoirs, telle que le réalise le programme NONSAT, apporte une amélioration dans la représentativité des hydrogrammes. Cette approche est cependant conceptuellement très insuffisante car elle considère que l'épaisseur de la zone non-saturée est constante, ce qui n'est pas le cas sur le bassin de la Somme où des fluctuations piézométriques d'une amplitude jusqu'à 15 m peuvent être communément observées. De telles fluctuations engendrent clairement des variations dans le nombre de réservoirs qu'il conviendrait de prendre en compte pour représenter une colonne de non-saturé, surtout lorsqu'elle est peu épaisse. Une solution devrait donc être recherchée pour établir une rétroaction de la nappe sur le non-saturé, ce qui n'est actuellement pas possible étant donnée l'exécution séquentielle des programmes NONSAT et MODCOU.

Une remarque finale peut être faite concernant l'aquifère. Les propriétés particulières de l'aquifère de la craie qui lui sont conférées par l'existence de fissures pouvant pénétrer en profondeur au sein du massif rocheux ne sont pas prises en compte par le modèle. Malgré

les résultats encourageants déjà obtenus avec le modèle en l'état, il serait sans aucun doute utile d'améliorer sa représentativité dans cette voie.

Conclusion :

Dans cette thèse, plusieurs contributions à la modélisation d'un système hydrologique ont été apportées. En premier lieu, au niveau des outils de modélisation, les meilleurs SIGMOD et SIGSOU ont été perfectionnés. Dans SIGMOD, le calcul de temps de transfert et l'algorithme de raffinement de maillage sur les limites du domaine ont été retouchés. Une sous-routine a été écrite pour réorganiser les sous-bassins. Dans SIGSOU, un fonctionnement correct de l'algorithme de regroupement des mailles a été assuré et des tests impliquant tous les critères de regroupement ont été exécutés. A propos de l'analyse du MNT, un algorithme de lissage a été développé. Cette procédure explore un MNT, identifie et corrige les irrégularités qui nuisent à la représentation du drainage des nappes par exfiltration. Une autre contribution importante est la procédure particulière de correction développée pour les élévations des mailles rivières le long des lignes de drainage de l'aquifère. Par ailleurs, le modèle couplé MODCOU a été modifié pour visualiser les lames d'exfiltration. Sur le plan méthodologique, la procédure de calibration de toutes les composantes du modèle a été décrite en détail, pouvant servir de guide pour une application future du modèle sur un autre bassin.

Globalement, une modélisation sophistiquée a été mise en œuvre. S'agissant de bassins comme la Somme qui sont fortement influencés par la nappe, de nombreux modèles échouent dans la représentation des événements correspondants à des situations hydrologiques diversifiées, car ils ne prennent pas en compte d'une manière suffisamment réaliste les échanges nappe-rivière. Dans cette recherche, les résultats obtenus pour les débits avec le modèle couplé sont relativement satisfaisants. Le comportement de la nappe et son effet sur la crue de 2001 sont bien représentés. La diversité des paramètres qui contrôlent l'écoulement de surface tels que les zones de production, les coefficients de transfert nappe-rivière et les coefficients de tarissement des mailles rivières confèrent au modèle une flexibilité qui semble lui permettre de s'adapter aux différentes situations hydrologiques rencontrées sur le bassin de la Somme. Cette flexibilité est encore renforcée par la structure du modèle en plusieurs modules qui peuvent être exécutés de manière indépendante et permet ainsi à l'utilisateur de mettre plus facilement l'accent sur les mécanismes prédominants au cours de la calibration. La contrepartie de cette flexibilité est qu'elle exige la manipulation d'un grand nombre de

paramètres discrétisés dans l'espace et dans le temps ; la technologie des Systèmes d'Information Géographique (SIG) devient alors indispensable pour mettre en forme, visualiser et interpréter les données spatiales et elle a ainsi ouvert une autre perspective à la modélisation.

Perspective :

Les outils de modélisation mis au point au cours de cette recherche vont servir au projet REXHYSS qui vise à estimer l'impact du changement climatique sur les ressources d'eau et sur les régimes hydrologiques des bassins de la Somme et de la Seine. REXHYSS est une partie du programme GICC (Gestion des Impacts du Changement Climatique) financé par le MEDAD (Ministère de l'Ecologie, du Développement et de l'Aménagement Durables). Au cours de ce projet, les effets du climat sur les basses et hautes eaux seront évalués au moyen des modèles hydrologiques et traduits par des analyses classiques en fréquences.

Le modèle du bassin de la Somme mis au point au cours de cette thèse sera en outre intégré au projet SIM-France qui exploite le système de modélisation hydrométéorologique Safran-Isba-MODCOU dans le but de produire une estimation prévisionnelle journalière des bilans d'eau et d'énergie sur l'ensemble de la France. L'humidité du sol, la température et lame de neige sont simulés par la composante Safran. La composante Isba-MODCOU produit les débits calculés en plus de 400 postes hydrométriques. Pour l'instant, les bassins de la Garonne, du Rhône et de la Seine ont fait l'objet d'une modélisation approfondie. Après la prise en compte du bassin de la Somme, de meilleurs résultats sont attendus pour le nord de la France.

TABLE OF CONTENTS

ABSTRACT.....	iv
RESUME	vi
ÖZ	viii
ACKNOWLEDGEMENTS	xi
SUMMARY OF THESIS IN FRENCH	xiii
TABLE OF CONTENTS.....	xxiii
LIST OF TABLES.....	xxvi
LIST OF FIGURES	xxvii
LIST OF SYMBOLS	xxxii
1. INTRODUCTION	1
1.1. Literature Survey	1
1.2. Objective	2
2. THEORETICAL BACKGROUND FOR GROUNDWATER FLOW	3
3. PRINCIPLES AND FUNCTIONING OF COUPLED HYDROLOGICAL MODEL 8	
3.1. Introduction	8
3.2. GEOCOU (Geometry of the Coupled Model).....	9
3.3. Computation of Water Budget – MODSUR.....	12
3.3.1. Production Function.....	12
3.3.2. Transfer of Surface Runoff	15
3.4. Transfer in the Unsaturated Zone – NONSAT	16
3.5. Steady-State Groundwater Flow Simulation – NEWSAM	18
3.5.1. Discretization	18
3.5.2. Boundary Conditions	23
3.5.3. Numerical Solution	24
3.6. Unsteady Simulation of Groundwater and Surface Flows – MODCOU	26
3.6.1. Groundwater Flow	26
3.6.2. Transfer in the Stream Network.....	28
3.6.3. Stream-Aquifer Interaction	31
3.7. Programming Toolkit	33

3.7.1.	Geographic Information System: Utilization of Digital Elevation Model in Hydrology	33
3.7.2.	Generation of the Surface Mesh – SIGMOD	35
3.7.3.	Generation of the Aquifer Mesh –SIGSOU	38
4.	THE SOMME RIVER BASIN	39
4.1.	Presentation of the Domain	39
4.1.1.	Geography	39
4.1.2.	Geologic and Hydrogeologic Context.....	41
4.2.	Basin Hydrology.....	43
4.2.1.	Pluviometry	43
4.2.2.	Hydrography	45
4.2.3.	Piezometry	49
4.2.4.	Springs	49
4.2.5.	Land Use	50
4.3.	Flood Problem	51
4.3.1.	Hydrologic Reaction	51
4.3.2.	Literature Survey.....	55
4.4.	Interrogation on Inundation.....	56
5.	APPLICATION OF THE COUPLED MODEL ON THE SOMME RIVER BASIN	58
5.1.	DEM Analysis	58
5.2.	Generation of the Surface Grid.....	63
5.3.	Generation of the Aquifer Grid	65
5.4.	Preparation of Data.....	66
5.4.1.	Composition of Production Zones	66
5.4.2.	Meteorologic Data.....	70
5.4.3.	Aquifer Data.....	72
5.4.4.	Surface Data.....	76
5.5.	Simulations.....	77
5.5.1.	Computation of the Water Budget	79
5.5.2.	Computation of Initial Piezometric Head Distribution	87
5.5.3.	Simulation of Surface and Groundwater Flows	88
5.5.4.	Simulation of Flow in Unsaturated Zone	115
5.6.	Validation and Analysis of the Results.....	120
5.7.	Sensitivity Analysis	131
6.	CONCLUSIONS	135
6.1.	Summary	135

6.2. Discussion	139
6.3. Conclusion.....	141
6.4. Perspective.....	142
REFERENCES	143
APPENDIX A.....	149
APPENDIX B.....	156
APPENDIX C.....	164
CURRICULUM VITAE.....	165

LIST OF TABLES

Table 4.1 Discharges observed on the Somme and its tributaries.....	49
Table 4.2 Flood discharges observed at the streamgage stations.....	53
Table 5.1 Production zones and their percentages.....	69
Table 5.2 The values of production function variables.....	80
Table 5.3 The alteration of water budget during calibration.....	83
Table 5.4 The values of error criteria after the calibration of production function.....	86
Table 5.5 The effect of ‘fill’ procedure and river elevation corrections on the groundwater and surface water exchange in year 2001.....	98
Table 5.6 Error criteria for flow hydrographs.....	123
Table 5.7 The flowrate values concerning the test simulations with initial piezometric levels of 1/8/1999 and 1/8/1998.....	133

LIST OF FIGURES

Fig. 2.1 Flow in a leaky unconfined aquifer.	7
Fig. 3.1 Principle of the multi-layer schematization of coupled hydrological model.	10
Fig. 3.2 Discretization and the stream network of a surface layer.	11
Fig. 3.3 Schematization of a production function.	13
Fig. 3.4 Principle of the Nash model.	17
Fig. 3.5 The effect of storage constant on the outflows of a Nash cascade with 5 reservoirs; a) $\tau=1$ day, b) $\tau=2$ days.	18
Fig. 3.6 Continuity in an aquifer cell.	19
Fig. 3.7 Flow in a horizontally layered confined aquifer.	20
Fig. 3.8 Representation of flow in a nested grid system.	21
Fig. 3.9 Formation of segments on the stream network.	28
Fig. 3.10 Stream-aquifer interaction; (a) connected gaining stream, (b) connected losing stream, (c) disconnected losing stream.	31
Fig. 3.11 The storage of a raster image.	34
Fig. 3.12 Criteria for regrouping.	35
Fig. 3.13 Possible flow directions in a cell.	38
Fig. 4.1 The department of Somme in the north of France.	39
Fig. 4.2 The Somme river basin with major tributaries.	40
Fig. 4.3 Topography of the Somme river basin.	40
Fig. 4.4 Aquifer thickness of the Somme river basin.	42
Fig. 4.5 Thickness of the unsaturated zone.	43
Fig. 4.6 Monthly rainfall at Abbeville (following PPRI 2004).	44
Fig. 4.7 The spatially averaged monthly rainfall for the period 8/1985-7/2003.	44
Fig. 4.8 Isohyetal map of the Somme basin for the period 1971-2000 (from Météo- France, published by Amraoui et al. 2002).	45
Fig. 4.9 Streamflow measurements on the Somme at Abbeville (5560 km ²), monthly average of 43 years (1963-2005) (following Banque Hydro 2007).	46
Fig. 4.10 Monthly averages of streamflow measurements on the tributaries of the Somme (following Banque Hydro 2007).	47

Fig. 4.11 3-monthly averaged discharges observed at a) several locations on the Somme, b) the tributaries of the Somme (following Banque Hydro 2007).....	48
Fig. 4.12 The springs on the Somme basin (from BRGM, Amraoui et al. 2002).....	50
Fig. 4.13 The ratio of precipitation falling in the period Oct 2000-Apr 2001 to the average of 57 years at the Abbeville station.....	51
Fig. 4.14 Spatially averaged rainfall; (a) monthly depth, (b) bimonthly average depth. .	52
Fig. 4.15 Daily observed discharge on the Somme at Abbeville.	53
Fig. 4.16 Monthly discharges observed at several locations on the Somme.....	54
Fig. 4.17 Monthly discharges observed at the tributaries of the Somme.	54
Fig. 5.1 Digital Elevation Model of the Somme basin (Pixel size = 125 m).	58
Fig. 5.2 Flow directions.	59
Fig. 5.3 Comparison of stream networks obtained by HYDRODEM (blue) and D8 algorithm (red).....	60
Fig. 5.4 Subcatchments of the Somme river basin.....	61
Fig. 5.5 Final delineation of the Somme river basin with extended portions; initial basin area is 6433 km ² (in blue), total area after extension is 8205 km ²	62
Fig. 5.6 Surface grid of the Somme river basin.	64
Fig. 5.7 Normalized transfer times with the stream network.....	64
Fig. 5.8 Aquifer grid of the Somme river basin.	65
Fig. 5.9 Soil type distribution.	67
Fig. 5.10 Land use data (from CORINE Land Cover Database).	68
Fig. 5.11 Dominant production zones.....	69
Fig. 5.12 Interannual averages of monthly rainfall and <i>PET</i> values over the Somme basin (in the period 8/1985-7/2003).....	70
Fig. 5.13 Spatially averaged annual rainfall and <i>PET</i> values.	71
Fig. 5.14 Average annual precipitation for the period of 1985-2003 in mm (from Météo- France).....	72
Fig. 5.15 Average annual potential evapotranspiration for the period of 1985-2003 in mm (from Météo-France).	72
Fig. 5.16 Hydraulic conductivity zones (from BRGM).....	73
Fig. 5.17 Specific yield zones (from BRGM).....	73
Fig. 5.18 Groundwater depth (from BRGM).	74
Fig. 5.19 Initial transmissivity distribution on the modeled area.....	75
Fig. 5.20 Initial specific yield distribution on the modeled area.....	75
Fig. 5.21 Observed pumpage rates in the year 1995 by BRGM.	76

Fig. 5.22	Distribution of hydrometric and piezometric stations.	76
Fig. 5.23	The effect of the maximum value of infiltration (FN) on the flow measured at Abbeville (catchment area = 5560 km ²).	82
Fig. 5.24	The effect of depletion ratio of surface runoff reservoir (C_{QR}).	82
Fig. 5.25	The effect of the unsaturated model (NONSAT) run with a storage constant of $\tau = 5$ days.	82
Fig. 5.26	Calibration of parameters of Artificial Surfaces.	83
Fig. 5.27	Calibration of CRT and DCRT for Agricultural Zones.	83
Fig. 5.28	Evolution of measures of error; a) Deviation of runoff volumes (D_v), Root mean squared error ($RMSE$); b) Correlation coefficient (ρ), Nash-Sutcliffe coefficient (R^2), Coefficient of gain from daily mean (DG).	84
Fig. 5.29	The variation of Nash-Sutcliffe coefficient (R^2) for the Somme gauged at Abbeville and for its tributaries.	85
Fig. 5.30	Flow hydrograph of the Somme gauged at Abbeville (5560 km ²) including the validation period.	86
Fig. 5.31	Piezometric head distribution before the calibration of transmissivities.	87
Fig. 5.32	Piezometric head distribution after the calibration of transmissivities.	88
Fig. 5.33	The values of root mean squared error ($RMSE$) for piezometric heads before and after the initial calibration of transmissivities.	90
Fig. 5.34	The Nash-Sutcliffe coefficients (R^2) before and after the calibration of transmissivities.	90
Fig. 5.35	The root mean squared error ($RMSE$) values of piezometric heads before and after the modification in specific yield.	91
Fig. 5.36	The rises applied to the elevations with the application of 'fill' procedure.	92
Fig. 5.37	Modification of river elevations in a cross-sectional view; a) application of average slope line, b) modified elevations.	94
Fig. 5.38	Overflow depth in the center of the basin in year 2001; a) initial elevations, b) after the application of 'fill' procedure, c) after correction of river elevations.	95
Fig. 5.39	The effect of river elevation corrections on overflow depth and extent; a) before correction, b) after correction.	97
Fig. 5.40	The root mean squared error ($RMSE$) values of piezometric heads before and after the reassumption of initial specific yield values.	98
Fig. 5.41	The root mean squared error ($RMSE$) values of piezometric head fits before and after the calibration of specific yield values.	99
Fig. 5.42	Final values of specific yield.	100

Fig. 5.43	The piezometric heads before and after the calibration of specific yield for the well 0335x0005.	101
Fig. 5.44	The piezometric heads before and after the calibration of specific yield for the well 0625x0002.	102
Fig. 5.45	The Nash-Sutcliffe coefficients for piezometric head fits before (outer circles) and after (inner circles) the calibration of specific yield.	102
Fig. 5.46	The final transmissivity values.	104
Fig. 5.47	The effect of transmissivity modification; dashed line represent the initial water table in which $T_A = T_B = T$, continuous line represent the water table after the modification.	105
Fig. 5.48	Monthly flowrate of the Avre before and after the calibration of transmissivities.	105
Fig. 5.49	Monthly flowrate of the Selle before and after the calibration of transmissivities.	106
Fig. 5.50	The difference between the final and the previous transmissivity values, and approximate flow directions.	106
Fig. 5.51	The piezometric head at the point numbered 0613x0012 before and after the calibration of transmissivities.	107
Fig. 5.52	The difference between the final and the previous transmissivity values.	108
Fig. 5.53	The piezometric head hydrographs of a) 0474x0011 and b) 0478x0002 before and after the calibration of transmissivities.	109
Fig. 5.54	The Nash-Sutcliffe coefficients for piezometric heads before (larger circles) and after (smaller circles) the calibration; and for flowrates before (values in black) and after (values in red) calibration.	110
Fig. 5.55	The Nash-Sutcliffe coefficients of piezometric head fits before and after the calibration of transmissivities.	110
Fig. 5.56	The effect of discharge coefficient on the Nash-Sutcliffe coefficients.	111
Fig. 5.57	The effect of the discharge coefficient on flow hydrograph of the Avre.	112
Fig. 5.58	The root mean squared error (<i>RMSE</i>) values of piezometric head fits before and after the calibration of MODCOU.	114
Fig. 5.59	Measures of error before and after the calibration of MODCOU; a) Deviation of runoff volumes (D_v), b) Root mean squared error (<i>RMSE</i>), c) Correlation coefficient (ρ), d) Nash-Sutcliffe coefficient (R^2), e) Coefficient of gain from daily mean (<i>DG</i>).	114
Fig. 5.60	Number of reservoirs in the Nash cascade.	116

Fig. 5.61	The effect of the storage constant, τ , on the Nash-Sutcliffe coefficients of flow hydrograph fits (the first test).	117
Fig. 5.62	Monthly averaged flowrate of the Somme at Abbeville between 1/1999 and 12/2001 for different values of the storage constant, τ (the first test).....	118
Fig. 5.63	The effect of the storage constant, τ , on the Nash-Sutcliffe coefficients of flow hydrograph fits for the period 1/8/1985-31/7/2003 (the second test).	118
Fig. 5.64	The distribution of the values of storage constant, τ	119
Fig. 5.65	The effect of NONSAT calibration on the Nash-Sutcliffe coefficients of the Somme and its tributaries.	120
Fig. 5.66	The final results of simulations together with the calibration and validation periods; (a)-(c) at various locations on the Somme, (d)-(g) on the tributaries of the Somme.	121
Fig. 5.67	Monthly discharges on the Somme at Abbeville for the period 1986-2002... 125	
Fig. 5.68	Average annual discharge and baseflow.....	125
Fig. 5.69	Comparison of total exfiltration depth in year 2001 calculated by MODCOU (in blue) with a satellite derived image representing the flooded percentages of areas for the mesh given on April 21, 2001 when the flood reached its maximum extent (in red).	126
Fig. 5.70	Comparison of total exfiltration depths excluding the river cells in year 2001 between MODCOU (in blue) and MARTHE (in red); a) downstream portion of the Somme, b) upstream portion of the Somme.	127
Fig. 5.71	The spatial distribution of exfiltration fluxes of year 2001 in the East-West direction computed by; a) MARTHE, b) MODCOU.	129
Fig. 5.72	Flux exchange between the surface and the aquifer in the period 1/8/1985-31/7/2003.....	130
Fig. 5.73	Effect of transmissivity and specific yield change on the average root mean squared error obtained by using 50 head observation points.....	132
Fig. 5.74	Effect of transmissivity and specific yield change on the average groundwater level change obtained by using 50 head observation points.....	132
Fig. 5.75	The effect of streambed conductance on flux exchange.....	133

LIST OF SYMBOLS

AET	: actual evapotranspiration
a_C	: calibration parameter for the CEQUEAU model
b	: saturated thickness of aquifer
C_d	: conductance of the drain
C_{QI}	: depletion ratio of the aquifer feeding reservoir
C_{QR}	: depletion ratio of the surface runoff reservoir
C_{riv}	: streambed conductance
CRT	: mean value of soil water stock
Cd	: discharge coefficient of the cell
Cds	: discharge coefficient of the segment
$Cred$: redistribution coefficient
D_v	: deviation of runoff volumes
$DCRT$: minimum value of soil water stock
DG	: coefficient of gain from daily mean
FN	: maximum value of infiltration
g	: gravitational acceleration
H_0	: elevation of the water surface in the stream
\mathbf{h}	: piezometric head matrix
h	: piezometric head
h_0	: known value of piezometric head
\mathbf{K}	: hydraulic conductivity matrix
K	: hydraulic conductivity
K_{iz}	: number of isochronal zones
k	: intrinsic permeability
k_{ET}	: evapotranspiration coefficient
L	: length of sand filter
l	: length of a cell
N	: number of reservoirs in the Nash cascade
N_k	: number of cells inside the isochronal zone
Nup	: number of upstream segments

n	: number of grid cells with unknown piezometric head values
n_r	: number of river cells in the segment
n_{adj}	: number of adjacent cells
n	: direction normal to the surface
P	: precipitation
P_r	: pumping rate
PET	: potential evapotranspiration
Q	: flow exchange with surface
Q_C	: constant flowrate value
Q_{max}	: maximum infiltration rate
QI	: input of aquifer feeding reservoir
QI_{max}	: overflow level of aquifer feeding reservoir
QII	: aquifer recharge
QR	: input of surface runoff reservoir
QR_{max}	: overflow level of the surface runoff reservoir.
QRR	: surface runoff
Qaq	: sum of the volume of water exchanged with the aquifer in the segment
Qr	: sum of surface runoff volume flowing into the segment
Q_w	: volume of water outflowing from the balance reservoir
q	: specific discharge
q_{low}	: exchange of flowrate with the lower aquifer layer
qaq	: volume of water exchanged between a river cell and the aquifer cell beneath
qr	: surface runoff volume into a river cell
R	: recharge rate
$RMSE$: root mean squared error
R^2	: Nash-Sutcliffe coefficient
R_{aq}	: level of the aquifer feeding reservoir
R_b	: level of balance reservoir
R_{bmax}	: maximum level of balance reservoir
R_b^{new}	: new level of balance reservoir
R_{sur}	: level of the surface runoff reservoir
r	: residue for convergence
S	: storage coefficient
S_{CA}	: catchment area of the river cell
S_{DA}	: accumulated drainage area of a cell

S_W	: area of the free water surface in the cell
S_c	: confined storage
S_s	: specific storage
S_y	: specific yield
Sl	: slope between two cells
\mathbf{T}	: transmissivity matrix
T	: transmissivity
T_{max}	: maximum of transfer times
t	: time
t_{tra}	: transition time
t_{tr}	: transfer time
V	: volume of water in the cell
V_s	: volume of water in the segment
α	: constant of discharge time
β	: calibration parameter for transition time calculation
Δh	: difference in piezometric heads
Δl	: distance between the centers of two cells
Δt	: time step
Δtc	: critical time step
ε	: error limit
λ_{max}	: residue for overrelaxation factor
μ	: dynamic viscosity of water
ρ	: correlation coefficient
ρ_w	: density of water
τ	: storage constant of reservoir
ω	: overrelaxation factor
ω_o	: optimum value of overrelaxation factor

CHAPTER 1

INTRODUCTION

1.1. Literature Survey

The interactions between groundwater and surface water have received considerable attention by many researchers. The problem of stream-aquifer interactions is important to watershed management efforts aiming at mitigating hazardous flood events, optimizing surface water and groundwater resources and also has significant ecological implications (Hantush et al. 2002). As Sophocleous (2002) points out, groundwater and surface water are not isolated components of the hydrologic system, but instead interact in a variety of physiographic and climatic landscapes. Thus, development or contamination of one commonly affects the other.

According to their relative position in space, Tóth (1963) defines three distinct types of flow systems: local, intermediate and regional, which could be superimposed on one another within a groundwater basin. In a local flow system, water flows to a nearby discharge area, such as a pond or stream. In a regional flow system, it travels a greater distance to major rivers, large lakes, or to oceans. An intermediate flow system is characterized by one or more topographic highs and lows located between its reach and discharge areas, but, unlike the regional flow system, it does not occupy both the major topographic high and the bottom of the basin.

Groundwater discharge is not only confined along the stream channel but also extends throughout the discharge area downgradient from the basin hinge line which is an imaginary line separating areas of upward (discharge) from downward (recharge) flow. Therefore, if baseflow calculations are used as indicators of average recharge, significant error may be introduced, because baseflow may represent only a relatively small part of the total discharge occurring downgradient from the hinge line (Sophocleous 2002).

Larkin and Sharp (1992) classify stream-aquifer systems as (1) underflow component dominated (the groundwater flux moves parallel to the river and in the same direction as the streamflow); (2) baseflow component dominated (the groundwater flux moves perpendicular to or from the river depending on whether the river is effluent or influent); (3) mixed. The dominant component can be deduced from geomorphologic data, such as, channel slope, river sinuosity, degree of river incision through its alluvium, the width-to-depth ratio of the bankfull river channel, and the character of the fluvial depositional system.

Sophocleous (2002) defines baseflow as water that enters a stream from persistent, slowly varying sources and maintains stream flow between water-input events. Subsurface flow can also enter streams quickly enough to contribute to the event response which is then called subsurface storm flow or interflow.

There are also researchers stressing the influence of the groundwater domain on hydrological basins. For example, Beven (2000) points out, one of the problems involved in having a complete understanding of hydrological systems is that most of the water flows takes place underground in the soil or bedrock and our ability to measure and assess subsurface flow processes is generally very limited.

1.2. Objective

The Somme river basin was influenced by a strong flood in year 2001 in which water levels reached to exceptional levels and caused an immense damage to the surroundings. This event has stressed the contribution of aquifers on the hydrology of basins. According to an estimation of BRGM (Bureau de Recherches Géologiques et Minières), nearly 75% of the flood volume was groundwater-induced as both exfiltration onto the surface and exchange between groundwater and river. The same event played an important role in the maintenance of discharges and causing attenuation of the consequences of dry seasons such as the spring and summer of 2003. Accordingly, in this research work a complete hydrogeological model of the Somme river basin in the north of France is aimed to be established with special emphasis on stream-aquifer interaction.

CHAPTER 2

THEORETICAL BACKGROUND FOR GROUNDWATER FLOW

In this chapter the principles of unsteady groundwater flow are described. While developing numerical methods for the analysis of field problems concerning groundwater flow, it is essential to build a mathematical model by defining the governing equations in the form of partial differential equations. These equations are considered as the mathematical representations of the physical phenomena occurring at a point in the flow domain (Aral 1990). The conceptual basis for the transient (or unsteady) fluid flow equation is the law of conservation of mass and Darcy's law. In the following, a brief description of the groundwater flow equations is provided.

In 1856 Henry Darcy carried out experiments with sand-filled tubes for a water supply system for the city of Dijon, France (Darcy 1856). He discovered an important physical relationship in the science of porous-media hydrodynamics which is now called as *Darcy's Law*:

$$q = -K \frac{\Delta h}{L} \quad (2.1)$$

where q is the specific discharge or volumetric flowrate per unit area of porous medium, K is the hydraulic conductivity of the porous medium, Δh is the difference in piezometric head across the filter of length L , i.e. $\Delta h = h_2 - h_1$, as the piezometric head describes the sum of pressure head and potential head of the fluid, the term, $(h_2 - h_1)/L$ is to be interpreted as hydraulic gradient along the flow path. By convention, the negative sign implies that flow is along the direction of decreasing gradient. The hydraulic conductivity is defined as:

$$K = \frac{k\rho_w g}{\mu} \quad (2.2)$$

where k is the intrinsic permeability, ρ_w is the density of water, g is the gravitational acceleration, and μ is the dynamic viscosity of water.

Further information regarding the generalization or limitations of Darcy's law can be found in Bear (1972), Delleur (1999) and Rushton (2003). Furthermore, sample values for the hydraulic conductivity and storage properties of unconsolidated and consolidated media are presented by Bear (1972), Bouwer (1978) and by Todd and Mays (2005). However, for actual models field investigations are essential.

Although it is common to use hydraulic conductivity in a general sense in describing the hydraulic properties of a porous medium, it is more advantageous to use the term, transmissivity to describe the ease with which water moves through a large porous medium such as a horizontal or layered aquifer. Transmissivity, T , is the product of hydraulic conductivity, K , and saturated thickness, b , of aquifer.

$$T = Kb \quad (2.3)$$

Transmissivity is defined in essentially horizontal flow as the discharge of water through the entire thickness of the aquifer per unit horizontal length of aquifer perpendicular to the direction of flow and per unit hydraulic gradient (Bear 1972).

In anisotropic porous media, where due to some direction related properties such as preferential lining of fractures, stratifications or layering, the conductivity changes depending upon direction (Delleur 1999). Such situations can be described by an extension of Darcy's Law, where the hydraulic conductivity becomes a second order symmetrical matrix, \mathbf{K} , with following components:

$$\mathbf{K} = \begin{bmatrix} K_{xx} & K_{xy} & K_{xz} \\ K_{xy} & K_{yy} & K_{yz} \\ K_{xz} & K_{yz} & K_{zz} \end{bmatrix} \quad (2.4)$$

where the quantities K_{xx} , K_{xy} and so forth are called the conductivity coefficients. Further, in Cartesian coordinates, Darcy's law becomes (Aral 1990):

$$q_x = -K_{xx} \frac{\partial h}{\partial x} - K_{xy} \frac{\partial h}{\partial y} - K_{xz} \frac{\partial h}{\partial z} \quad (2.5)$$

$$q_y = -K_{xy} \frac{\partial h}{\partial x} - K_{yy} \frac{\partial h}{\partial y} - K_{yz} \frac{\partial h}{\partial z} \quad (2.6)$$

$$q_z = -K_{xz} \frac{\partial h}{\partial x} - K_{yz} \frac{\partial h}{\partial y} - K_{zz} \frac{\partial h}{\partial z} \quad (2.7)$$

where q_x , q_y and q_z are the specific discharges in x, y and z directions, respectively.

As can be seen from Eqs. (2.5) to (2.7) potential gradients in one direction can yield flows in other directions. In practice, these equations are not much used, because it is not feasible to assess all conductivity components accurately. Whereas, in an anisotropic medium, where the principle hydraulic conductivity directions are parallel to the main coordinate directions chosen, the specific discharge vectors can be defined as:

$$q_x = -K_x \frac{\partial h}{\partial x} \quad (2.8)$$

$$q_y = -K_y \frac{\partial h}{\partial y} \quad (2.9)$$

$$q_z = -K_z \frac{\partial h}{\partial z} \quad (2.10)$$

The specific discharge vectors constitute three of the four unknowns in a typical groundwater study. The remaining unknown is the piezometric head, h . Therefore a fourth equation is needed. The fourth equation is the continuity equation. Among different approaches, the most popular technique to derive the continuity equation is the representative elementary volume (REV) approach developed by Bear (1972), where macroscopic variables are defined as mean values over a REV. While the exact size of the REV is not determined, it is assumed that the size is much larger than the pore scale and much smaller than the scale of the porous medium. The results obtained with this approach yield macroscopic values for the groundwater flow, representing the average behavior of the fluid over the REV (Delleur 1999).

After employing the control volume approach, for a unit three-dimensional element, the following equation can be written:

$$\frac{\partial}{\partial x} \left(K_x \frac{\partial h}{\partial x} \right) + \frac{\partial}{\partial y} \left(K_y \frac{\partial h}{\partial y} \right) + \frac{\partial}{\partial z} \left(K_z \frac{\partial h}{\partial z} \right) = S_s \frac{\partial h}{\partial t} \quad (2.11)$$

where S_s is the specific storage of the aquifer assuming an elastic mechanical behavior for the REV.

Eq. (2.11) is the governing equation for unsteady three-dimensional groundwater flow in an anisotropic porous medium. However, due to practical reasons, that is, difficulty assessing the conductivity components correctly in all directions, a simpler mathematical model for multi-layered aquifers is rather preferred in the solution of groundwater problems. Eq. (2.11) is reduced to a quasi three-dimensional form by employing the following assumptions (Aral 1990):

1. The flow in the main aquifers is two-dimensional in the horizontal plane of the aquifer and the variation in the aquifer thickness is much smaller than the horizontal dimensions of aquifer. For an unconfined aquifer, this assumption is an extension to the well known Dupuit assumption, in which the vertical flow component is neglected and the potential lines are assumed to be vertical and the streamlines horizontal. The error introduced by this assumption is discussed by Bear (1972). In addition, solutions to two common groundwater problems with and without employing the Dupuit assumption are provided by Korkmaz and Önder (2006) and by Önder and Korkmaz (2007).
2. Main aquifer layers are hydraulically connected to each other by confining layers (aquitards). The direction of flow in the confining layers is vertical and the difference between the hydraulic conductivity of the main aquifers and the confining layers is large.

For a confined aquifer, Eq. (2.11) becomes

$$\frac{\partial}{\partial x} \left(T_x \frac{\partial h}{\partial x} \right) + \frac{\partial}{\partial y} \left(T_y \frac{\partial h}{\partial y} \right) = S_c \frac{\partial h}{\partial t} + Q \quad (2.12)$$

where S_c is the confined storage and the term Q accounts for the flow exchange with surface as well as other aquifer layers.

For an unconfined aquifer (Fig. 2.1), Eq. (2.11) is reduced to

$$\frac{\partial}{\partial x} \left(K_x (h - z_b) \frac{\partial h}{\partial x} \right) + \frac{\partial}{\partial y} \left(K_y (h - z_b) \frac{\partial h}{\partial y} \right) + R - P_r = S_y \frac{\partial h}{\partial t} \quad (2.13)$$

where R is the recharge or injection rate from the surface, P_r is the pumping rate, S_y is the specific yield and the term $(h - z_b)$ represents the thickness of the groundwater. R , P_r and Q in Eq. (2.12) are defined in terms of volumetric flowrate per unit area.

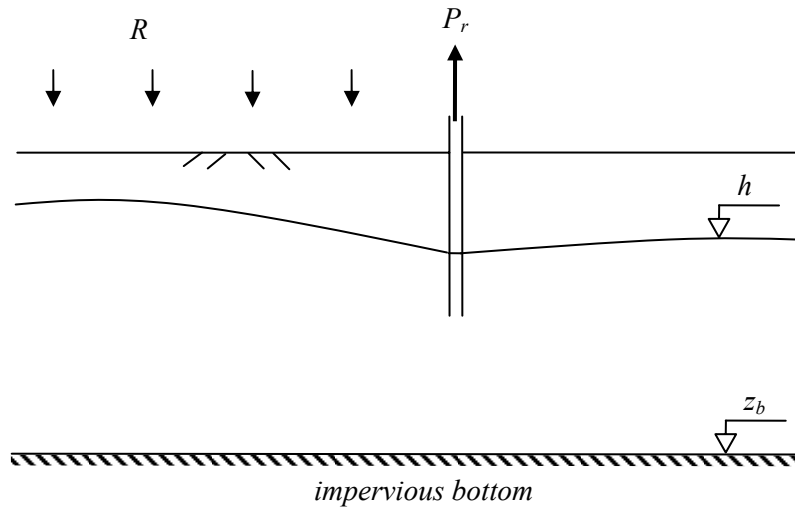


FIG. 2.1 Flow in a leaky unconfined aquifer.

In the solutions of certain problems in unconfined aquifer, some researchers as Bouwer et al. (1999) prefer to use transmissivity instead of hydraulic conductivity. In such cases, the product of hydraulic conductivity (K) with the average saturated thickness $(h - z_b)$ gives the transmissivity. When the vertical variations of the groundwater table are small compared to the saturated thickness, this is a useful assumption as it avoids the non-linearity of governing equation (Bear and Verruijt 1987). In this case a similar form of Eq. (2.12) is used.

CHAPTER 3

PRINCIPLES AND FUNCTIONING OF COUPLED HYDROLOGICAL MODEL

3.1. Introduction

The coupled hydrological model is used to simulate the surface runoff and groundwater flow in a multilayered hydrogeological system (Ledoux 1980; Ledoux et al. 1984). It was recently applied to the Seine (Gomez 2002) and the Rhône (Golaz-Cavazzi 1999) river basins which have important aquifers as the Somme and satisfying results were obtained. The model uses the method of finite differences on a mesh composed of square cells of several sizes. In addition, it can account for the heterogeneity of parameters controlling the flow in the domain. The model structure is schematized in Fig. C. 1 in Appendix C. The primary characteristic of the model is to decompose the water cycle into several stages. These stages can be considered to be independent and their outputs are separately controlled. Hence, it is possible to verify the validity of internal mechanisms while running the whole model. The model consists of five interconnected functions to represent the water cycle:

- a. **The input function:** It essentially includes the precipitation and the exchange of water through the boundaries of the domain. The modeling of input function is not covered in this research, however, its results are taken as input to the problem. The most important ones are the precipitation and potential evapotranspiration (*PET*).
- b. **The production function:** The domain is divided into production zones on each of which a production function is associated. A production function defines the mechanisms that construct the pathway of water entering the system. It

distributes the surface water input among infiltration, overland flow, evapotranspiration and soil water stock using several parameters. In order to extend the applicability of the coupled model, the production function is involved in one single module which facilitates the adaptation to particular problems.

- c. **The surface transfer function:** This function transports the available surface water down to the outlet section. This flow has two sources, namely, the overland flow already partitioned by the production function and the exfiltration to the surface from interactions with the aquifer. Because of this interaction with the groundwater transfer function, this function is embedded in “the coupled model” and it is used simultaneously with the groundwater transfer function.
- d. **The groundwater transfer function:** It simulates the groundwater flow according to equations of flow through porous media. The origins of this flow are the infiltration partitioned by the production function and the flow exchange with the stream network.
- e. **The surface-aquifer exchange function:** It computes the exchange between surface and aquifer domains at the points falling on and beneath the stream network. This computation is made simultaneously with the surface and groundwater transfer functions.

The model was articulated in several modules written in FORTRAN, which are intended to operate sequentially, to include and perform the above described functions. These modules are GEOCOU (Geometry of the Coupled Model), MODSUR (Surface Model), NEWSAM (Groundwater Model), NONSAT (Unsaturated-zone Model), MODCOU (Coupled Model).

3.2. GEOCOU (Geometry of the Coupled Model)

The solution domain is composed of several layers of which the uppermost one is called the surface layer and the others as aquifers (Fig. 3.1). The partition of precipitation into infiltration and surface runoff, and the transfer of surface runoff take place on the surface layer. On the other hand, groundwater flow takes place in the aquifer layers which are

hydraulically connected to each other with confining layers. GEOCOU is used to construct the geometric and physiographic characteristics of the domain. It takes the initial grid information generated by the codes SIGMOD and SIGSOU, and combines them by establishing connectivity. SIGMOD and SIGSOU are two recently created modules used to generate surface and aquifer grids respectively, by using topographic information derived from Digital Elevation Model (DEM) analysis. SIGMOD and SIGSOU are explained in detail in following chapters.

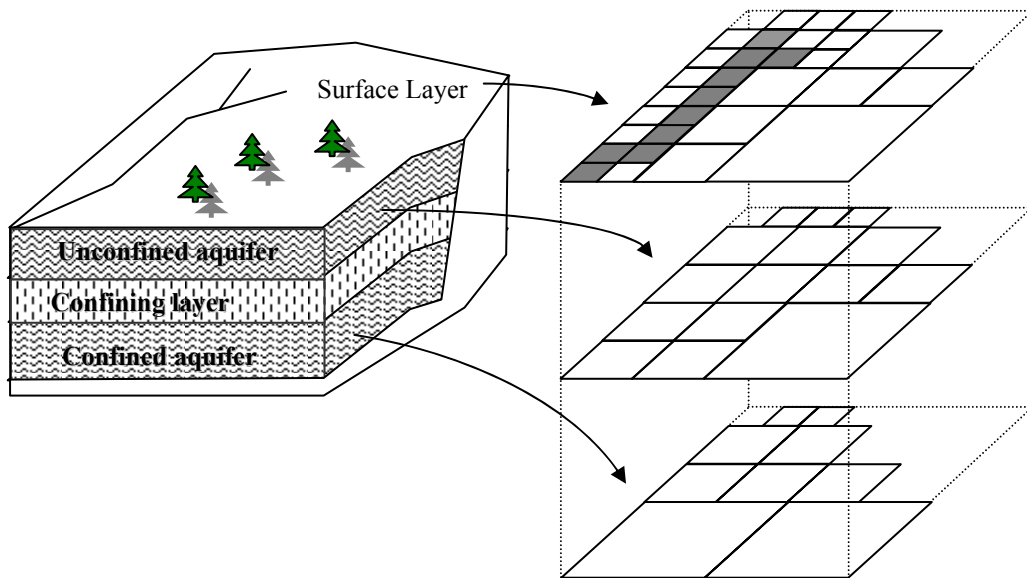


FIG. 3.1 Principle of the multi-layer schematization of coupled hydrological model.

The spatial discretization used in the coupled model is a multi-layered nested grid system using square cells. The characteristics of the flow domain are represented by these cells. For example, flow direction and elevation values are assigned to a surface cell; on the other hand, transmissivity and specific yield values are assigned to an aquifer cell.

The flow network on the surface has the form of one or more arborescent structures. This is defined by assigning each cell a unique flow direction which is the direction having the steepest slope between the cell and its neighbors. Afterwards, this flow network is divided into two categories: stream network and the zone of surface runoff (Fig. 3.2).

Stream network: The network consisting of the cells that are considered to represent the river (grey-colored cells in Fig. 3.2). The interaction between surface and groundwater flows takes place on the stream network. The stream network terminates at an outlet and

any outlet in a flow domain corresponds to a basin. The outlet of a basin is most of the time on its boundary and each basin has an independent catchment and stream network.

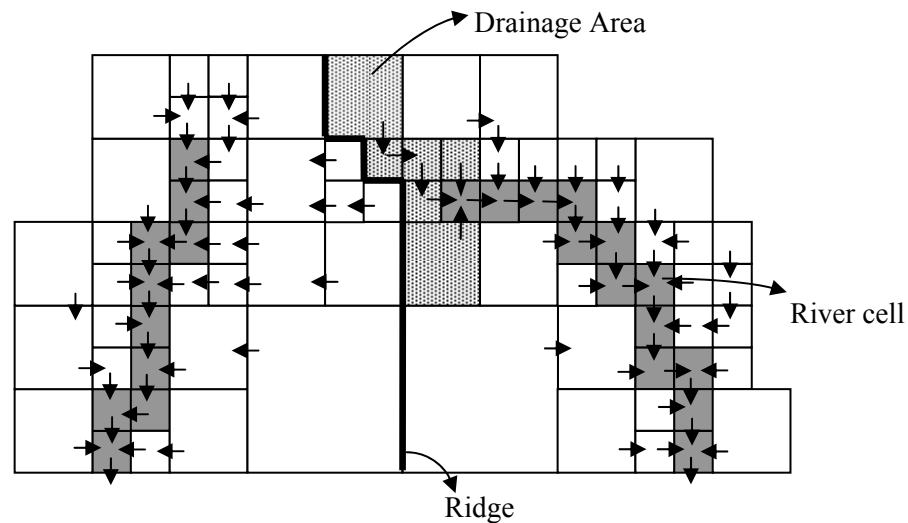


FIG. 3.2 Discretization and the stream network of a surface layer.

Zone of surface runoff: The cells on the surface which are not selected to be a river cell fall into two categories:

- Those falling into the main river basin (right side of the ridge in Fig. 3.2). These cells are partitioned as *drainage areas* on which the infiltration to aquifer and transfer of surface water to the hydraulically closest river cell will be calculated.
- Those falling on a basin which does not comprise the main river network (left side of the ridge in Fig. 3.2). In these zones neither the stream-aquifer interaction nor the transfer of surface water is calculated. The only purpose to keep these zones inside the computation domain is to calculate the infiltration to the aquifer, because the aquifer boundaries are not always related to surface topographic features (e.g. ridges, hillslopes) and maybe larger than the surface domain.

This separation of surface flow into two types renders less computation time and demonstrates the flexibility of the model used. According to the problem encountered different configurations are possible. For example, if the problem is to calculate only the amount of groundwater flow then there would not be any river cell on the surface layer to avoid computation on the stream network, and the surface layer would only be used to

compute the infiltration to the aquifer layer. On the other hand, a stronger interaction with the aquifer layer can be made possible by marking every cell on the surface as a source cell to enable the exfiltration of groundwater onto the surface.

3.3. Computation of Water Budget – MODSUR

MODSUR is the surface module calculating the partition of precipitation among infiltration, surface runoff, evapotranspiration and soil stock. The calculation is made in the time steps of meteorological data, for each production zone inside all the meteorological zones. The partitioning of meteorological zones can be done using any method, such as Thiessen polygons in which each zone is linked to the nearest rain gage. Inside a meteorological zone, the inputs (precipitations and potential evapotranspiration) are homogeneous.

3.3.1. Production Function

The production function is used to calculate the hydrological balance in all the cells on the surface mesh. The production function is expressed in terms of several parameters belonging to the reservoir system defined in Fig. 3.3. At each time step the levels and outflow of these reservoirs are calculated. The outputs from the production function are actual evapotranspiration (*AET*), volume of water to infiltrate to the aquifer domain and volume of water to join the surface runoff.

The comparison of simulated flowrate and piezometric levels with the measured flowrate and piezometric levels allows the calibration of parameters related to these reservoirs. A brief description of the reservoirs is provided below.

Balance Reservoir: The partition of the available water is a function of surface water input (i.e. precipitation), *P*, the level of reservoir, *R_b* and the parameters *DCRT* and *CRT*. *DCRT* is the minimum value of soil water stock usually defined in mm which determines the role of initial rainfall after a dry period. On the other hand, *CRT* is the mean value of soil water stock and is effective on the value of *AET*. The following calculation is performed in the balance reservoir:

$$R_{bmax} = 2(CRT - DCRT) + DCRT$$

$$RBA = \max(DCRT, R_b) - DCRT$$

$$RHA = \min(R_b + P, R_{bmax}) - DCRT$$

$$\Delta R = \max(0, RHA - RBA)$$

$$Q_w = \max(R_b + P - R_{bmax}, 0) + \Delta R (2RBA + \Delta R) / (4(CRT - DCRT))$$

$$AET = \min(PET, R_b + P - Q_w)$$

$$R_b^{new} = R_b + P - Q_w - AET$$

where R_{bmax} is the maximum level of balance reservoir, R_b^{new} is the new level of balance reservoir, Q_w is the volume of water outflowing from the balance reservoir.

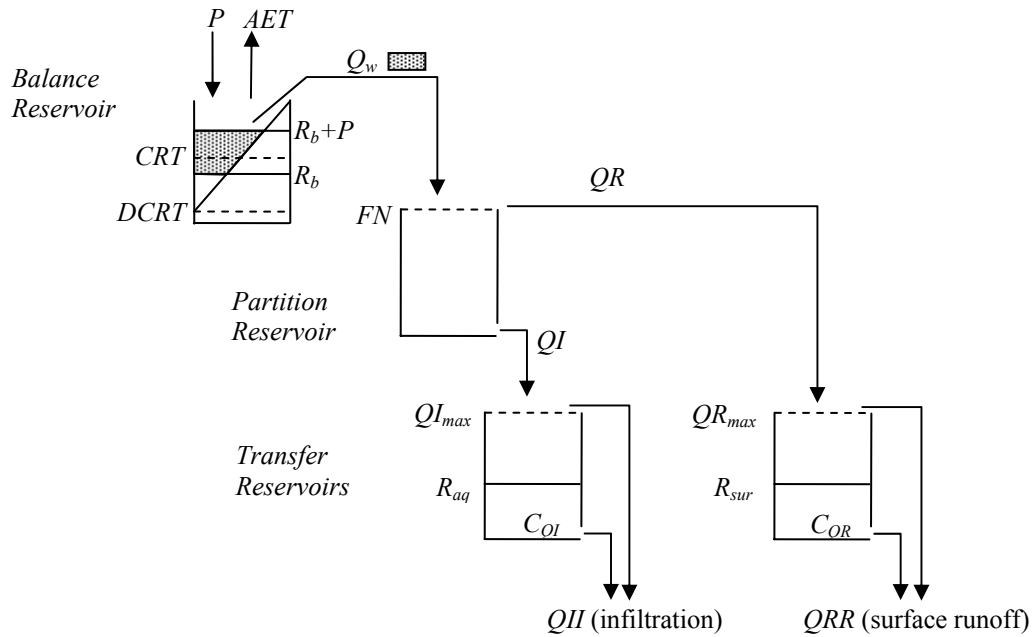


FIG. 3.3 Schematization of a production function.

Unlike other models, for instance, the TOPMODEL (Beven and Kirkby 1979), interception by the vegetation is not included as a separate reservoir in this model. However, interception is handled to a certain degree by the variables $DCRT$ and CRT . Forest canopies intercept the precipitation causing a delayed evaporation with values much more than prairies. Therefore, for the same soil type, the difference ($CRT - DCRT$) will be higher for a forest cover than any other covering. This will cause a reduction in the volume of water, Q_w , to be partitioned between surface runoff and infiltration, and thus, there will be more available water for evapotranspiration. Further, in the areas covered with forests, the root depth is also important. In the forests with deep roots the soil water stock capacity is more and thus, the value of $DCRT$ is higher.

Partition Reservoir: In partition reservoir, the output of balance reservoir is distributed between the aquifer feeding reservoir and the surface runoff reservoir. The distribution of water to infiltration (QI) or surface runoff (QR) is controlled by the parameter FN which stands for the maximum value of infiltration in a time step. These are expressed as follows:

$$QI = \min(Q_w, FN)$$

$$QR = \max(0, Q_w - QI)$$

In MODSUR, surface runoff is created by exceeding the infiltration capacity of soil. If the level of available water is not high enough to spill over the partition reservoir, then there will be no surface runoff and all the water will infiltrate.

Transfer Reservoirs: There are two transfer reservoirs, namely, aquifer feeding reservoir and surface runoff reservoir.

Aquifer feeding reservoir introduces retardation between the infiltration (QI) and aquifer recharge (QII). The reservoir is defined by the parameters R_{aq} , C_{QI} and QI_{max} . These are defined below:

R_{aq} : Level of the aquifer feeding reservoir.

C_{QI} : Depletion ratio of the aquifer feeding reservoir.

QI_{max} : Overflow level of aquifer feeding reservoir.

The recharge to the aquifer is calculated as follows:

$$R_{aq} = R_{aq} + QI$$

$$\text{If } R_{aq} < QI_{max} \text{ then } QII = C_{QI} \times R_{aq}$$

$$\text{If } R_{aq} \geq QI_{max} \text{ then } QII = C_{QI} \times R_{aq} + \max[0, (R_{aq} - C_{QI} \times R_{aq} - QI_{max})]$$

As can be seen from above relations, infiltration is always tried to be conducted with retardation.

Surface runoff reservoir works in a similar way. It introduces retardation for the surface runoff, QRR . The parameters related to this reservoir are described below:

R_{sur} : Level of the surface runoff reservoir.

C_{QR} : Depletion ratio of the surface runoff reservoir.

QR_{max} : Overflow level of the surface runoff reservoir.

The surface runoff is calculated as follows:

$$R_{sur} = R_{sur} + QR$$

$$\text{If } R_{sur} < QR_{max} \text{ then } QRR = C_{QR} \times R_{sur}$$

$$\text{If } R_{sur} \geq QR_{max} \text{ then } QRR = C_{QR} \times R_{sur} + \max[0, (R_{sur} - C_{QR} \times R_{sur} - QR_{max})]$$

In the same way, the surface runoff is tried to be generated with retardation.

There is yet one exception in the calculation of production functions. In the case of “water bodies”, the above parameters are not defined. Instead, the following is used:

$$AET = k_{ET} PET$$

where k_{ET} is a coefficient derived empirically, (e.g. $k_{ET} = 0.8$).

Furthermore, there is one single reservoir, in which $QR = P - AET$ is used to calculate the surface runoff.

3.3.2. Transfer of Surface Runoff

MODSUR computes the transfer of surface runoff until it reaches the main stream network. This is performed by using isochronal zones. Each cell on the main stream network is considered to be the outlet of its drainage area (see Fig. 3.2). Each drainage area is divided into a number of isochronal zones equal to that of time steps (Δt) necessary for flow of the most upstream point to reach the cell.

The flowrate of surface runoff into a river cell, qr , at any time, t , is described as follows:

$$qr_i(t) = \sum_{k=0}^{k=K_i-1} \sum_{j=1}^{j=N_k} QRR_j(t - k \cdot \Delta t) \quad (3.1)$$

where K_{iz} is the number of isochronal zones, N_k is the number of cells inside the isochronal zone, QRR_j is the surface runoff produced in cell j , coming from production function calculations.

As can be seen in Eq. (3.1), the transfer of surface runoff is carried out on the drainage areas of all the river cells. These surface runoff values are stored on the river cells for every time step to be later used by MODCOU. In addition, this overland flow cannot infiltrate along its way down to the river, because, as mentioned before, stream-aquifer interaction is made only on the main stream network. In case the interaction with the aquifer domain is required, the number of river cells can be increased by defining a more detailed stream network.

To sum up, the necessary input for MODSUR is given below:

- Association of a meteorological zone to each surface cell in the basin.
- Preparation of necessary meteorological input, precipitation and *PET*.
- Selection of production zones and determination of their parameters.
- Evaluation of the concentration time of the basin, which is necessary for the formation of isochronal zones. The normalized transfer times calculated in the previous stages (by SIGMOD) are multiplied by the concentration time to give the absolute transfer times.

As output, for each time step, it gives:

- The infiltration in every surface cell.
- The surface runoff to every cell on the main stream network.

3.4. Transfer in the Unsaturated Zone – NONSAT

The aim of the unsaturated-zone module is to transfer the infiltrated water calculated by the production functions vertically to the groundwater table. In MODSUR, the retardation in the unsaturated zone is not sufficiently represented because the thickness of the unsaturated zone may vary greatly in large basins. The unsaturated-zone module is based on the studies of Besbes (1978) who made observations of retardation between the infiltration into aquifer and the groundwater recharge. Besbes (1978) proposes the use of the Nash cascade model (Nash 1959). In Fig. 3.4 a representation of a Nash cascade is

provided. According to the thickness of the unsaturated zone, the unsaturated domain is discretized vertically and represented by the parameters N and τ . N is the number of reservoirs in the Nash cascade, which represents a certain thickness of the unsaturated zone (e.g. 5m) and τ is the storage constant of reservoir. The outflow of the reservoir k is calculated as follows:

$$Q_k(t) = \frac{\Delta Q_{II}(t_0)}{\tau \cdot (k-1)!} \cdot e^{-(t-t_0)/\tau} \cdot \left(\frac{t-t_0}{\tau} \right)^{k-1} \quad (3.2)$$

where $\Delta Q_{II}(t_0)$ is an instantaneous volume given to the first reservoir at time $t=t_0$.

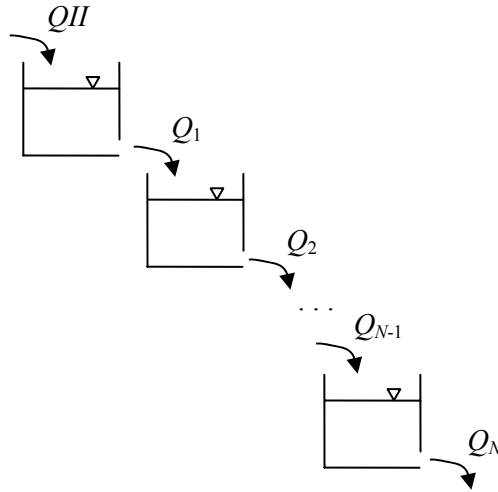


FIG. 3.4 Principle of the Nash model.

As input the number of reservoirs, N , at each cell of the surface grid, the storage constant, τ , for each of the reservoirs and the infiltration rates, Q_{II} , which are computed by MODSUR, are given. As output it gives the same output file as MODSUR, but with the recharge rate of groundwater instead of the infiltration rate into the aquifer. Therefore, the usage NONSAT is optional and it may yield varying results depending on the storage constant and the number of reservoirs provided for an unsaturated zone. An example demonstrating the effect of storage constant is provided in Fig. 3.5.

As can be seen in Fig. 3.5, the value of storage constant is highly determinant on the reduction of the effects an intense inflow. It causes the reservoirs to transmit the flow with delay. Similarly, the number of reservoirs is also determinant on the peak flow. The optimum values of these parameters are determined by calibration.

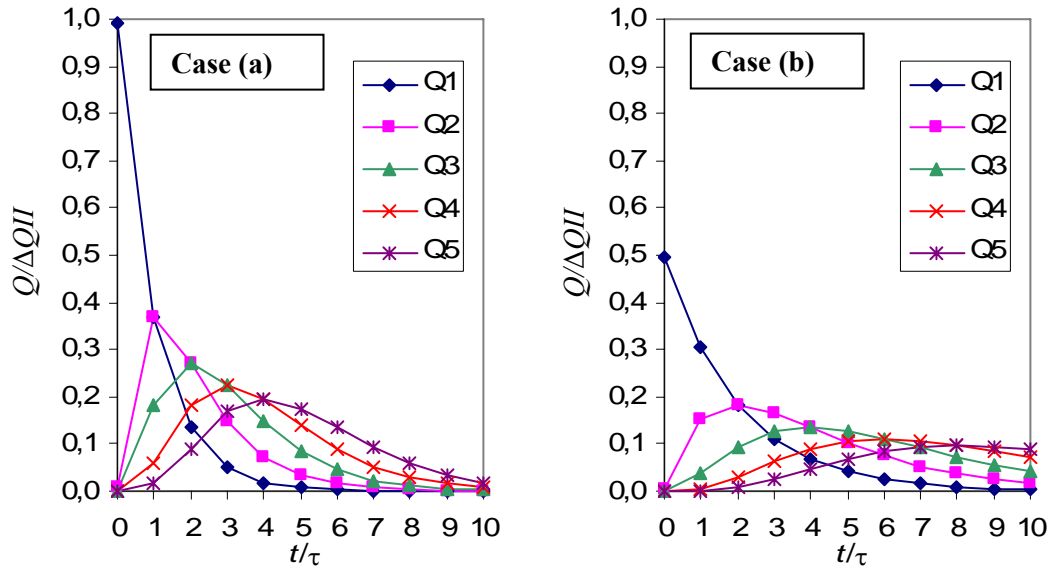


FIG. 3.5 The effect of storage constant on the outflows of a Nash cascade with 5 reservoirs; **a)** $\tau=1$ day, **b)** $\tau=2$ days.

3.5. Steady-State Groundwater Flow Simulation – NEWSAM

NEWSAM is the module simulating transient or steady-state groundwater flow and solute transport (Levassor and Ledoux 1996). In this research, it is used to obtain a steady-state groundwater level in the aquifer to form the initial condition of the coupled model, MODCOU.

The general form of the governing equation solved by NEWSAM is a steady-state, two-dimensional flow equation, similar to Eq. (2.12).

$$\frac{\partial}{\partial x} \left(T_x \frac{\partial h}{\partial x} \right) + \frac{\partial}{\partial y} \left(T_y \frac{\partial h}{\partial y} \right) = Q \quad (3.3)$$

where h is the piezometric head; T_x, T_y are the transmissivities in x and y directions; and Q represents the recharge-leakage term of the aquifer.

3.5.1. Discretization

The discretization is made using the method of finite differences. The grid is generated by GEOCOU and the unknown $h(x, y)$ is located at the center of each grid cell. Each layer represents an individual aquifer and connected to other aquifers by confining layers. Each

cell in a layer is vertically connected to other cells, if any, in upper or lower aquifer layers. Continuity relation for an aquifer cell is shown in Fig. 3.6 where the grid is assumed to consist of identical square cells.

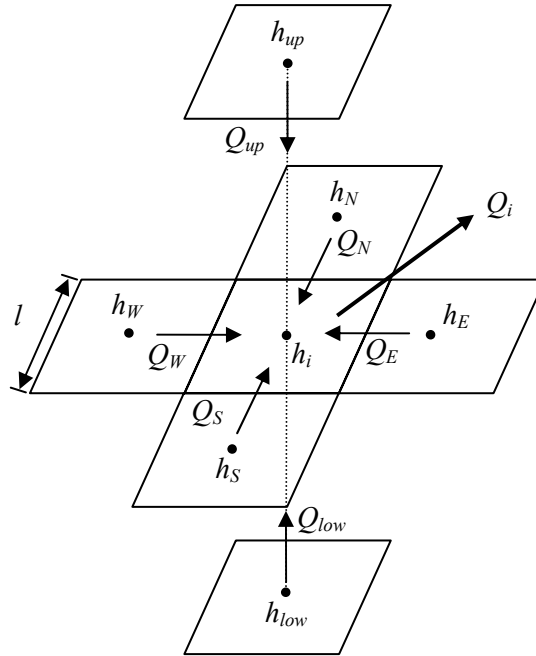


FIG. 3.6 Continuity in an aquifer cell.

The directions of neighboring cells are represented by four main compass directions. h_i is the piezometric head at the current cell; h_N , h_E , h_S , h_W are the piezometric heads in the neighboring cells falling to north, east, south and west, respectively; whereas h_{up} and h_{low} are the piezometric heads in the neighboring cells of upper and lower aquifer layers; and, l is the length of a cell. The flows entering and leaving the cell are shown with related directions. By applying the continuity principle, the following can be written in a cell:

$$Q_N + Q_E + Q_S + Q_W + Q_{up} + Q_{low} - Q_i = 0 \quad (3.4)$$

where Q_N , Q_E , Q_S , Q_W are the flows entering into the cell from north, east, south and west directions, respectively; Q_{up} and Q_{low} are the flows entering into the cell from upper and lower aquifer layers through a confining layer; and Q_i is the flowrate pumped from the cell. If there is recharge or injection then there should be a negative sign before Q_i .

The flowrate entering the cell i from any horizontally neighboring cell j can be defined using Darcy's law:

$$Q_j = T_{ij}l \frac{h_j - h_i}{l} = T_{ij}(h_j - h_i) \quad (3.5)$$

where T_{ij} is the transmissivity between the cells i and j . It is defined by using the principle of flow normal to layers in a confined aquifer (Bear 1972). For the confined aquifer shown in Fig. 3.7, the following relation can be written:

$$\frac{L}{T_{eq}} = \sum_{k=1}^n \frac{L_k}{T_k} \quad (3.6)$$

where T_{eq} is the equivalent transmissivity of the horizontally layered aquifer.

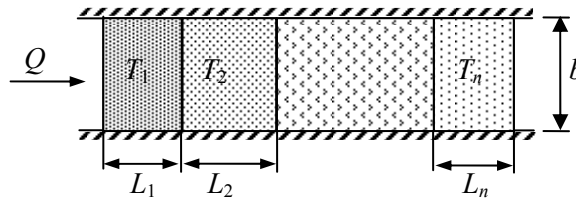


FIG. 3.7 Flow in a horizontally layered confined aquifer.

When the plan view is considered, for two identical cells, according to Eq. (3.6), T_{ij} becomes

$$T_{ij} = \frac{2T_i T_j}{T_i + T_j} \quad (3.7)$$

which is the harmonic mean of the transmissivities of two cells.

There is yet one special case that has to be considered. In the present model, refinement in the cell size is made where additional precision is required (e.g. see Fig. 3.2). This is achieved by a nested grid generation, details of which will be described in the following chapters. Because of the nested grid system employed, there can be neighboring cells having different sizes. When the case schematized in Fig. 3.8 is considered, the flowrates entering the cell i can be defined as:

$$Q_j = T_{ij} l \frac{h_j - h_i}{3l/2} = \frac{2}{3} T_{ij} (h_j - h_i) \quad (3.8)$$

$$Q_k = T_{ik} l \frac{h_k - h_i}{3l/2} = \frac{2}{3} T_{ik} (h_k - h_i) \quad (3.9)$$

where T_{ij} and T_{jk} are the equivalent transmissivities of two adjacent cells, indicated by the indices. These are defined again by using the relation given in Eq. (3.6):

$$\frac{3l/2}{T_{ij}} = \frac{l}{T_i} + \frac{l/2}{T_j} = \frac{l(2T_j + T_i)}{2T_i T_j}$$

and therefore

$$T_{ij} = \frac{3T_i T_j}{T_i + 2T_j} \quad \text{and} \quad T_{ik} = \frac{3T_i T_k}{T_i + 2T_k} \quad (3.10)$$

which are again harmonic means of transmissivities.

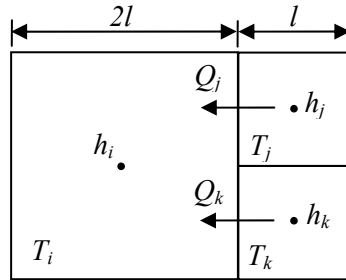


FIG. 3.8 Representation of flow in a nested grid system.

The flowrates of leakage from upper and lower aquifer layers are expressed as:

$$Q_{up} = K_{up} l^2 \frac{h_{up} - h_i}{b_{up}} \quad (3.11)$$

$$Q_{low} = K_{low} l^2 \frac{h_{low} - h_i}{b_{low}} \quad (3.12)$$

where K_{up} and K_{low} are the hydraulic conductivities of upper and lower confining layers; b_{up} and b_{low} are the thicknesses of confining layers. Instead of hydraulic conductivities, $T_{up} = K_{up} \frac{l^2}{b_{up}}$ and $T_{low} = K_{low} \frac{l^2}{b_{low}}$ can be used, where T_{up} and T_{low} are the transfer coefficients of confining layers.

Therefore Eq. (3.4) can be discretized as follows:

$$T_N(h_N - h_i) + T_E(h_E - h_i) + T_S(h_S - h_i) + T_W(h_W - h_i) + T_{up}(h_{up} - h_i) + T_{low}(h_{low} - h_i) = Q_i \quad (3.13)$$

Eq. (3.13) is the discretized form of the linear differential equation solved by NEWSAM. It is written for every node i inside the problem domain, therefore a linear system of equations with n unknowns, where n is the number of grid cells with unknown piezometric head values, are obtained. For simplicity, the following matrix form can be written:

$$\mathbf{T}\mathbf{h} = \mathbf{Q} \quad (3.14)$$

Where \mathbf{T} is the transmissivity matrix of dimensions $n \times n$:

$$\mathbf{T} = \begin{bmatrix} T_{11} & T_{12} & \cdot & T_{1n} \\ T_{21} & T_{22} & \cdot & T_{2n} \\ \cdot & \cdot & \cdot & \cdot \\ T_{n1} & T_{n2} & \cdot & T_{nn} \end{bmatrix} \quad (3.15)$$

And \mathbf{h} is the piezometric head matrix of dimension n :

$$\mathbf{h} = \begin{bmatrix} h_1 \\ \cdot \\ \cdot \\ h_n \end{bmatrix} \quad (3.16)$$

\mathbf{Q} is the flowrate matrix of dimension n :

$$\mathbf{Q} = \begin{bmatrix} Q_1 \\ \cdot \\ \cdot \\ Q_n \end{bmatrix} \quad (3.17)$$

3.5.2. Boundary Conditions

There are three types of boundary conditions in such a groundwater flow problem:

1. Dirichlet Boundary Condition: Also referred to as prescribed head boundary condition, where the piezometric head is known and constant on a particular region of the domain, for example, along a reservoir, lake or sea boundary. In this case, the following can be written:

$$h = h_0 = \text{const} \quad (3.18)$$

where h_0 is the known value of the piezometric head.

2. Neumann Boundary Condition: Also referred to as prescribed flux boundary condition, where there is constant and known inflow or outflow normal to the boundary surface. The most common form of this boundary condition exists for impervious boundaries or groundwater divides where the flux across the boundary is zero. This boundary condition can be expressed as:

$$q = q_0 = T \frac{\partial h}{\partial n} = \text{const} \quad (3.19)$$

where n is the direction normal to the surface.

3. Cauchy Boundary Condition: Also referred to as head-dependent boundary condition, where the direction and magnitude of flow is not constant and depends on the head on the boundary. This boundary condition exists mainly on stream and outlet boundaries. The flow drained by a stream or outlet can be written as:

$$Q = C_d (h - h_0) \quad (3.20)$$

where C_d is the conductance of the drain and h_0 is the head of the drain.

In order to prevent an inverse flow, the following condition can be added:

$$Q \geq Q_C \quad (3.21)$$

where Q_C is a constant flowrate value, for example, with $Q_C = 0$, an inverse flow from the outlet to the aquifer is prevented.

This boundary condition can also be used to represent the sources. By Eq. (3.20) flooding can occur when the piezometric head of groundwater rises above the surface and by Eq. (3.21) re-infiltration from the surface is prevented, thus, forming a saturation excess overland flow.

In case of contact with stream, Q_C can take a negative value to represent the condition that the groundwater head falls below the elevation of the river bottom. An unsaturated zone occurs beneath the streambed and Eq. (3.20) can not be used. As a consequence, the flow is represented by a constant value, Q_C .

3.5.3. Numerical Solution

The solution technique used by NEWSAM is Point Successive Overrelaxation (PSOR) method. PSOR is an iterative procedure usually employed when there are a large number of nodes inside the problem domain. The fundamentals of this method are presented by Varga (1962). Eq. (3.13) can be rearranged as:

$$h_i = \frac{T_N h_N + T_E h_E + T_S h_S + T_W h_W + T_{up} h_{up} + T_{low} h_{low} - Q_i}{T_N + T_E + T_S + T_W + T_{up} + T_{low}} \quad (3.22)$$

As mentioned before, Eq. (3.22) is written for every grid node inside the problem domain. Incorporating the PSOR method, Eq. (3.22) becomes

$$h_i^{k+1} = \omega \frac{T_N h_N^{k+1} + T_E h_E^k + T_S h_S^k + T_W h_W^{k+1} + T_{up} h_{up}^{k+1} + T_{low} h_{low}^k - Q_i}{T_N + T_E + T_S + T_W + T_{up} + T_{low}} + (1 - \omega) h_i^k \quad (3.23)$$

where k is the iteration level and ω is the overrelaxation factor.

The grid is scanned in an orderly fashion. The first calculation is made on the cell located at the upper left-hand corner of the uppermost layer and the sweep is considered to proceed from left to right. When one layer is completely finished, the computation proceeds from the layer right below. As can be seen in Eq. (3.23), while calculating the new value at a cell, the most recent values in the north, west and upper cells are used. The overrelaxation factor, ω , has a value between 1 and 2. It is calculated by using Carré's method (Carré 1961). The algorithm used to calculate the optimum value of overrelaxation factor can be outlined as follows:

1. One iteration is performed with $\omega = 1$.
2. Twelve iterations are performed using $\omega = 1.375$.
3. Find the residue λ_{\max} using

$$\lambda_{\max} = \max \left(\frac{|h_i^{k+1} - h_i^k|}{|h_i^k - h_i^{k-1}|} \right) \quad (3.24)$$

4. Find the optimum value of overrelaxation factor, ω_o , using

$$\omega_o = 2 \left[1 + \left[1 - \frac{(\lambda_{\max} + \omega - 1)^2}{\lambda_{\max} \omega^2} \right]^{1/2} \right]^{-1} \quad (3.25)$$

5. Calculate

$$\omega = \omega_o - \frac{2 - \omega_o}{4} \quad (3.26)$$

6. Go to step 2 and use this value of ω .
7. Repeat the complete procedure until two estimates of ω_o are within a specified tolerance.

It should be noted that Carré's method is economical of time as the optimum value is found during regular iteration process.

The convergence is checked using a residue defined as follows:

$$r = \frac{\sum_{i=1}^n |h_i^{k+1} - h_i^k|}{n} \quad (3.27)$$

where n is the number of cells with unknown heads on the grid.

In the end of each time step the value of r is compared to an error limit, such as $\varepsilon = 1. \times 10^{-4}$, and when $r < \varepsilon$ convergence is satisfied.

3.6. Unsteady Simulation of Groundwater and Surface Flows – MODCOU

MODCOU simulates the water flow in both surface and aquifer domains by taking into consideration their interaction. In this last step, the simulated flowrates at the outlets and hydrometric stations and also the piezometric heads up to 50 points inside the basin are obtained. The inputs of MODCOU are; initial piezometric head distribution from NEWSAM, the recharge rate of groundwater from NONSAT and flowrate of overland flow reaching at each stream cell from MODSUR.

3.6.1. Groundwater Flow

Groundwater flow is simulated by using the diffusion equation in porous medium. The underground domain has a multilayered representation, that is, there are the aquifer layers and the semi-permeable layers connecting these aquifers. The model assumes that the flow is horizontally two-dimensional (2D) inside the aquifers and vertical in the semi-permeable layers. The simulation of groundwater flow by MODCOU is similar to that carried out by NEWSAM. The only difference is the unsteady simulation of flow. The related governing differential equation for a 2D unsteady groundwater flow is given below:

$$\frac{\partial}{\partial x} \left(T_x \frac{\partial h}{\partial x} \right) + \frac{\partial}{\partial y} \left(T_y \frac{\partial h}{\partial y} \right) = S \frac{\partial h}{\partial t} + Q_{sur} + Q_{up} + Q_{low} \quad (3.28)$$

where h is the piezometric head; T is the transmissivity; S is the storage coefficient; Q_{sur} is the exchange of flowrate with the surface; Q_{up} is the exchange of flowrate with the upper aquifer layer; Q_{low} is the exchange of flowrate with the lower aquifer layer. S becomes

specific yield, S_y , for an unconfined aquifer and confined storage, S_c , for a confined aquifer. Q_{up} and Q_{low} are already defined by Eqs. (3.11) and (3.12).

Discretization and Numerical Solution:

The method of discretization is the same as in NEWSAM. By considering the storage term, Eq. (3.13) can be rewritten as follows:

$$\sum_{j=1}^{nadj} T_{ij} (h_j^{t'} - h_i^{t'}) = \frac{S_i \cdot l^2}{\Delta t} \cdot (h_i^{t+1} - h_i^t) + Q_i^{t'} \quad (3.29)$$

where $nadj$ is the number of adjacent cells; T_{ij} is the harmonic mean of the transmissivities of cells i and j , as already defined by Eq. (3.7) for two identical cells and by Eq. (3.10) for two different sized cells; Q_i is the recharge/leakage term; and t' is the time level depending on the scheme used. The calculation is made using either explicit or implicit schemes depending on the stability condition. In Eq. (3.29), $t' = t$ is used for an explicit scheme and $t' = t + 1$ for an implicit scheme where $t+1$ represents the new time step. As mentioned by Delleur (1999), explicit finite-difference equations are simple and straightforward to solve, but they may have associated stability criteria. That is, if time increments are too large, small numerical errors or perturbations may propagate into larger errors at later stages of computation. According to Von Neumann stability analysis (Trefethen 1996), the exact stability restriction to the heat equation, $u_t = u_{xx}$, is $\sigma \leq \frac{1}{2}$

where $\sigma = \frac{\Delta t}{(\Delta x)^2}$. When this criterion is adapted to the problem considered, a critical time step (Δtc) can be defined as follows:

$$\Delta tc = \min \left(\frac{S_i \cdot l^2}{\sum_{j=1}^{nadj} T_{ij} (+ C_{rivi})} \right) \quad (3.30)$$

where C_{rivi} is the streambed conductance (see Section 3.6.3 below), that is, a term added for the aquifer cells beneath a river cell.

If the simulation time step, Δt , is greater than the critical time step, Δt_c , the explicit approximation becomes unstable and in this case, an implicit approximation is used. When an implicit scheme is considered, there would be a system of n equations containing n unknowns. Such a system can be solved simultaneously. Even though the solution is more complicated, implicit scheme has the advantage of being unconditionally stable. In the coupled model, successive overrelaxation method is used to perform iterations for convergence within each time step.

3.6.2. Transfer in the Stream Network

The amount of surface water arriving at each river cell for every time step has already been calculated by MODSUR. However it has not been transferred to the outlet and the exchange with the aquifer has not yet been done. The flow in the stream network by taking into consideration the stream-aquifer interaction is handled by MODCOU.

This part of the model is derived from the CEQUEAU model (Girard et al. 1972). The stream network is divided into segments as in Fig. 3.9 by using isochrones.

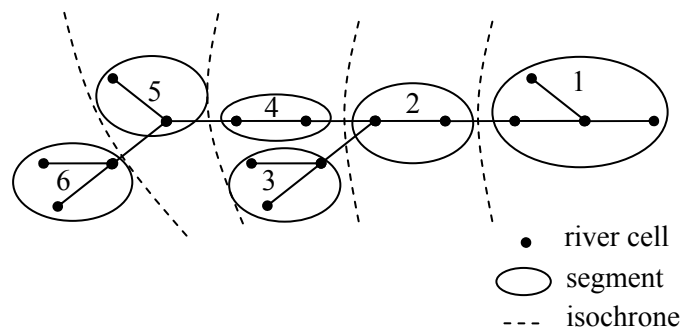


FIG. 3.9 Formation of segments on the stream network.

Each segment represents a group of river cells between two isochrones and has a drainage coefficient. The segments are formed in such a way that water in each cell inside a segment arrives at the outlet of the basin within the same time step. Therefore, the surface water stock contained in a segment in a given time step is the sum of the water stock in all the river cells forming that segment.

The transfer is carried out as follows:

$$Vs_i^{t+1} = (1 - Cds_i) \cdot (Vs_i^t + Qr_i^t + Qaq_i^t) + \sum_{j=1}^{Nup} Cds_j \cdot (Vs_j^t + Qr_j^t + Qaq_j^t) \quad (3.31)$$

where Vs_i^{t+1} is the volume of water in segment i at time $t+1$; Cds_i is the discharge coefficient of segment i ; Nup is the number of upstream segments which flow directly into segment i (e.g. segments 3 and 4 for segment 2 in Fig. 3.9); Qr_i is the total volume of surface runoff flowing into segment i within the time step; Qaq_i is the total volume of water exchanged with the aquifer in segment i within the time step. For any given segment, Qr and Qaq are computed with the following equations:

$$Qr^t = \sum_{i=1}^{n_r} qr_i^t \quad (3.32)$$

where qr_i is the volume of surface runoff arriving at the river cell i (Eq. 3.1), and n_r is the number of river cells in the segment.

$$Qaq^t = \sum_{i=1}^{n_r} qaq_i^t \quad (3.33)$$

where qaq is the volume of water exchanged between a river cell and the aquifer cell beneath in a time step.

Eq. (3.31) can be considered to be the equation of continuity for a segment, which means that the volume of water in a segment is equal to the volume of water retained after discharge and plus, the discharged volumes coming from upstream segments.

Contrary to the transfer of surface runoff carried out by MODSUR (section 3.3.2), the stream flow may be simulated at any point on the stream network in order to output the flow hydrograph and compare it with the measured stream flow data.

Once the transfer between the segments is completed, the total amount of water in a segment is distributed among the river cells by using a redistribution coefficient:

$$Cred_i = \frac{l_i / Cd_i}{\sum_{k=1}^{n_r} l_k / Cd_k} \quad (3.34)$$

where n_r is the number of river cells in the segment, l is the size of the cell, and Cd is the discharge coefficient of the cell.

And redistribution of the volume of water for a cell is made using the following:

$$V_i^{t+1} = Cred_i \cdot V_s^{t+1} \quad (3.35)$$

Thus, this redistribution privileges the cells having a low discharge coefficient.

Computation of Discharge Coefficient:

The volume of water flowing into a cell is described according to the law of exponential depletion:

$$\frac{\partial V}{\partial t} = -\alpha \cdot V \quad (3.36)$$

which gives after integration from 0 to Δt :

$$\Delta V = (1 - e^{-\alpha \cdot \Delta t}) \cdot V \quad (3.37)$$

and the discharge coefficient of a cell is:

$$Cd = (1 - e^{-\alpha \cdot \Delta t}) \quad (3.38)$$

where α is a constant of discharge time; and it is expressed using the CEQUEAU model (Girard et al. 1972):

$$\alpha = a_C \cdot \frac{S_{CA}}{S_W + \frac{1}{100} \cdot \sqrt{S_{CA}}} \quad (3.39)$$

where S_{CA} is the catchment area of the river cell; S_W is the area of the free water surface (lake area) in the cell; and a_C is a calibration parameter in terms of a time constant having a dimension of $[T]^{-1}$.

As can be seen in Eq. (3.39), the discharge coefficient for each cell can be different. It depends on the storage of water in the cell. If there is no storage reservoir in a cell other than that supplied by the streambed, the discharge coefficient will be close to unity. On the other hand, when there is a large lake inside the cell, during a flood a considerable storage of water can take place. In this case, according to the value of S_w , the discharge coefficient, Cd , will decrease.

For any segment, the minimum of the discharge coefficients of the cells is assumed to be the discharge coefficient of the segment to be used in Eq. (3.31), as it will be the controlling value of the flow between two segments. In MODCOU, it is also possible to introduce the discharge coefficients of river cells directly as input, instead of computing with Eqs. (3.38) and (3.39).

3.6.3. Stream-Aquifer Interaction

MODCOU calculates the flux exchange between the aquifer and the stream at each time step. As can be seen in Fig. 3.10, three possible cases of this interaction are considered.

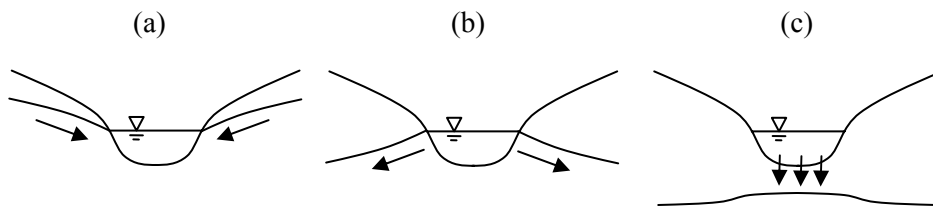


FIG. 3.10 Stream-aquifer interaction; (a) connected gaining stream, (b) connected losing stream, (c) disconnected losing stream.

Case (a) and (b):

The free surface on a groundwater mound rises from the shallow regional water table to intercept the water level in the channel; the stream-aquifer system is *hydraulically connected*. In this case, the surface water is represented as a constant head boundary and the flowrate to or from the boundary is computed using Darcy's law:

$$q_{aq} = C_{riv} \cdot (H_0 - h) \quad (3.40)$$

where H_0 is the elevation of the water surface in the stream; h is the groundwater head; and C_{riv} is the streambed conductance.

Therefore, the value of qaq is positive for case (b) and negative for case (a).

Case (c):

In this case, unsaturated sediments exist between the channel and the regional water table and thus, the system is *hydraulically disconnected* (Stephens 1996). There is an unsaturated flow between the stream and the aquifer. This flow is expressed as a constant value:

$$qaq = Q_{\max} \quad (3.41)$$

where Q_{\max} is the maximum infiltration rate.

The annual variations in the hydraulic regime of the system cause changes between the cases explained above. In addition, the volume of water infiltrating to the aquifer is limited with the available water in a cell within a time step. Considering all these, the exchange function is treated by the following non-linear relation:

$$qaq = \min \begin{cases} C_{riv} \cdot (H_0 - h) \\ Q_{\max} \\ V/\Delta t \end{cases} \quad (3.42)$$

where V is the available volume of water in the stream cell calculated by Eq. (3.35).

The head in the stream is the elevation of the water surface. However, for the sake of simplicity, in this model this value is not related to the volume of water stored in the stream, but it is equal to the elevation of the topography. Therefore the water level in the stream remains constant all the time.

Streambed conductance term represents the product of hydraulic conductivity, K , of the sediment layer and cross-sectional area of flow (i.e. area of the cell) divided by the length of the flow path. However, these parameters are each difficult to estimate and it should be recognized that formulation of a single conductance term to account for three-

dimensional flow processes is inherently an empirical exercise, and that adjustment during calibration is almost always required (McDonald and Harbaugh 1988). In the same way, the maximum infiltration rate, Q_{\max} , is as well subject to calibration.

3.7. Programming Toolkit

Other than the modules contained in the conceptual model, there are some programs used to prepare the necessary input data for the conceptual model and also to visualize the output of modules.

In the following, the programs HYDRODEM, SIGMOD and SIGSOU are described. These are supplementary programs used to prepare initial data to GEOCOU most of which already existed, however, in this research they were developed in order to fit the model being used.

3.7.1. Geographic Information System: Utilization of Digital Elevation Model in Hydrology

A Digital Elevation Model (DEM) is a numerical representation of a topographic surface (Beven and Kirkby 1993). There is a diversity of current and developing technologies for generating digital elevation data ranging from interpolation of digitized contour lines to photogrammetric analysis of aircraft or satellite derived stereo images. In many developed countries of the world digital elevation or terrain models (DEM or DTM) are becoming available at resolutions fine enough to represent the form of hillslopes. As Beven (2000) describes, resolution is clearly an issue, coarse-resolution DEMs will not be able to provide adequate description of hillslope flow pathways. On the other hand, the available models may not be able to use all the information in a fine-resolution DEM due to computational constraints. Recently, McMaster (2002) has made a study examining the effect of DEM resolution on the positional accuracy of derived hydrologic networks and this study quantitatively confirms that DEM resolution should be greater than the average hillslope length when used for hydrologic modeling. Furthermore, comparison between predicted and mapped streams reveals that accuracy of predicted stream locations decays quickly beyond a DEM resolution of 180 m (McMaster 2002). On the other hand, analyses suggest that resolutions coarser than 100 m will not suffice (Beven 2000).

The analysis of DEM is equally important as the rainfall-runoff model, as it constitutes one of the initial stages of modeling process. This is where the geographic information systems (GIS) come in. GIS is a technology that is used to view and analyze data from a geographic perspective. GIS links location to information and layers that information to give a better understanding of how it all interrelates. The analysis of a DEM consists of deriving flow directions, drained surfaces, major flow pathways, basin boundaries and subcatchment partitioning.

In this research, in order to carry out DEM analysis, the program HYDRODEM written by Leblois (CEMAGREF Lyon, personal communication, 2005) was used. It is employed to obtain the initial input of the coupled model and contains some hydrologic functions. Other programs for the same purpose can be found; for example, Arc Hydro Tools (Arc Hydro 2007) is a commonly used toolbar inside the ArcMap software.

While finding the flow direction at a point, there may be several surrounding grid elements with elevations lower than the cell being considered. The problem is how to distribute the potential flow to different possible pathways. Beven (2000) suggests the use of the multiple flow direction algorithm of Quinn et al. (1995) and the resultant vector method of Tarboton (1997). The methods based on the approach of O'Callaghan and Mark (1984) are also widely used.

In a DEM, the resolution is referred to as the length of a pixel in the terrain. In raster format, each cell (or pixel) has a line and column number and contains a numerical or alphanumeric value (Fig. 3.11).

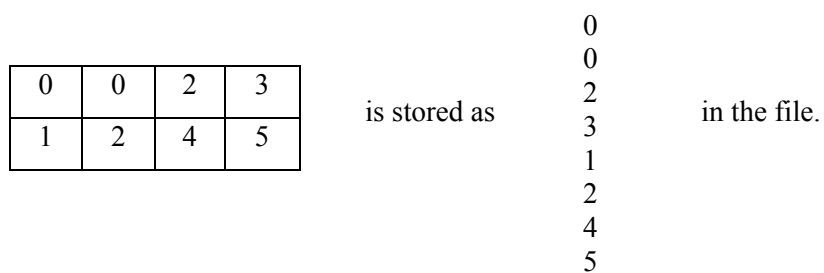


FIG. 3.11 The storage of a raster image.

The details of the steps of DEM analysis are given under the application section.

3.7.2. Generation of the Surface Mesh – SIGMOD

In this step, SIGMOD (Golaz-Cavazzi, 1995), written in FORTRAN is used. It generates the surface mesh of a basin by using a nested grid system. As input, the files containing topographic and hydrographic information derived from a Digital Elevation Model analysis are supplied. It also defines the drainage network, computes normalized transfer times and production zones.

Input files of SIGMOD contain flow directions, accumulated drainage areas, delimitation of the basin, stream network, subcatchment partitioning and elevations. Additionally, production zones may be defined at this stage or they may be later incorporated into the output file of SIGMOD. In SIGMOD, the data regarding production zones can be supplied in two forms; one single production zone per cell or percentages of all the available production zones per cell.

The input data is given for each cell on the regular mesh of the DEM. However, this is unnecessarily fine. While generating the mesh, SIGMOD aims at reducing the total number of cells by combining them according to certain topological and hydrological criteria (Fig. 3.12).

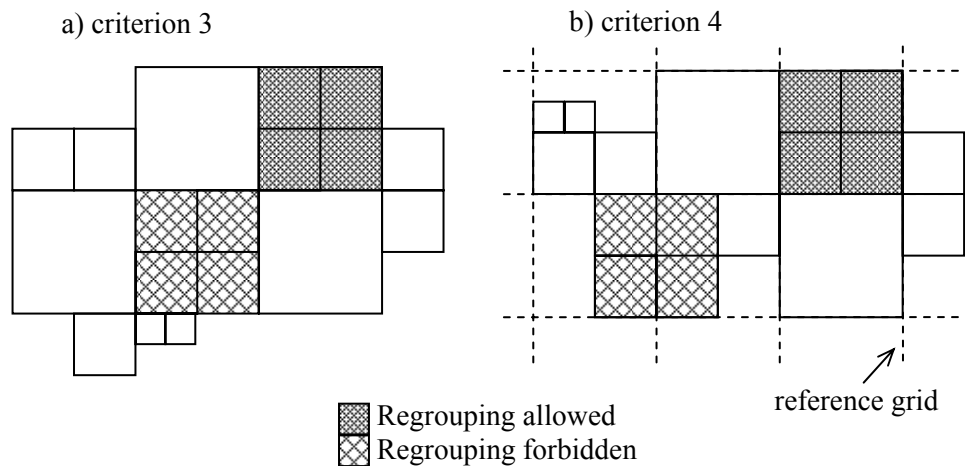


FIG. 3.12 Criteria for regrouping.

The topological criteria can be listed as follows:

1. The 4 cells to be regrouped should be of the same size.
2. After regrouping, the 4 cells should form a square.

3. The regrouping must obey neighboring rules, such that, any cell cannot have a neighboring cell with a size less than half of it.
4. The regrouping is made by the help of an imaginary reference grid. The cells of the reference grid are all of the biggest size that could be achieved after maximum amount of regrouping and all the 4 cells to be regrouped must fall into the same reference cell.

The hydrological criteria are based on theoretical aspects, such that:

1. The stream-aquifer interaction is important and requires a fine discretization. Thus, it is possible to choose to forbid regrouping on the river cells.
2. The 4 cells to be regrouped must belong to the same subcatchment. Otherwise, there will be transfer of water from one subcatchment to another. Therefore, regrouping can be prohibited on the subcatchment boundaries.

There are several variables affecting the number of cells on the mesh generated by SIGMOD. For example, regrouping can be made several times by obeying the criteria listed above to reduce the total number of cells to a reasonable value. Moreover, the threshold value for the accumulated drainage area in DEM analyses also affects the complexity of the stream network and therefore the number of the subcatchments. More subcatchments will cause SIGMOD to do less regrouping, because there will be more irregular subcatchment boundaries on which regrouping is not permitted.

In order to have a mesh composed of regrouped cells, SIGMOD is run two times. In the first run, regrouping option is not selected and some preliminary files are prepared. The following are calculated:

- If the file containing the slopes is not given, it calculates the slopes at each cell considering the distance and elevation difference between a cell and the cell at its downstream.
- Transition time from a cell to the neighboring downstream cell by using

$$t_{tra} = \frac{\Delta l}{\sqrt{Sl} \cdot (S_{DA})^\beta} \quad (3.43)$$

where Δl is the distance between the centers of two cells, Sl is the slope between the two cells, S_{DA} is the accumulated drainage area in km^2 , β is a calibration parameter (e.g. $\beta = 0.25$)

In Eq. (3.43), transition time is calculated by taking into consideration the accumulated drainage area, that is, the larger the area the bigger the flowrate will be and the transition from one cell to another will be faster.

- Transfer times (travel time of a point in a basin to the outlet)

At any point, it is the summation of all the transition times from the point to the outlet in the downstream direction:

$$t_{yf}(i) = \sum_{k=i}^{\text{outlet}} t_{tra}(k) \quad (3.44)$$

In final output, these values are normalized by dividing them by the maximum value and therefore given on a scale from 0. to 1.. The maximum value is calculated as follows:

$$T_{\max} = \max(t_{yf}(i), i = 1 \rightarrow \text{lastcell}) \quad (3.45)$$

- Initial structure of the grid and links all the necessary information to the cells on the grid.

In the second run, regrouping is enabled. However, it is possible not to let regrouping on the river cells. This is a commonly employed option, especially when the DEM resolution is not very high.

After regrouping 4 cells, the maximum of transfer times, the minimum of elevations and the average of production functions are assigned to the new cell. Flow directions can take values from 1 to 9. This is shown in Fig. 3.13.

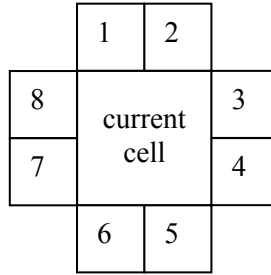


FIG. 3.13 Possible flow directions in a cell.

If the value is 9, then the current cell is an outlet cell. For the cells having the same size the possible values are 2, 4, 6, 8 and 9.

3.7.3. Generation of the Aquifer Mesh –SIGSOU

Once the surface mesh is generated, it is possible to generate the aquifer mesh by using the SIGSOU module. As input it requires an output file of SIGMOD which includes information on each surface cell, i.e., the coordinates, the size, the accumulated drainage areas in km², the number of the subcatchment it belongs, the river index, the flow direction, the elevation, the transfer time, the percentages of the production functions. In addition, it requires the mask of the underground layers and optionally, a mask of the zones where regrouping is not desired.

All the other topological and hydrological criteria are the same as those for the surface mesh. In addition, the neighboring rules are applied not only horizontally but also vertically in this case. Such that, a cell of order n can have neighboring cells of order $n-1$, n or $n+1$ both horizontally and vertically. This is already schematized in Fig. 3.1.

In present study the programming of SIGSOU was highly contributed. Proper functioning was ensured by using a small test basin and all the criteria for regrouping were tested on this basin. Connectivity with the surface mesh was established. The output was made compatible with the coupled model.

CHAPTER 4

THE SOMME RIVER BASIN

4.1. Presentation of the Domain

4.1.1. Geography

The Somme river basin covers an area of almost whole the department of Somme (see Fig. 4.1) and northwest of Aisne in the region of Picardie lying in the north of France. The basin is adjacent to that of Authie in the north, Bresle in the south, Escaut, Scarpe and Sensée in northeast, and that of the Seine in the southeast which is represented by the Oise river (PPRI 2004).



FIG. 4.1 The department of Somme in the north of France.

It has a catchment area of 6433 km². The river is 245 km long, from its source in the high ground of the former Forest of Arrouaise at Fonsommès near Saint-Quentin to the Somme Bay in the English Channel. It lies in a geological syncline which gives it a fairly constant

and mild topographic gradient. The major tributaries of the Somme river are the Nièvre, Avre, Selle, Hallue and Ancre (Fig. 4.2). The length of the basin in the east-west direction is about 160 km, and the elevations vary between 0 and 221 m where the highest values are observed is the southwestern portion of the basin (Fig. 4.3).

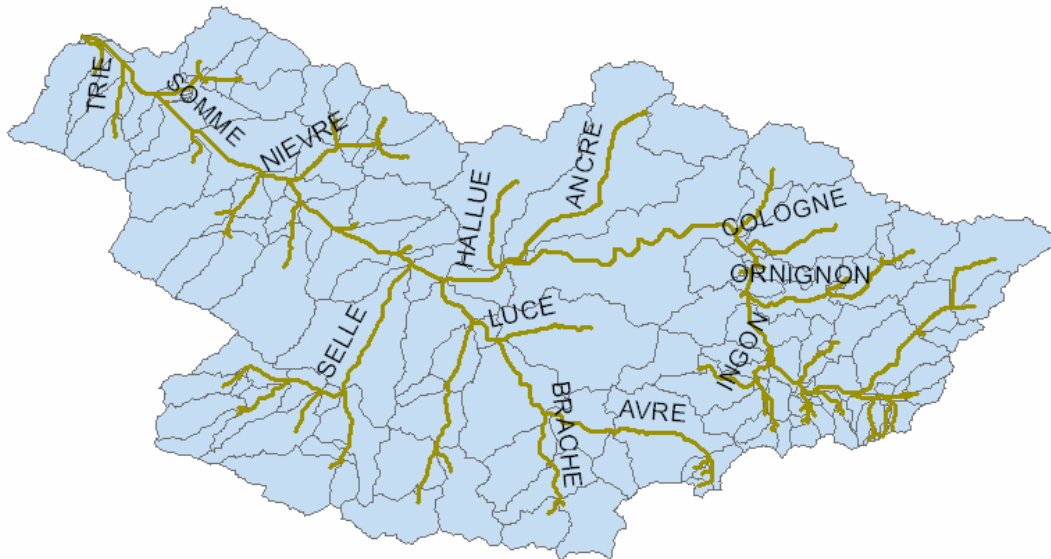


FIG. 4.2 The Somme river basin with major tributaries.

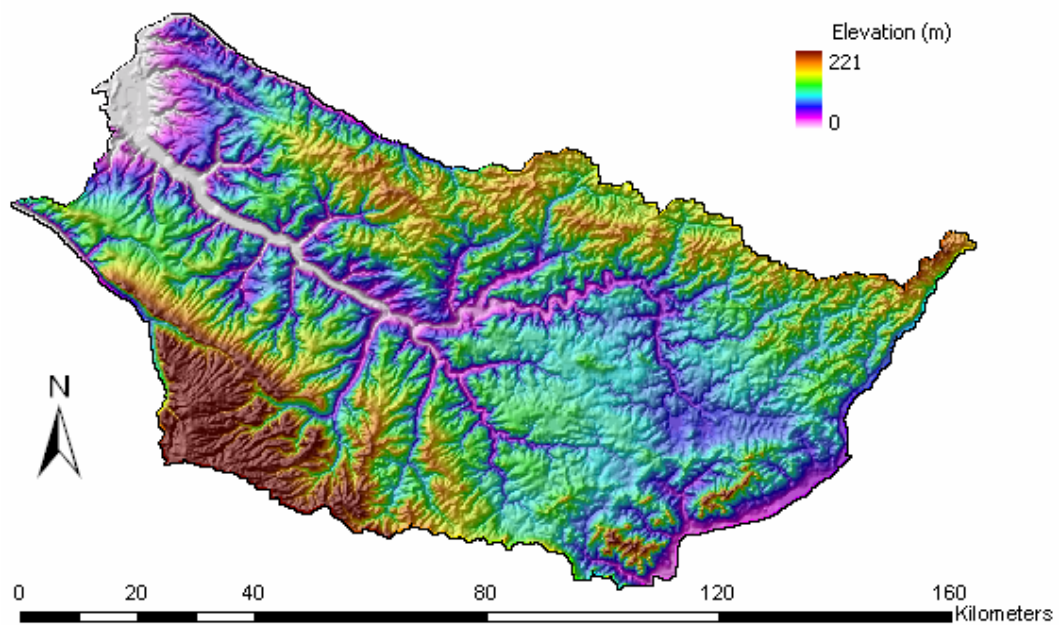


FIG. 4.3 Topography of the Somme river basin.

The Somme basin contains various natural environments; such as, agricultural terrains dominating the surface, valleys and forests like Crécy-en-Ponthieu, and particularly, the Somme possesses a maritime facade of 67 km.

4.1.2. Geologic and Hydrogeologic Context

Brief geological history of the Somme is provided by Amraoui et al. (2002) and Crampon et al. (1993). The stratigraphic series of the accumulation of main geological formations outcropping over the Somme basin from bottom to top can be summarized as follows (Pinault et al. 2005):

1. Early and Middle Turonian marl
2. Late Turonian and Senonian chalk
3. Tertiary sands and clays
4. Quaternary alluvium in the valleys and silt on the plateaus

The thickness of the alluvium layer varies between 0 to 16 m. Whereas, the average thickness of the fissured chalk layer is about 60 m. The chalk groundwater drains into the Somme River and its tributaries.

The main structure of the aquifer is composed of white chalk of early Senonian with small amounts of flint and grey chalk of late Turonian with large flints (Amraoui et al. 2002). In wet valleys, there are riverbank sediments composed of sand, gravel and ancient alluvium. The Turonian marl is considered to be impermeable and represent the substratum of the aquifer. Aquifer thickness was determined by using the data provided by BRGM. This data includes the elevations of the topography and the substratum, the difference of which varies between 17 and 141 m (Fig. 4.4).

The Cretaceous Chalk is a very pure and fine-grained limestone which is quite heterogeneous, and lateral and vertical facies variations are common (Crampon et al. 1993). Accordingly, different chemical signatures in groundwater are explained by lateral facies variations. These facies variations can cause the aquifer to be multi-layered (Négre and Petelet-Giraud 2005). The attribute of the chalk aquifer depends not only on the facies but also on the degree of fissuring which are enlarged by the dissolution of

carbonates in water. Hence, these fissures are more developed in the valleys (Crampon et al. 1993).

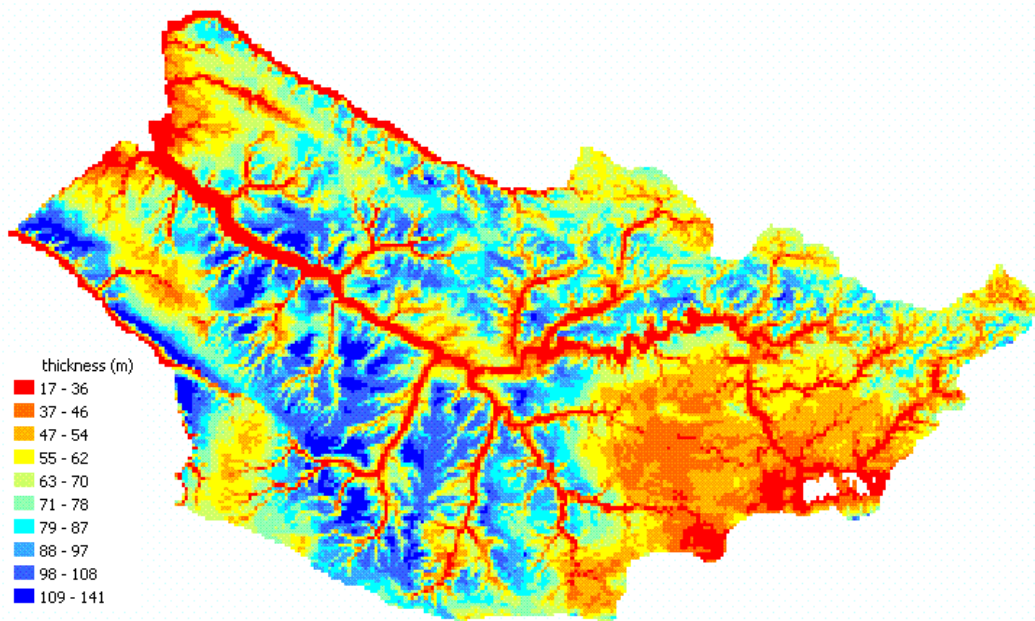


FIG. 4.4 Aquifer thickness of the Somme river basin.

Carbonate rock has a dual porosity of which the matrix microporosity varies between 20 and 40%, whereas fissure porosity ranges from 1% on the plateaus to 2-10% on the valleys and controls the groundwater flow. The hydraulic interaction between these porosities is usually complex which can explain the unsatisfactory representation of simple models. According to Pinault et al. (2005) the value of fissure porosity reaches up to 30% in the wet valleys which is a property rendering the unsaturated zone more important.

According to some field tests carried out in a similar chalk aquifer in the east of Paris, aquifer is heterogeneous and possesses preferential flows in certain depths depending on the condition of the fissures (Bénédicte 2002). In addition, the transmissivity measurements give different values in dry and wet periods of the year which is due to the vertical heterogeneity. This spatial and temporal variability of the chalk conductivity poses a classical hydrogeological problem. Nevertheless, it can always be assumed that chalk has higher conductivities in the valleys and lower in the crests.

The thickness of unsaturated zone of the Somme river basin is shown in (Fig. 4.5). It was obtained by taking the difference between surface topography and average groundwater head supplied by BRGM.

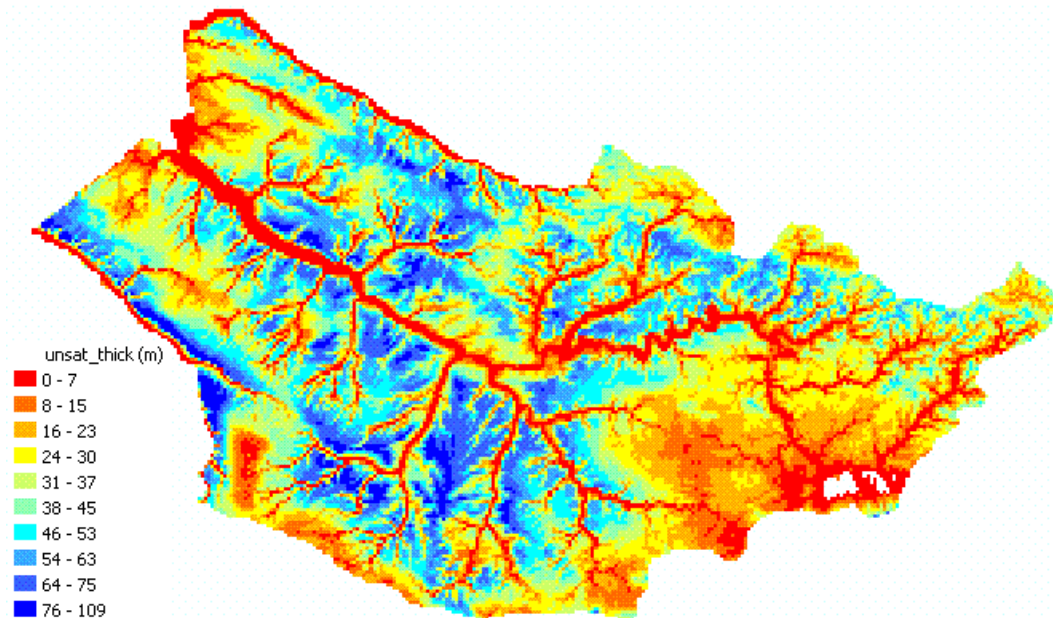


FIG. 4.5 Thickness of the unsaturated zone.

4.2. Basin Hydrology

The Somme river basin has the characteristics of generally an oceanic climate and slightly continental on the eastern region (PPRI 2004). The basin is remarked by the abundance of dry valleys. The portion of wet valleys with respect to dry valleys is very small. Only the main valleys and the main tributaries are fed by permanent flow (Amraoui et al. 2002).

The chalk aquifer contributes substantially to the discharge in the Somme. In the Somme valley groundwater always feeds the rivers both in dry and wet seasons. According to the distributed model constructed by Amraoui et al. (2002), for the Selle, up to 80% of the flow originates from the aquifer in dry seasons.

4.2.1. Pluviometry

The determination of the available water for the aquifer is related to the pluviometric analysis. In Fig. 4.6, the values of monthly precipitations averaged over the period 1973-2001 is given for the Abbeville meteorologic station (PPRI 2004).

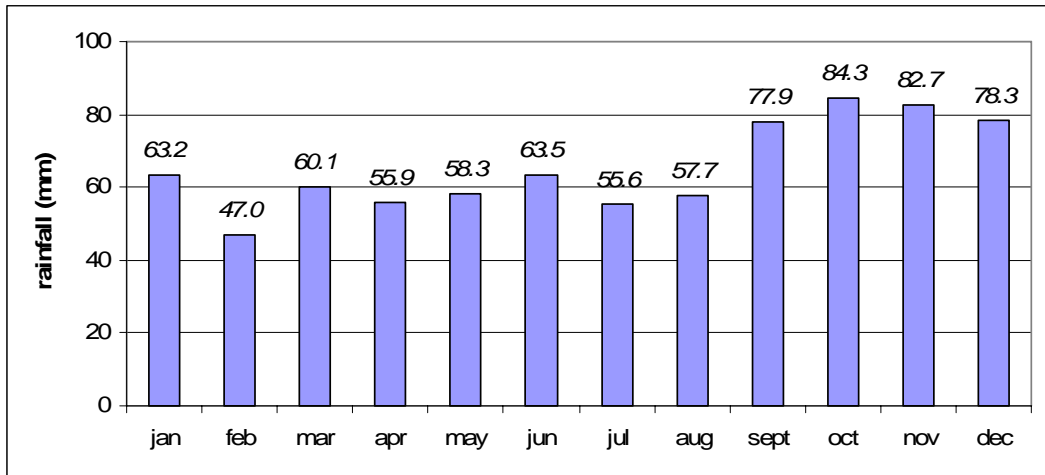


FIG. 4.6 Monthly rainfall at Abbeville (following PPRI 2004).

It is observed that September, October, November and December are the most pluvial months of the year. In the analyzed period, the least pluvial month is June 1976 by 3.4 mm and the most pluvial is October 2000 by 216.4 mm. Average annual precipitation is 788 mm (PPRI 2004). On the other hand, spatially averaged monthly rainfall falling on the basin surface is demonstrated in Fig. 4.7. In this figure, it is observed that the highest rates are observed in December and the lowest in May.

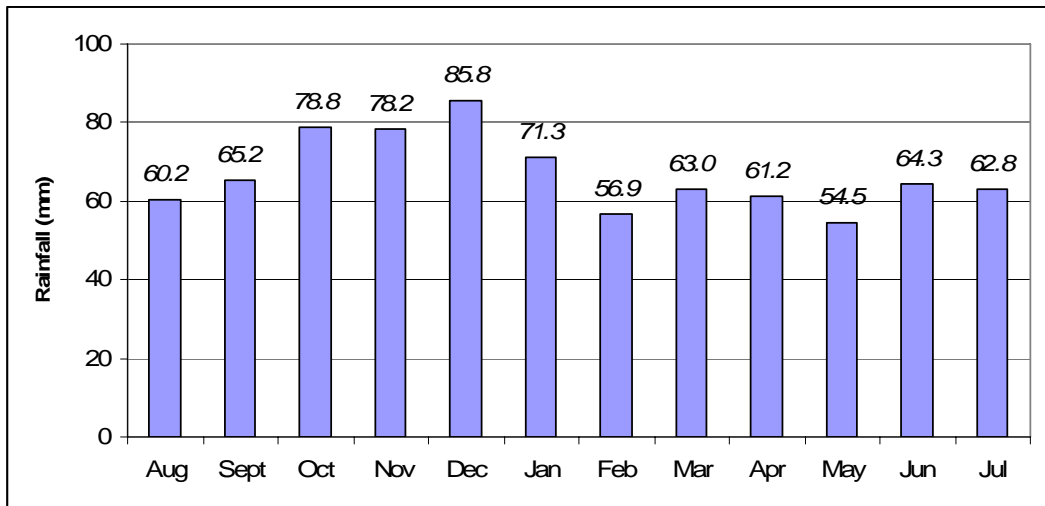


FIG. 4.7 The spatially averaged monthly rainfall for the period 8/1985-7/2003.

The spatial variability of rainfall can be observed from the isohyetal map of Météo-France provided in Fig. 4.8 (Amraoui et al. 2002). According to this map, the basin

receives more rainfall on the northern and western regions with values around 850 mm and less rainfall on the southern regions with values around 650 mm.

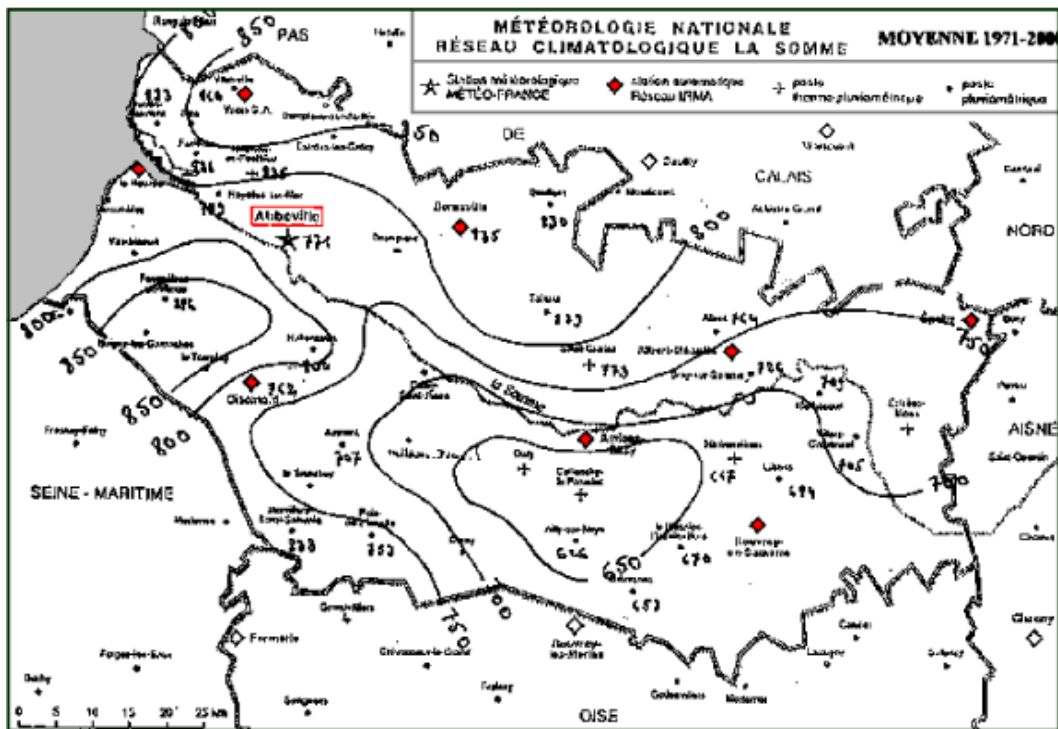


FIG. 4.8 Isohyetal map of the Somme basin for the period 1971-2000 (from Météo-France, published by Amraoui et al. 2002).

4.2.2. Hydrography

The Somme river basin has a complex formation in terms of water resources, such as rivers, marshes, ponds, trenches, ditches, channels and diverse hydraulic works. There is a great contribution of groundwater to the superficial waters (Deneux and Martin 2001).

The river is characterized by a very mild slope and a steady flow. The valley is more or less steep-sided but its bottom is flat with fens and pools. Steady flow and the flooded valley bottom are due to strong groundwater contribution.

The Somme river has several tributaries. On the right bank, the Omignon, Ancre, Hallue, Nièvre and Scardon; and on the left bank, the Avre, Selle, Saint-Landon, Airaine and Ambroise are the principal tributaries (Deneux and Martin 2001).

Until Amiens, the river follows several meanders, and the valley is narrow and embanked. Towards the downstream of the valley, the river gets broader and takes the northwest direction. All along its path to the sea, the Somme flows rarely naturally. It was canalized along the majority of its path in order to serve for navigation. This channel is 156.5 km long from Saint-Simon to the Somme bay where it outflows (Deneux and Martin 2001).

There are streamgauge stations on the Somme and its tributaries measuring the daily average discharge for a long time. The station at Abbeville started functioning as early as in 1963.

The average monthly flowrate of 43 years measured at the hydrometric station on the Somme at Abbeville, which has a catchment area of 5560 km², is shown in Fig. 4.9. The river exhibits low flowrates between August and October with values around 25 to 30 m³/s, while high flowrates are generally observed between January and May with values around 40 m³/s. The average monthly flowrate of 43 years is 34.90 m³/s.

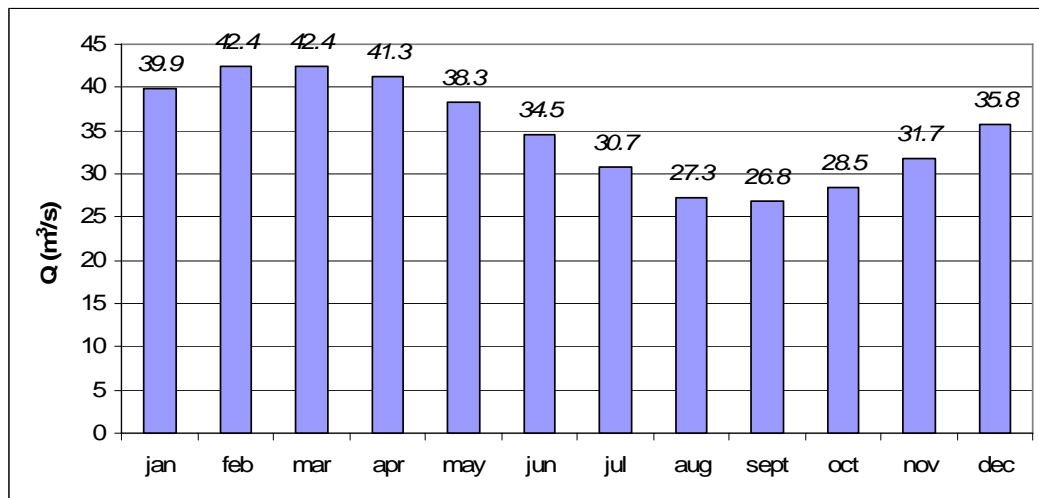


FIG. 4.9 Streamflow measurements on the Somme at Abbeville (5560 km²), monthly average of 43 years (1963-2005) (following Banque Hydro 2007).

When compared to the spatial rainfall (Fig. 4.7), it is observed that there is a shift of 3 months between the highest rainfall and the highest flowrates. This represents the influence of groundwater on the river flow and highlights the importance of the properties of the aquifer such as storage, baseflow and the characteristics of unsaturated zone.

For the hydrometric station on the Selle at Plachy-Buyon, which has a catchment area of 524 km², the average monthly flowrate of 27 years is given in Fig. 4.10. Low flowrates are observed between August and October with values around 3.6 m³/s, while high flowrates are observed between January and June with values around 4.3 m³/s. The average flowrate of 27 years is 4.07 m³/s.

For the hydrometric station on the Avre at Moreuil having a catchment area of 642 km², the average flowrate of 40 years is 2.28 m³/s. Low flowrates are observed between August and October with values around 1.8 m³/s, while high flowrates are observed January and May with values around 2.6 m³/s. The Nièvre is gaged at l'Etoile (269 km²), the average flowrate obtained for 28 years is 2.14 m³/s. Low flowrates are between September and November with values of about 1.8 m³/s and high flowrates are between March and May with values around 2.5 m³/s. Flowrate of the Hallue is measured at Bavelincourt (115 km²). The average flowrate of 32 years is 0.541 m³/s. Low flowrates are between October and November with values around 0.3 m³/s and high flowrates are observed on April and May with values around 0.8 m³/s.

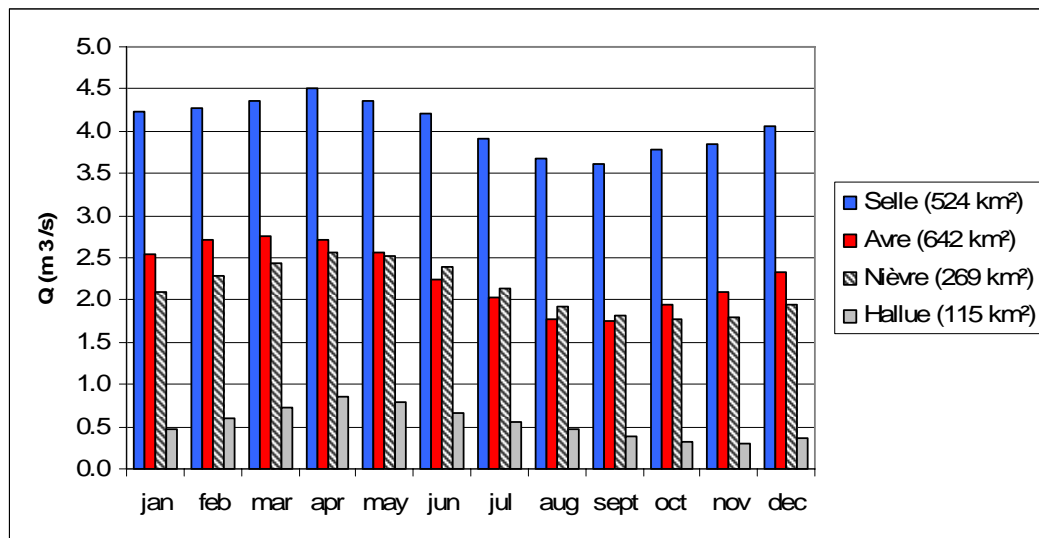


FIG. 4.10 Monthly averages of streamflow measurements on the tributaries of the Somme (following Banque Hydro 2007).

In Fig. 4.10, it is observed that the flows in the tributaries have more or less similar behaviors. However, the Avre has almost the same average flowrate as the Nièvre even though it has a catchment area 2.4 times larger than that of the Nièvre. In addition, the flowrate of the Avre is fluctuating more than the Nièvre. These observations indicate that

the Avre is less affected by the groundwater. As can be seen in Fig. 4.4, the aquifer is shallower at the catchment of the Avre.

Three-monthly discharges between 1970 and 2004 are shown in Fig. 4.11 for the Somme and its tributaries. Generally the peaks are in the first quarter of the year. Five major peaks of flowrate are observed; in 1982, 1988, 1994, 1995 and 2001. Unlike the others, in 2001 the peaks are mainly in the second quarter of the year.

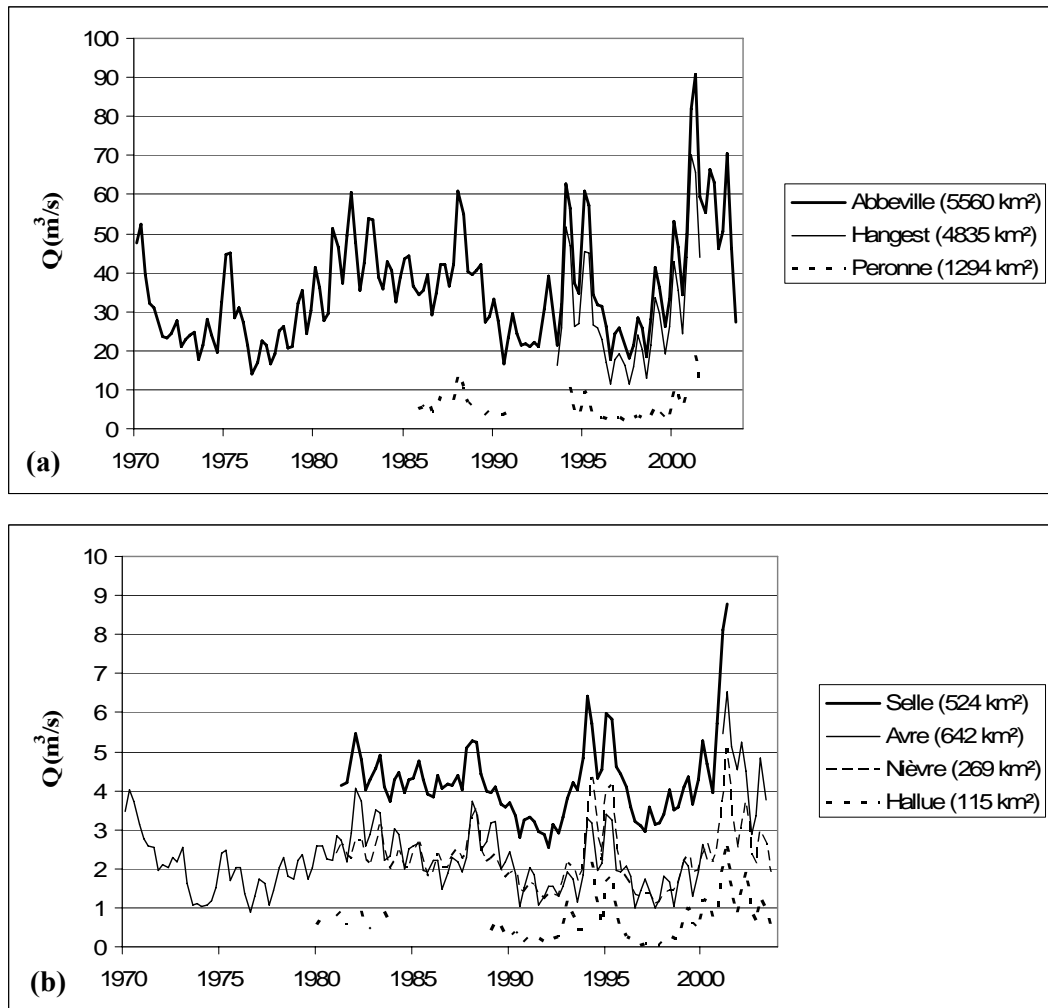


FIG. 4.11 3-monthly averaged discharges observed at **a)** several locations on the Somme, **b)** the tributaries of the Somme (following Banque Hydro 2007).

The values of maximum (Q_{max}), minimum (Q_{min}), average annual (Q_{an}) and specific (Q_s) discharges observed on the Somme and its tributaries are summarized in Table 4.1 where A_C is the catchment area of streamgauge station. The specific discharges were calculated using the values of average annual flowrate ($Q_s = Q_{an} / A_C$). The Avre has the smallest

value which shows a weaker groundwater contribution. On the other hand, the Nièvre receives the highest groundwater contribution.

TABLE 4.1 Discharges observed on the Somme and its tributaries.

River and Location of Station	A_C (km²)	Q_{an} (m³/s)	Q_{max}(m³/s)	Q_{min}(m³/s)	Q_s (l/s/km²)
Somme at Abbeville	5560	34.9	104.0	10.30	6.28
Somme at Hangest-sur-Somme	4835		90.5	5.43	
Somme at Peronne	1294	6.54	24.3	0.91	5.05
Avre at Moreuil	642	2.28	10.1	0.65	3.84
Selle at Plachy-Buyon	524	4.07	11.0	2.36	7.77
Nièvre at l'Etoile	269	2.14	6.5	1.04	7.96
Hallue at Bavelincourt	115	0.54	3.3	0.02	4.70

4.2.3. Piezometry

The piezometry of the Somme river basin is observed by BRGM using 63 observation wells located all around the basin. Under normal circumstances, the piezometric level of the aquifer varies between 0 and 180 m. The shape of groundwater table is coherent to surface topography while attenuating small irregularities (Lefrou 2001).

Hubert (2001) has studied the piezometry of the Somme for the period 1995-2001 and found that certain piezometers were more sensitive to local geologic and climatic conditions as well as to their relative position in regional flow systems. The maximum groundwater levels are reached in the first 4 months of the year, being fed by the infiltration of fall and winter precipitations.

4.2.4. Springs

A total of 207 springs have been recognized and georeferenced by BRGM (Amraoui et al. 2002). The majority of these springs are either depressions or thalwegs, such that, they appear in the valleys where the groundwater level reaches the surface (Fig. 4.12).

These springs fall into three categories: i) Those on the heads of the wet valleys which composes the headwaters of the perennial rivers. The location of these springs can shift in upstream or downstream direction for several kilometers depending on the level of the groundwater. ii) Artesian springs, which emerge on the alluvial zones by passing through clayey peat layers. iii) Flooding springs, which emerge on the downstream portion of the

valleys by passing through chalk and alluvium, and as well as on the maritime fields. When Fig. 4.12 is considered, abundance of springs at the bottom of valley and at the middle and upstream portion of the Selle can be recognized.

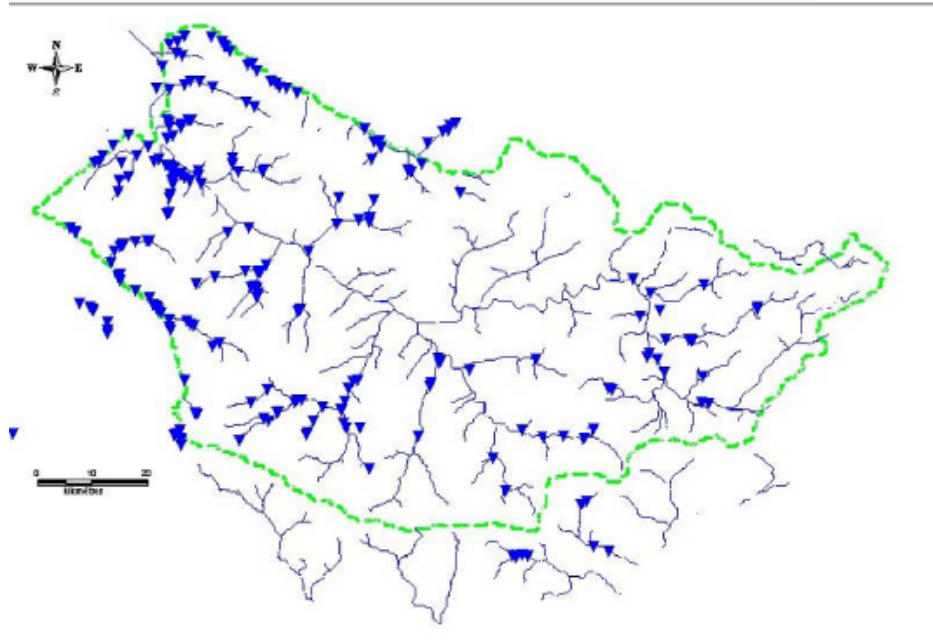


FIG. 4.12 The springs on the Somme basin (from BRGM, Amraoui et al. 2002).

4.2.5. Land Use

There are yet four other causes affecting the contribution of surface water to the groundwater which are considerably less important than the amount of precipitation. (Amraoui et al. 2002). These are:

1. The covering formations: Among the formations existing on the basin surface, the lignite-clayey formations provide lower permeability values than others. However, this is only seen in the southern and southeastern borders of the basin.
2. Forest-covered areas: The lands covered with forests act as a buffer zone and reduce the contribution of rainfall to groundwater.
3. Alluvial terrains: The aquifer beneath the alluvial terrains is generally confined or semi-confined under loamy and peat covered zones. In these regions, the recharge of groundwater by the rainfall is usually weak and approaches to zero during the period when high levels are observed and the aquifer overflows due to water bodies.
4. Urban areas: Because of being impermeable, in urban areas there is very small or no recharge to the groundwater.

4.3. Flood Problem

In the end of 2000 and spring 2001 the Somme basin was influenced by severe inundations in which the chalk aquifer played an important role. Beginning from October 2000, the Somme valley received exceptional amounts of precipitation. This catastrophic event led to the evacuation of 1100 persons and the flooding of more than 100 communes, 2800 houses, 20 roads and the railroad between Abbeville and Amiens. Agriculture was also severely affected all around the Somme valley by the extraordinary precipitation from the first months of 2001. Even when not flooded, there occurred immense loss of crop as well as soil. The submersion of permanent prairies on the valley bottom during several months destroyed its vegetative cover completely (Lefrou 2001).

4.3.1. Hydrologic Reaction

Hubert (2001) has studied the pluviometry of the Somme valley and found out that the annual average rainfall observed at the Abbeville station for 1999-2000 is 1044 mm whereas the average for the period 1945-1998 is 736 mm. Lefrou (2001) has also observed the precipitations supplied by Météo-France between October 2000 and April 2001 at the Abbeville station (Fig. 4.13). The precipitation falling in this period is twice as high as the average of 57 years. As can be seen in the figure, for the given period monthly rainfall depths reach excessive values in all the months except February.

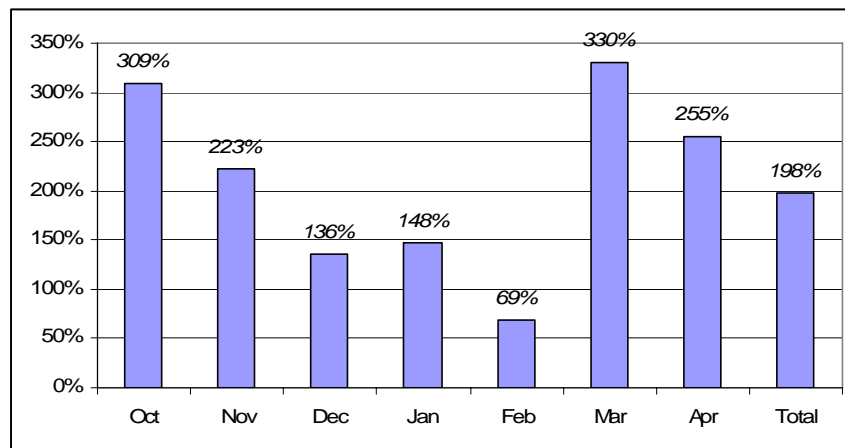


FIG. 4.13 The ratio of precipitation falling in the period Oct 2000-Apr 2001 to the average of 57 years at the Abbeville station.

The spatially averaged monthly and bimonthly rainfall depth is illustrated for the period between January 1986 and July 2003 in Fig. 4.14. When the monthly rainfall is considered, March 2001 is on the third rank with a value of 171.3 mm, the first is December 1993 by 197.1 mm and the second is December 1999 by 194.7 mm whereas the mean for the whole period is 67.4 mm. However, when the averages of two succeeding months are considered March-April 2001 becomes the first by 150.4 mm.

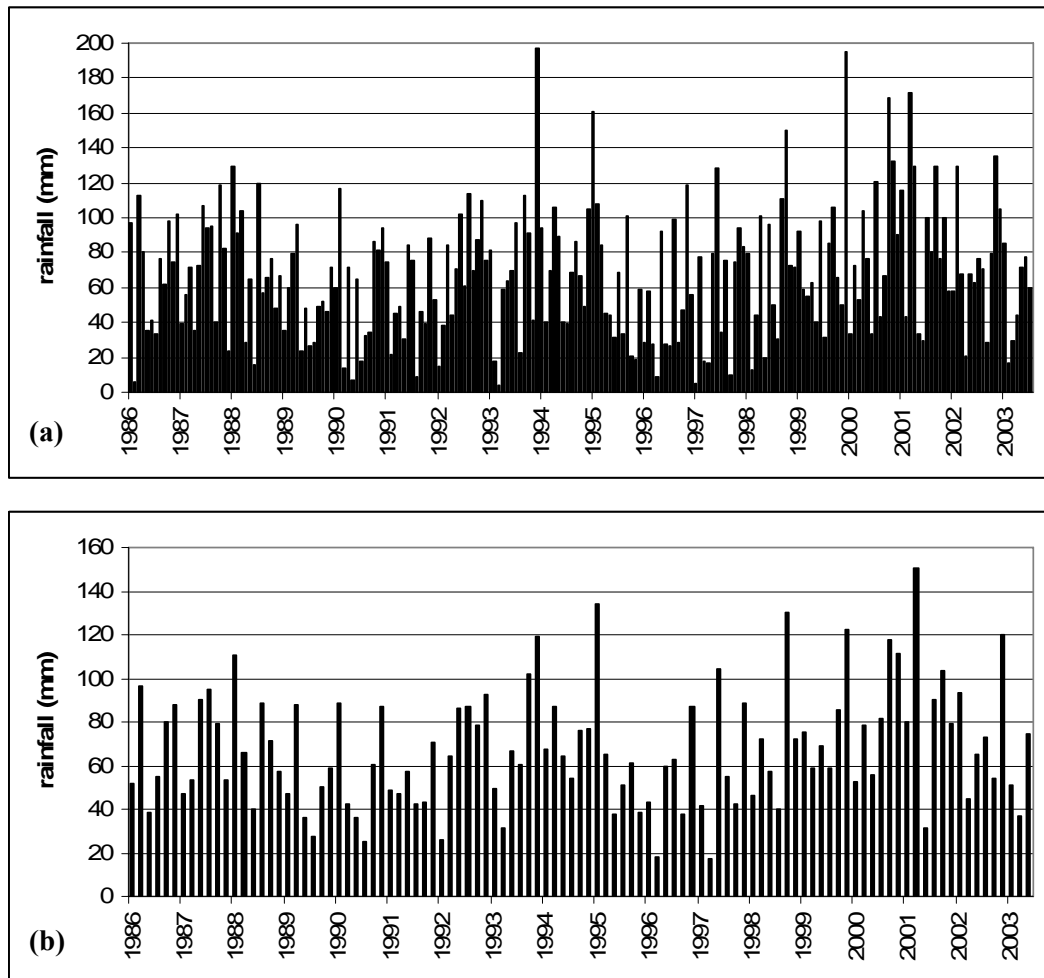


FIG. 4.14 Spatially averaged rainfall; (a) monthly depth, (b) bimonthly average depth.

Pinault et al. (2005) made a similar analysis using the observed rainfall data at the Glisy raingage station. According to this study, when the accumulated value of two succeeding months is considered March–April 2001 attains a value of 246 mm while the mean of 1900 to 2002 is 109 mm. In the same analysis, the annual rainfall for the period July 2000 – June 2001 is 922 mm whereas the mean from 1900 to 2002 is 648 mm.

The flowrate of the Somme observed at Abbeville streamgauge station (5560 km²) beginning from 1996 and comprising the period of flood is given in Fig. 4.15. The spatially averaged rainfall falling on the whole basin surface is also drawn on this figure. In some days, the daily rainfall approaches to almost 30 mm which is equal to a volume of $167 \times 10^6 \text{ m}^3$ of water falling onto the surface.

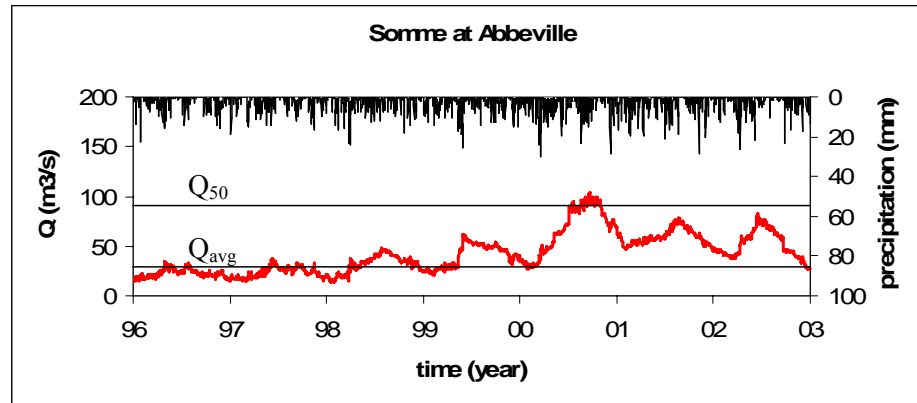


FIG. 4.15 Daily observed discharge on the Somme at Abbeville.

The values concerning the average annual discharges and the discharges observed during the flood event of 2001 for the Somme and its tributaries are summarized in Table 4.2. In this table, A_C is the area of the catchment, Q_{an} is the average annual discharge, Q_f is the discharge during the flood event.

TABLE 4.2 Flood discharges observed at the streamgauge stations.

River and Location of Station	A_C (km ²)	Q_{an} (m ³ /s)	Q_f (m ³ /s)
Somme at Abbeville	5560	34.90	104.0
Somme at Hangest-sur-Somme	4835		90.5
Somme at Peronne	1294	6.54	24.3
Avre at Moreuil	642	2.28	8.6
Selle at Plachy-Buyon	524	4.07	11.0
Nièvre at l'Etoile	269	2.14	6.2
Hallue at Bavelincourt	115	0.54	3.3

The maximum daily discharge at Abbeville was observed on April 20, 2001 as 104.0 m³/s (Fig. 4.15). This value is at the same time the maximum of the period 1963-2005. Moreover, it is three times greater than the average of 43 years, which is $Q_{avg} = 34.9 \text{ m}^3/\text{s}$. The previous record was in 1994 with 74 m³/s and the flowrate of a flood with a 50-year return period is $Q_{50} = 91 \text{ m}^3/\text{s}$. According to Hubert (2001), this value could have risen up

to $130 \text{ m}^3/\text{s}$, if there were not an inundation. Because a considerable amount of water was stored on the surface.

The evolution of discharges using monthly averages from January 1999 to December 2001 is illustrated in Fig. 4.16 for the Somme and in Fig. 4.17 for its tributaries. Spatially averaged monthly rainfall is also drawn in a reverse scale on the right axis on these figures.

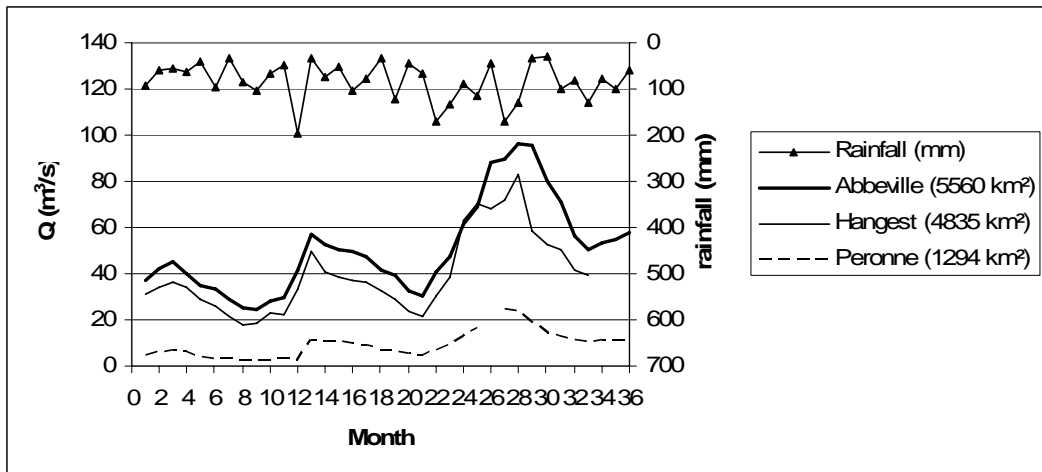


FIG. 4.16 Monthly discharges observed at several locations on the Somme.

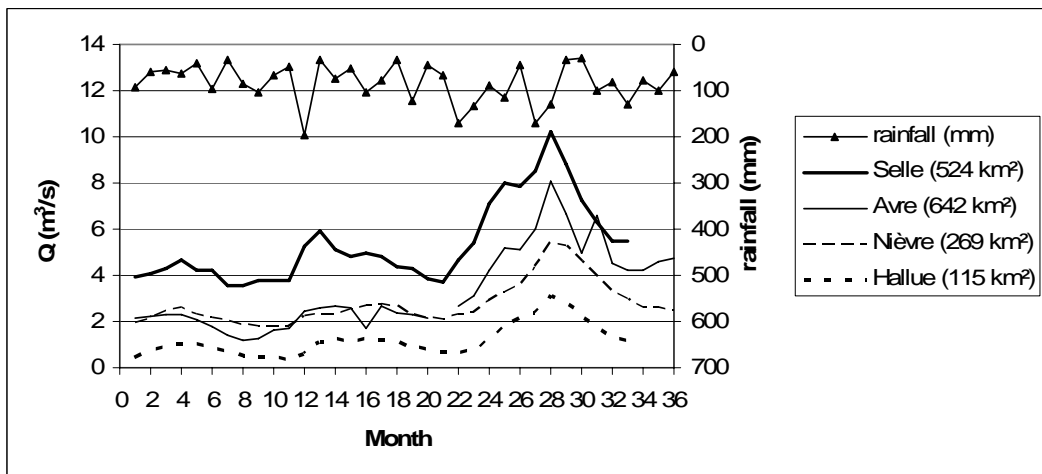


FIG. 4.17 Monthly discharges observed at the tributaries of the Somme.

From these figures several conclusions may be derived. By considering, in particular, the recession period it can be said that the Somme is highly affected by the groundwater. This can be observed in two ways. The former way is that many months after heavy rainfall, a strong baseflow continues to feed the river. The latter way is to consider the rising limb.

Even if the rainfall of the spring seems to be responsible for the flood, this may not be the actual case. Because the increase in the discharge is already triggered by the intense rainfall of October and November 2000, and even though there is a weaker rainfall until spring 2001, the discharges keep increasing at a constant rate which demonstrates a strong groundwater contribution. There is yet one exception to these cases. The Avre seems to be less affected by groundwater and more by superficial recharge as sharp variations is observed in the hydrograph. This can also be determined by considering the specific discharges given in Table 4.1. The Avre has the smallest and the Nièvre has the highest value. The ratio of their specific discharges is 2.07 which is too large to be explained by spatial variability of rainfall. In the same sense, the Nièvre is the tributary which can be considered to be most affected by the groundwater.

4.3.2. Literature Survey

To resolve the mechanisms involved in the flood of 2001, and to assess the flood risk on the Somme basin, two approaches namely, global and distributed, have been presented by BRGM (Amroui et al. 2002). Among these two models, distributed model is more complete in the sense that it represents better the heterogeneity of the porous medium as well as that of the stream network and the interaction of surface and groundwater. For the related catastrophic event in 2001, the contribution of the groundwater of the chalk aquifer has been estimated to be 80% of the total discharge of the Somme river. According to Pointet et al. (2003), this contribution closes to 100% in dry periods.

Further, the contribution of groundwater to floods has been investigated in a chemical sense by taking samples of groundwater from different locations of the aquifer and also from the Somme and its tributaries during two seasons; April 2001 (high levels) and October 2001 (low levels) (Pointet et al. 2003). It was found that the chemistry of water evolves towards the downstream direction. The flow gets progressively diluted by the groundwater having diverse chemical contents coming from the subcatchments. This contribution increases in such a way that the chemistry of the Somme approaches to that of the groundwater towards downstream. Moreover, Négrel and Petelet-Giraud (2005) point out that, among the tributaries of the Somme, the Hallue, Selle and Ancre present geochemical characteristics very similar to that of groundwater which demonstrates a strong groundwater contribution and that the Avre is rather more influenced by surface water than groundwater.

Carli (2005) used a model named CaB (Catchment Based) on the Somme basin. It is a land surface model based on TOPMODEL (Beven and Kirkby 1979). The domain is discretized into elementary catchments on which the topographic gradient is assumed to represent the hydraulic gradient at the same time. The depth of groundwater is spatially distributed according to average humidity of the catchments. However, despite some modification and calibrations, CaB represents weakly the actual groundwater phenomena in the Somme river basin because it is based on TOPMODEL which is conceived to work for small basins with shallow aquifers. For that reason, a coupling with MODCOU is suggested.

In literature, there are also some studies concentrated peculiarly on the structure of chalk aquifers. Price et al. (2000) remark that the volume of water draining from chalk catchments in recession periods are significantly greater than that can be explained by gravity drainage from fissure porosity and the most likely source of this water is slow drainage from the matrix porosity above the water table. Because of this storage in the unsaturated zone, the position of the water table may not be an accurate indicator of groundwater resources. Pinault et al. (2005) and Lewis et al. (1993) explain the discharge from a chalk aquifer in a similar manner. They studied chalk aquifers and found out that substantially more water had left the catchments as streamflow than could be explained by the change in position of the water table which indicates the importance of the unsaturated zone. Price et al. (2000) explains further the flow in chalk blocks, such that, more water drains from blocks having rougher surfaces and smaller blocks have higher matrix specific yield values as their ratio of surface area to volume is greater than large blocks and therefore specific yield decreases with depth as the block size and fissure spacing increase with depth.

4.4. Interrogation on Inundation

Given a brief synthesis of the Somme river basin and the event of a catastrophic flood that affected it severely, there are still some unresolved issues. These are mainly about the hydrology of this particular basin which is not yet well understood and how the aquifer reacts under heavy rainfall. In order to find answers to these questions, a complete distributed hydrogeological model will be constructed by using the coupled model developed at Ecole des Mines. The factors affecting the flowpath of water on the surface,

in the unsaturated zone and in the saturated zone will be analyzed in detail. A correspondence between the observed and simulated discharges and piezometric levels will be sought. Comparison of the results with those of other hydrological models will be made. As using a distributed model involves the analysis and adjustment of data in a spatial sense, in all the stages of modeling the GIS (Geographic Information Systems) will be integrated.

CHAPTER 5

APPLICATION OF THE COUPLED MODEL ON THE SOMME RIVER BASIN

5.1. DEM Analysis

In present study, HYDRODEM, written by Leblois (CEMAGREF Lyon, personal communication, 2005) was used. HYDRODEM was employed to derive the stream network. The DEM for the Somme basin is a satellite-derived raster image of the topography with a resolution of 125 m (Fig. 5.1).

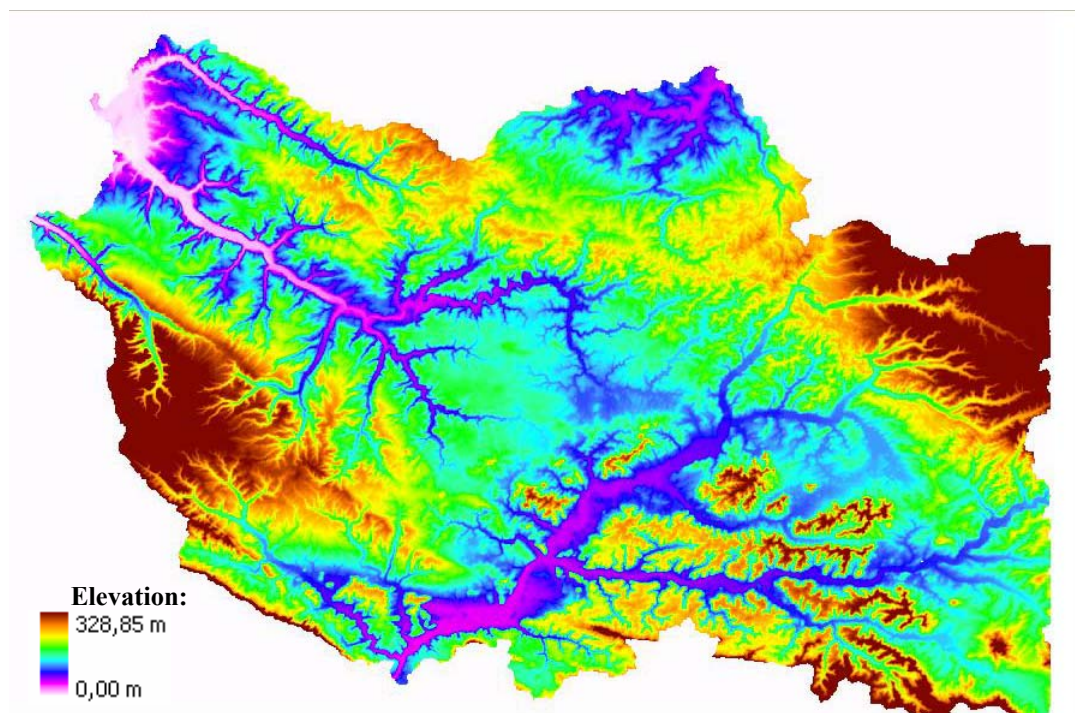


FIG. 5.1 Digital Elevation Model of the Somme basin (Pixel size = 125 m).

The first step is to create a depressionless DEM. The aim is to allow all cells inside the DEM to drain to a boundary. The procedure begins with the exclusion of flat areas. The cells which have neighboring cells of equal elevations are marked. Then local slope and aspect are calculated for each cell except the flat ones that have been marked in order to find an initial flow path. Then a removal procedure for pits (or sinks) ran in which the elevations of the cells inside the pit were raised to the lowest elevation at the rim of the pit to conduct flow downstream. At this stage, there might still exist some problems in the flow path, these are corrected manually by assigning correction vectors towards downstream direction. After these corrections flow directions are assigned. The flow directions derived for the Somme is given in Fig. 5.2. As the coupled model transfers water in 4 main compass directions a D4 (4 flow directions) algorithm was used to find the flow directions. There are other algorithms available; for example, D8 (8 flow directions) algorithm initially introduced by O'Callaghan and Mark (1984) or D_{∞} (an infinite number of possible single flow directions) of Tarboton (1997).

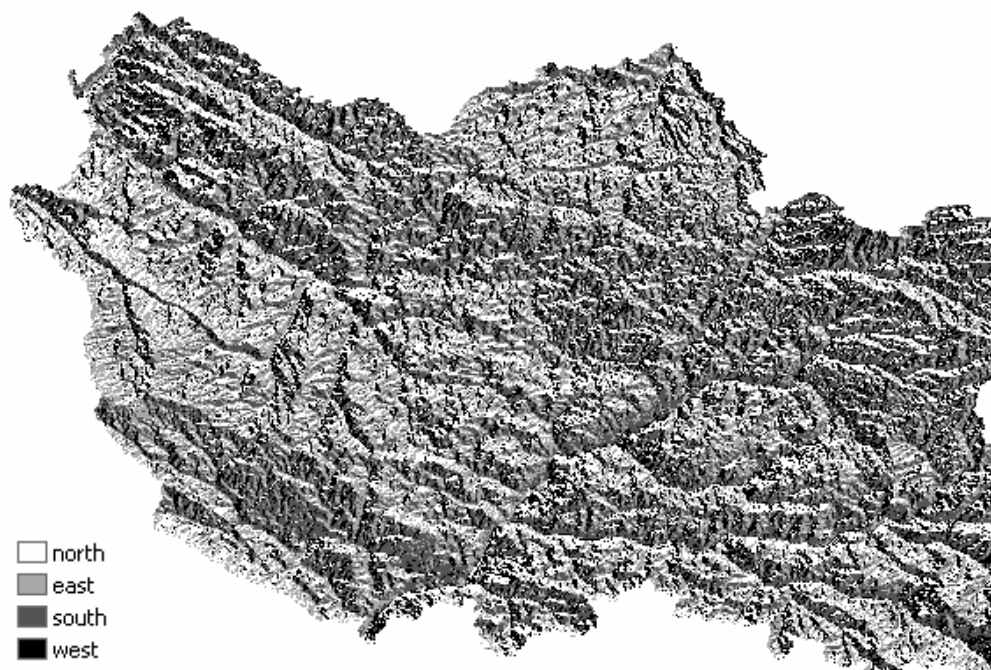


FIG. 5.2 Flow directions.

The next step is to calculate the accumulated drainage areas for each cell. This process begins at the most upstream portions of the basin, that is, at the cells located on the ridge lines and which do not have an upstream cell. A threshold value for the accumulated drainage area is given to obtain a stream network. The cells which drain an area of equal

or greater than this threshold value are marked as river cells. Initially, a very small threshold value was given to obtain a detailed network and then this threshold was modified with small increments. It is possible to obtain many different stream networks by using varying threshold values. The point is to find a reasonable one, that is, the one the most compatible with the mapped stream accounting for the portion on which stream-aquifer exchange takes place. In Fig. 5.3 the comparison of stream networks obtained by HYDRODEM (D4 algorithm) and D8 algorithm is demonstrated. Both of them were obtained by a threshold of 2500 cells. This corresponds to an area of 39 km². As can be seen from the figure, there is not a considerable difference between the two networks.

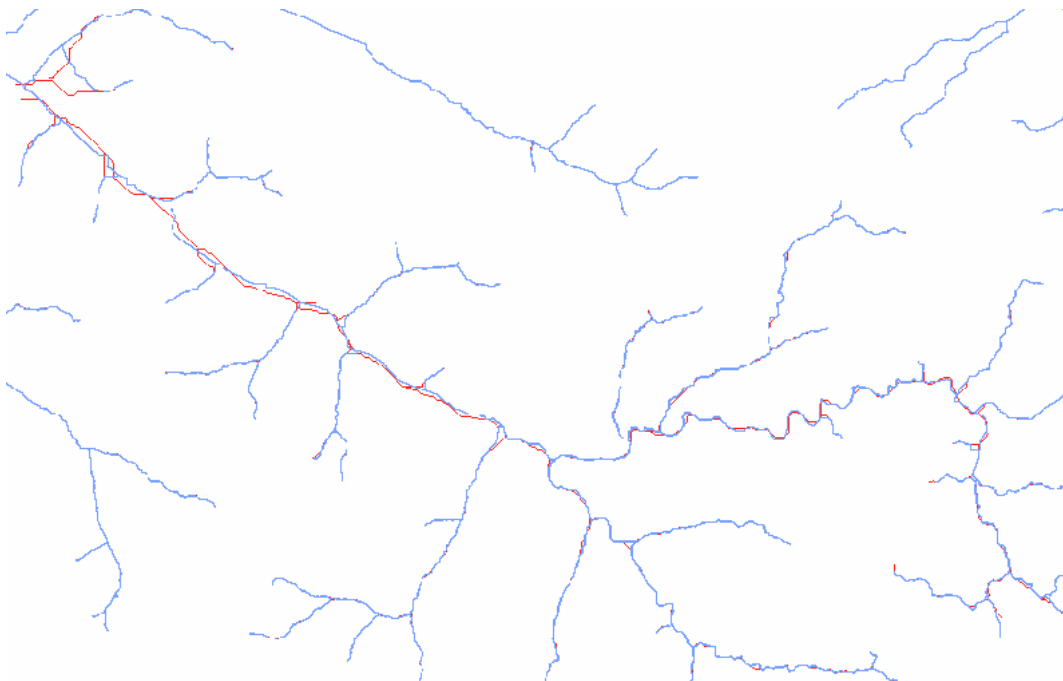


FIG. 5.3 Comparison of stream networks obtained by HYDRODEM (blue) and D8 algorithm (red).

While incurring a stream network, all the segments of stream between a source and a junction or between two junctions or between the last junction and the outlet are given a unique id number to be used in the determination of subcatchments. The cell in each link that has the largest flow accumulation value is considered an outlet of a subcatchment. Therefore, a subcatchment is defined as a zone of cells having the same cell value as the first outlet cell they drain through. The number of subcatchments is directly related to the complexity of the stream network. As each link in the stream network corresponds to a subcatchment, the more stream network is detailed the more subcatchments occur. For the stream network in Fig. 5.3 the subcatchments were too many in number and their sizes

were unnecessarily too small. In grid generation process, this would cause to a high number of small sized cells all around the basin. For this reason, a code was written in FORTRAN to combine small subcatchments. Finally 32 subcatchments were formed inside the basin (Fig. 5.4).

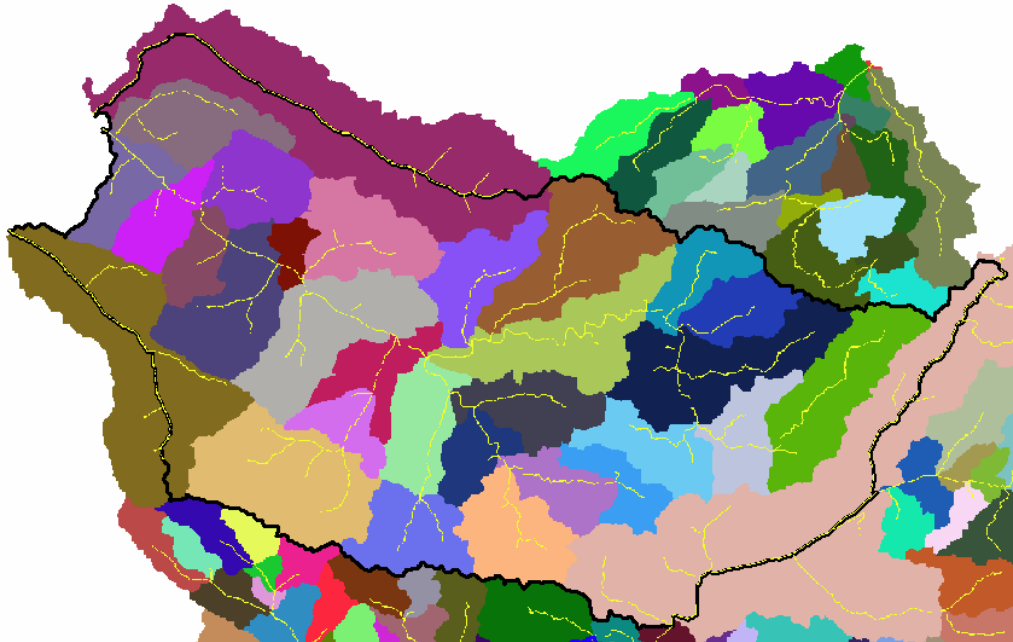


FIG. 5.4 Subcatchments of the Somme river basin.

In order to obtain the boundaries of the basin, all the outlets are sorted according to their accumulated drainage areas. The outlet having the biggest value is the main outlet of the basin considered. All the cells draining through the same outlet belong to the same basin. However, this is a delineation drawn by considering only the surface topography. When the subsurface topography of the Somme basin is considered, the aquifer domain is found to be larger in extent. Moreover, the exact locations of groundwater divides are unknown. Therefore, the aquifer domain was considered to extend to the closest natural hydrogeological boundaries; that is, to the rivers in the north, southwest and east. In order to sustain hydraulic correspondence between the surface and aquifer domains, such as, for the calculation of infiltration, the surface domain was also extended. In the extended portions the rainfall partitioned as surface flow will definitely drain into the corresponding rivers. However, the infiltrating water will enter the aquifer domain and according to the position of the groundwater divide it may contribute to the groundwater beneath the Somme river basin and eventually flow out through the same outlet as the Somme. In Fig. 5.5 the final delineation of the basin is shown; the blue region is the

initial basin area (6433 km²), and the other colors represent the extended portions. Total modeled area is 8205 km².

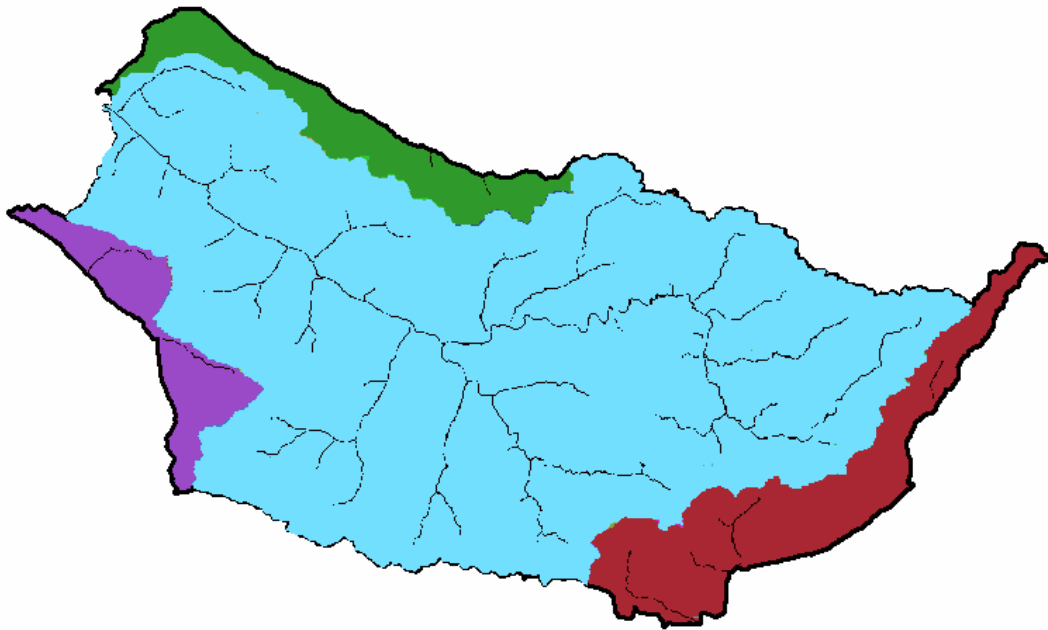


FIG. 5.5 Final delineation of the Somme river basin with extended portions; initial basin area is 6433 km² (in blue), total area after extension is 8205 km².

As a DEM may occupy an area larger than a basin, a mask was built at this stage in order to not deal with unnecessary data. The mask assigns a value of 1 to the cells inside the basin and 0 outside. This allows all further computations to be limited by the boundaries of the basin. For example, the stream network was clipped using this mask (Fig. 5.5).

To sum up, in the end of DEM analysis the following information was acquired on the basin:

- Mask of the basin (0 outside the basin and 1 inside)
- Subcatchments (0 outside the basin and the number of the subcatchment within a subcatchment, there are a total of 32 subcatchments in Somme)
- Flow directions in degrees with respect to north (0. or 90. or 180. or 270.) in clockwise direction.
- Mask of the river obtained with the minimum threshold value (in Somme basin, it is 500 cells or 7.8 km²)
- Mask of the river obtained with a reasonable threshold value (2500 cells or 39 km² for the Somme basin)
- Natural logarithms of accumulated drainage areas (initially in m²)

- Elevations, slopes (optional)

5.2. Generation of the Surface Grid

For the grid generation, the SIGMOD module was utilized. In order to generate the grid, the files obtained from DEM analysis were used. Regrouping option was enabled in order to have a nested grid system. As the minimum cell size is 125 m which is already large for a river and because of the fact that increasing further the cell size on the streams would highly decrease the precision of solution, regrouping of cells was not permitted on the stream network. In addition, by default regrouping is not done on the cells falling on subcatchment boundaries in order to avoid transfer of water between subcatchments.

As mentioned before, to generate a grid a sequence of two runs representing two essential steps is performed. In the first run, preliminary files are prepared without any regrouping and in the second run regrouping is done by using these preliminary files. In the final grid, the number of cells created after the first run was 525136 and this number decreased to 71653 after the second run (Fig. 5.6). The reason is that three levels of regrouping were used, and therefore, the cell sizes obtained are 125, 250, 500 and 1000 m. As can be seen in the figure the smallest cells are on the stream network and subcatchment boundaries. In addition there are a total of 10871 river cells.

Transfer times were also computed by SIGMOD (Fig. 5.7). These are dimensionless normalized values varying between 0. and 1. (Eq. 3.44). Later, these values will be multiplied by the concentration time of the basin which is estimated during the calibration of the surface model and expressed in days. As can be seen in Fig. 5.7, in the extended portions transfers times are zero. This means that no computation of surface runoff will be made in these areas and the rainfall partitioned as surface flow will directly enter the corresponding streams and reach their outlets in no time. The only purpose to keep these portions in the model is to calculate the infiltration into the aquifer domain. On the other hand, inside the surface basin area the transfer times are gradually increasing in the upstream direction.

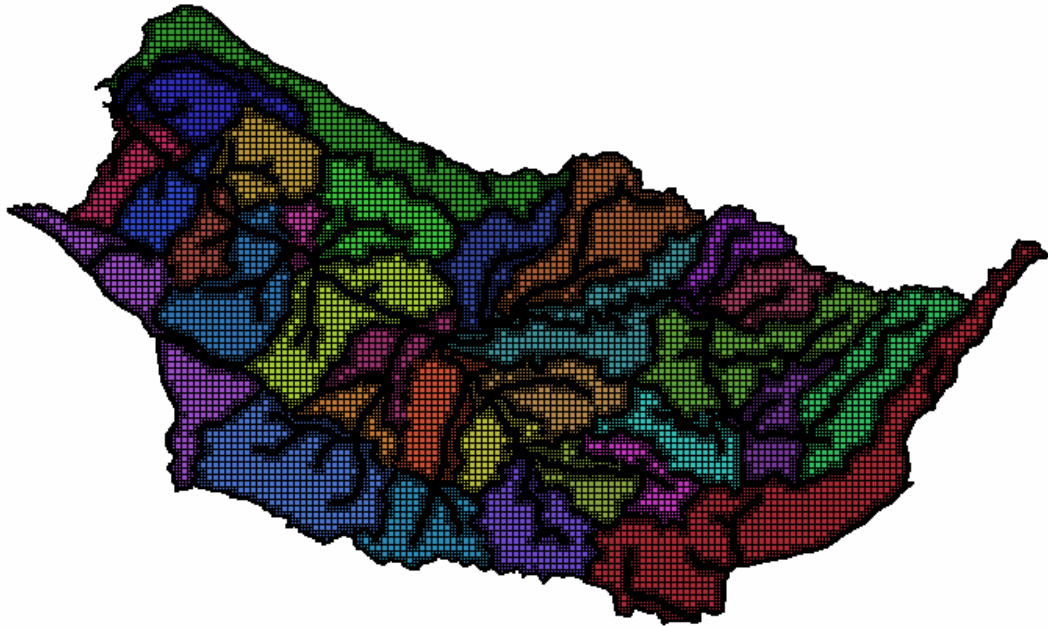


FIG. 5.6 Surface grid of the Somme river basin.

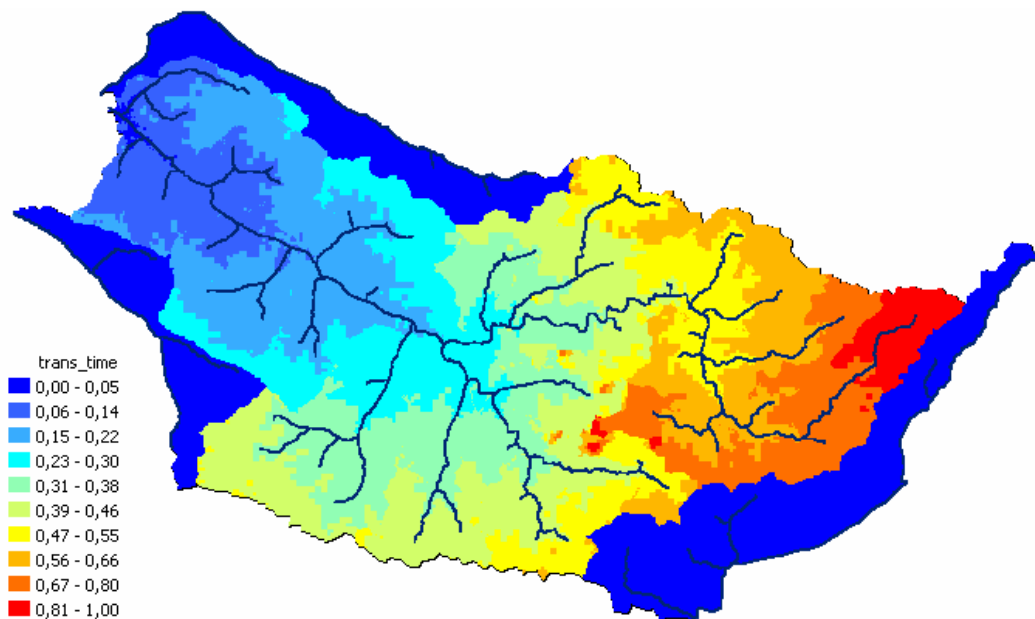


FIG. 5.7 Normalized transfer times with the stream network.

In the modeling of the Somme basin, HYDRODEM and SIGMOD were run several times for the following reasons;

1. To extend the boundaries of the basin up to the natural boundaries.
2. To trim the part of the mesh falling on the other side of the natural boundaries.

3. To see the results of different threshold values of accumulated drainage area while extracting the stream network. As previously mentioned, the optimum threshold value can only be determined by trial and error.
4. To make the reference grid coincide with the grid of meteorological data which has a cell size of 8 km.
5. To combine the subcatchments and therefore, to decrease the total number of cells. In the beginning, there were unnecessarily too many small sized cells. To overcome this situation, a simple procedure was written in FORTRAN to merge several small subcatchments.
6. To debug or modify the code for changes.

5.3. Generation of the Aquifer Grid

Once the surface grid is generated, it is possible to generate the aquifer grid (Fig. 5.8) by using the SIGSOU module.

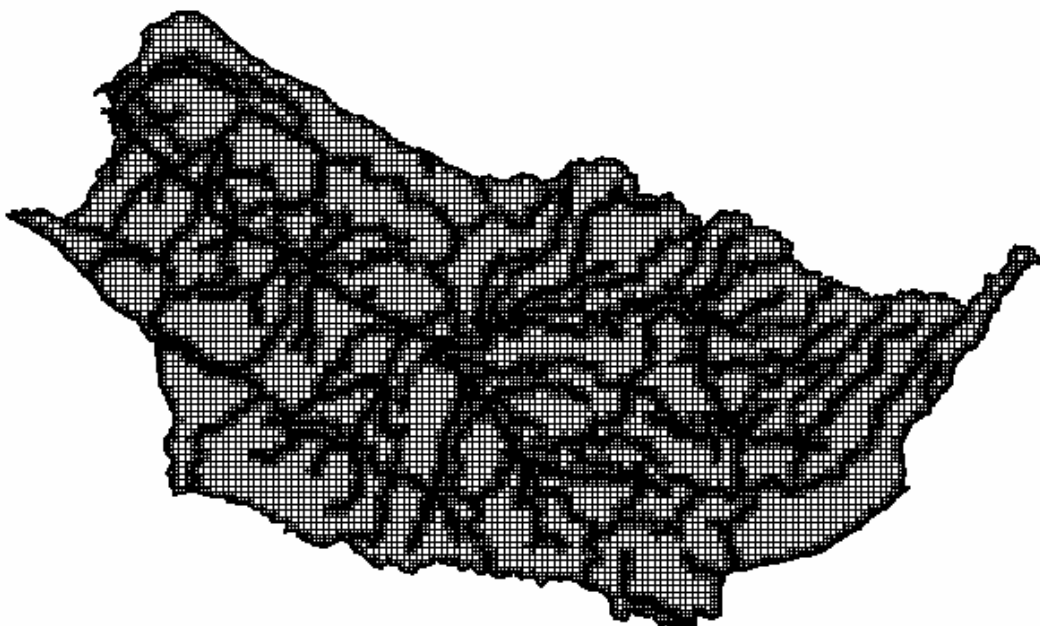


FIG. 5.8 Aquifer grid of the Somme river basin.

For the Somme basin, the mask of the surface layer was as well used as the mask of the aquifer and one more level of regrouping was enabled while the reference grid size was kept constant (1000 m). Additional regrouping of small cells with respect to surface mesh was mainly made on the cells below subcatchment boundaries because subcatchment partitioning does not make any sense in the aquifer as the flow is conducted by

piezometric head gradient. In addition, regrouping was again not allowed on the cells beneath the stream network in order to maintain a high accuracy for the solution of stream-aquifer interaction. Therefore, these cells are of the smallest size (125 m).

In Fig. 5.8, the aquifer grid composed of 63226 cells is shown. In the figure, it is observed that small cells on subcatchment boundaries still exist. The reason is that due to vertical neighboring rules, a cell can not have an adjacent cell having a size less than half of it. When a surface cell size is 125 m on a subcatchment boundary, the size of an aquifer cell beneath can not be greater than 250 m.

5.4. Preparation of Data

In order to have a well constituted model, the most important thing is to have as much information as possible on the basin. In order to run the surface model (MODSUR), soil type and land use data to form the production zones, and also meteorologic input data are essential. For NONSAT (Unsaturated Model), the unsaturated thickness of the aquifer is needed. For NEWSAM, the aquifer parameters, namely, transmissivity and specific yield of the porous medium are needed. Finally for MODCOU, other than the aquifer parameters, the piezometric level observations and streamgage measurements on the river and its tributaries are essential. The longer the period of observations the better the model will be.

5.4.1. Composition of Production Zones

The production zones are used to partition the rainfall between surface runoff and infiltration according to surface properties. The production zones for the Somme basin were built by crossing two types of data in GIS environment. These are, namely, soil type and land use. Soil type data was acquired from INRA Database (King et al. 1995) and land use data from CORINE Land Cover Database (Collectif 1996).

From these databases 9 indices for soil type and 5 indices for land use were supplied to be used for the modeling. Soil type indices are; alluvial deposits, calcareous rocks, clayey materials, sandy materials, loamy materials, detrital formations, crystalline rocks and migmatites, volcanic rocks, other rocks, undefined soil. However, among the supplied data detrital formations, crystalline rocks and migmatites, volcanic rocks did not exist in the Somme basin. Whereas, within the index of other rocks, organic soil was detected in

the proximity of river beds and estimated to be “peat”. On the other hand, a small portion of water bodies was detected and later added to land use data. Soil type classification composed of combinations of 9 indices listed above can be seen in Fig. 5.9. In the figure, the percentages of soils are given in parenthesis. Each zone enclosed by a contour line represents a cartographic unit and each cartographic unit corresponds to percentages of several types of soil.

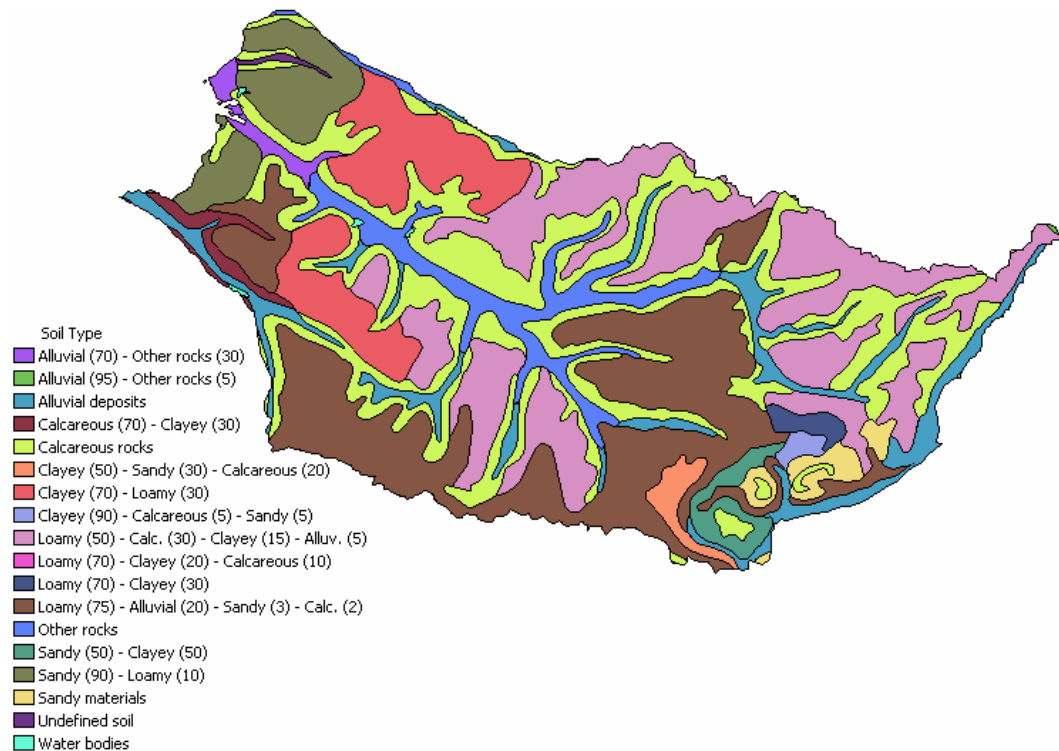


FIG. 5.9 Soil type distribution.

Land use indices are; artificial surfaces, water bodies, wetlands, agricultural areas, forest and semi-natural areas (Fig. 5.10). While incorporating soil type data into land use data, artificial surfaces, water bodies and wetlands indices from land use were taken as dominant indices and were not included in combination. Whereas, the other two indices, namely, agricultural areas, and forest and semi-natural areas were superposed with 7 types of soil indices and 14 combinations were obtained. Together with 3 dominant features of land use, initially, 17 production zones were formed. Among these 17 production zones, undefined soil-agricultural areas, undefined soil-forests and organic soil-forests combinations had negligible percentages. Therefore, undefined soil-agricultural areas were added to calcareous-agricultural areas and undefined soil-forests were added to calcareous-forests as chalk is the most abundant material in the aquifer.

Further, organic soil-forests are combined with organic soil-agricultural areas. As a result, a total of 14 production zones were obtained due to the limitation of the code.

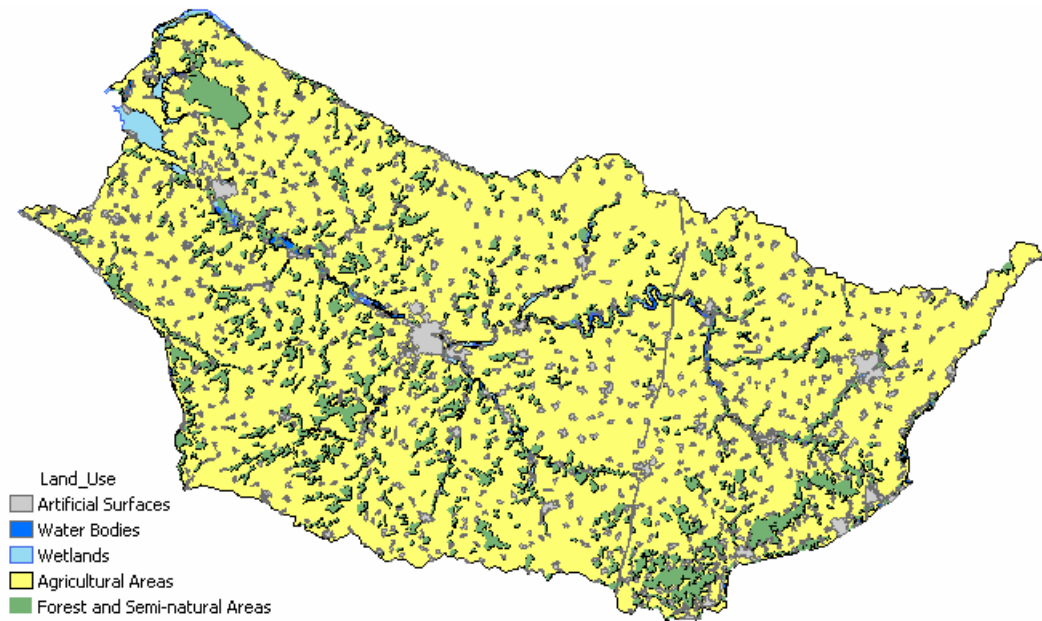


FIG. 5.10 Land use data (from CORINE Land Cover Database).

Afterwards, the resultant 14 production zones were joined to the surface mesh. Therefore every cell on the surface mesh was assigned the percentages of these 14 production zones. In Table 5.1, the percentages of productions zones in basin scale are given. The most abundant productions zone is calcareous-agricultural areas and then loamy-agricultural areas.

The dominant zone in each cell is schematized in Fig. 5.11. To obtain this figure, in each cell, the production zone having the maximum percentage was assumed to represent the cell. However, in the model all of the 14 values are considered during calculations. During simulations, it was observed that artificial surfaces were highly effective in rainfall partitioning which was due to their overestimation and therefore they were made less effective by adding artificial surfaces less than 80% to the zone having the highest percentage in the cell. Table 5.1 and Fig. 5.11 present the latest values. There is a dominance of calcareous and loamy soil covered with agricultural areas. This is followed by alluvial deposits covered with agricultural areas. With these 14 values, it is possible to calibrate the surface model (MODSUR) and have different surface runoff-infiltration partitionings around the basin.

TABLE 5.1 Production zones and their percentages.

Zone no.	Name of zone	Percentage (%)
1	Artificial Surfaces	5.4
2	Water Bodies	2.6
3	Wetlands	3.2
4	Alluvial-agricultural areas	13.1
5	Calcareous-agricultural areas	24.8
6	Clayey-agricultural areas	7.7
7	Sandy-agricultural areas	4.8
8	Loamy-agricultural areas	20.7
9	Organic-agricultural areas	8.2
10	Alluvial forests	2.6
11	Calcareous forests	3.6
12	Clayey forests	0.7
13	Sandy forests	0.8
14	Loamy forests	1.8

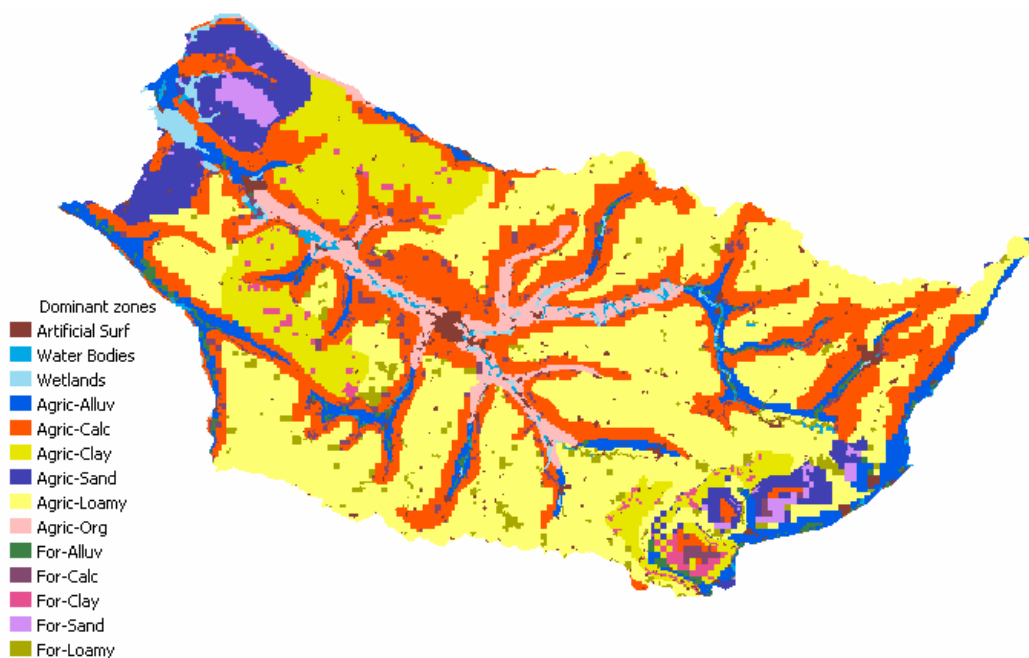


FIG. 5.11 Dominant production zones.

5.4.2. Meteorologic Data

The necessary meteorologic forcing to be used by the coupled model includes rainfall and potential evapotranspiration (*PET*). These were supplied by Météo-France in a daily time step on a regular grid covering the whole Somme basin. This grid consists of 235 cells where the cell size is 8 km. This input data was provided by SAFRAN (Système d'Analyse Fournissant des Renseignements Atmosphérique à la Neige) analysis system processing the meteorologic data; such as, liquid and solid precipitation, temperature, wind speed, humidity, incoming short wave and long wave radiation and surface pressure (Durand et al. 1993, Quintana-Segui et al. 2007). SAFRAN uses an interpolation method based on the output of a mesoscale model (20 to 100 km²) and the available observations coming from synoptic stations and stations of climatic network of the state over the Somme basin.

The meteorological data, obtained from SAFRAN was redistributed on a mesh called “météo” as described above. The atmospheric forcing was supplied for the period August 1985 – July 2003. This data have already been visualized in certain figures. The spatially averaged monthly rainfall is demonstrated in Fig. 4.7 and the annual progress of spatially averaged monthly and bimonthly rainfall depths in Fig. 4.14. In Fig. 5.12, seasonal variations are shown.

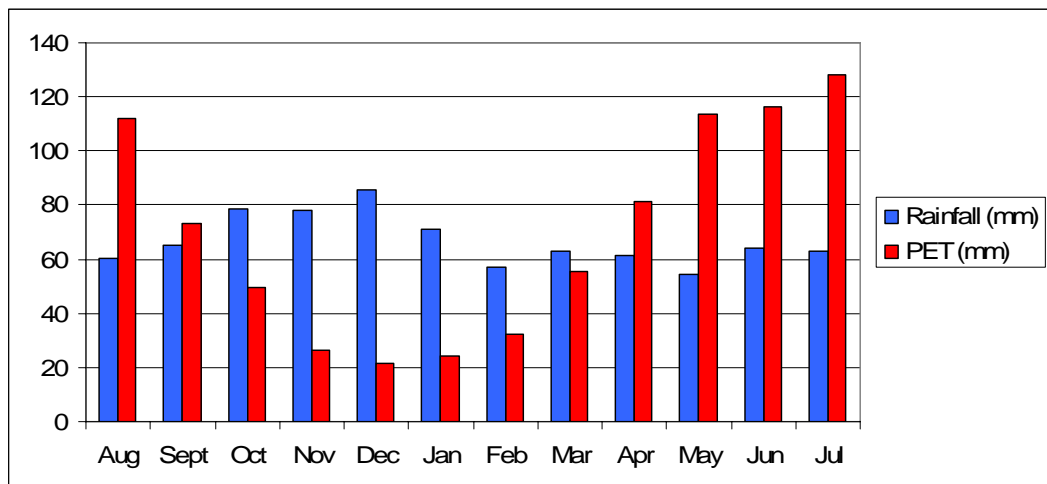


FIG. 5.12 Interannual averages of monthly rainfall and *PET* values over the Somme basin (in the period 8/1985-7/2003).

Fig. 5.12 was obtained for a period of 18 years (8/1985-7/2003) by taking interannual averages of spatially averaged monthly cumulative rainfall and *PET* values. The *PET*

values vary between 21.7 mm in December and 128.0 mm in July. Whereas, the rainfall values alter less, that is, from 54.5 mm in May to 85.8 mm in December.

Annual rainfall and *PET* values for the same period are illustrated in Fig. 5.13. For rainfall data, the highest values are observed in 2000-2001 (1123 mm) and 1999-2000 (994 mm). The third peak is in 1993-1994 (942 mm). On the other hand, *PET* values are more or less in a regular form where the highest value is in 1989-1990 (958 mm).

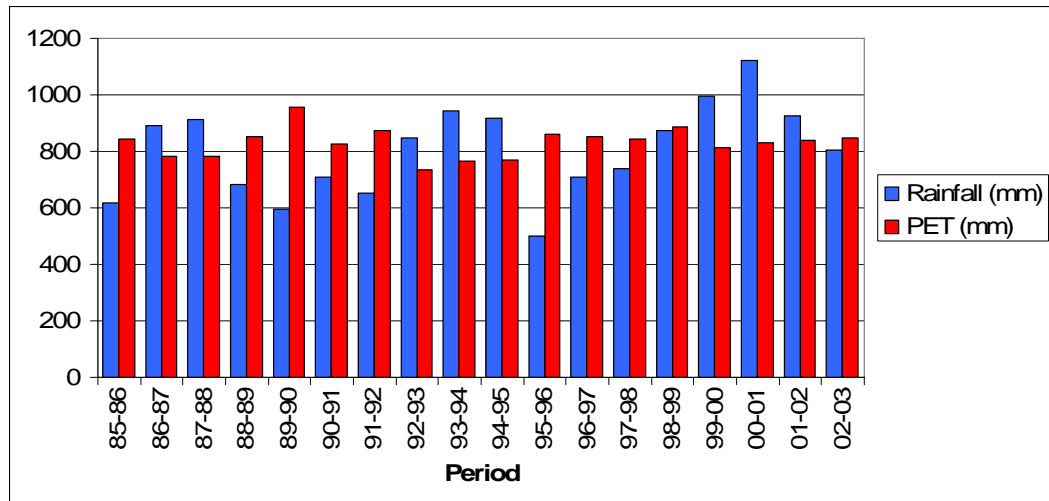


FIG. 5.13 Spatially averaged annual rainfall and *PET* values.

The average annual precipitation is visualized in Fig. 5.14 and the average annual *PET* in Fig. 5.15. While obtaining the precipitation values, it is assumed that snow melts directly without forming a cover on the terrain. Therefore, the values of rainfall and snowfall are directly summed up to give the precipitation. As observed from Fig. 5.14, rainfall values are higher in the northern and western regions, and smaller values are mainly in the mid-eastern portion. The difference between the highest and lowest values is well above 200 mm. In addition, there is a resemblance with the isohyetal map of Météo-France provided in Fig. 4.8.

On the other hand, when Fig. 5.15 is considered, it is seen that *PET* values are higher on the inner valleys and south-eastern portion of the basin. *PET* is dependent on many factors such as solar radiation, humidity, temperature and wind.

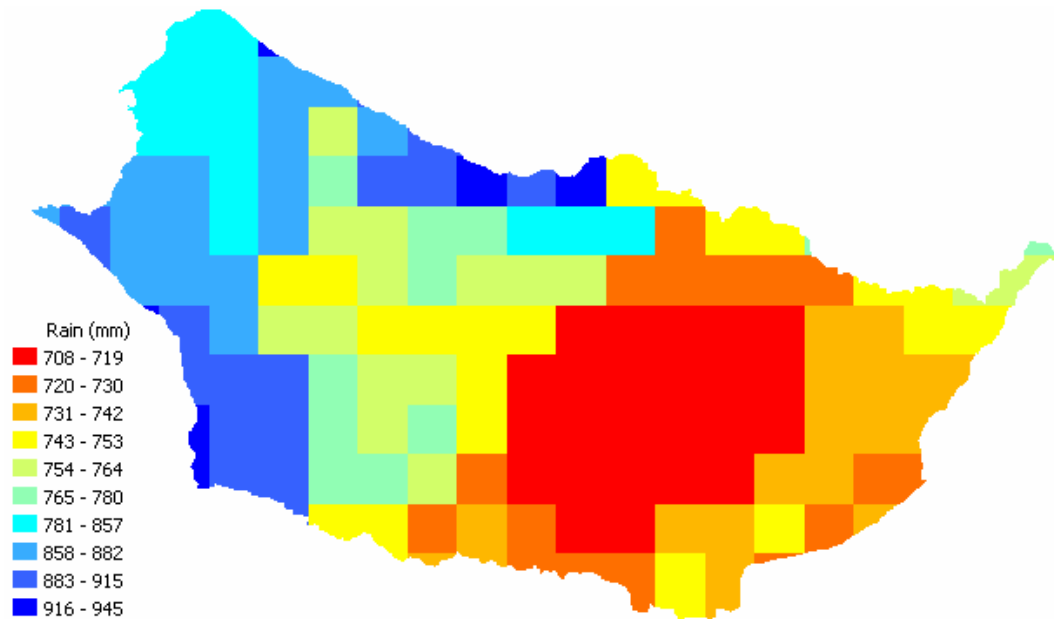


FIG. 5.14 Average annual precipitation for the period of 1985-2003 in mm (from Météo-France).

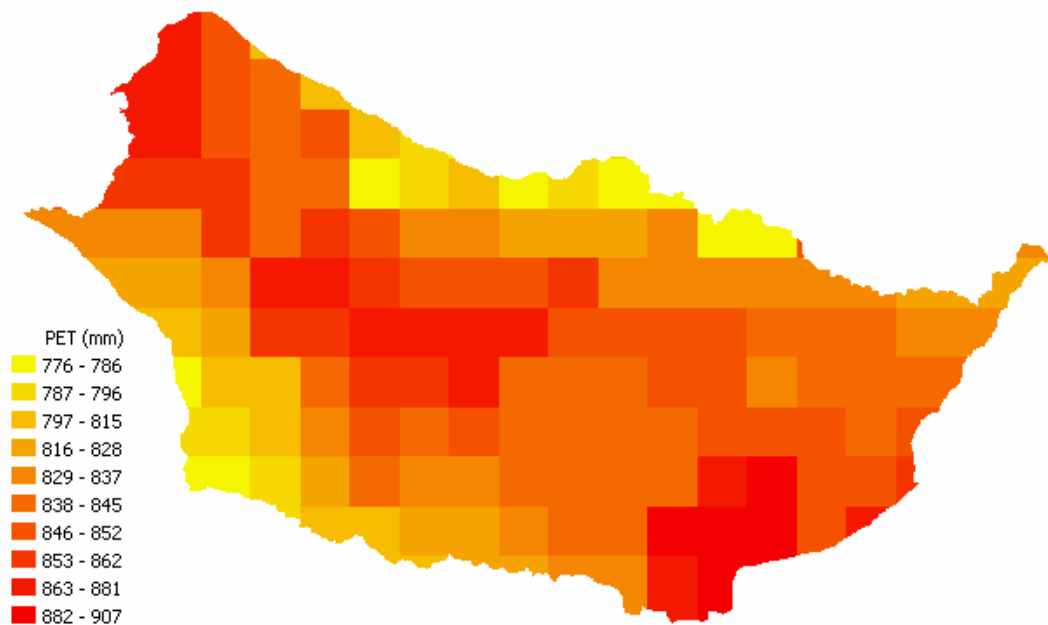


FIG. 5.15 Average annual potential evapotranspiration for the period of 1985-2003 in mm (from Météo-France).

5.4.3. Aquifer Data

The initial aquifer data was supplied by BRGM on a regular grid composed of cells all having a size of 500 m. This data includes 5 hydraulic conductivity zones, 3 specific yield zones, altitude of topography, altitude of substratum, piezometric head distribution,

pumping rates involving both irrigation and industrial pumping, flooding index marking where the groundwater may overflow and river index marking river cells. Hydraulic conductivity zones are visualized in Fig. 5.16. The highest values are observed in the Somme river valley. These values slightly decrease towards the downstream portion and the lowest values are observed in high regions. Specific yield zones are shown in Fig. 5.17. As can be seen, this figure demonstrates a rough estimate of specific yield values.

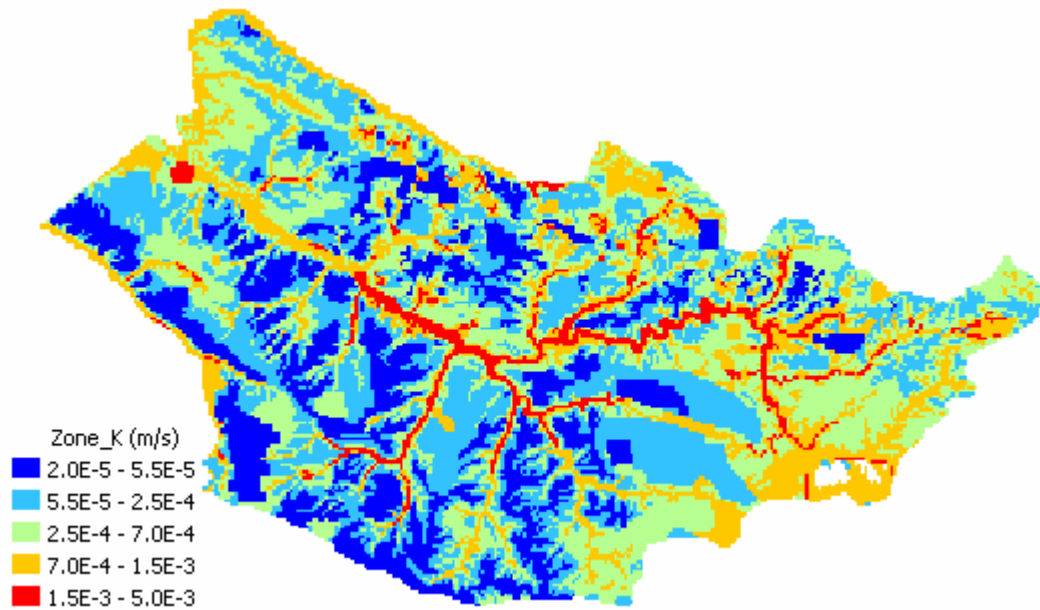


FIG. 5.16 Hydraulic conductivity zones (from BRGM).

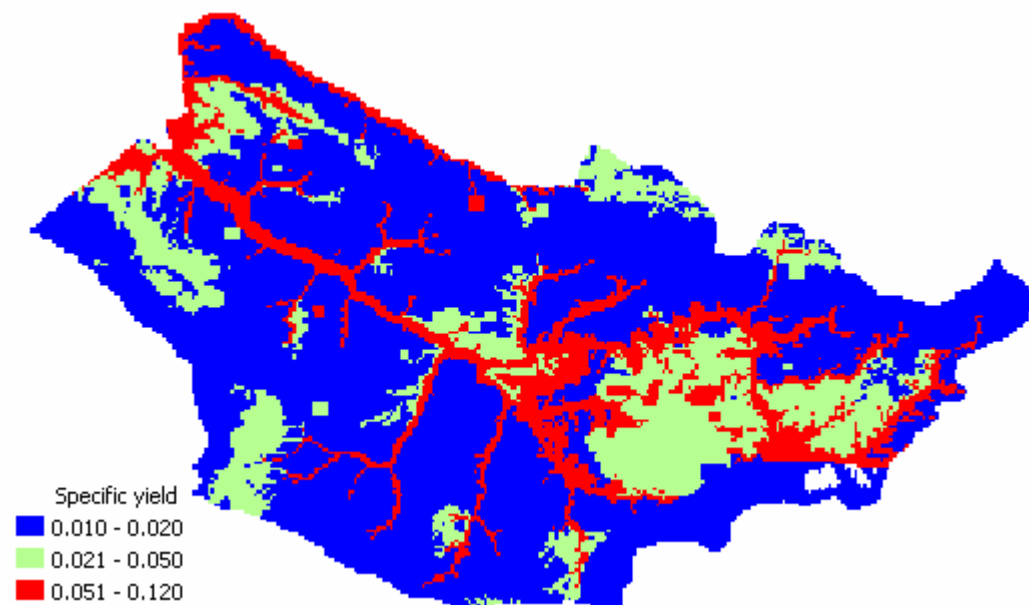


FIG. 5.17 Specific yield zones (from BRGM).

In the current model, the surface and aquifer grids occupy a wider area than the one supplied by BRGM. In addition, transmissivity is used instead of hydraulic conductivity as can be seen in Eqs. (3.23) and (3.29). For these reasons, some modifications were carried out.

To establish the transmissivity map, the hydraulic conductivity values were multiplied by the groundwater depth which is the difference between average piezometric head and altitude of substratum (Fig. 5.18). For the eastern region of the grid, where the hydraulic conductivities were not supplied, a distribution of transmissivity was made according to surface topography (Fig. 5.19). As for specific yield, the most abundant value (0.015) was assigned to missing portions (Fig. 5.20).

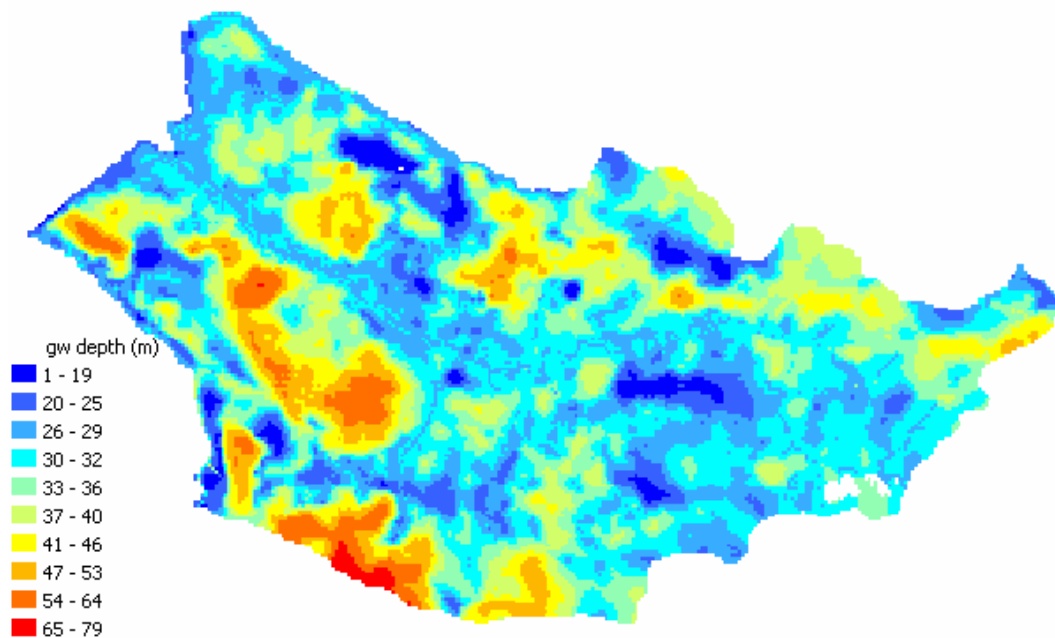


Fig. 5.18 Groundwater depth (from BRGM).

Fig. 5.19 represent merely the initial values of the transmissivity and Fig. 5.20 those of the specific yield. These are subject to change during calibration of the model. In order to have correspondence between the observed and simulated flowrates or piezometric heads, transmissivity and specific yield values are altered. In fact, in different models it is possible to obtain different distributions that give similar results. The point is to stay within reasonable limits of these values. In addition to these figures, the unsaturated thickness, which will be used by the unsaturated model (NONSAT), has already been visualized in Fig. 4.5. Moreover, the pumpage rates acquired in 1995 by BRGM including

both industrial and irrigation purposes are shown in Fig. 5.21. Pumpage is concentrated mainly on the northwestern and eastern regions of the basin.

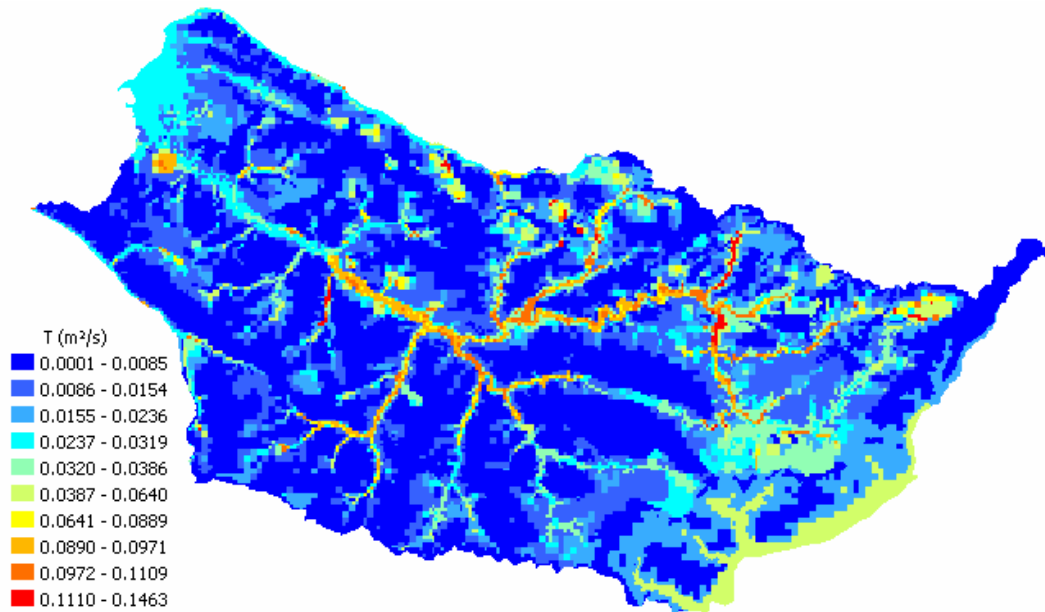


FIG. 5.19 Initial transmissivity distribution on the modeled area.

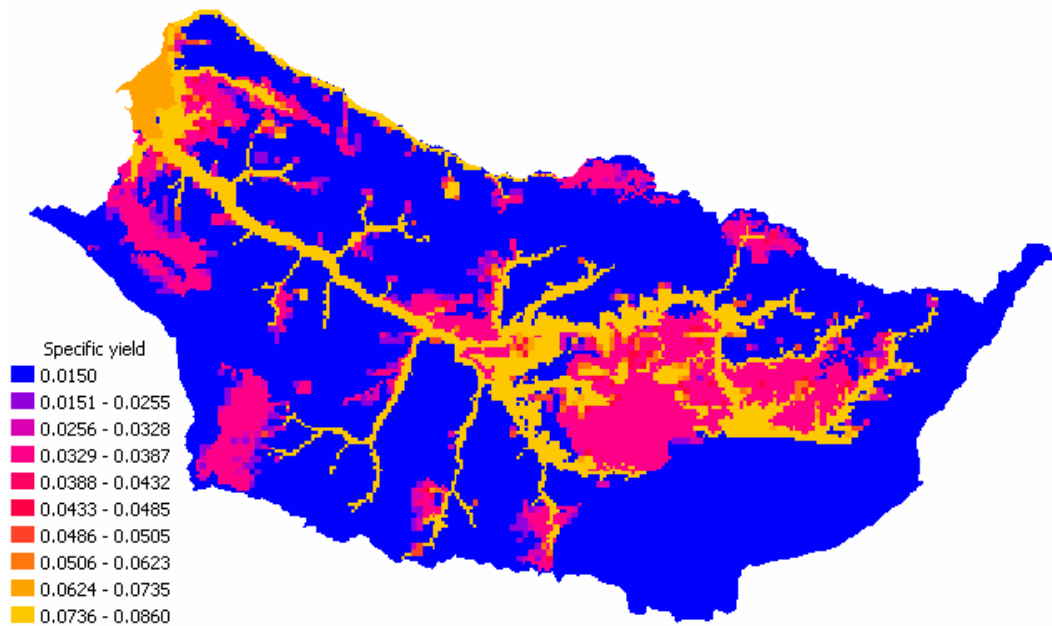


FIG. 5.20 Initial specific yield distribution on the modeled area.

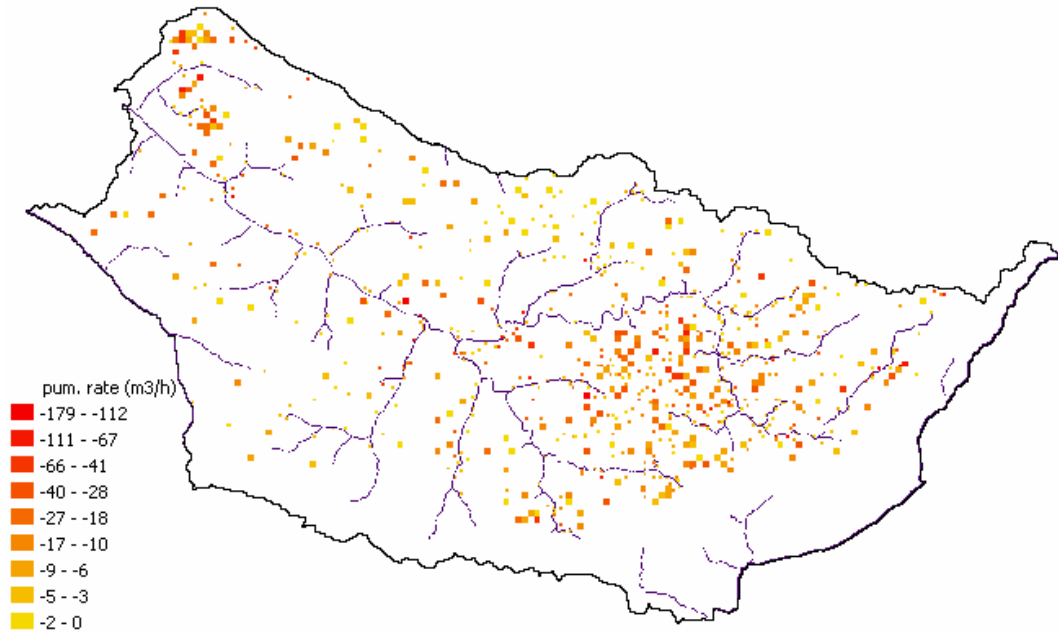


FIG. 5.21 Observed pumpage rates in the year 1995 by BRGM.

5.4.4. Surface Data

Streamflow measurements and piezometric level observations constitute the surface data. 7 hydrometric and 62 piezometric stations were chosen to be used for calibration and validation purposes. In Fig. 5.22, the distribution of hydrometric and piezometric stations is given.

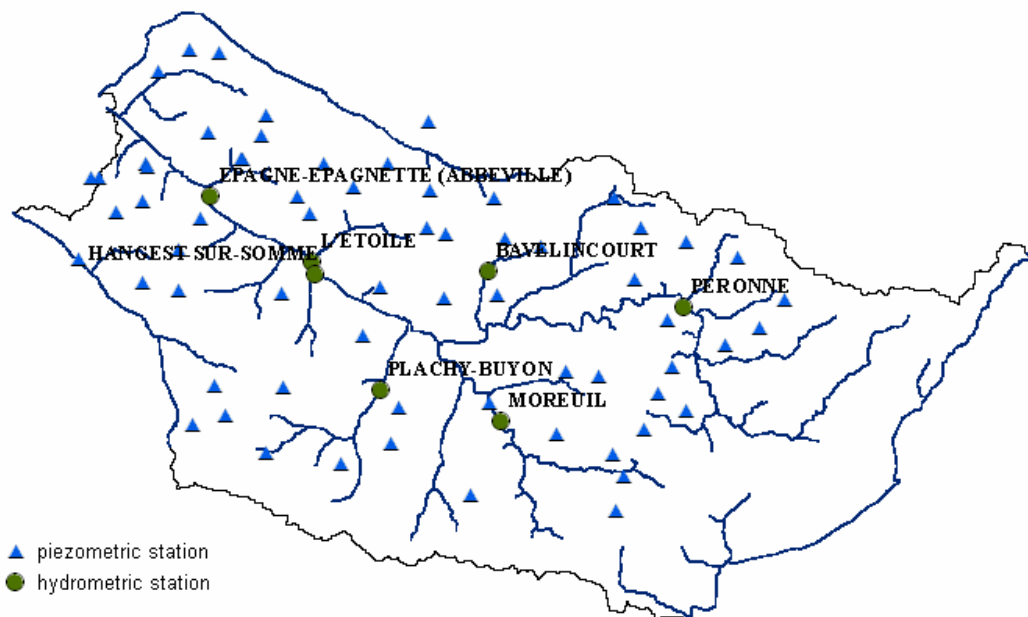


FIG. 5.22 Distribution of hydrometric and piezometric stations.

Streamflow measurements were obtained from Banque Hydro (2007). This data has been analyzed in detail in Sections 4.2.2 and 4.3.1. 3 of the stations are on the Somme and the others are located on the tributaries. The catchment areas, annual, maximum, minimum and specific discharges of these stations are given in Table 4.1.

Initially, the streamflow data supplied from hydrometric stations will be used to calibrate the production function parameters, and then the transmissivity and specific yield. On the other hand, piezometric level measurements are used to calibrate the transmissivity and specific yield of the aquifer.

5.5. Simulations

After the preparation of the necessary data, model simulations can begin. Simulations are performed over two periods; namely, calibration and validation. Calibration is the process of adjusting parameter values in order to optimize model performance according to a set of predefined criteria (Wilby 1997). Whereas, validation is assessing model performance against a data set not used for calibration. In time series models, the validation period is usually of the same length as the calibration period.

Generally, all the available data for calibration is collated and split into two periods of equal length. These are expected to have similar conditions; however, the model is tested more rigorously if the hydrological conditions differ in these two periods. Another way is to carry out calibration and validation on the subsets of the available data. Ideally, the model should perform as well over the validation period as it does over the calibration period.

In order to determine which set of parameters provides the best results certain criteria for measuring the quality of results must be defined. In present study, the following criteria were used in order to assess goodness of fit; Root Mean Squared Error, Deviation of Runoff Volumes, Correlation Coefficient, Nash-Sutcliffe Coefficient (Nash and Sutcliffe 1970), Coefficient of Gain from Daily Mean.

Root Mean Squared Error:

The root mean squared error (*RMSE*) or the standard deviation is the average of squared differences between observed and calculated values. It is a measure of the spread of data

about the observed values. The *RMSE* is usually considered to be the best measure of error if errors are normally distributed (Anderson and Woessner 1992).

$$RMSE = \sqrt{\frac{\sum_{i=1}^n (Q_{obs} - Q_{sim})^2}{n}} \quad (5.1)$$

where Q_{obs} is the observed flowrate, Q_{sim} is the simulated flowrate and n is the number of days of simulation.

Deviation of Runoff Volumes:

Deviation of runoff volumes (D_v) is numerically equivalent to the percentage difference in mean flow and is a measure of the water balance of the model (Wilby 1997).

$$D_v (\%) = \frac{V_{obs} - V_{sim}}{V_{obs}} \times 100 \quad (5.2)$$

where V_{obs} is the volume of the observed flow, V_{sim} is the volume of the simulated flow.

Correlation Coefficient:

Correlation coefficient indicates the strength and direction of a linear relationship between two random variables. It is sometimes referred to as *Pearson product moment correlation coefficient*.

$$\rho = \frac{1}{n-1} \times \frac{\sum_{i=1}^n (Q_{obs} - \bar{Q}_{obs})(Q_{sim} - \bar{Q}_{sim})}{\sigma_{obs} \times \sigma_{sim}} \quad (5.3)$$

where \bar{Q}_{obs} is the mean of observed flowrate, \bar{Q}_{sim} is the mean of simulated flowrate, σ_{obs} and σ_{sim} are the standard deviations of observed and simulated flowrates.

The value of ρ varies between -1 and 1. A negative value indicates a negative linear correlation and a positive value a positive correlation whereas values close to 0 means that there is no or weak linear correlation between the two variables.

Nash-Sutcliffe Coefficient:

$$R^2 = 1 - \frac{\sum_{i=1}^n (Q_{obs} - Q_{sim})^2}{\sum_{i=1}^n (Q_{obs} - \bar{Q}_{obs})^2} \quad (5.4)$$

The Nash-Sutcliffe coefficient measures the performance of the model against the overall mean flow. R^2 varies between $-\infty$ and 1 where a value of 1 represents a perfect model. A value of 0 indicates that the model predicts no better than using the mean of the flows.

Coefficient of Gain from Daily Mean:

$$DG = 1 - \frac{\sum_{i=1}^n (Q_{obs} - Q_{sim})^2}{\sum_{i=1}^n (Q_{obs} - Q'_{obs})^2} \quad (5.5)$$

where Q'_{obs} is the mean of observed flowrate in previous years for that day.

The criterion is similar to the Nash-Sutcliffe coefficient but this time the performance of the model is tested against the mean flow on each day.

Deviation of runoff volumes (D_v), Nash-Sutcliffe coefficient (R^2) and coefficient of gain from daily mean (DG) are the three criteria suggested by American Society of Civil Engineers (ASCE 1993) for continuous hydrographs.

5.5.1. Computation of the Water Budget

Computation of the water budget was performed by MODSUR. For the calibration of production function variables such as CRT and DCRT, initially the values from an earlier project were used (Gomez 2002, Ledoux et al. 2007). To concentrate on the period of high flows which is 2000 – 2003, the period 8/1995 – 7/2003 was chosen for calibration and the period 8/1985 – 7/1995 for validation.

Simulation was done with a daily time step. The calibration of the concentration time was done by comparing the flood peaks of simulated and observed values in flow hydrographs. The concentration time was estimated to be 5 days.

The final values of production function variables are given in Table 5.2. The effect of each variable on the flow hydrograph was examined. Increasing CRT reduces the effect of a flood which is the maximum value of flowrate in a flow hydrograph. This was mainly increased for *Artificial Surfaces*. Increasing $DCRT$ increases the AET (Actual Evapotranspiration) therefore decreases the available water for surface flow and infiltration. This was increased for *Artificial Surfaces* and decreased for *Agricultural Zones*.

TABLE 5.2 The values of production function variables.

Prod. Zone	CRT	$DCRT$	R_b	FN	C_{OR}	QR_{max}	C_{OI}	QI_{max}	R_{aq}
Artificial S.	20	10	0	10	0.05	100	0.1	100	0
Water Bod.	0.8								
Wetlands	50	10	0	10	0.01	20	0.08	30	0
AG-Alluv	20	5	0	20	0.04	20	0.1	30	0
AG-Calc	115	5	0	20	0.01	90	0.1	10	0
AG-Clay	140	10	0	10	0.03	20	0.1	30	0
AG-Sand	110	15	0	20	0.03	15	0.1	30	0
AG-Loamy	60	20	0	10	0.02	90	0.1	50	0
AG-Org	70	20	0	10	0.02	50	0.1	50	0
FOR-Alluv	95	20	0	10	0.05	20	0.1	30	0
FOR-Calc	80	25	0	20	0.03	25	0.1	10	0
FOR-Clay	130	25	0	10	0.03	30	0.1	30	0
FOR-Sand	110	5	0	20	0.04	20	0.1	30	0
FOR-Loamy	85	30	0	10	0.03	90	0.1	50	0

The initial level of balance reservoir, R_b was taken as 0. for all of the production zones for the simulations started on the 1st of August which is a dry period. FN , the maximum daily value of infiltration, was increased for all of the zones as there were too many peaks in the flow hydrograph which demonstrated a too strong surface runoff. Therefore, the water was transferred to the aquifer by increasing FN . C_{OR} , depletion ratio of the surface runoff reservoir, strongly affects the magnitude of flow peaks by controlling the speed of surface runoff; therefore, it was decreased for all of the production zones to about one tenth of the initial value. QR_{max} , overflow level of the surface runoff reservoir, controls the highest flow peaks but not all. These high peaks were due to a low QR_{max} value for *Artificial Surfaces*; therefore, it was increased for only *Artificial Surfaces* by about 50 times. C_{OI} ,

depletion ratio of the aquifer feeding reservoir, affects the speed of infiltration. This value was kept constant for all of the production zones as the unsaturated model (NONSAT) already controls the groundwater recharge by using infiltration values and yields C_{QI} less effective. Accordingly, QI_{max} , overflow level of aquifer feeding reservoir, was kept constant for all of the production zones. R_{aq} , level of the aquifer feeding reservoir, was set to 0. for all zones.

In order to perform calibration, all the modules have to run. As MODSUR is the first module to run, and none of the other modules are calibrated, a rough coincidence between the observed and simulated flowrates was sought. The calibration steps of MODSUR are described in the following.

First, FN was increased for most of the production zones. The effect of FN can be seen in Fig. 5.23. In terms of water budget, for a precipitation of 6439 mm the infiltration increased from 1563.4 mm to 1726.3 mm and the surface runoff reduced from 296.9 mm to 133.9 mm.

Second, depletion ratio of the surface runoff reservoir, C_{QR} , was reduced. The effect of this reduction can be observed in Fig. 5.24. Modifying the value of C_{QR} did not affect the water balance as it is a parameter inside the surface runoff reservoir which controls the speed of surface runoff output.

Third, the effect of the unsaturated model (NONSAT) was investigated (Fig. 5.25). At this stage, the calibration of NONSAT was not made, therefore, a rough parameter set was employed. It highly improved the flow hydrograph. The calibration of parameters of NONSAT is described in the following sections.

Next, the parameters of *Artificial Surfaces* were investigated; $DCRT$, CRT , FN and QR_{max} were increased (Fig. 5.26). With the calibration of parameters of *Artificial Surfaces*, infiltration slightly decreased from 1726.3 mm to 1706.2 mm and surface runoff 133.8 to 101.8 mm which demonstrates a loss of water by AET .

Finally, the parameters CRT and $DCRT$ were adjusted for *Agricultural Zones* (Fig. 5.27). They were increased for some and decreased for others. As a result, infiltration increased from 1706.2 mm to 1784.8 mm and surface runoff from 101.8 mm to 102.6 mm.

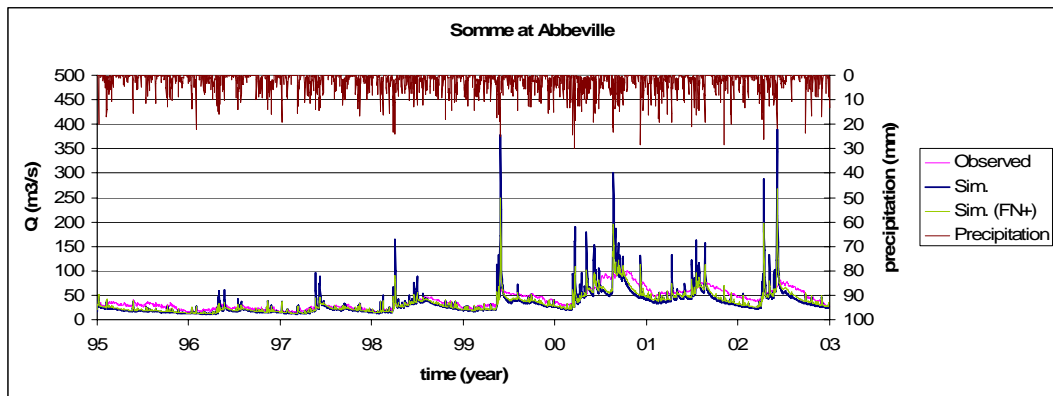


FIG. 5.23 The effect of the maximum value of infiltration (FN) on the flow measured at Abbeville (catchment area = 5560 km²).

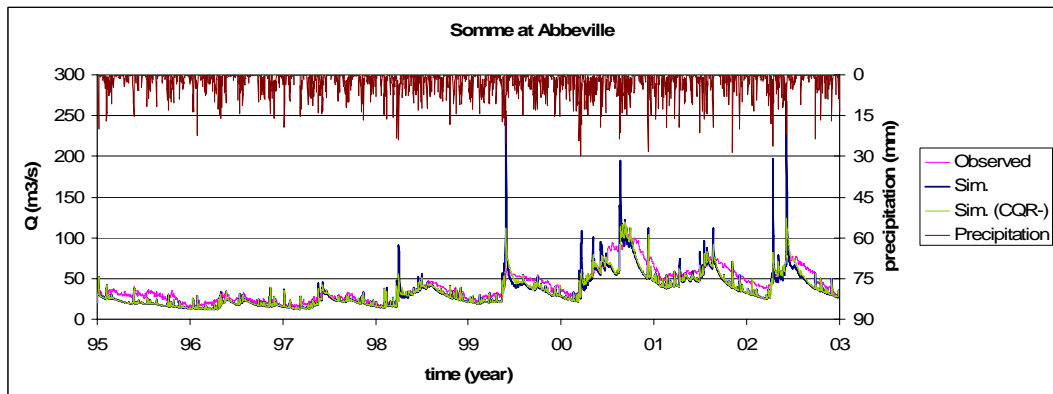


FIG. 5.24 The effect of depletion ratio of surface runoff reservoir (C_{QR}).

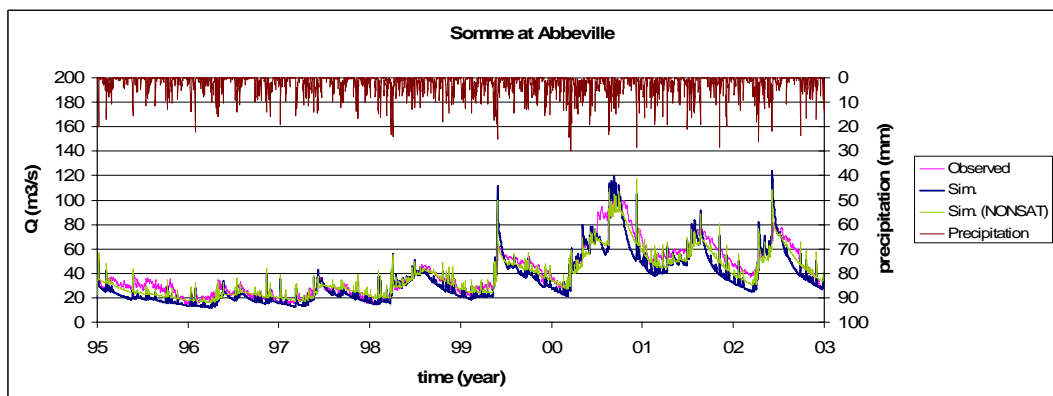


FIG. 5.25 The effect of the unsaturated model (NONSAT) run with a storage constant of $\tau = 5$ days.

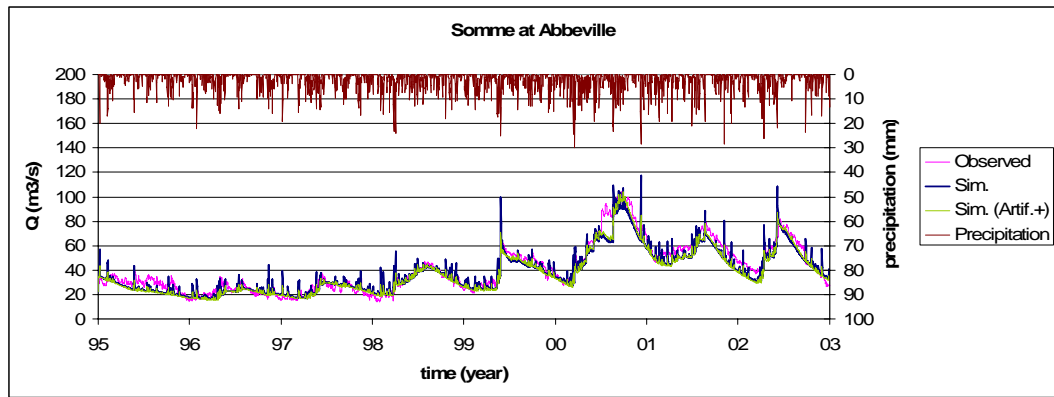


FIG. 5.26 Calibration of parameters of Artificial Surfaces.

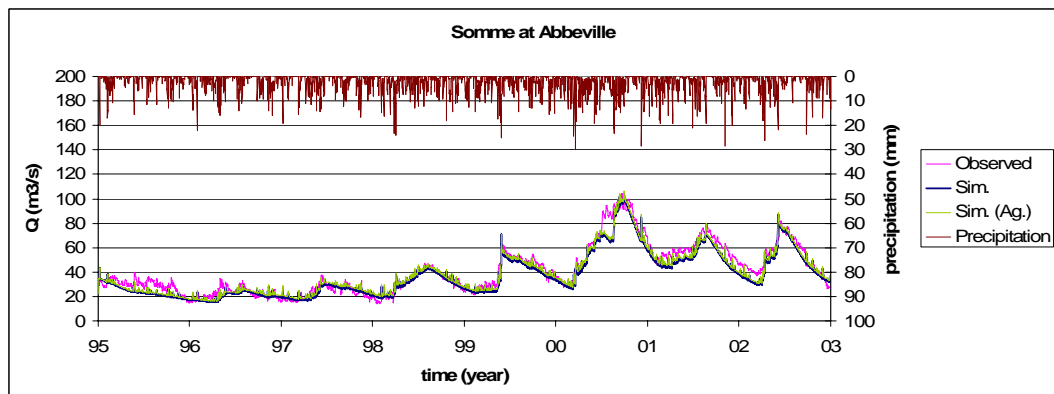


FIG. 5.27 Calibration of CRT and DCRT for Agricultural Zones.

The alteration of the elements of water budget during the calibration process is summarized in Table 5.3. The biggest alteration was caused by changing *FN*. During calibration, as the infiltration increases, surface runoff decreases. This means that intense flow peaks appeared because of excessive surface runoff and they diminished as the infiltration capacity of the production zones were increased. In addition, *AET* and water stock slightly decreased during the calibration.

TABLE 5.3 The alteration of water budget during calibration.

Calibration Step	precipitation (mm)	infiltration (mm)	sur. runoff (mm)	<i>AET</i> (mm)	water stock (mm)
1) Initial values	6439	1563.4	296.9	4599.2	10.2
2) <i>FN</i> increased	6439	1726.3	133.9	4599.2	10.2
3) <i>CQR</i> decreased	6439	1726.3	133.8	4599.2	10.2
4) NONSAT run	6439	1726.3	133.8	4599.2	10.2
5) Artif. Surfaces	6439	1706.2	101.8	4651.3	10.4
6) Agricul. Zones	6439	1784.8	102.6	4573.0	9.9

In Fig. 5.28, the evolution of measures of error for the Somme gauged at Abbeville (5560 km²) is shown. The order of calibration steps on the x-axis are given in Table 5.3. *RMSE* decreases parabolically while D_v decreases by fluctuations. Whereas, ρ , R^2 and *DG* increases parabolically and approaches to 1. The biggest improvement is observed in the 2nd calibration step such that all the criteria except D_v are approaching their ideal values.

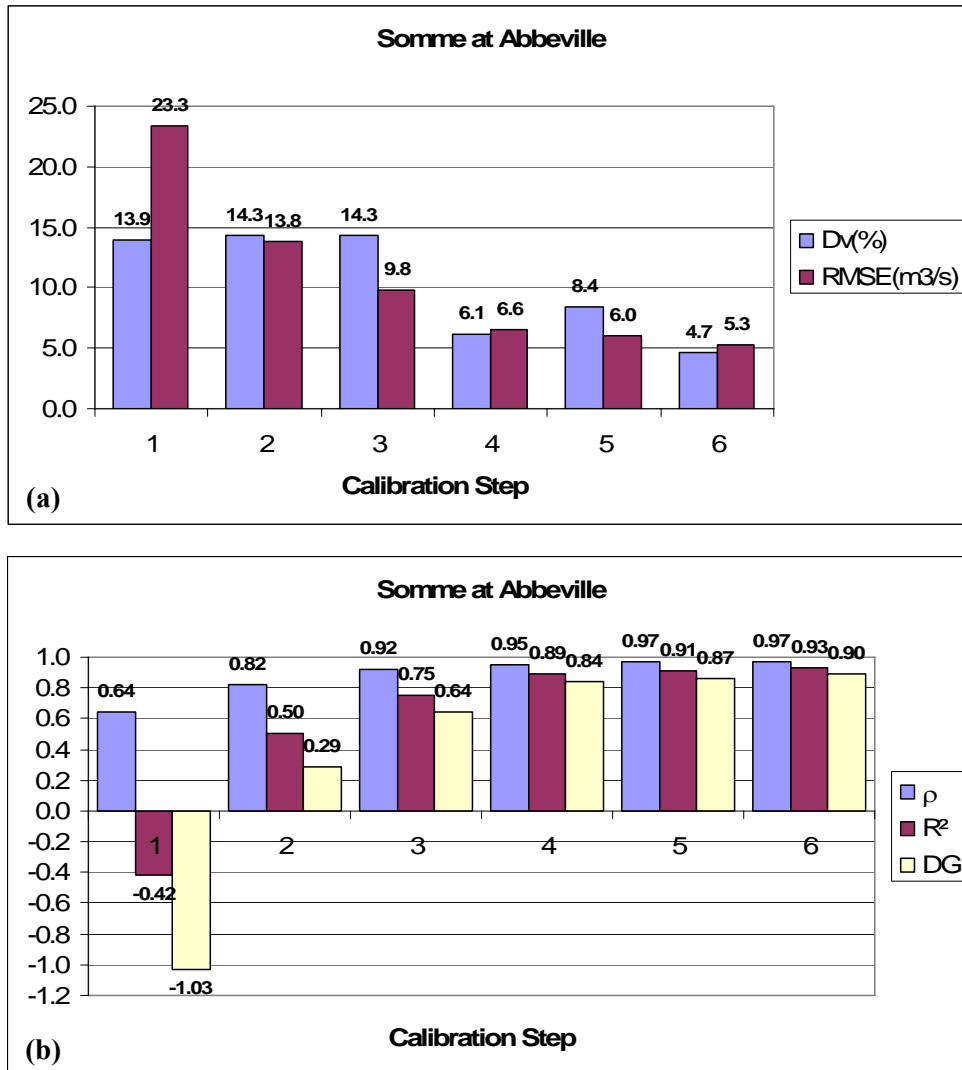


FIG. 5.28 Evolution of measures of error; **a)** Deviation of runoff volumes (D_v), Root mean squared error (*RMSE*); **b)** Correlation coefficient (ρ), Nash-Sutcliffe coefficient (R^2), Coefficient of gain from daily mean (*DG*).

The figures representing the calibration steps for the tributaries of the Somme are provided in Fig. A. 1 to Fig. A. 4 (Appendix A), and the corresponding error criteria in Fig. A. 5. When these figures are considered, it is observed that the simulated flow hydrographs of all the tributaries were improved. However, the Avre fails to improve in

the 4th (inclusion of NONSAT module) and 6th steps (calibration of the parameters of Agricultural Zones). This can be due to different aquifer characteristics of the Avre as mentioned in Sections 4.3.1 and 4.3.2. In addition, an approximate parameter set had been used for the NONSAT module at this stage. The Nièvre slightly degrades in the 5th step (calibration of the parameters of Agricultural Zones) and the Selle in the 5th and 6th steps, however, when the correlation coefficient is considered they both keep improving. This means that even when the performance of the model against the mean flow decreases, the linear relationship between the observed and simulated flows increases.

The validation of this calibration process was realized over the period 8/1985 – 7/1995. The model was run for the whole period 8/1985 – 7/2003. As initial conditions of the calibration period (8/1995 – 7/2003) have changed, the measures of error for this period were also slightly changed. For the sake of continuity one single run comprising both periods was performed. The variation of the Nash-Sutcliffe coefficient (R^2) is shown in Fig. 5.29. The validation value of the Somme gauged at Abbeville is 0.72 which can be considered satisfactory at this stage. The Nièvre and the Selle demonstrate a poor performance in the validation period while the Avre and the Hallue improves the fit.

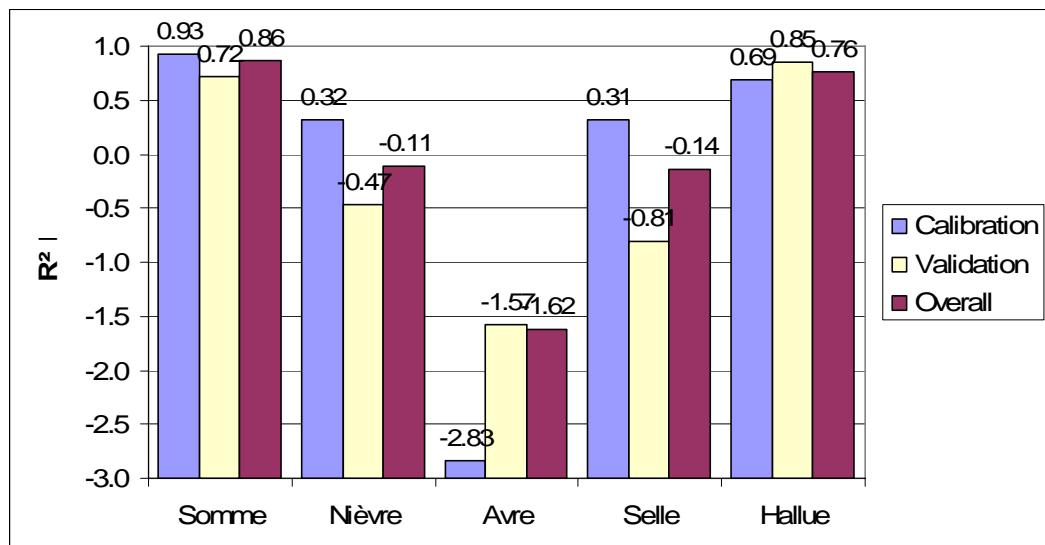


FIG. 5.29 The variation of Nash-Sutcliffe coefficient (R^2) for the Somme gauged at Abbeville and for its tributaries.

The values of all measures of error used are summarized in Table 5.4. DG has a tendency similar to R^2 . $RMSE$ increases in all, D_v improves in the Somme and the Avre, and ρ slightly decrease in all except the Hallue.

TABLE 5.4 The values of error criteria after the calibration of production function.

Period	Somme	Nièvre	Avre	Selle	Hallue
	<i>Deviation of runoff volumes, D_v (%)</i>				
calibration	2.15	34.34	-52.86	-22.51	5.03
validation	-1.31	41.37	-48.99	-24.50	-18.46
overall	0.33	38.86	-50.20	-23.72	-7.00
<i>Root mean squared error, RMSE</i>					
calibration	5.14	0.77	1.05	1.27	0.38
validation	6.87	0.99	1.22	1.36	0.47
overall	6.16	0.91	1.17	1.33	0.44
<i>Correlation coefficient, ρ</i>					
calibration	0.97	0.97	0.88	0.95	0.96
validation	0.88	0.91	0.83	0.83	0.96
overall	0.93	0.93	0.85	0.89	0.92
<i>Nash-Sutcliffe coefficient, R^2</i>					
calibration	0.93	0.32	-2.83	0.31	0.69
validation	0.72	-0.47	-1.57	-0.81	0.85
overall	0.86	-0.11	-1.62	-0.14	0.76
<i>Coefficient of gain from daily mean, DG</i>					
calibration	0.90	0.06	-8.49	0.05	0.57
validation	0.57	-1.09	-3.73	-1.31	0.78
overall	0.81	-0.44	-3.49	-0.38	0.69

The flow hydrograph of the Somme resulting from the validation run is shown in Fig. 5.30. The better fit in the calibration period can be observed easily. The flow hydrographs for the tributaries of the Somme are provided in Fig. A. 6. It is recognized that the Nièvre is below the observation line whereas the Avre and the Selle are above which means that the water balance is not satisfied in their subcatchments.

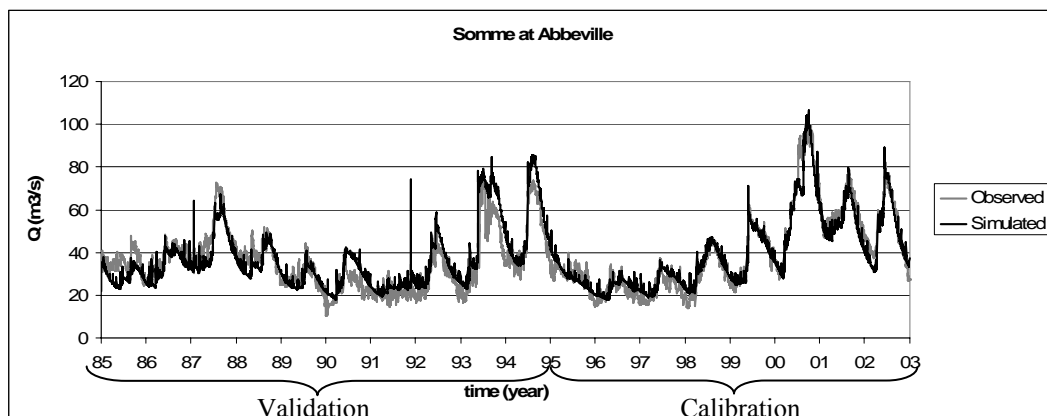


FIG. 5.30 Flow hydrograph of the Somme gauged at Abbeville (5560 km²) including the validation period.

5.5.2. Computation of Initial Piezometric Head Distribution

NEWSAM is the module run after the partition of rainfall between infiltration and surface runoff by MODSUR. After daily infiltration values are calculated for every surface cell, a steady-state piezometric head distribution can be obtained so as to constitute the initial condition of MODCOU. As the result serves as an initial condition, NEWSAM is run in steady-state mode by averaging the infiltration values calculated for every time step.

The transmissivities were initially obtained by multiplying the groundwater thickness by the hydraulic conductivities which are defined on 5 different zones by BRGM (Fig. 5.19). Afterwards, they were calibrated to fit the observed piezometric levels. As the values of transmissivity were modified during calibration, the initial piezometric head distribution was also modified. Here, two of the results are presented; the distribution with the initial transmissivity values (Fig. 5.31) and the distribution with the values obtained after the calibration (Fig. 5.32). As can be observed in these figures, the highest value in the south-western portion decreases from 200.5 m to 194.8 m. This decrease is not limited to that portion only. There is a general decline in the piezometric head, in particular, in the subcatchments of the Avre, the Selle, the Nièvre and the Hallue. This can be recognized by considering the gap between two isolines. As the gap expands, groundwater table becomes milder and therefore the maximum value on the peaks decreases. This is an indication of a general increase in the values of transmissivity.

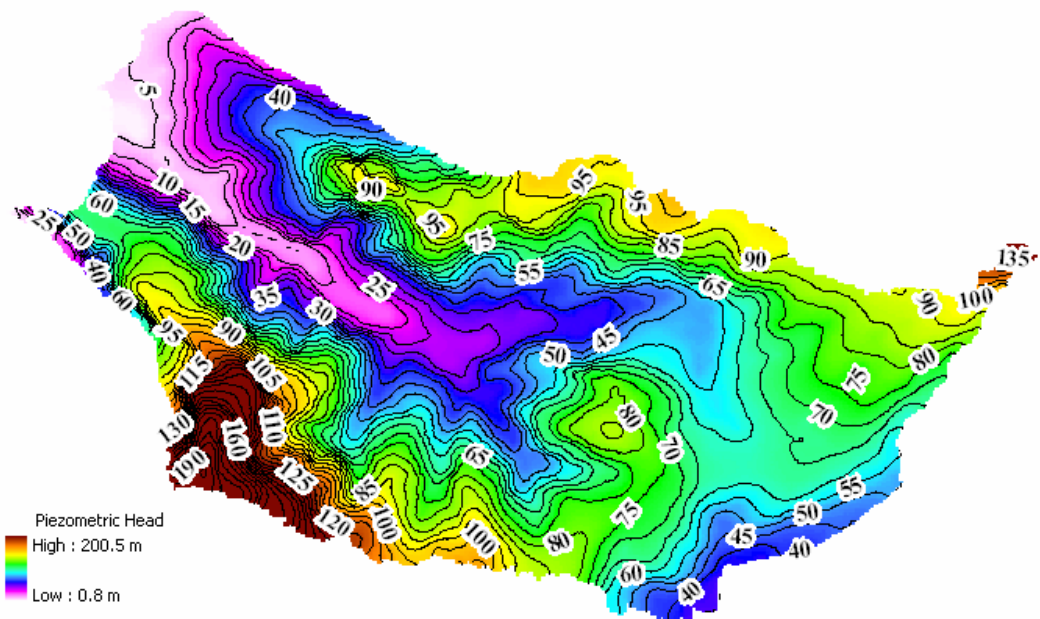


FIG. 5.31 Piezometric head distribution before the calibration of transmissivities.

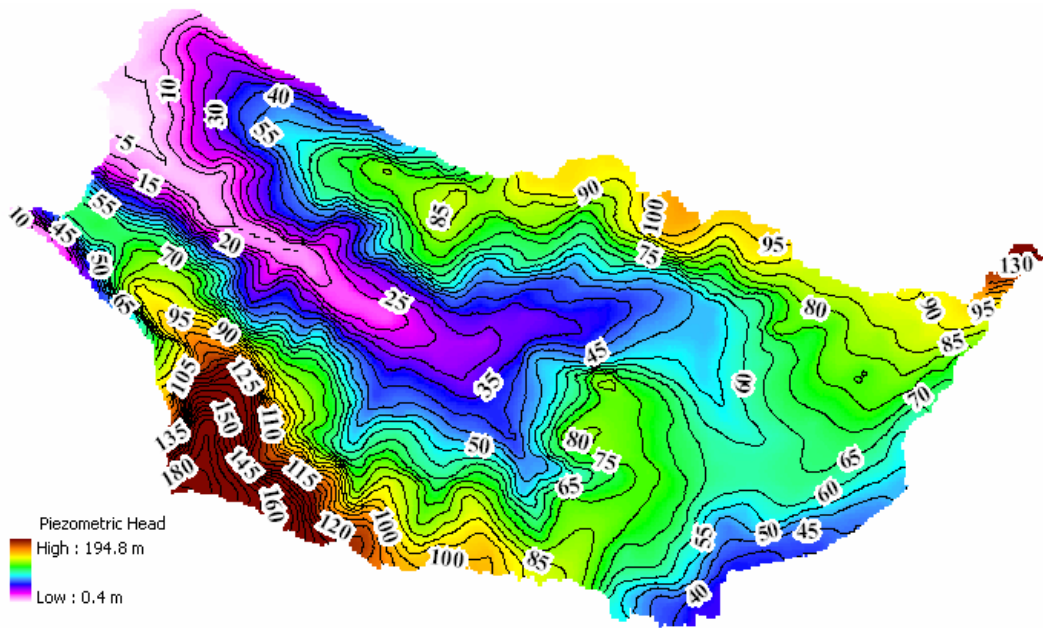


FIG. 5.32 Piezometric head distribution after the calibration of transmissivities.

The details of calibration of transmissivity is explained in MODCOU as aquifer parameters are calibrated by comparing time-dependent observed piezometric heads with simulated ones.

5.5.3. Simulation of Surface and Groundwater Flows

The unsteady simulation of surface and groundwater flows by considering their interaction was performed by MODCOU. The necessary input data are as follows; the daily surface runoff values arriving at each river cell (from MODSUR), the daily values of groundwater recharge (from NONSAT), an initial piezometric head distribution supplied by NEWSAM, transmissivity, specific yield, pumpage rate, maximum infiltration rate, and streambed conductance.

As output, MODCOU gives daily flowrate values for each streamgage station and for outlets of the rivers defined on the boundaries of the basin, daily piezometric head values in up to 50 locations inside the domain, and the piezometric head value at every grid cell in the end of each year.

As obtaining the best fit requires the calibration of all the parameters of a model, the calibration was made step by step. Before finalizing the calibration of a parameter, other

parameters were also adjusted. Therefore, in order to obtain the best fit, reasonable values for each parameter were determined by trial-and-error. Many combinations of values for these parameters are possible, however, the aim is to select a set of reasonable values among those.

Simulations of MODCOU began with the adjustment of parameters concerning stream-aquifer interaction. In order to enable overflowing of groundwater onto the surface, every grid cell of the aquifer layer was marked as a source by allocating a streambed conductance value of $C_{riv} = 0.1 \text{ m}^2/\text{s}$. For the actual river cells the maximum infiltration rate, Q_{max} , was set to $1.E-3 \text{ m}^3/\text{s}$ in order to enable a two-way stream-aquifer interaction. However, Q_{max} , was set to 0. for those marked as source cells and re-infiltration from the surface to the aquifer was avoided. Therefore, in these cells once the groundwater exfiltrates onto the surface, it can not re-infiltrate until reaching a river cell. After these modifications the calibration was performed.

First Step: Initial calibration of transmissivity

In the first step, the transmissivity values were calibrated to a certain degree which means that in further stages one other elaborate calibration was also performed. The highest and the lowest initial values were accepted as limits and were not passed. The simulated piezometric head values were compared with the observed ones. In 41 out of 50 locations improvement in the fit has been observed. On the other hand, a slight loss of fit was observed for the flows in the Nièvre and the Hallue, while a better fit was seen in the Avre after this calibration. The values of root mean squared error (*RMSE*) of the piezometric heads before and after this calibration in these 50 locations are shown in Fig. 5.33.

A visual interpretation of the results of this initial transmissivity calibration can be seen in Fig. 5.34. In this figure, circles of two different sizes representing the Nash-Sutcliffe coefficients are superimposed. Larger circles represent initial values and smaller ones on top of them represent the values after calibration. According to these, an improvement is observed in the downstream portion of the aquifer on both sides of the Somme such that values higher than 0.3 were attained in 4 locations. Other improvements are observed in the northern and eastern portion, especially in the subcatchment of the Avre. Whereas, poor fits still exist in the central, southern and northeastern portions of the basin.

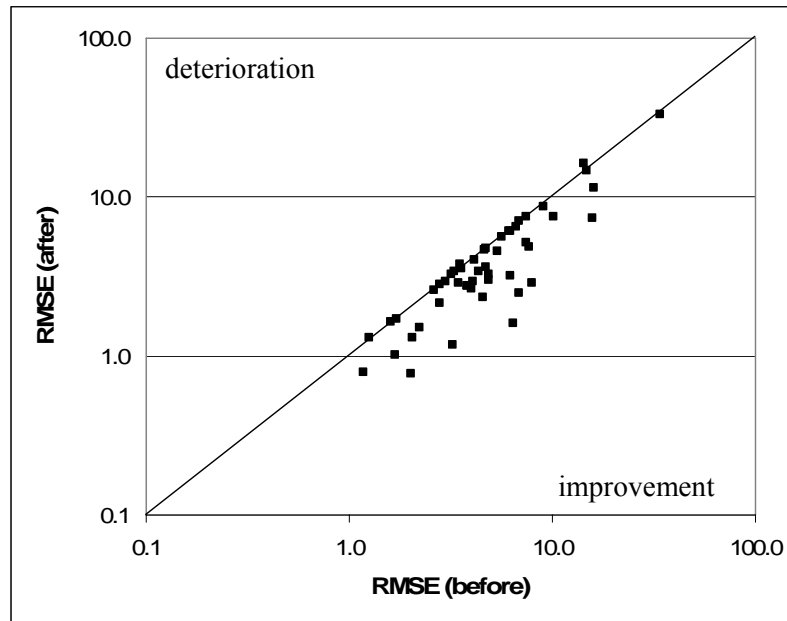


FIG. 5.33 The values of root mean squared error ($RMSE$) for piezometric heads before and after the initial calibration of transmissivities.

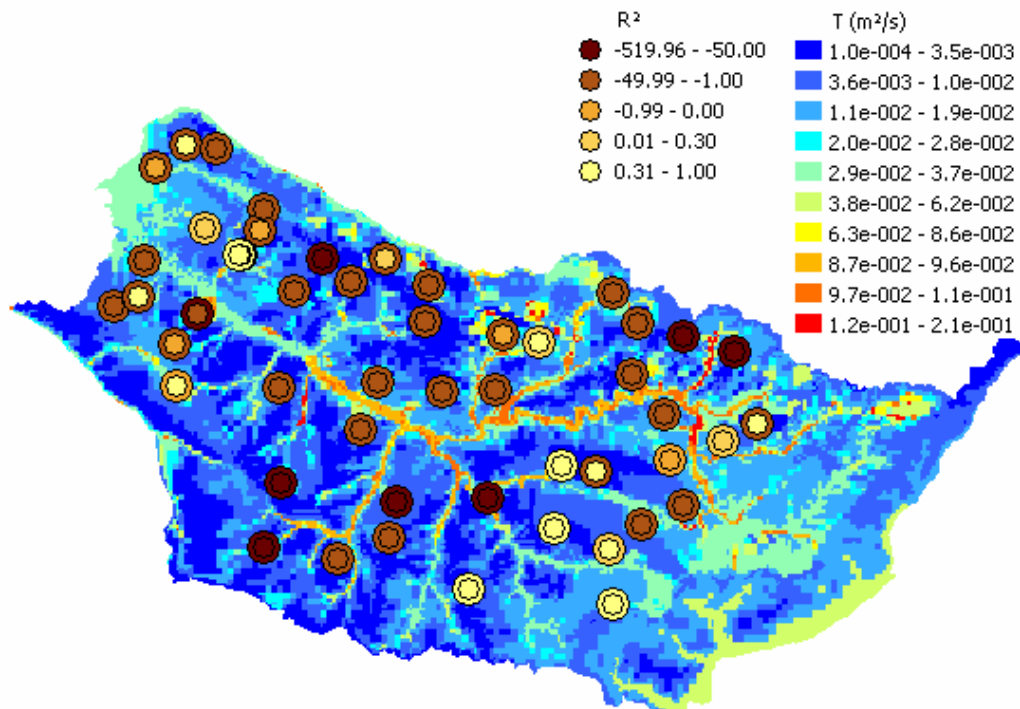


FIG. 5.34 The Nash-Sutcliffe coefficients (R^2) before and after the calibration of transmissivities.

Second Step: Initial calibration of specific yield

Second, a rough calibration of specific yield (S_y) was performed. The initial values were supplied in three zones by BRGM and were composed of approximate values (Fig. 5.17).

As the first zone seemed to be abundant and have a considerably low value, the values less than 0.018 were multiplied by 2 to observe the effect of specific yield on the piezometric surface. The root mean squared error (*RMSE*) values before and after this change are shown in Fig. 5.35. In this calibration improvement in the fit was observed in 37 locations which proves that initial values were low. However, this was a very rough calibration which had to be taken back in further stages.

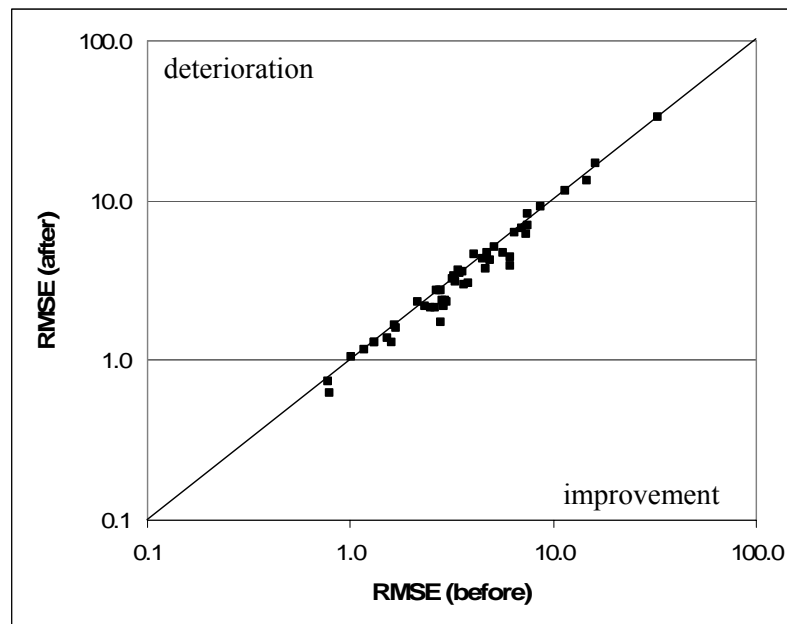


FIG. 5.35 The root mean squared error (*RMSE*) values of piezometric heads before and after the modification in specific yield.

Third Step: Topographic correction

A topographic problem was discovered, such that, due to inaccuracy of the DEM, in a given flow direction some neighboring cells downstream of a cell had higher elevation than the cell being considered. This problem was discovered after visualizing the total flooded volume in each cell in one year. The groundwater flooding onto the surface was found to be high in quantity and interrupted in spatial extent. For this reason, a correction consisting of two steps was applied. In the former step, a ‘fill’ algorithm was developed and applied to the whole domain. A ‘fill’ algorithm is in fact one of the initial stages of a DEM analysis. It is used to get rid of the sinks in a raster topographic map. Therefore it was applied to the elevation file. The algorithm of the code developed through current study is as follows:

1. Find the slopes in 4 directions.

2. If the maximum of slopes is negative then it is a single cell sink and raise the cell up to the elevation of the lowest neighbor.
3. If the maximum of slopes is zero then it is a part of a flat area. Search the neighboring cells having the same elevation for a *flat area id*, if they already have a *flat area id*, give the current cell the same id. If they do not, assign a new id. Also calculate the size of each flat area.
4. In case there appears to exist neighboring flat areas with different ids, combine them.
5. If an exit with a lower elevation is encountered then the flat area is a non-sink flat area. Erase the *flat area id* of non-sink flat areas.
6. Find and apply the lowest rise necessary for remaining flat areas.
7. Check the number of flat areas to which a rise is applied. If it is more than one, go to step 3.
8. Give the output elevation file.

After the application of the code, the maximum rise applied was 9.4 m and the mean rise in the basin was 0.029 m. This is visualized in Fig. 5.36.

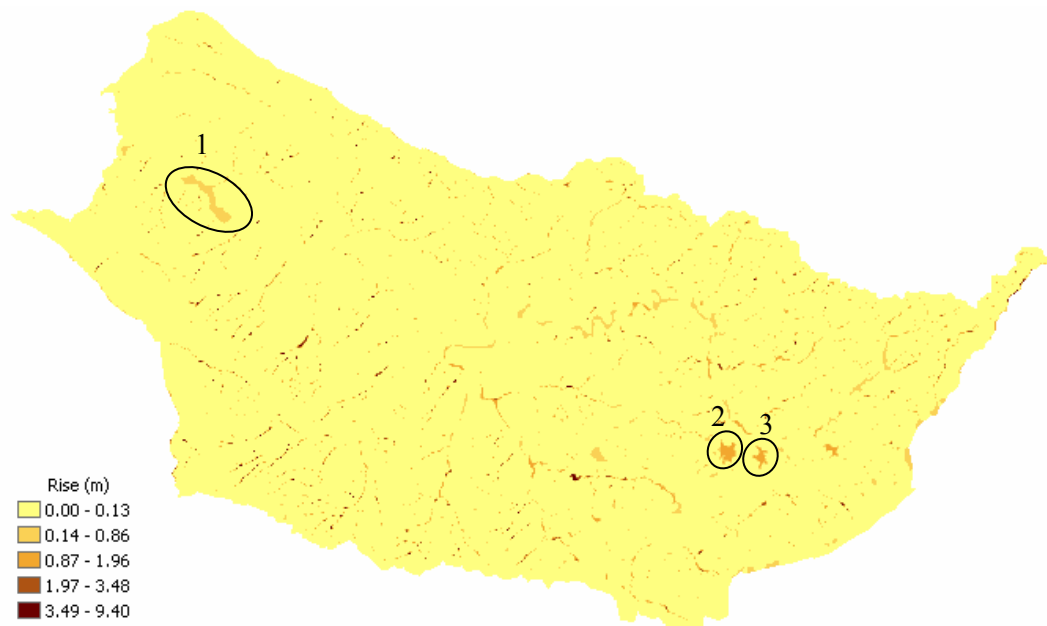


FIG. 5.36 The rises applied to the elevations with the application of ‘fill’ procedure.

The rises are observed about everywhere inside the basin. Three major groups are easily recognized. The first one is in the downstream portion of the basin and a rise of 0.16 m was applied. The second and the third groups are in the upstream portion of the basin, and respectively, rises of 1.08 and 1.52 m were applied. These are group of cells all flowing

through the same downstream cell which has a higher elevation than all the cells in the group. The program raised the elevations of all the cells in those groups in order to maintain an uninterrupted streamline.

In the latter step of the corrections, the elevations of the river cells were slightly modified. There were two reasons for this correction. First, as mentioned before, the flooding of groundwater onto the surface was high, because the drainage supplied by the stream network was not enough. Second, the direction of the flow exchange between river and aquifer cells was interrupted. The reason was that the vertical flow was continuously changing direction such as from river to aquifer and from aquifer to river. In order to overcome this situation, a modification in the elevations of the river cells was made. This was achieved with the help of another code developed through current study, of which the algorithm is as follows:

1. Every source, junction and outlet on the stream network is marked on the surface mesh manually.
2. Program scans the surface mesh from top left corner to bottom right corner. When it encounters a source or a junction, it records the elevation and begins to go downstream by using the flow directions until it reaches a junction or an outlet. There, it stops and records the second elevation. These values represent the upstream and downstream elevations of a reach.
3. The difference of elevations is divided by the length followed and an average slope for that reach is obtained.
4. This time, calculation is made in upstream direction by calculating elevations corresponding to the average slope line. If the current elevation is of the cell above the new elevation then the new elevation is assigned to the cell. If not, then the elevation of the cell remains the same.
5. The treated reach is marked, and step 2 is resumed until all the reaches are marked as treated.

This procedure is schematized in Fig. 5.37 in which bold arrows represent the interrupted groundwater exfiltration and thin arrows represent the reduction of elevations above the average slope line. In the second part of the figure, dashed lines represent the piezometric head of the groundwater where a less interrupted exfiltration is assured. This was a reasonable correction, because the resolution of the DEM is 125 m and it is very probable

to have measured the bank elevations and assumed them as river elevations. Therefore, the error was assumed to be only in positive direction in altitude and a reduction procedure was applied.

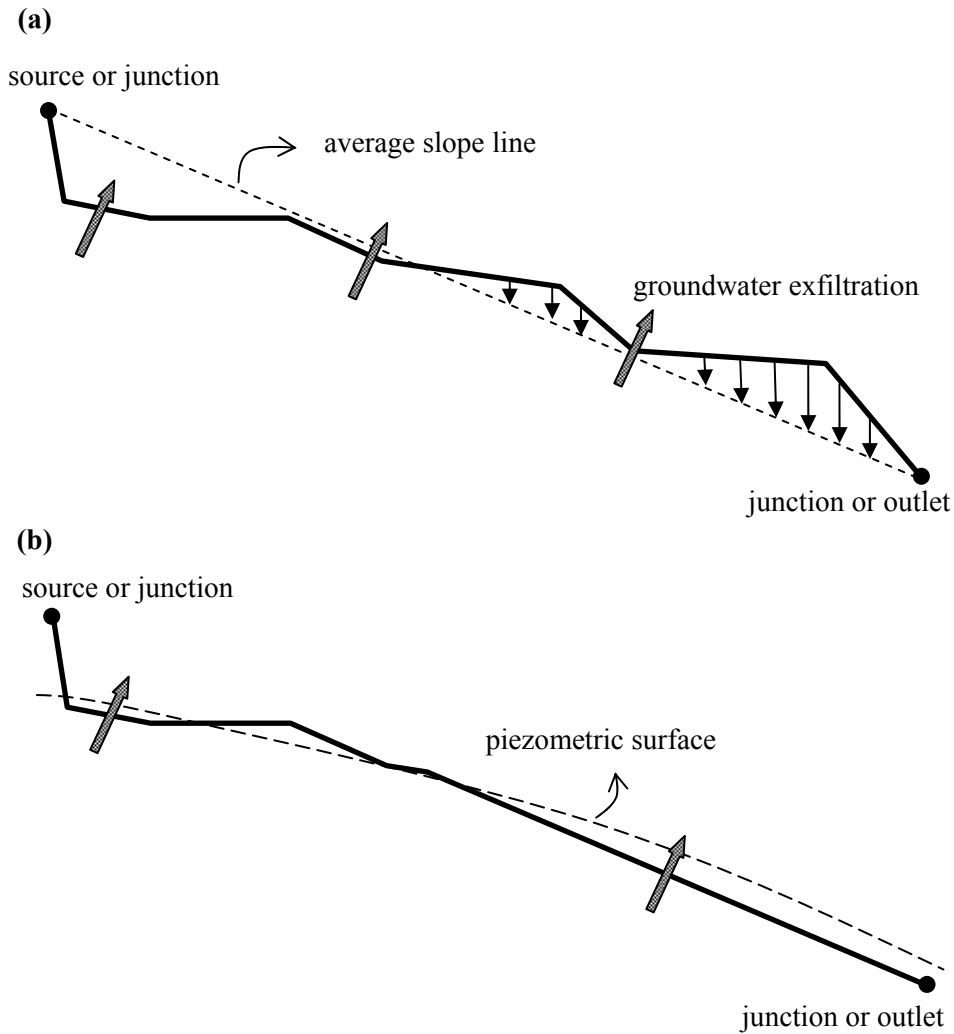


FIG. 5.37 Modification of river elevations in a cross-sectional view; **a)** application of average slope line, **b)** modified elevations.

The effect of these corrections can be observed by visualizing the cells at which groundwater has overflowed to the surface in year 2001. In Fig. 5.38, three figures from the center of the basin are shown. The first one corresponds to the result obtained with initial elevations. The overflowing locations are interrupted and the thickness of the blue lines represent that overflowing is not limited to river cells. In some places it occurs several kilometers away from the river. This is an indication of that river is not draining the groundwater enough.

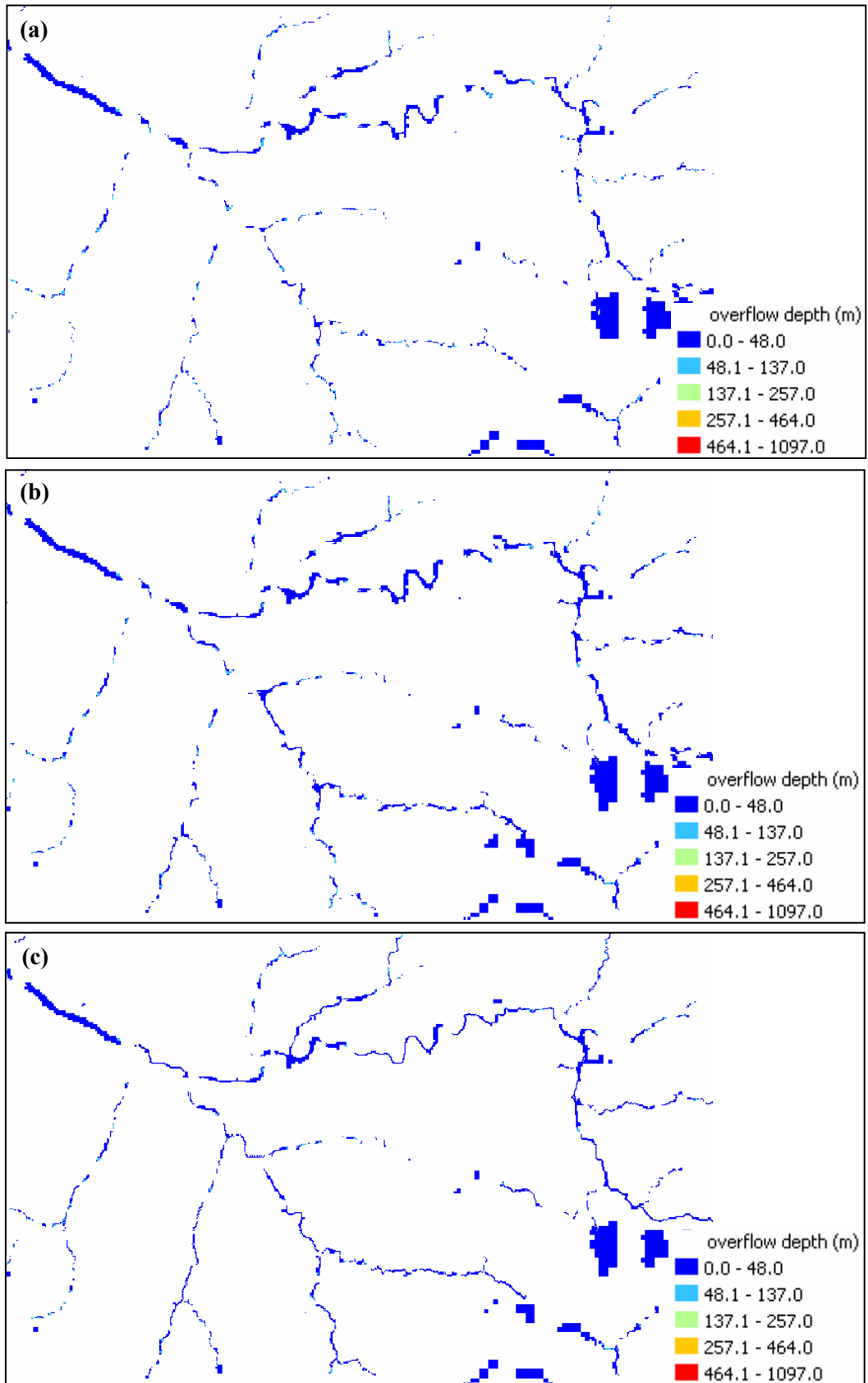


FIG. 5.38 Overflow depth in the center of the basin in year 2001; **a)** initial elevations, **b)** after the application of 'fill' procedure, **c)** after correction of river elevations.

In the second part of the figure, the result after the application of 'fill' procedure is shown. It can be observed that overflowing has even more dispersed, because by the application of 'fill' procedure the elevations of the pits were raised everywhere inside the basin including the river cells and therefore drainage by rivers got weaker. In the third part of the figure, the effect of river elevation modifications can be easily recognized. Blue lines are more continuous and at the same time they are thinner. This means that vertical flow exchange does not change direction as often as in previous cases, and moreover, groundwater overflow is more limited to riverbeds than its surroundings.

In Fig. 5.39 the upstream portion of the Somme and the Ancre tributary is seen. The river cells of which the elevations were corrected are marked by transparent boxes. In the first part, the overflow map before the correction is shown. The boxes are mainly empty because they represent the river cells having elevations above the average slope line and therefore overflowing is not abundant in those cells. On the other hand, in the second part, the situation after the correction is observed. Overflowing takes place on the corrected river cells, therefore, it is more continuous and less widespread as the river drains the groundwater better.

The result of this modification can also be explained with values as in Table 5.5. These values are presented in two formats; namely, as volume exchanged in year 2001, and as depth exchanged which was obtained by dividing the volume exchanged by the surface area of the basin. The total sums are almost the same and in favor of overflow (exfiltration) with a value of $3.22E+09 \text{ m}^3$ or 0.39 m. With the application of 'fill' procedure surface overflow reaches the highest value and river overflow decreases to the lowest value. As the elevations of river cells are at maximum, overcharged groundwater reaches the surface through surface cells instead of river cells. This situation is reversed with the application of river elevation corrections where the river overflow reaches its highest value and surface overflow to its lowest.

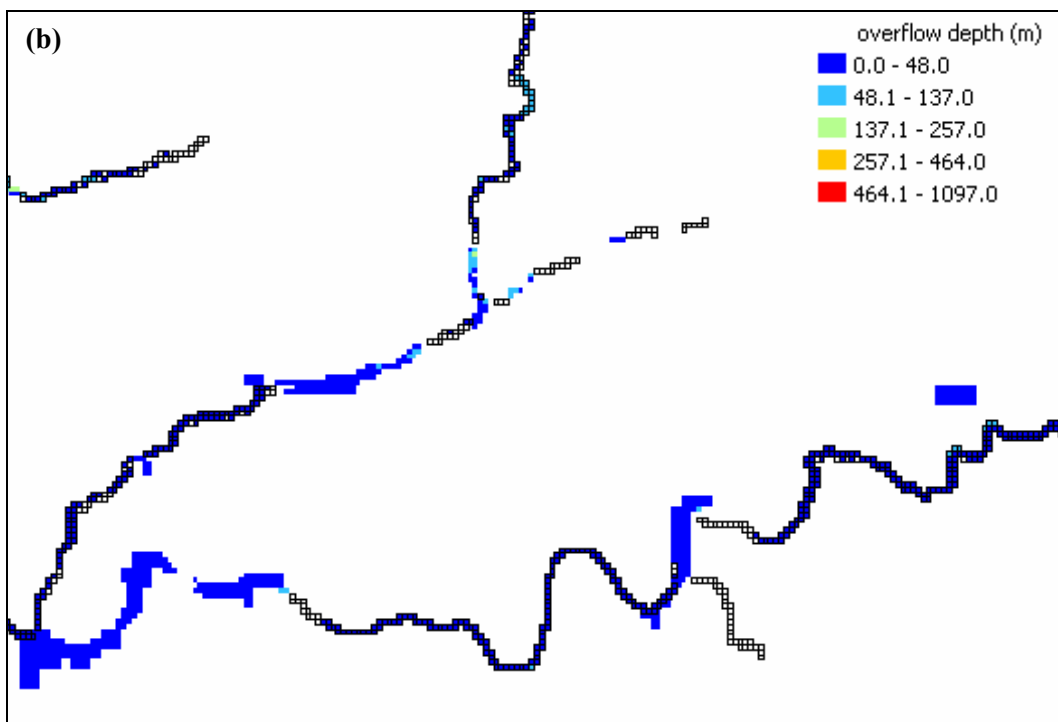
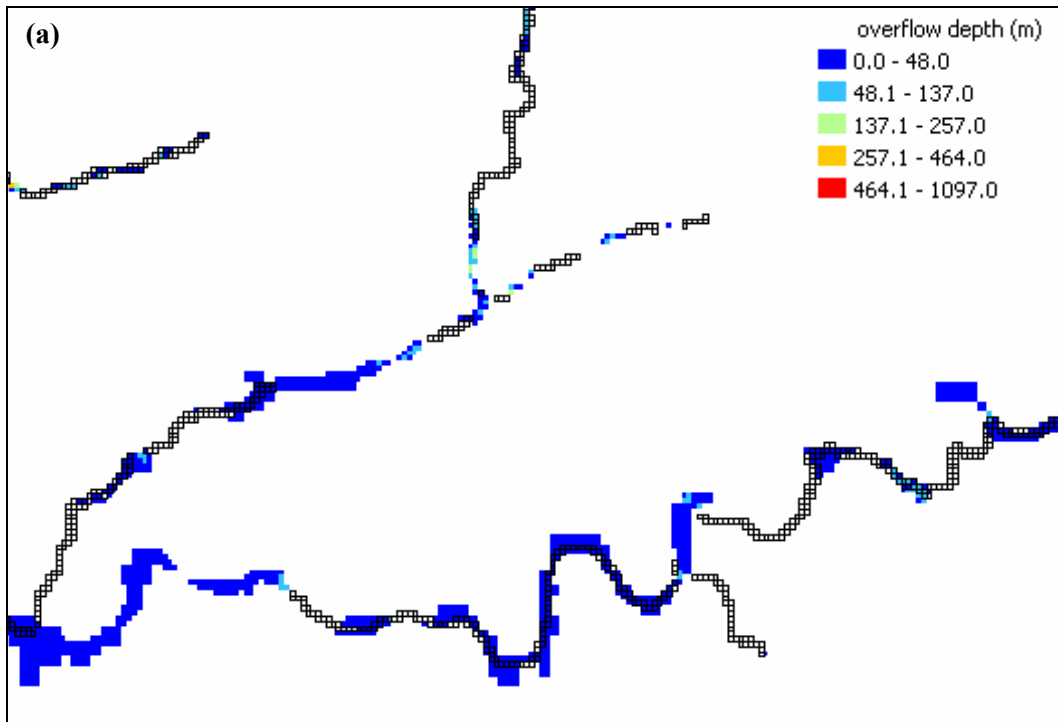


FIG. 5.39 The effect of river elevation corrections on overflow depth and extent; **a)** before correction, **b)** after correction.

TABLE 5.5 The effect of ‘fill’ procedure and river elevation corrections on the groundwater and surface water exchange in year 2001.

Area = 8205.25 km ²	initial	‘fill’	‘fill’+correction
surface overflow (m ³)	1.07E+09	1.22E+09	9.97E+08
river overflow (m ³)	2.34E+09	2.16E+09	2.36E+09
river infiltration (m ³)	-1.98E+08	-1.66E+08	-1.31E+08
river sum (m ³)	2.14E+09	1.99E+09	2.22E+09
total sum (m ³)	3.21E+09	3.22E+09	3.22E+09
surface overflow (m)	0.130	0.149	0.121
river overflow (m)	0.286	0.263	0.287
river infiltration (m)	-0.024	-0.020	-0.016
river sum (m)	0.261	0.243	0.271
total sum (m)	0.391	0.392	0.393

Fourth Step: Re-assumption of initial specific yield values

In this step, the initial values of specific yield were re-assumed. As mentioned in step 2, a rough calibration that caused an increase in the lowest values of specific yield was performed. Contrarily, this time a slight decline in the root mean squared error (*RMSE*) values of piezometric heads was observed (Fig. 5.40). However, the simulated flows of the Somme at Abbeville, the Nièvre and the Hallue improved. Actually, this was rather a transition to the initial state of specific yield in order to carry out a reasonable calibration in the following step.

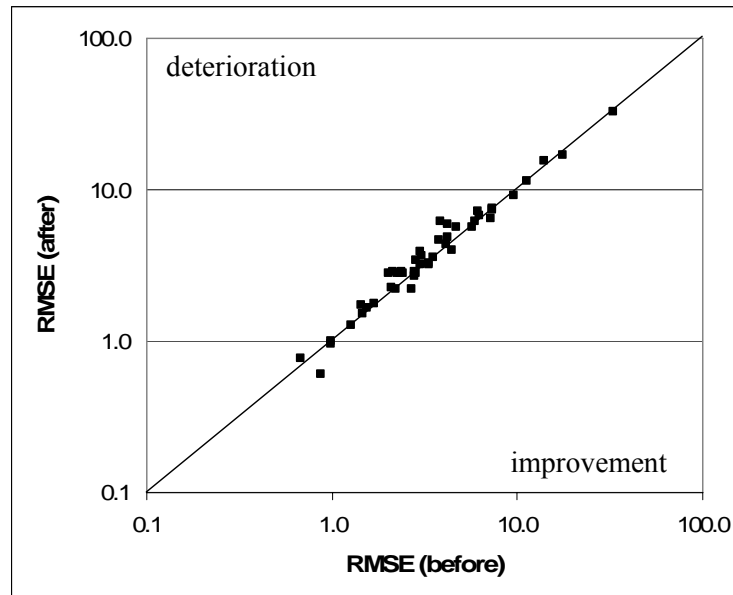


FIG. 5.40 The root mean squared error (*RMSE*) values of piezometric heads before and after the re-assumption of initial specific yield values.

Fifth Step: Final calibration of specific yield

In the fifth calibration step, specific yield values were calibrated regionally and not globally. This means that in each run, the values of specific yield in only one or two locations were altered, and in addition, these were selected in regions that do not belong to the same subcatchment. Otherwise, it is almost impossible to distinguish the effect of each calibration on the piezometric head, whether positive or negative. For example, if two locations in the same subcatchment are calibrated and an improvement in the piezometric heads or in the flow hydrograph is observed, there are three possibilities. First, calibration of the first location might have affected positively and that of the second location negatively. Second, calibration of the first location might have affected negatively and that of the second location positively. Third, calibration of both locations might have affected positively.

The locations subject to calibration were chosen mainly in relation with the piezometric head observation points and also less often in relation with locations of streamgage stations where piezometric head observations were not provided. As a result, in almost every location of calibration, an increase in specific yield value had to be made in order to obtain good fits between the simulated and the observed values. Finally, an improvement in piezometric head fits in 42 locations out of 50 was observed. In Fig. 5.41, the root mean squared error (*RMSE*) values of piezometric heads are presented.

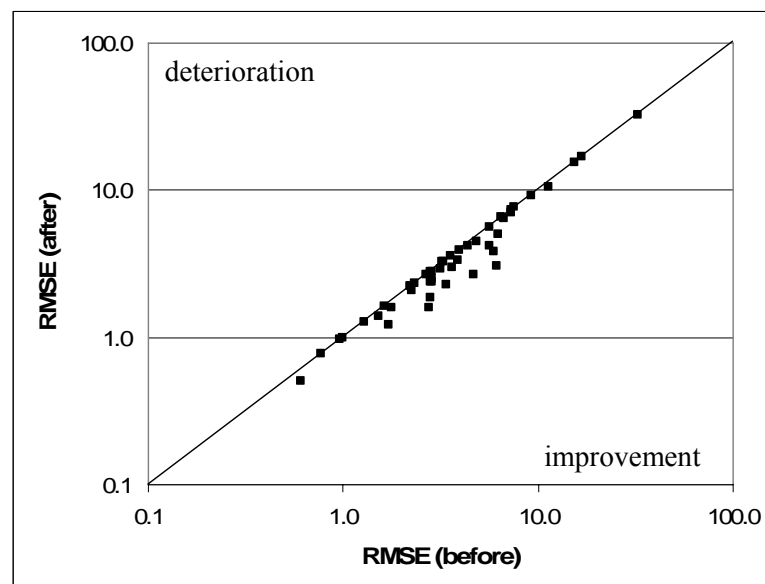


FIG. 5.41 The root mean squared error (*RMSE*) values of piezometric head fits before and after the calibration of specific yield values.

The final values of specific yield are presented in Fig. 5.42. Specific yield represents the storage capability of the aquifer. Therefore, different values mean different storage capabilities. As can be seen in the figure, a wide range of values varying between 0.0150 and 0.0864 are observed. In the areas where small values are observed, the aquifer is less capable of holding water, therefore in these areas short-term fluctuations are easily observed in piezometric head graphs. These fluctuations represent the storage difference between dry and pluvial months of a year. On the other hand, in the areas where large values of specific yield are observed, there are only long-term fluctuations which represent major storage differences between dry and pluvial years. In these types of areas, the effects of short-term events are not clearly observed, and in some cases, even the effects of long-term events are hardly recognized.

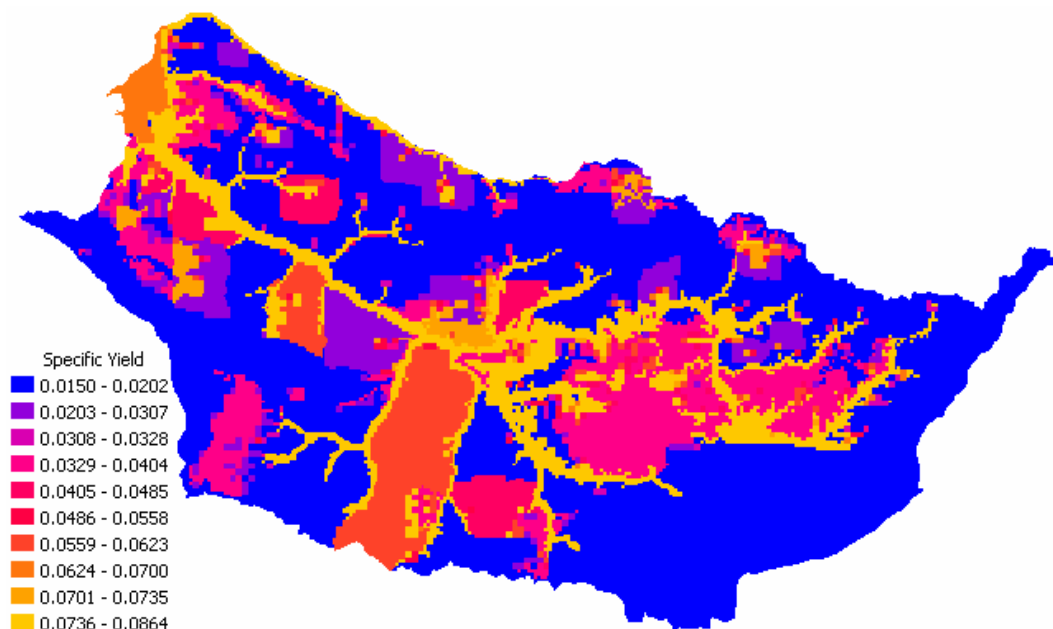


FIG. 5.42 Final values of specific yield.

When Fig. 5.42 is compared to Fig. 5.20, a considerable increase in specific yield values is easily recognized. In the region on the east side of the Selle, the values were increased by 4 times, that is, from 0.015 to 0.060 all the way from the river to the impervious boundary in the south. The values in small portions in the west of the Avre and on both sides of the Hallue were increased by about 2 or 3 times. On the other hand, the values in the region between the upstream portion of the Somme and the Avre were not altered much as there were already good fits of piezometric head in that region. Beginning from the confluence with the Hallue, small increments are observed on both sides of the Somme towards downstream direction until reaching the outlet. In addition to these, a

general widening of the largest values situated mainly on the rivers and riverbanks is observed. The reason is that when the initial values of specific yield supplied by BRGM (Fig. 5.17) were superposed with the stream network of the present model, it was observed that the large values were shifted aside. In order to make these values correspond to the stream network and maintain continuity in specific yield values, the zones having the largest values were slightly widened.

The short-term and long-term variations mentioned above can be observed in Fig. 5.43. In this figure, piezometric head variations concerning observation well numbered 0335x0005 are shown. Before the calibration there are two types of fluctuations. The one with the smaller amplitude represents the short-term or annual fluctuation, whereas, the one with the larger amplitude represents a long-term fluctuation of which the wavelength is variable. After the calibration, the specific yield value around that region was increased by about 3 times the initial value. This increment caused the amplitude of all fluctuations to diminish and the *RMSE* to decrease from 1.72 to 1.21 m. As shown, specific yield affects the amplitude of fluctuations but not the vertical position of the piezometric surface. Vertical correspondence between the observed and simulated values is sought by transmissivity calibrations.

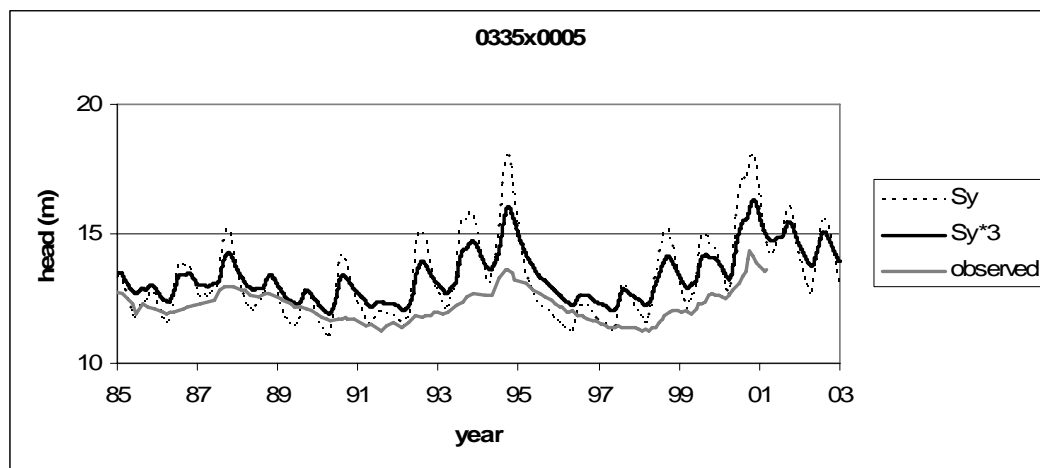


FIG. 5.43 The piezometric heads before and after the calibration of specific yield for the well 0335x0005.

Another example for specific yield calibration can be given regarding the observation well numbered 0625x0002. In Fig. 5.44, a major difference between the behaviors of simulated and observed heads are recognized. While the observed head exhibits more or less a stable behavior, the simulated head exhibits both long-term and short-term

fluctuations. Moreover, the amplitudes of the both fluctuations are highly remarkable. During calibration, the specific yield value in that region was multiplied by 4 which caused attenuation in the fluctuations and the *RMSE* value decreased from 6.11 to 3.03 m. Hence, a better fit was obtained by increasing the specific yield value. As there was not a considerable vertical difference between the observed and simulated heads, calibration of transmissivity was not performed on this region.

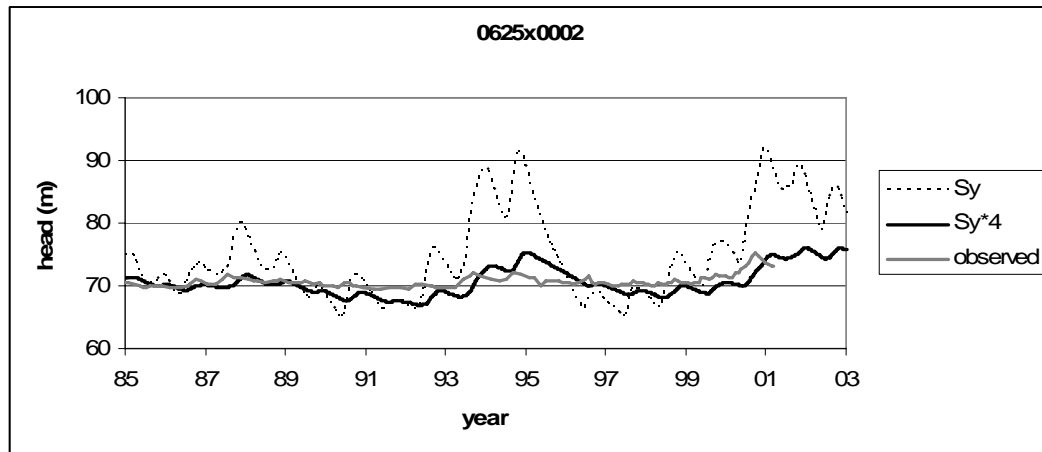


FIG. 5.44 The piezometric heads before and after the calibration of specific yield for the well 0625x0002.

The improvement with the calibration of specific yield values is visualized in Fig. 5.45.

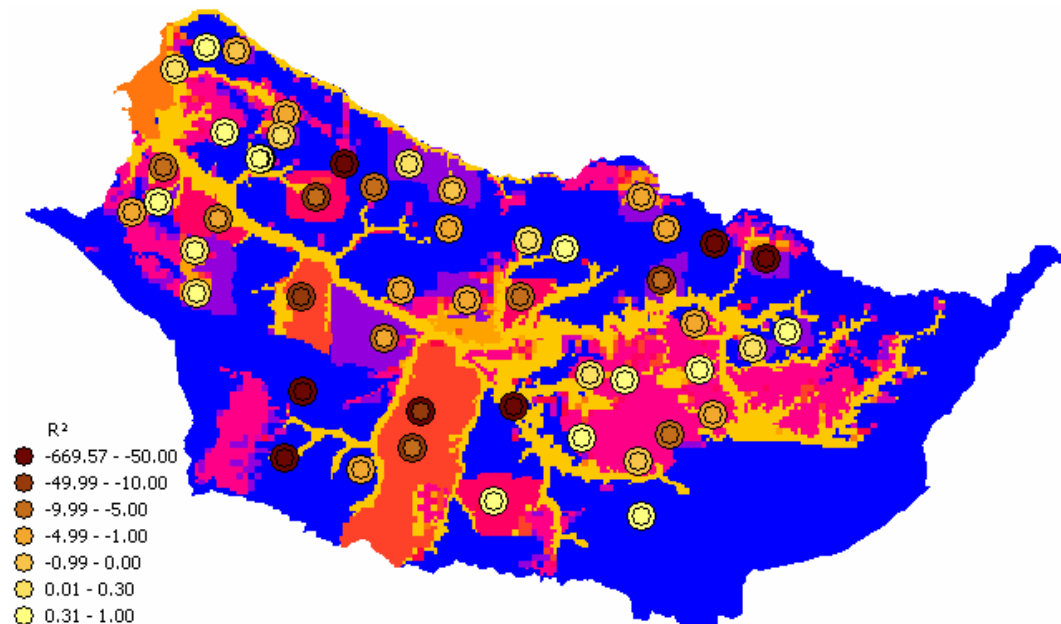


FIG. 5.45 The Nash-Sutcliffe coefficients for piezometric head fits before (outer circles) and after (inner circles) the calibration of specific yield.

In this figure outer circles represent the values before calibration and the inner circles represent the values after calibration. The biggest improvements are observed in the downstream portion of the Somme and in the subcatchment of the Selle. A slighter improvement occurs in the upstream portions of the Somme.

Sixth Step: Final calibration of transmissivity

In the sixth calibration step, transmissivity values were calibrated for the second and the last time. This was a rather detailed calibration, performed both in a regional and global scale. As it constituted one of the last steps of the whole modeling process, goodness of fit was looked for not only in piezometric heads but also in flow hydrographs.

The locations of calibration were initially chosen around the piezometric observation wells and where satisfactory results could not be obtained, a larger selection was made. The larger selection included areas mainly in the upstream or downstream portions of a river, particularly, those of a tributary. As a result, water balance between the subcatchments could be partially controlled. Satisfying the water balance of a subcatchment means to have a good correspondence between the observed and simulated flowrates. The reason is that flowrates are usually measured at a point close to the outlet of a tributary. Therefore having a good fit of flow hydrographs means that the correct amount of water is contained in the subcatchment. Until this step, this had been an unresolved issue especially for the tributaries. As can be observed in Fig. A. 1 to Fig. A. 6, there is a difficulty in obtaining good fits. The reason is that a detailed and regional calibration of production function in MODSUR was not possible because the production zones are scattered to such an extent that every zone could be found in any part of the basin and changing the parameter regarding a zone had a global effect. In addition, MODSUR was the first model to be calibrated and it would be unreasonable to seek a good fit in all of the flow hydrographs. Thus, at that stage a rough calibration was performed by considering the goodness of fit mainly in the flow of the Somme at Abbeville which has a catchment area of 5560 km². Until this point, satisfactory results for the flowrate fits could not be obtained for the tributaries other than the Hallue.

The values after the transmissivity calibration are shown in Fig. 5.46. When compared to Fig. 5.34 a considerable difference is easily recognized. The modifications were made in about everywhere inside the basin.

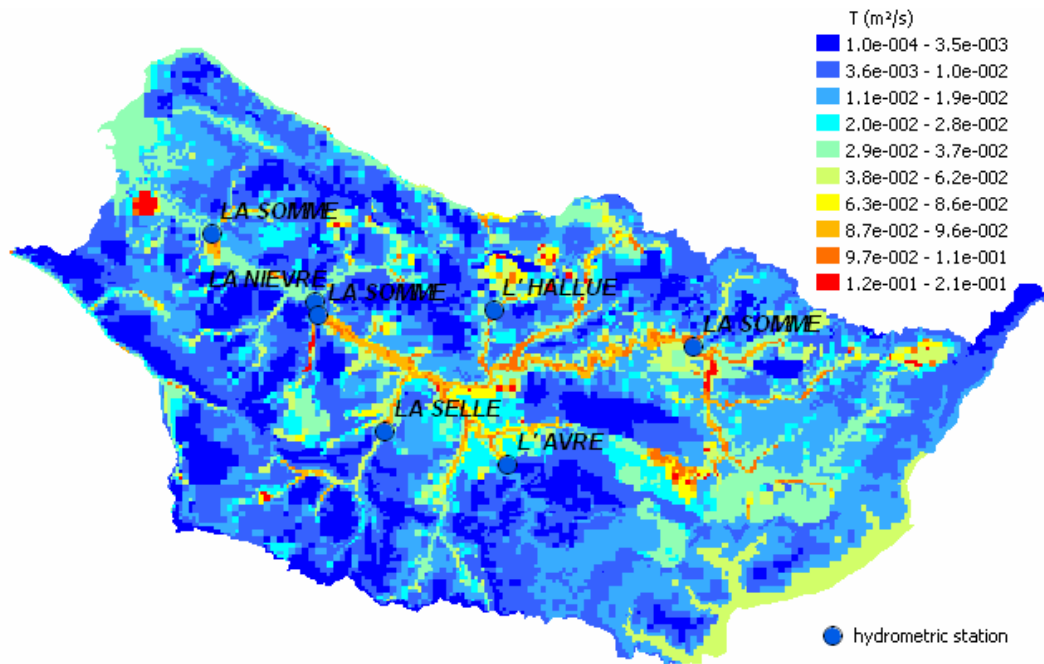


FIG. 5.46 The final transmissivity values.

A major calibration was realized in the subcatchment of the Avre and the Selle. Because when the flow hydrograph of the Avre and the Selle were considered, the simulated flows and thus the amounts of water were well above the observed values. As observed in Fig. 5.46, a general reduction in the transmissivity values was applied inside both subcatchments and increments were applied to the portions immediately downstream of the gauging stations and also to the portion located north-east of the Avre subcatchment and both sides of the Selle subcatchment. This is a method followed to adjust the water balance or piezometric surface of a region. The reduction of transmissivity inside an area causes the groundwater to move slower and the groundwater table to curve outward like a mound due to recharge. If the modification is left here, there might be an increase in the piezometric heads inside the region because of this mound. However, if the transmissivity of the surrounding regions is increased, there will be a sharp interface between the two regions and the region with higher transmissivity will drain the other one (Fig. 5.47). This modification causes an area to lose water to surrounding areas. Therefore, it is used to adjust the piezometric head at a point as well as the water balance of an area. At this interface, a decline in the groundwater table is observed. If the point considered is at this interface, its piezometric head will decrease. If a flowrate measurement is performed at point *P*, a reduction of flowrate due to the decline in the baseflow will be observed. If an

inverse modification is made, then the piezometric head or the flowrate of stream will increase.

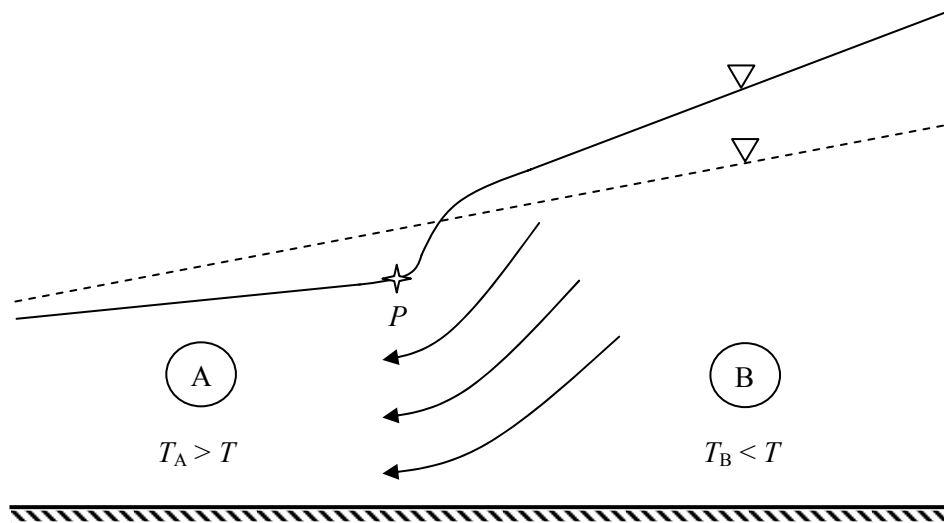


FIG. 5.47 The effect of transmissivity modification; dashed line represent the initial water table in which $T_A = T_B = T$, continuous line represent the water table after the modification.

In the case regarding the Avre and the Selle, this method was used to diminish the simulated flowrates. With the calibration, a considerable reduction in baseflow is observed in both hydrographs. The improvement in the flow hydrographs of the Avre and the Selle can be seen in Fig. 5.48 and Fig. 5.49 respectively.

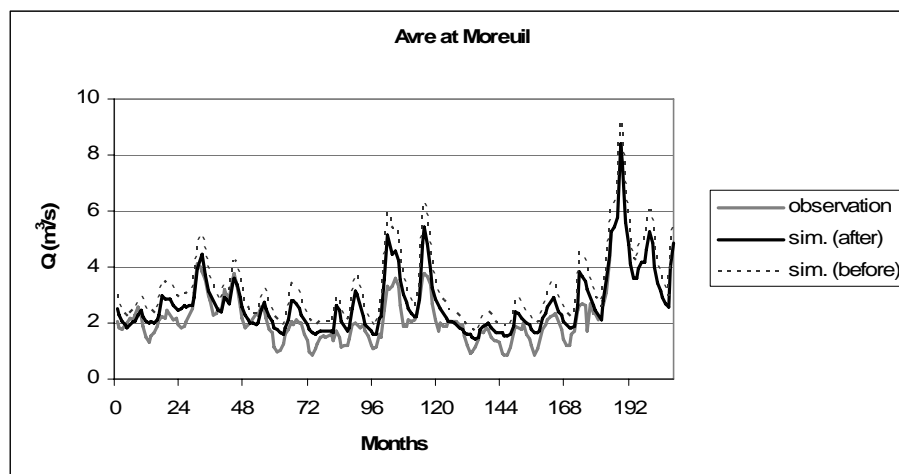


FIG. 5.48 Monthly flowrate of the Avre before and after the calibration of transmissivities.

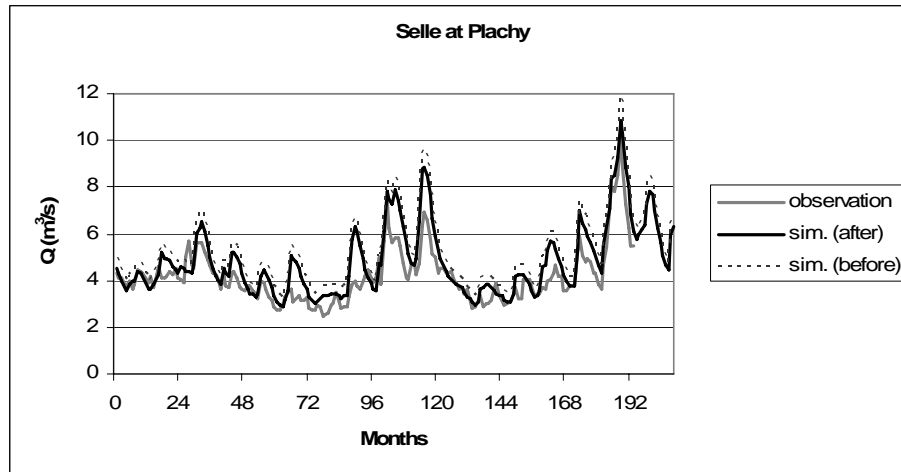


FIG. 5.49 Monthly flowrate of the Selle before and after the calibration of transmissivities.

After this calibration, the ratio of mean flows decreased from 1.44 to 1.21 for the Avre and from 1.23 to 1.12 for the Selle, and the Nash-Sutcliffe coefficient increased from -0.83 to 0.35 for the Avre and from 0.04 to 0.51 for the Selle.

As an example to piezometric head adjustments, observation well numbered 0613x0012 can be considered (Fig. 5.50).

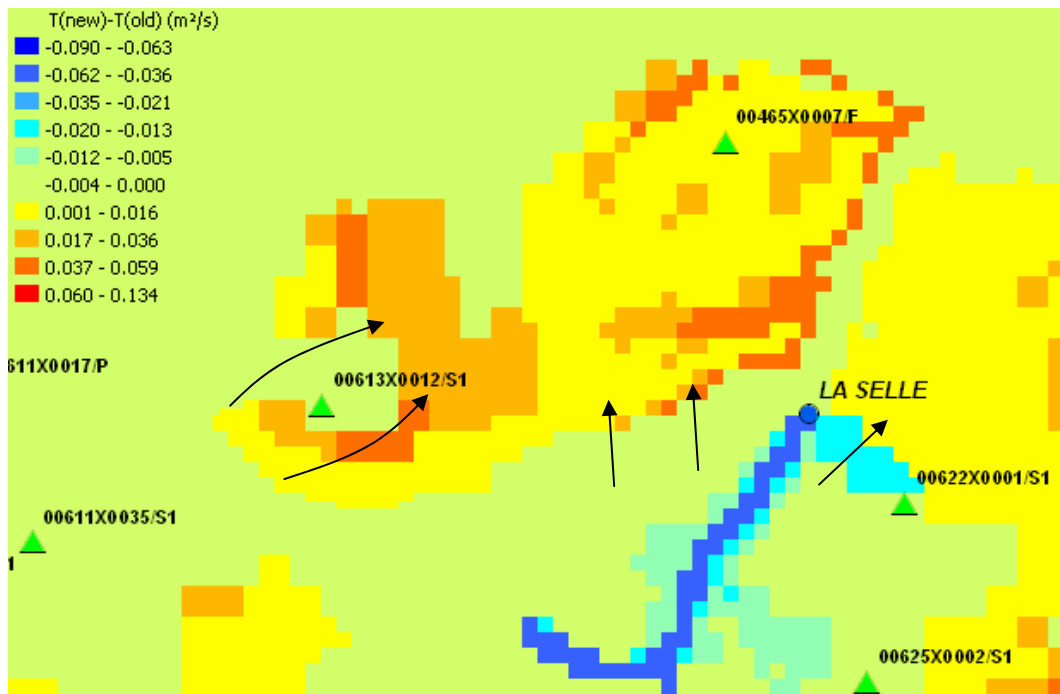


FIG. 5.50 The difference between the final and the previous transmissivity values, and approximate flow directions.

In Fig. 5.50, it is observed that the transmissivity values in the surrounding region of the observation point were increased while the values in the close vicinity were not changed. The estimates of flow directions are also shown in this figure. The flows coming from the upstream bend away from the observation well and approach to each other again at the downstream of the well. The reason is that the high transmissivity eases the flow of water while low transmissivity hinders it. In the same figure, the situation of the Selle described above can also be observed. Decrease of transmissivity along the streambed and increment in the surrounding regions causes the groundwater to flow away from the subcatchment.

In Fig. 5.51, the change of piezometric level at the well 0613x0012 can be seen. With the modification, the mean of the simulated head decreases from 104.14 m to 90.53 m while the mean of the observed head is 90.12 m, whereas the Nash-Sutcliffe coefficient increases from -573.53 to -85.95. This was a point which was difficult to calibrate. Contrary to the modifications in the specific yield it was not possible to obtain the same trend. The reason may be due to the scarcity of the measurements, that is, there were a total of 205 measurements supplied in the period April 25, 1995 – September 27, 2001 which means almost 6.5 years. The frequency of readings varies from once a month in the first years to 4 times a month in the last years. Therefore, it is probable to have missed the fluctuations. As a close mean in the piezometric head was obtained, the calibration was left at this point.

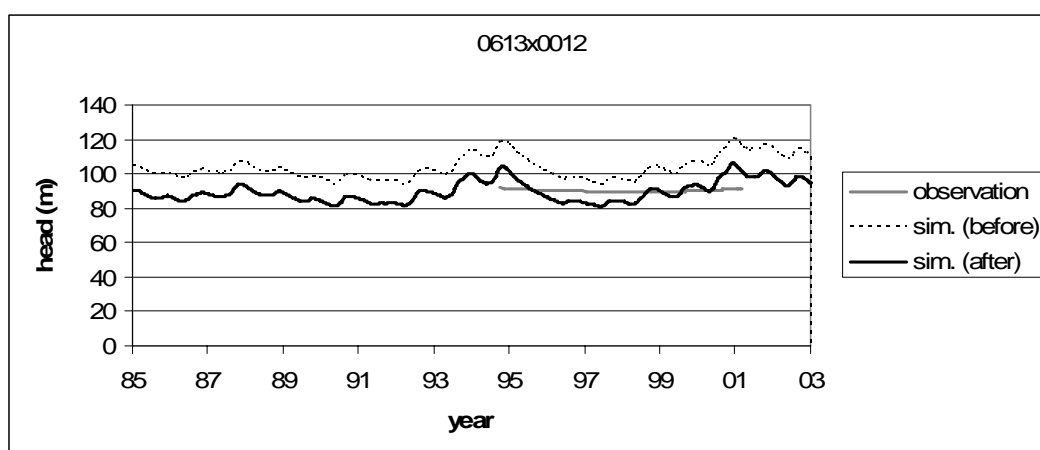


FIG. 5.51 The piezometric head at the point numbered 0613x0012 before and after the calibration of transmissivities.

Other examples of transmissivity calibration can be given for the observation wells numbered as 0474x0011 and 0478x0002. The difference between the last and the previous transmissivity values are shown in Fig. 5.52. For the well 0474x0011, a decrease in the region from around the well to the upstream and an increment in the downstream portion were made.

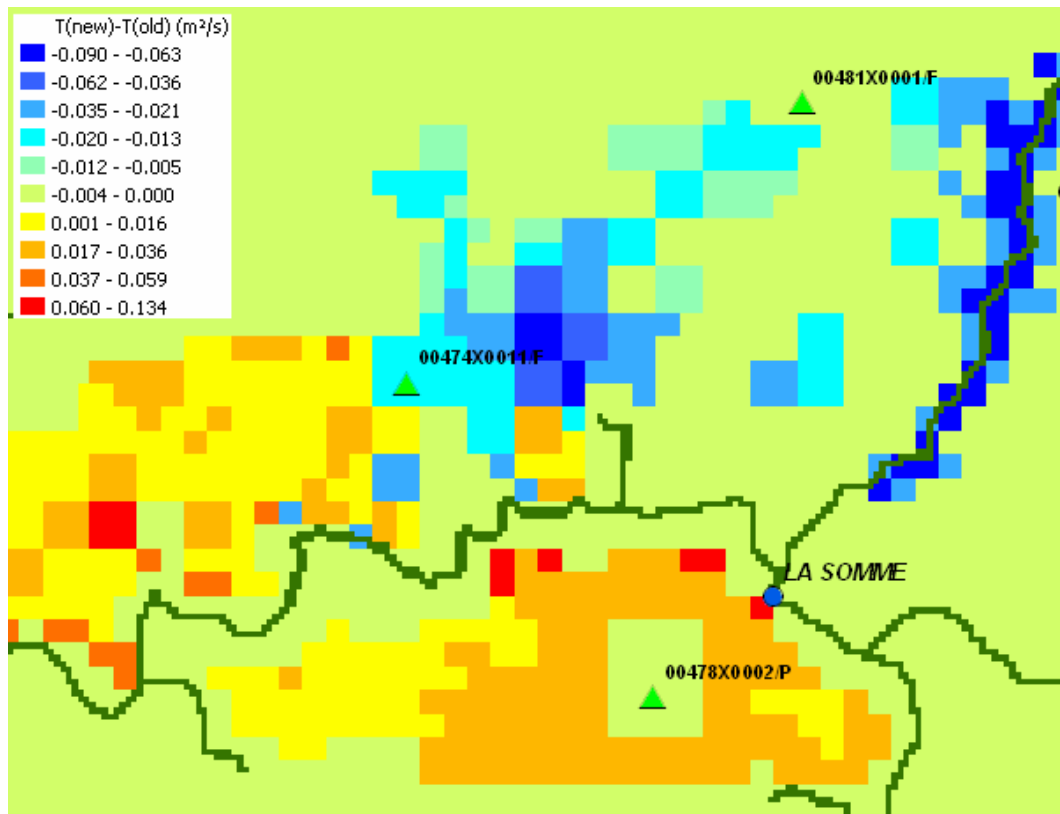


FIG. 5.52 The difference between the final and the previous transmissivity values.

As for the well 0478x0002, increments were made all around the well and the values in the close vicinity of the well were not modified. An increment for those was also tried. However, this caused to an attraction of water from the surrounding cells and therefore the simulated piezometric head was increased further instead of decreasing. The improvements in the piezometric head hydrographs of the wells 0474x0011 and 0478x0002 can be observed in Fig. 5.53.

The cases described above proves that simple rules usually employed in one-dimensional (1D) groundwater problems, such as ‘*increasing transmissivity decreases the piezometric head*’ do not always hold true because in a 1D flow problem the aquifer characteristics are assumed to be the same and extend to infinity in the direction perpendicular to the

flow. However, in a more realistic problem the aquifer characteristics are heterogeneous in both directions and there is no such thing as infinite horizontal extent. In conclusion, the fact that ‘*increasing transmissivity may drain water from the surrounding area*’ should also be taken into consideration during the calibration of a region.

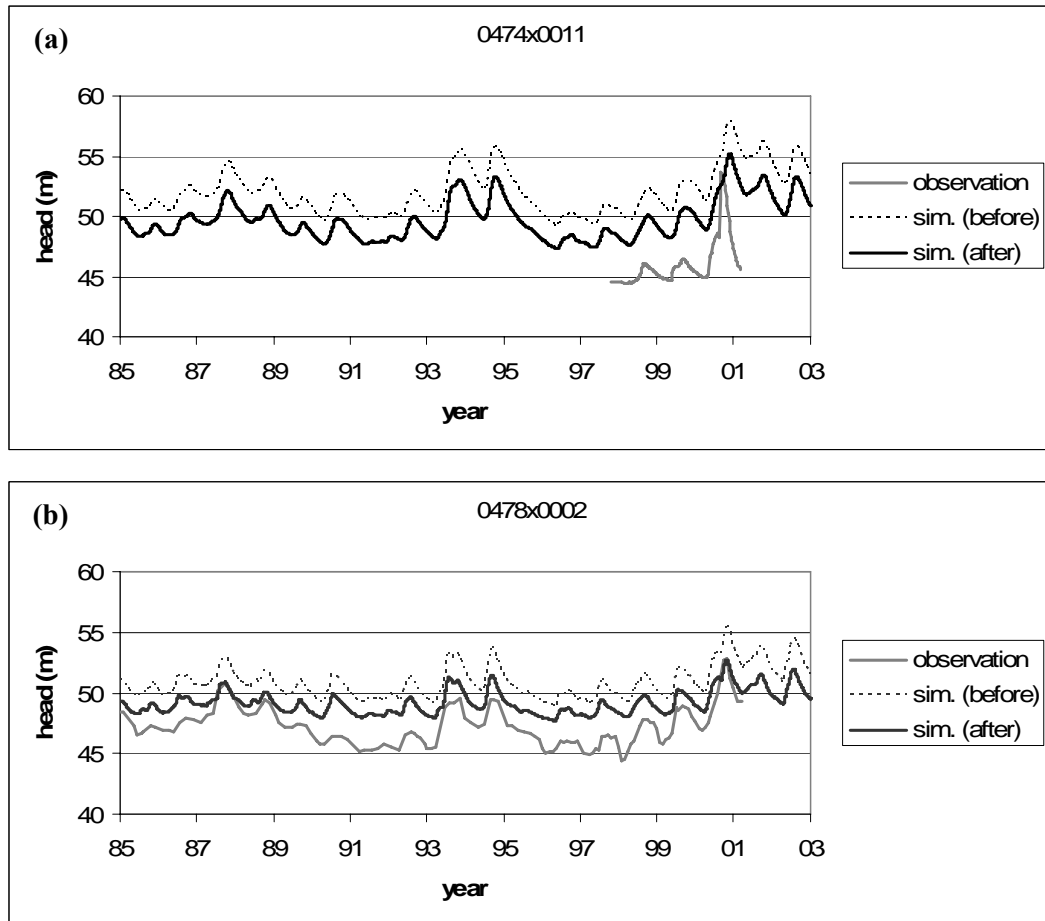


FIG. 5.53 The piezometric head hydrographs of a) 0474x0011 and b) 0478x0002 before and after the calibration of transmissivities.

Consequently, improvements in 37 of the piezometric heads and in flow hydrographs of 3 tributaries, namely, the Nièvre, the Avre and the Selle were observed (Fig. 5.54). However, there was a loss of fit in several piezometric head observation points in the subcatchment of the Nièvre. The reason is that the runoff volume of the Nièvre was underestimated and in order to increase this volume, increments in transmissivity values were made in the upstream portion of the subcatchment and this gave rise to a decline of head in that portion. Nevertheless, the Nash-Sutcliffe coefficient of the Nièvre increased from -0.20 to 0.35 with this modification which rendered it reasonable.

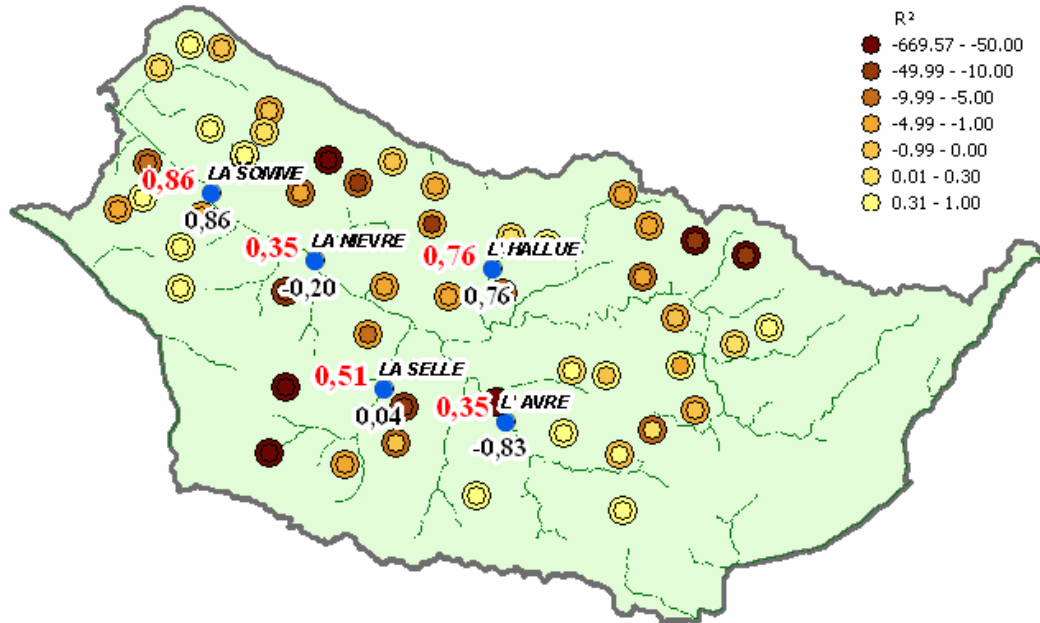


FIG. 5.54 The Nash-Sutcliffe coefficients for piezometric heads before (larger circles) and after (smaller circles) the calibration; and for flowrates before (values in black) and after (values in red) calibration.

In Fig. 5.55, the improvement in the piezometric head fits can be observed in a graphical form. Major improvements were realized in some problematic points while in a few locations a loss of fit took place due to the reason explained above. In addition, minor adjustments can also be observed from the figure.

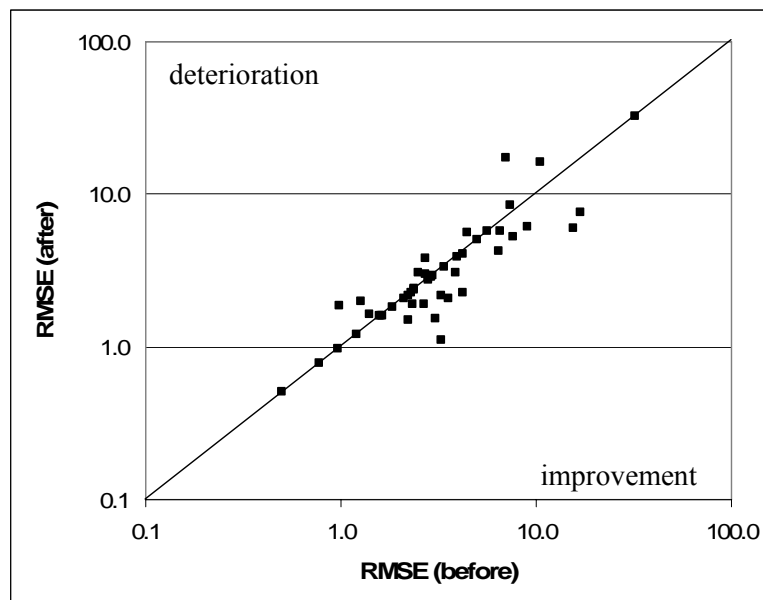


FIG. 5.55 The Nash-Sutcliffe coefficients of piezometric head fits before and after the calibration of transmissivities.

Seventh Step: Calibration of discharge coefficient

In this step, the discharge coefficients, Cd , of river cells were calibrated. It is a parameter controlling the discharge from a river cell to the neighboring downstream cell. It is formulated in Eq. (3.38). While calculating the surface flow transfer, MODCOU divides the stream network into segments according to the concentration time of the basin. The discharge from one segment to the downstream segment is controlled by the discharge coefficient of the segment, which is the smallest of the discharge coefficients of river cells falling in that segment. This surface flow computation is described by Eq. (3.31).

So far, a value of 0.99 was used for all the river cells in the stream network. In order to see the effect of this parameter on the flowrates, various values of Cd were initially assigned to every river cell individually and several test simulations were performed. The tested values are 0.70, 0.55 and 0.40. The effect of each value on the Nash-Sutcliffe coefficients is illustrated in Fig. 5.56. The Hallue, the Avre and the Selle were positively affected by the decrease while the Nièvre lost the fit and the Somme at Abbeville remained almost the same. The optimum values for the tributaries were as follows; 0.40 for the Avre and the Hallue, 0.55 for the Selle and 0.99 for the Nièvre.

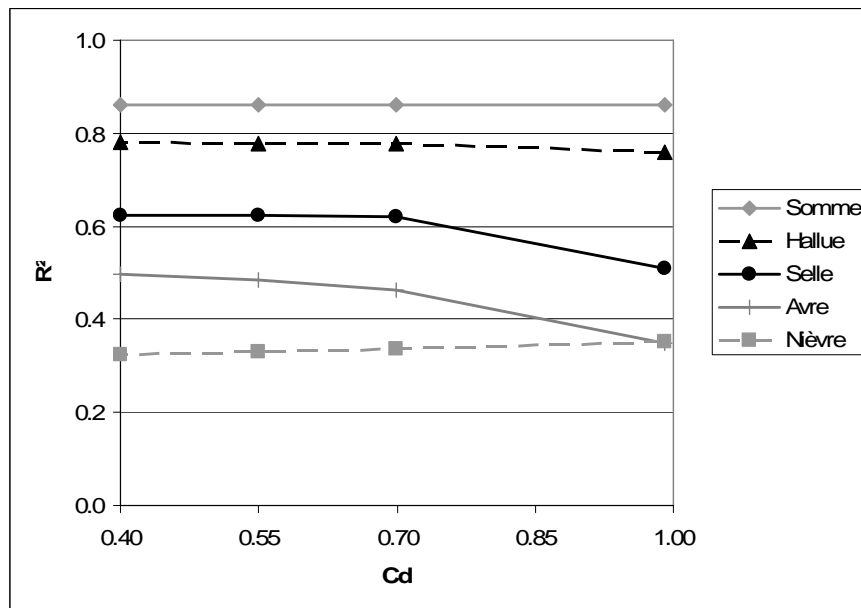


FIG. 5.56 The effect of discharge coefficient on the Nash-Sutcliffe coefficients.

Hence, in the tributaries the optimum values listed above were assigned to the river cells and for the rest of the Somme no change was made. The resulting simulation was satisfactory for all the stations except the Nièvre. Even though its coefficient was not

modified, it slightly lost the fit. The Hallue, the Avre and the Selle attained exactly the same values of R^2 as those obtained during the test (Fig. 5.56) and the value for the Somme increased from 0.861 to 0.867 while for the Nièvre it decreased from 0.352 to 0.320. A remarkable effect of this calibration was the attenuation of sudden peaks in flow hydrographs. The reason is that as the values of Cd were decreased, the discharge of flow was slowed down and the storage in the river cells was increased.

As an example the flow hydrograph of the Avre is shown in Fig. 5.57. The sharp peak observed in 1992 reduces to a value less than half of the initial value. The mean flowrate at the outlet of the Somme (6433 km²) decreased from 72.7 to 71.9 m³/s, and the water stocked in the whole stream network increased from 3.91×10^7 to 4.32×10^7 m³ in the period 8/2000 – 7/2001 with this modification. As for the piezometric heads, there was not a significant change.

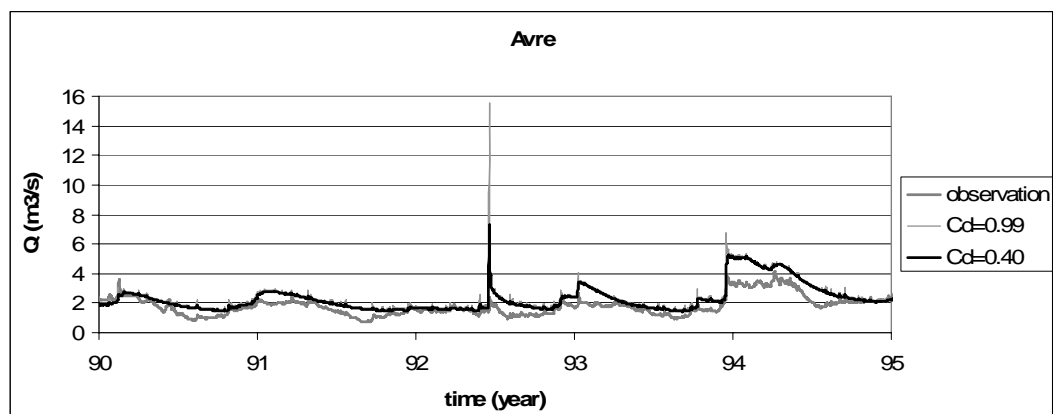


FIG. 5.57 The effect of the discharge coefficient on flow hydrograph of the Avre.

Summary of the calibration procedure:

To sum up, during the calibration of MODCOU a stepwise procedure was followed. Initially the parameters regarding the stream-aquifer interaction were adjusted. Exfiltration of groundwater was enabled in every surface cell while the infiltration of surface water was enabled only in the river cells. With this modification a stream-aquifer interaction was assured. Next, the transmissivity values were calibrated to a certain level but not finalized. In 42 out of 50 well locations improvement in the fit was observed. Afterwards, a very rough calibration of specific yield values was made. The initial values were found to be too low and thus the lowest values, which are at the same time the most abundant, were multiplied by 2. A general improvement was observed in the majority of the piezometric head fits, however, this was a very rough calibration and was taken back

later. In the following step, a topographic problem was detected, such that, along a streamline on the surface some downstream cells had higher elevations than the cell being considered. This was hydraulically impossible and caused to flooding of groundwater on the unexpected regions such as elevated plateaus. Therefore a “fill” procedure written in FORTRAN was implemented and the *sinks* in the DEM were corrected. Accordingly, a similar correction was made with regard to elevations of river cells. As the resolution of the DEM was 125 m, it was possible to have measured the bank elevations and assumed them as river elevations. This caused to an interrupted exfiltration in river cells. An average slope line, that is, an imaginary line connecting both ends of a river branch, was drawn for every single branch of river and the elevations of river cells over this line were reduced to the elevation of the line. Therefore a smoother riverbed and a more continuous groundwater exfiltration were assured. In the next step, the initial values of specific yield were re-assumed and a detailed calibration was made. In almost every region where a calibration was made the values of specific yield were increased and finally improvement in 43 out of 50 piezometric head fits was observed. This proved that initial values were really small. Later, transmissivity calibration was made for the second and the last time. As it was one of the last steps and the transmissivity was highly effective on both the piezometry and flow hydrographs, a very detailed calibration was made. The conditions about how to adjust the piezometry of a point were analyzed elaborately. Especially in the Avre and the Selle, the goodness of fit was improved substantially. In the final calibration step of MODCOU, a parameter called *the discharge coefficient* was calibrated for each tributary and as a result a satisfactory fit was obtained in the flow hydrographs.

The root mean squared error (*RMSE*) values of piezometric heads before and after the whole calibration process of MODCOU is given in Fig. 5.58. There is an improvement in almost everywhere except a few points.

The measures of error for the flow hydrographs before and after the calibration of MODCOU are depicted in Fig. 5.59. The highest improvement is observed in the Avre and then in the Selle and the Nièvre. The Somme gauged at Abbeville (5560 km²) and the Hallue improve fairly. When the deviations of runoff volume (D_v) are considered, the Nièvre underestimates the flow, whereas the Avre, and the Selle and the Hallue overestimate it. According to R^2 and DG values, the worst fit is the Nièvre while according to ρ , it is the Avre.

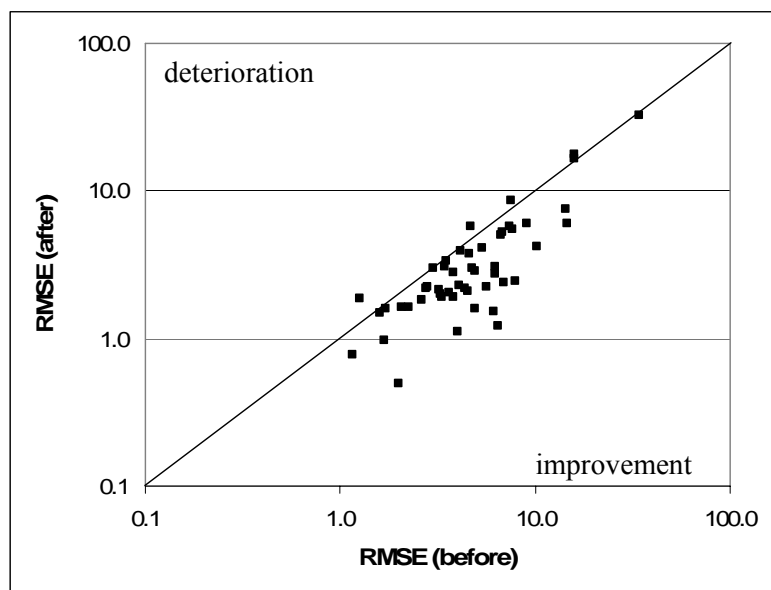


FIG. 5.58 The root mean squared error (*RMSE*) values of piezometric head fits before and after the calibration of MODCOU.

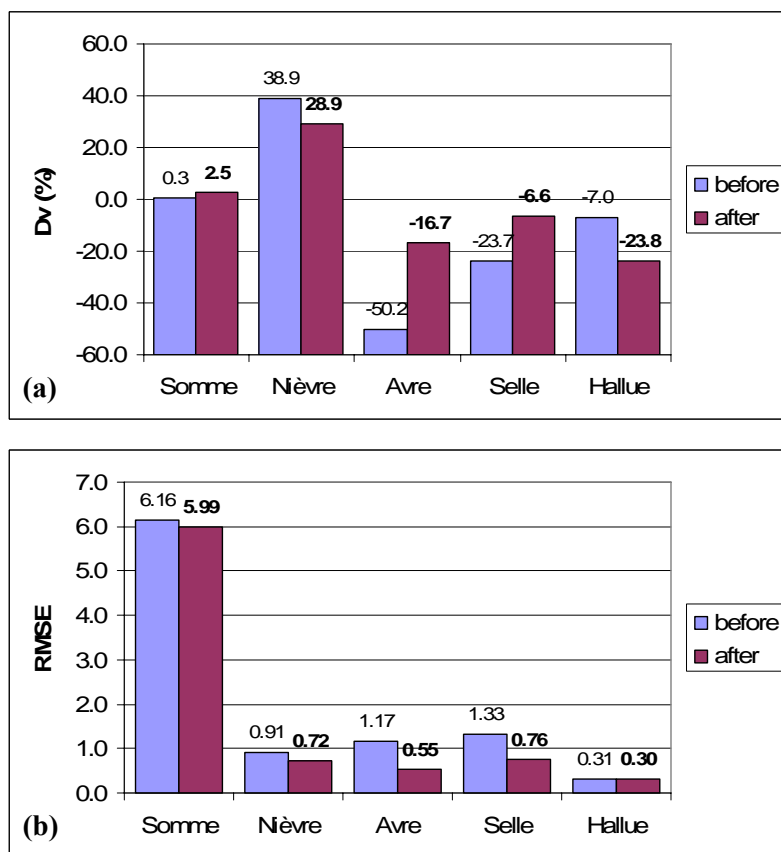


FIG. 5.59 Measures of error before and after the calibration of MODCOU; **a)** Deviation of runoff volumes (D_v), **b)** Root mean squared error (*RMSE*), **c)** Correlation coefficient (ρ), **d)** Nash-Sutcliffe coefficient (R^2), **e)** Coefficient of gain from daily mean (DG).

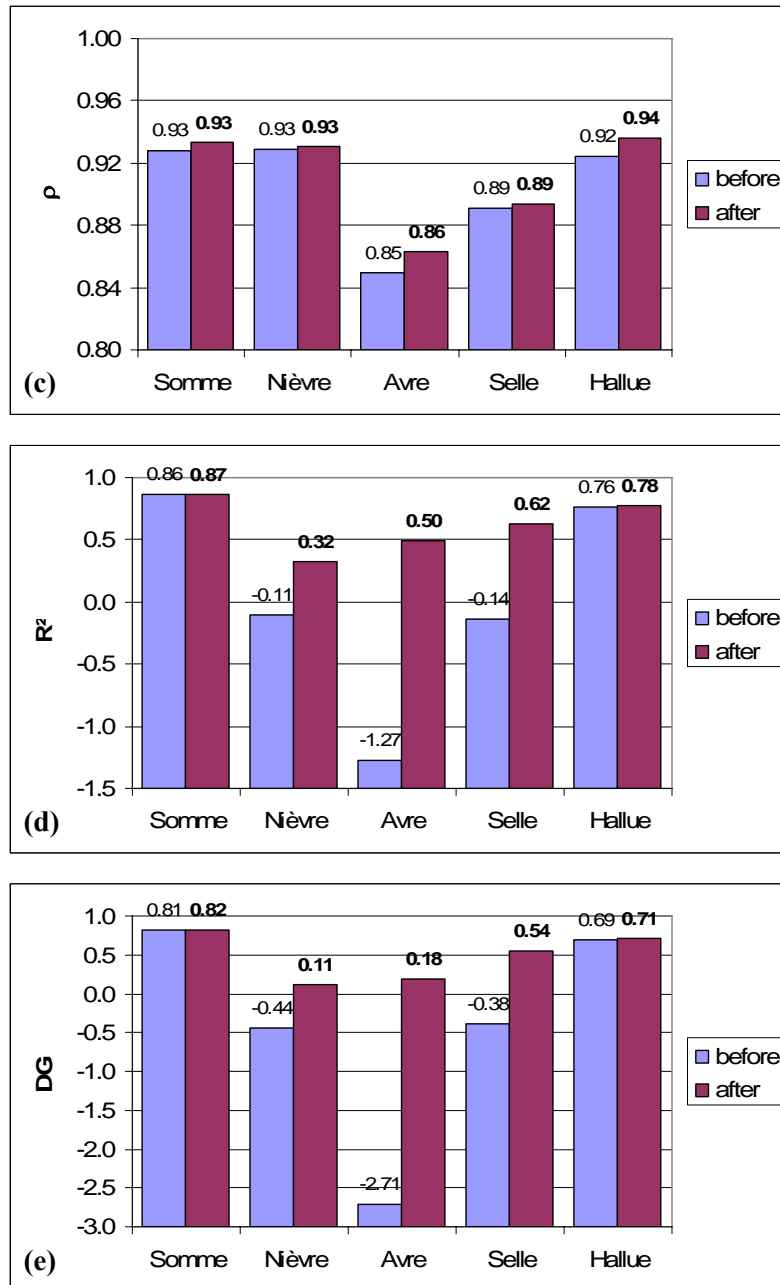


FIG. 5.59 (continued)

5.5.4. Simulation of Flow in Unsaturated Zone

The simulation of flow in unsaturated zone was performed by NONSAT module. The modeling of transfer in the unsaturated zone entails the division of this zone into several homogeneous layers. Each layer represents a certain thickness of the unsaturated zone and is represented by a reservoir and a storage constant, τ . The effects of the number of reservoirs and the storage constant are illustrated in Fig. 3.5. Increasing the number of

reservoirs or the value of storage constant both have similar effects in the attenuation of an instantaneous inflow. However, storage constant is somewhat more effective in the milding of the slope of recession curve.

The total thickness of the unsaturated zone was calculated by using the difference between the surface topography and the average groundwater head supplied by BRGM for the basin area. This thickness varies between 0 and 109 m as shown in Fig. 4.5. Initially the whole unsaturated zone was divided into layers each having a thickness of 5 m, and therefore, 1 to 22 reservoirs were allocated to each surface cell (Fig. 5.60). There were some portions of the basin, namely, one in the north of the outlet of the Somme and another in the southeast of the basin, average groundwater head data was missing because the basin area covered by BRGM was different. The cells falling in these regions were assumed to have an unsaturated thickness of 10 m and were assigned 2 reservoirs.

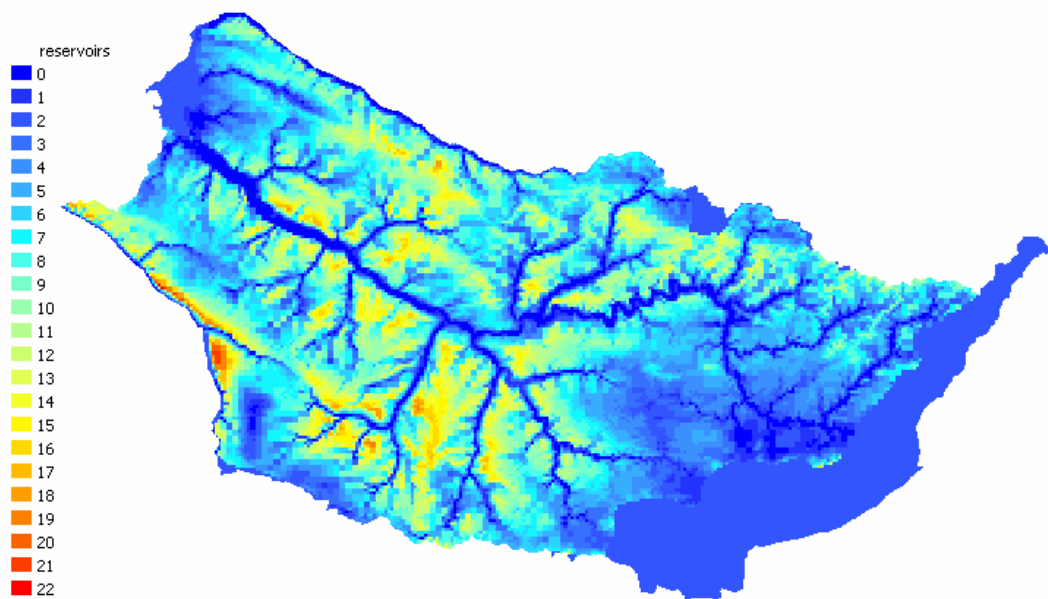


FIG. 5.60 Number of reservoirs in the Nash cascade.

Up to this point, a detailed calibration of NONSAT was not made. A simple calibration was made during adjustment of production function parameters. As an example to the effect of NONSAT, Fig. 5.25 can be observed. The division of layers was always kept the same as described above which is one reservoir for each 5 m of the unsaturated zone, however, the aim is to find the best value of storage constant. During the calibration of production functions 3 values of the storage constant were tested which are 1, 5 and 10 days. These values were assigned to all the reservoirs in all the cells. The effect of the

storage constant on the Nash-Sutcliffe coefficients is shown in Fig. 5.61. For the Somme and the Nièvre 5 days, for the Avre and the Selle 10 days and for the Hallue 1 day gave the best result. The monthly averaged flowrate for the Somme simulated with these 3 values for the period 1/1999 – 12/2001 is given in Fig. 5.62. When the portion pertaining to the flood of 2001 is considered, it is observed that a value of 1 day gives a steep hydrograph and the flood peak is overestimated, whereas a value of 10 day results in a smooth hydrograph where the flood peak is underestimated. The best result was obtained with a value of 5 days. As the flowrate of the Somme at Abbeville represents the whole basin, a storage constant of 5 days was used in all the reservoirs in the basin until the end of the calibration of MODCOU.

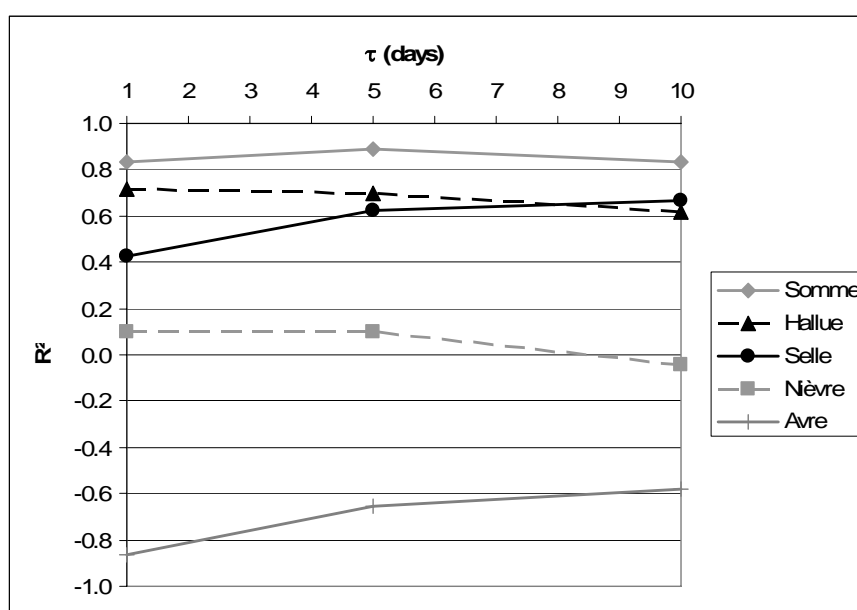


FIG. 5.61 The effect of the storage constant, τ , on the Nash-Sutcliffe coefficients of flow hydrograph fits (the first test).

Another test with the values of 1, 3, 5, 6 and 8 days was carried out in the end of the calibration of MODCOU. The test was performed in the whole period (1/8/1985-31/7/2003) however the results were analyzed in two more sub-periods, namely, 8/1985-7/1995 and 8/1995-7/2003. The effect of each value on the Nash-Sutcliffe coefficients for the whole period is shown in Fig. 5.63. The reason for not testing values greater than 8 is due to the different behaviors of the flow hydrographs in two sub-periods. When the former period is considered the Avre and the Selle improves continuously as the value of storage constant is increased, however, when the latter period is considered slightly better

values were obtained with a storage constant of 6 days. In order to conserve the overall performance of the flow hydrographs, further values were not tested.

A similar behavior was also observed for the Hallue. In the first sub-period a storage constant of 5 days gave the best fit whereas in the second sub-period a value of 3 days resulted in a better fit.

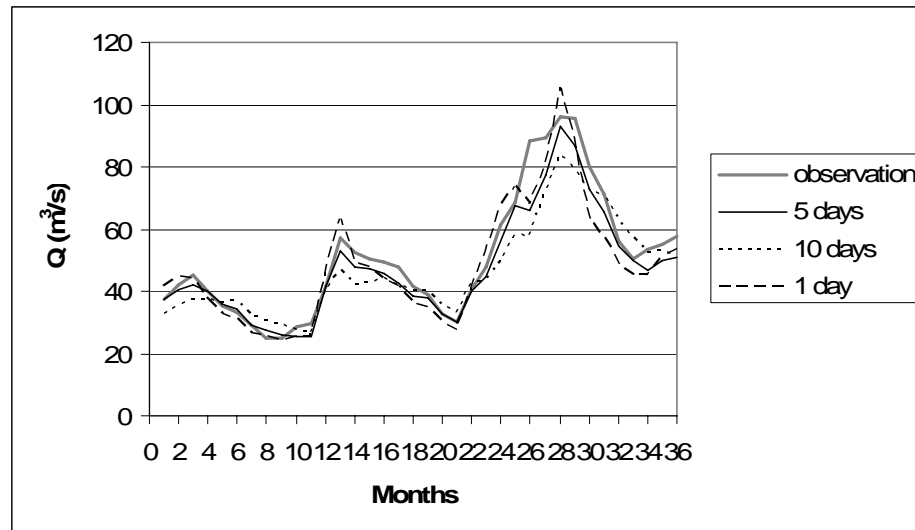


FIG. 5.62 Monthly averaged flowrate of the Somme at Abbeville between 1/1999 and 12/2001 for different values of the storage constant, τ (the first test).

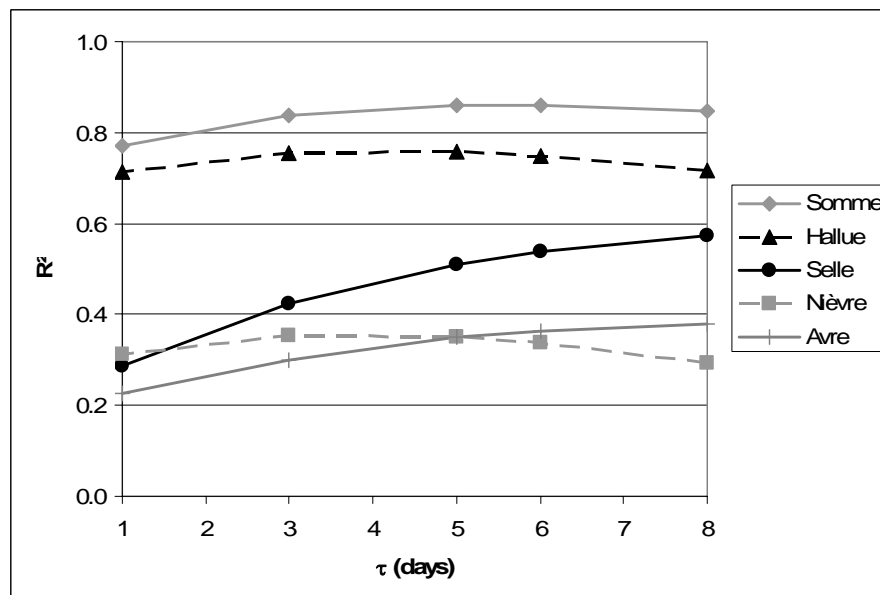


FIG. 5.63 The effect of the storage constant, τ , on the Nash-Sutcliffe coefficients of flow hydrograph fits for the period 1/8/1985-31/7/2003 (the second test).

Therefore the decision was made using the overall results (Fig. 5.63). 5 and 6 days gave almost the same result for the Somme, for the Hallue 5 days gave the best result, for the Avre and the Selle 8 days, and for the Nièvre 3 and 5 days gave the best results. According to these values, 8 days was used for the Avre and the Selle, a value of 4 days was estimated by linear interpolation for the Nièvre and for the rest of the basin 5 days was assumed to be the storage constant of the reservoirs. The distribution of these values is depicted in Fig. 5.64. The outcome of this calibration can be seen in Fig. 5.65. The highest improvement is observed in the Avre and the Selle and then in the Nièvre and the Somme. However, there was not a significant change in the piezometric heads.



FIG. 5.64 The distribution of the values of storage constant, τ .

In conclusion, the effect of NONSAT on the flow hydrographs was examined. Shortly, it is a model simulating the flow in the unsaturated zone which takes the infiltration as input and converts it into groundwater recharge. It adjusts the steepness of the rising and falling limbs, and the recession curves in a flow hydrograph. One drawback is that the piezometric head is assumed to be constant during all the simulation period. However, piezometric level is constantly changing in the Somme basin and even in some years there are many regions inside the basin where the groundwater exfiltrates or approaches the surface so close that the unsaturated zone completely disappears. This is the reason why better fits were obtained in the period 8/1995-7/2003 with lower values of storage constant. Because, lower values represent a quick flow between surface and the

groundwater table. Similar results can be obtained with the same storage constant but using fewer reservoirs which represent a shallower unsaturated zone.

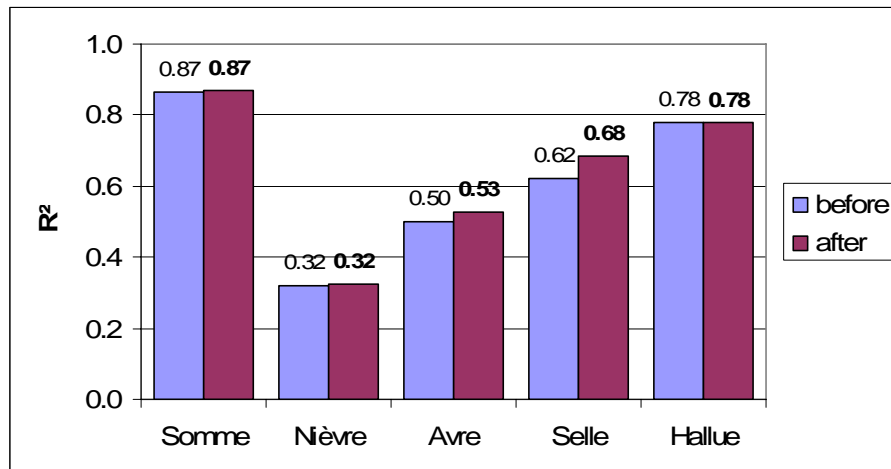


FIG. 5.65 The effect of NONSAT calibration on the Nash-Sutcliffe coefficients of the Somme and its tributaries.

5.6. Validation and Analysis of the Results

The validation of the model was made once in the end of the calibration of production function parameters. The calibration was carried out in the period 8/1985-7/1995 and the validation was performed in the period 8/1995-7/2003. The results were presented in the end of section 5.5.1.

Another validation was carried out after completing the calibration of MODCOU and NONSAT. It was made using the two other streamgage stations on the Somme, namely, at Hangest-sur-Somme (4835 km²) and Peronne (1294 km²) which were not used until this stage. In Table 4.1 and Table 4.2 several values regarding these two stations and in Fig. 4.16 their monthly observed flowrates are presented. Their exact locations inside the basin are illustrated in Fig. 5.22. In addition, the flowrate observations in the end periods of the Avre, the Nièvre and the Hallue were acquired in later stages of the modeling process and kept for the validation. These periods are as follows; Feb 1, 2001 to Jul 31, 2003 for the Avre, Aug 20, 2001 to Jul 31, 2003 for the Nièvre and Sept 4, 2001 to Jul 31, 2003 for the Hallue. The final results of simulations are given in Fig. 5.66. On the figures, the calibration and validation periods are also indicated.

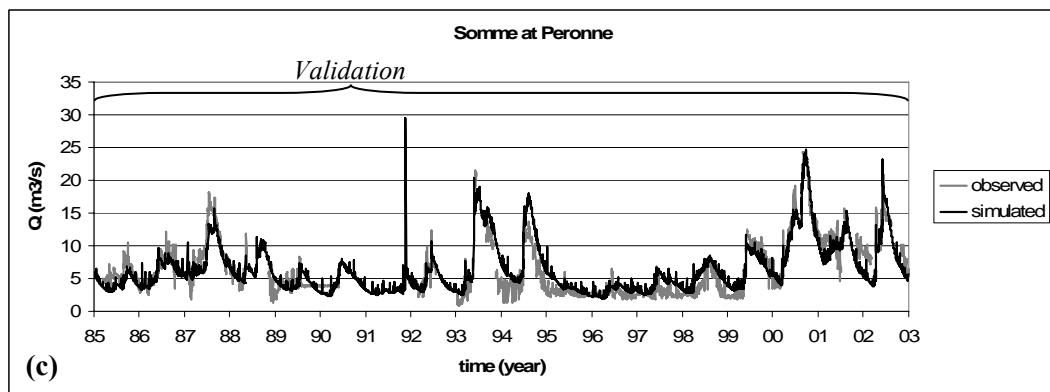
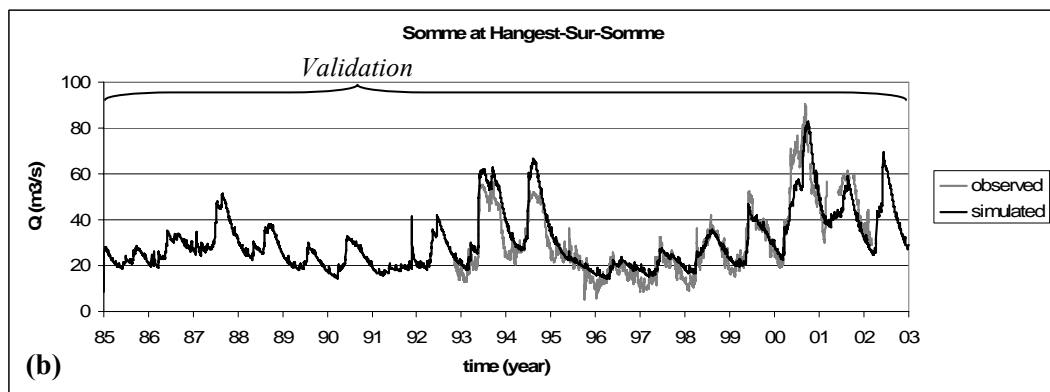
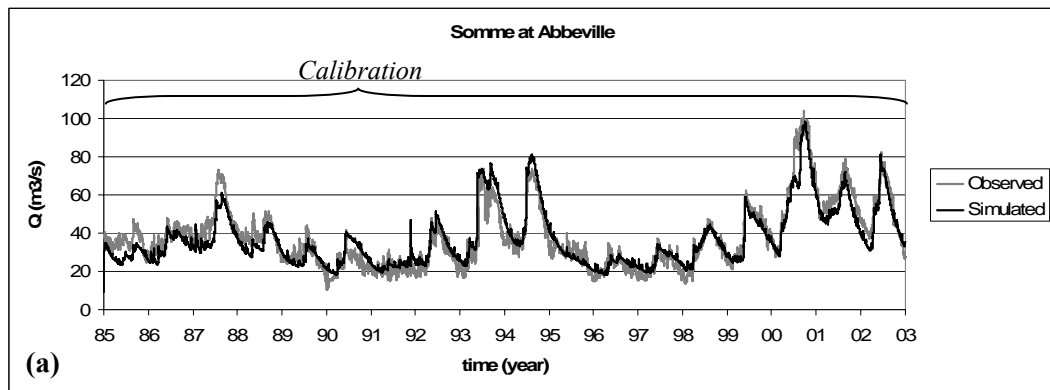


FIG. 5.66 The final results of simulations together with the calibration and validation periods; **(a)-(c)** at various locations on the Somme, **(d)-(g)** on the tributaries of the Somme.

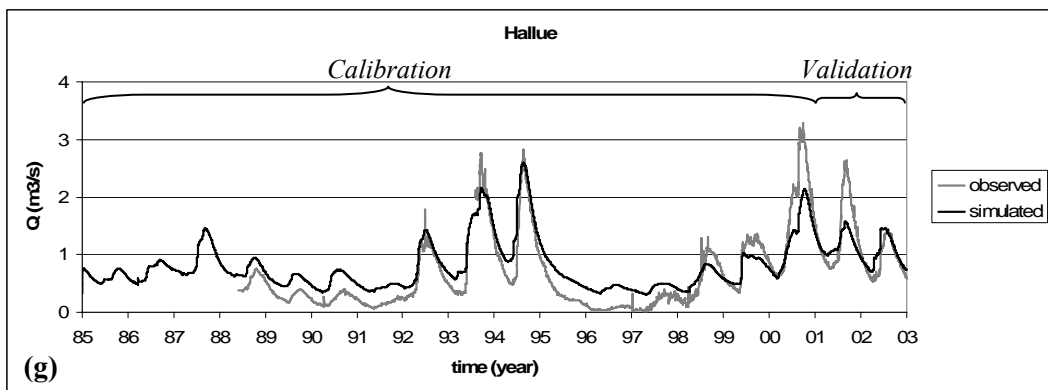
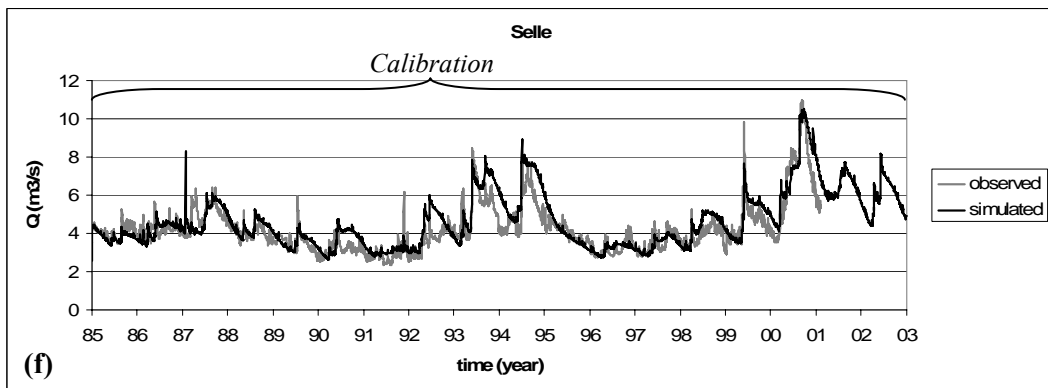
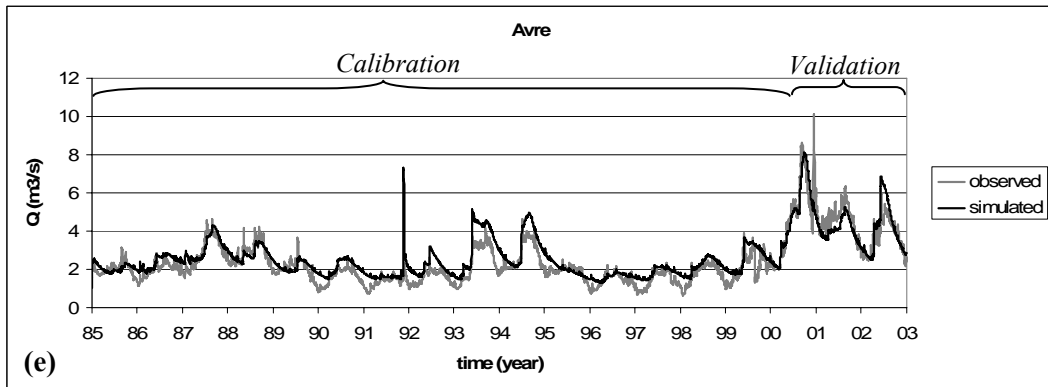
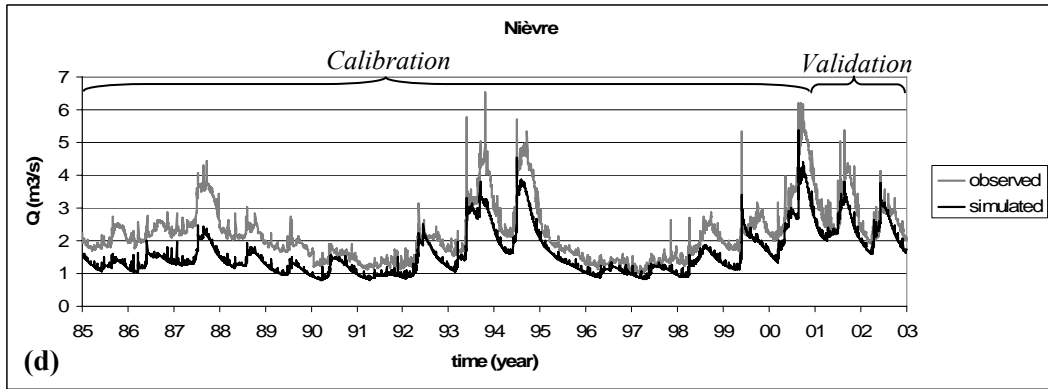


FIG. 5.66 (continued)

The statistical values for the goodness of fits are given in Table 5.6.

TABLE 5.6 Error criteria for flow hydrographs.

Period	Somme (Abbeville)	Somme (Hangest.)	Somme (Peronne)	Nièvre	Avre	Selle	Hallue
	<i>Deviation of runoff volumes, D_v (%)</i>						
calibration	2.56			28.83	-16.37	-6.36	-23.85
validation		-5.04	-1.83	14.91	1.40		2.91
overall	2.56	-5.04	-1.83	26.96	-11.66	-6.36	-18.11
	<i>Root mean squared error, RMSE</i>						
calibration	5.98			0.71	0.53	0.70	0.30
validation		6.34	1.93	0.55	0.80		0.35
overall	5.98	6.34	1.93	0.70	0.58	0.70	0.31
	<i>Correlation coefficient, ρ</i>						
calibration	0.93			0.93	0.86	0.89	0.94
validation		0.92	0.88	0.80	0.82		0.82
overall	0.93	0.92	0.88	0.91	0.91	0.89	0.93
	<i>Nash-Sutcliffe coefficient, R^2</i>						
calibration	0.868			0.323	0.526	0.683	0.780
validation		0.840	0.780	0.189	0.653		0.539
overall	0.868	0.840	0.780	0.349	0.781	0.683	0.775
	<i>Coefficient of gain from daily mean, DG</i>						
calibration	0.822			0.118	0.227	0.616	0.706
validation		0.739	0.702	-2.594	0.008		-1.318
overall	0.822	0.739	0.702	0.148	0.717	0.616	0.696

According to deviation of runoff volumes (D_v) the Somme at Abbeville very slightly underestimates the mean flow while at Hangest-Sur-Somme and at Peronne it is the contrary. As for tributaries, the Nièvre highly underestimates during calibration and approaches the mean flow during validation. The Avre, the Selle and the Hallue overestimate the mean flow while during validation the Avre and the Hallue gets very close to it.

When the values of root mean squared error ($RMSE$) are considered, the Somme gives a higher value at Hangest-Sur-Somme than at Abbeville although the catchment area at Hangest-Sur-Somme is smaller. This shows that there are more perturbations in the flow hydrograph of Hangest-Sur-Somme which can be due to two parameters; namely, the discharge coefficient, Cd , and the storage constant in NONSAT, τ , which were not calibrated in that region. As described before, Cd has an effect on reducing the sharp flow peaks and τ controls mainly the slope of the recession curve. When the $RMSE$ of other hydrographs are considered, small values are observed, particularly, in the Nièvre a better value was obtained in validation period.

As the correlation coefficients are considered, all the values are above 0.80 which demonstrates that a strong linear correlation is assured between the simulated and observed values.

As for the values of Nash-Sutcliffe coefficient, which is one of the most commonly employed measure of error, a high value of 0.868 was achieved during the calibration of the Somme at Abbeville and this goodness of fit was validated with values of 0.840 at Hangest-Sur-Somme and 0.780 at Peronne even though no part of those two hydrographs was used in any stage of modeling. Values with regard to the tributaries are somewhat lower. The lowest value was obtained in the Nièvre, whereas the highest values were achieved for the Hallue and then the Selle. As for the Avre, a better value of 0.683 was obtained in validation than in calibration.

When the values of coefficient of gain from daily mean (*DG*) are considered, a value of 0.822 was reached during the calibration of the Somme at Abbeville and this performance was conserved during the validation at Hangest-Sur-Somme and Peronne. For the Hallue and the Selle fairly good values were achieved, however, during validation the Hallue gave a poor value. For the Nièvre and the Avre rather low values were achieved, the values got even lower during the validation. The reason is that the coefficient of gain from daily mean tests the model performance against the mean of the same day of previous years; however, for the tributaries the validation periods were too short to obtain a fair result. Therefore, coefficient of gain from daily mean must be discarded while considering the goodness of fit for the validation periods of the tributaries. On the other hand, when the performance on the overall period is considered, all except the Nièvre give successful results.

A comparison of the results of MODCOU was made with another model called CaB (Catchment Based) (Carli, 2005). CaB is a land surface model dealing with water and energy transfers using soil-vegetation-atmosphere transfer (SVAT) schemes (Ducharne et al. 2000; Koster et al. 2000). It is based on TOPMODEL, and therefore works better for basins with shallow aquifers. In Fig. 5.67, the monthly discharges on the Somme at Abbeville are depicted for the period 1986-2002. As can be seen in the figure, both models simulate satisfactorily the floods of 1994 and 1995, however, CaB slightly

underestimates the flood of 2001. The Nash-Sutcliffe coefficients for monthly discharges are 0.886 for the Somme and 0.797 for CaB.

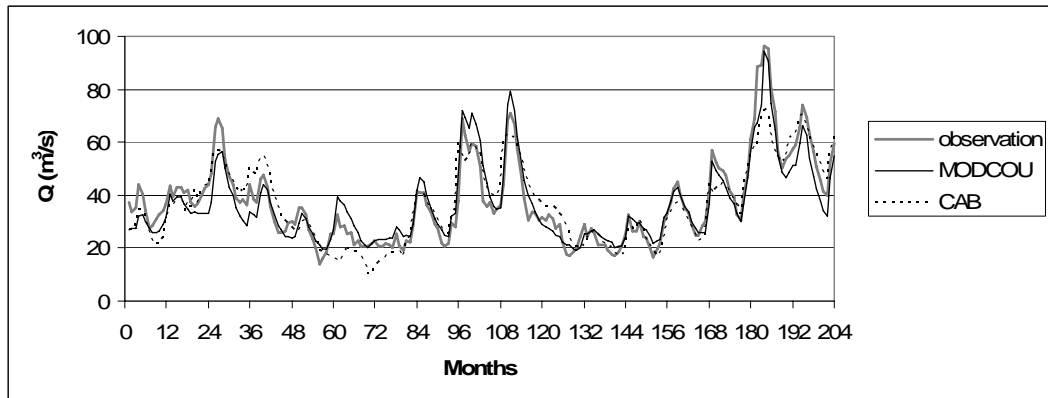


FIG. 5.67 Monthly discharges on the Somme at Abbeville for the period 1986-2002.

The baseflow contribution to the streamflow is depicted in Fig. 5.68. The values in the figure are average annual values. As can be observed, the percentage of baseflow contribution is higher for low-flow periods and lower for high-flow periods. The average baseflow contribution is 94% for the overall period of 18 years. For the period 2000-2001 in which the flood event took place, it is 92% and for the two-month period March-April 2001 in which the flood reached its maximum extent, the baseflow contribution is 89%. These high values indicate how the streamflow is fed by groundwater.

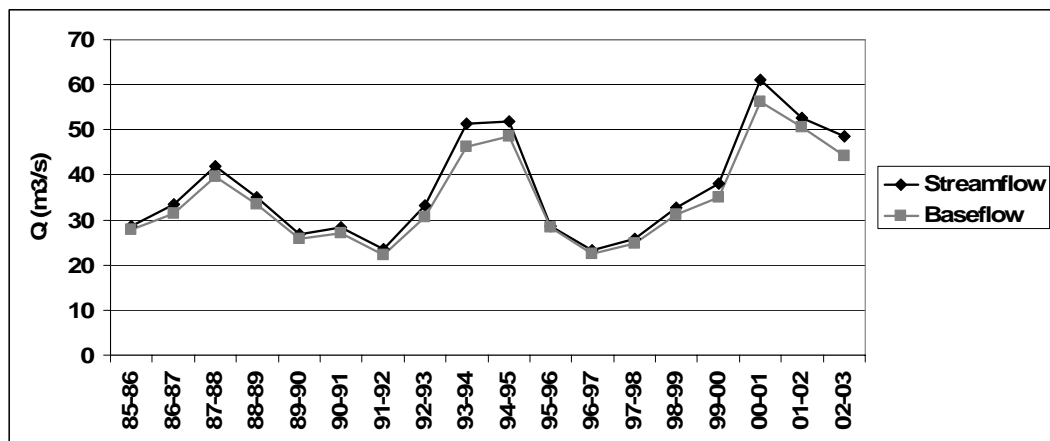


FIG. 5.68 Average annual discharge and baseflow.

Further analyses were carried out regarding the flood event in 2001. These analyses were partially covered during the calibration of MODCOU (Section 5.5.3 above). Continuity in

the flooded areas especially inside the stream network was sought. To do so, several topographical corrections were performed.

The final result concerning the flooded areas in year 2001 were compared with that of a satellite derived image covering a region between Abbeville and Hangest-Sur-Somme and extending to the northern boundary of the basin. In order to obtain this image, the images from the SAR radar of ERS1 satellite and the HRV instrument of SPOT satellite were acquired (Zribi et al. 2007). Further, the images from these two sources were treated with a DEM. In the final data, the values are provided on several days in year 2001 and represent the percentage of water surface covering the grid cell which has a size 1km x 1km. In order to have a reasonable comparison with the total exfiltration depth in 2001 calculated by MODCOU, the day in which the flood reached its maximum extent was chosen (April 21, 2001). This comparison is visualized in Fig. 5.69. The exfiltration depth of MODCOU was calculated by dividing the total exfiltrating volume in year 2001 by the surface area of the cell. When the figure is considered the spread of the flood between Abbeville and Hangest-Sur-Somme is well represented by the present study.

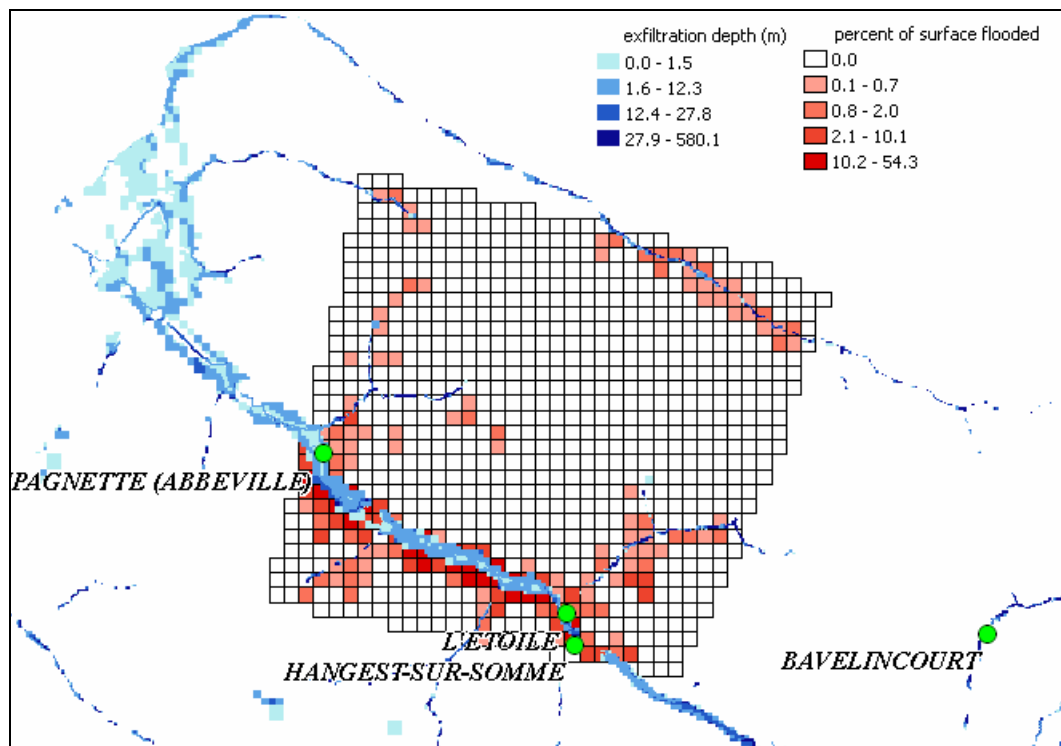


FIG. 5.69 Comparison of total exfiltration depth in year 2001 calculated by MODCOU (in blue) with a satellite derived image representing the flooded percentages of areas for the mesh given on April 21, 2001 when the flood reached its maximum extent (in red).

Another comparison was made between the exfiltration depths calculated by MODCOU and the model developed by BRGM called MARTHE (Thiéry 1990, Thiéry 1998) as shown in Fig. 5.70. MARTHE is another hydrogeological model comprising the simulation of flow in the unsaturated zone and a Manning-Strickler flow routing scheme with a stream-aquifer interaction support. The grid used by MARTHE covers an area of 7335.8 km² in which the cell sizes are 100 m inside and around the stream network, and 500 m elsewhere.

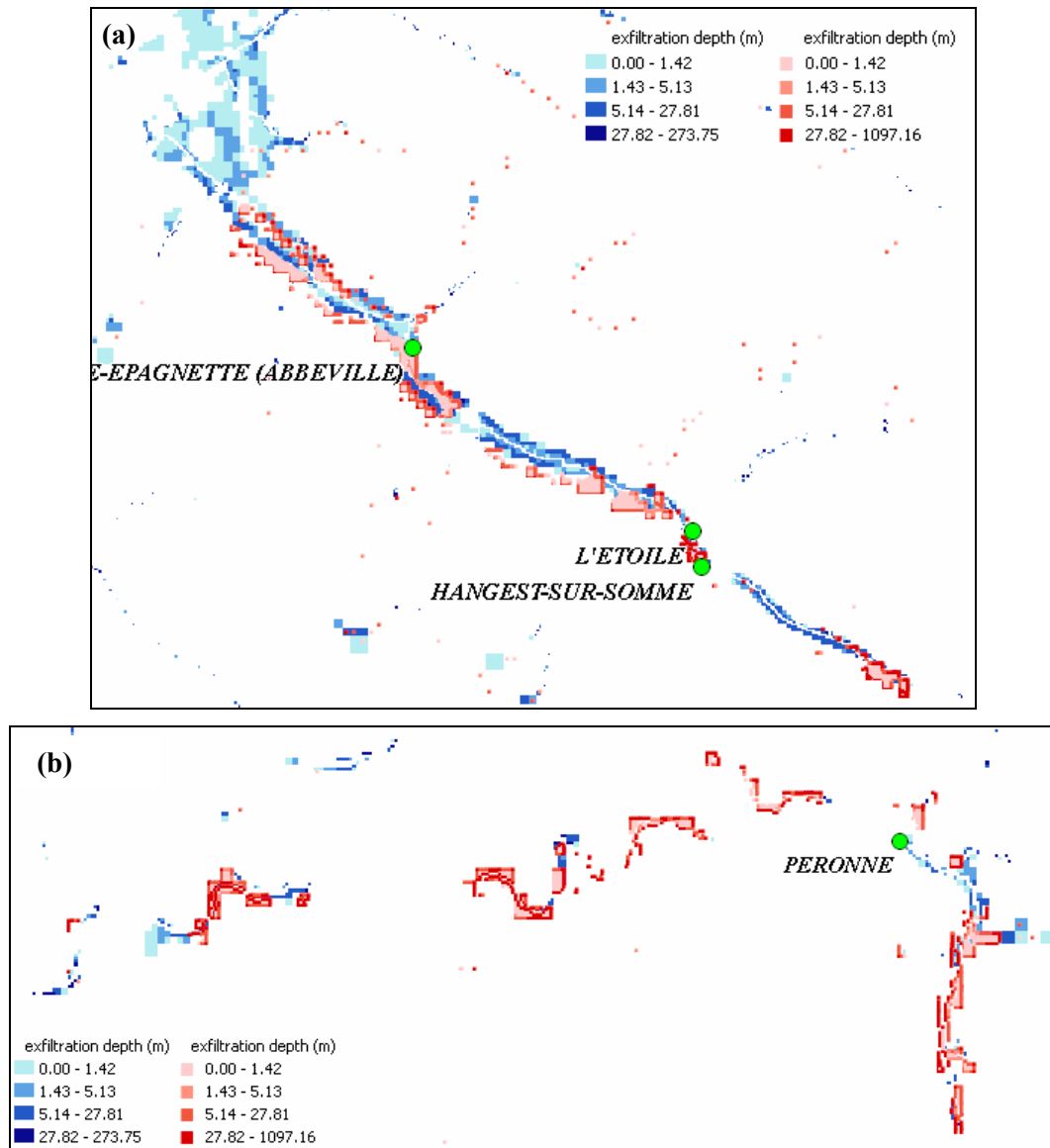


FIG. 5.70 Comparison of total exfiltration depths excluding the river cells in year 2001 between MODCOU (in blue) and MARTHE (in red); **a)** downstream portion of the Somme, **b)** upstream portion of the Somme.

Values supplied by MARTHE represent exfiltration depths everywhere except the river cells. In order to be coherent, the exfiltration depths in the river cells were excluded from MODCOU as well. For the year 2001, the maximum value is 273.75 m for MODCOU and 1097.16 m for MARTHE. On the other hand, mean exfiltration depth is 0.130 m for MODCOU and 0.238 m for MARTHE.

In the first part of Fig. 5.70, the downstream portion of the Somme can be seen. The values provided by MARTHE are more interrupted, especially, immediately upstream of Hangest-Sur-Somme for about 8 km there is not a considerable exfiltration. In addition, towards the outlet there are only the values of MODCOU because this region is outside the grid used by MARTHE. In the second part of the figure, the upstream portion of the Somme can be observed. The situation is almost reversed, that is, the values of MODCOU are more interrupted than those of MARTHE, because in this portion the majority of the exfiltration occurs in the river cells which are not considered in this comparison.

This spatial variation of exfiltration fluxes in the East-West direction is illustrated in Fig. 5.71. The values in the North-South direction are all projected on the figure but not summed up. According to these, MARTHE gives interrupted and high values while MODCOU is more homogeneous both in spatial extent and strength. This can be due to the different topographic maps employed by the two models. Moreover, in the third calibration step of MODCOU, several topographic corrections were made in order to establish a more continuous exfiltration (Section 5.5.3 above). Another difference is that MARTHE gives values more concentrated in the upstream half of the basin whereas MODCOU gives higher values in the downstream half which can be due to different piezometric variations in two models.

Further comparisons of the present model with three other models namely, MARTHE, CLSM and SIM were made by Habets et al. (2007). These comparisons are mainly focused on the period comprising the flood of year 2001. In the same study, it is found that 90% of the stream flow is supplied by the aquifer whereas according to the results of MARTHE this value is 80%. In addition, MARTHE simulates piezometric heads better and the discharges worse than MODCOU. On the other hand, the flow of the Nièvre is underestimated by MARTHE as well.

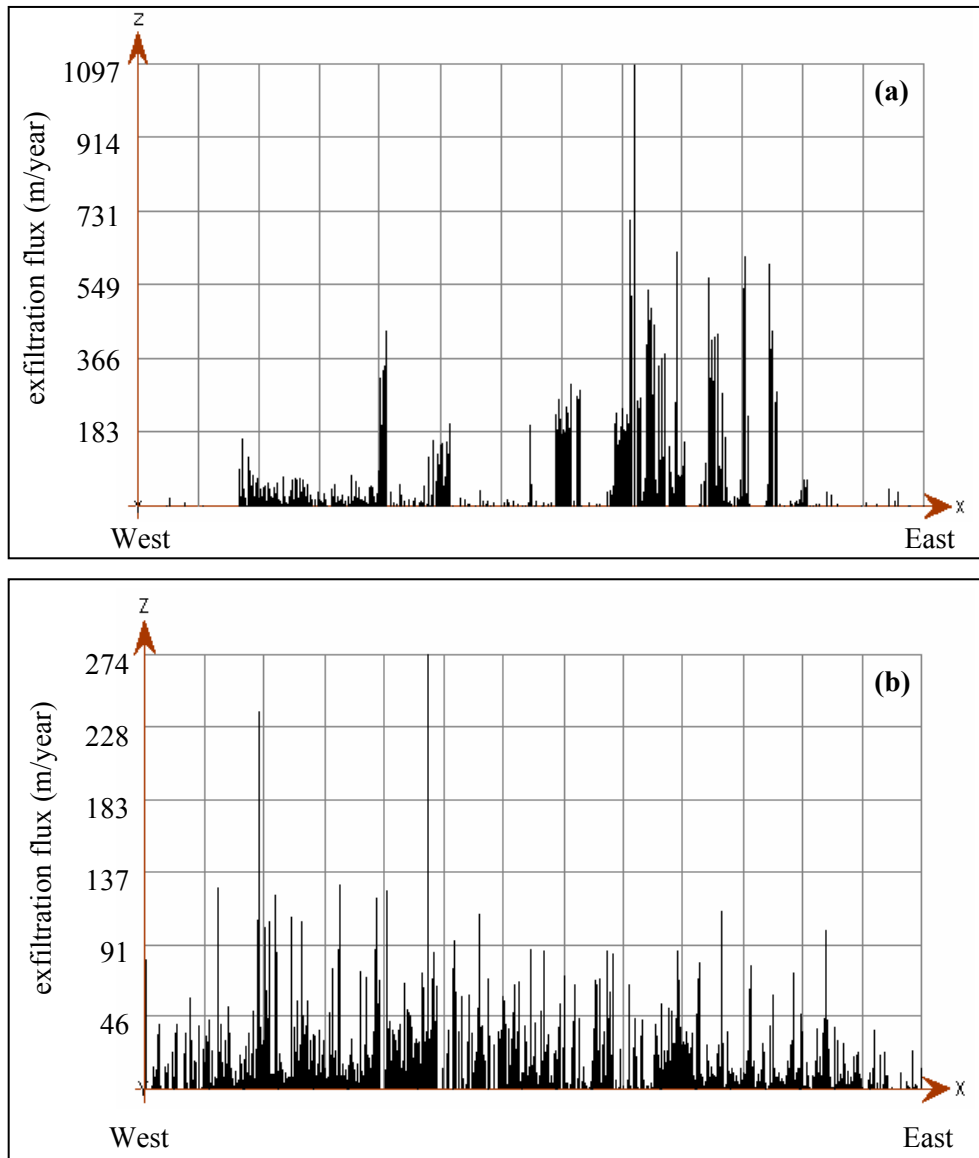


FIG. 5.71 The spatial distribution of exfiltration fluxes of year 2001 in the East-West direction computed by; **a)** MARTHE, **b)** MODCOU.

Finally the surface-aquifer flow exchange values were computed in a basin scale for each simulation year from 1/8/1985 to 31/7/2003. These values are illustrated in Fig. 5.72. As mentioned before, the flow exfiltrating onto the surface is not permitted to re-infiltrate until reaching a river cell, therefore there is infiltration only on the river cells. Furthermore, this infiltration is controlled by two parameters, namely, streambed conductance and maximum infiltration rate. When a spatial comparison is made, it is seen that exfiltration locations are approximately the same for all years, however, the intensities are different. The highest values are observed in year 2001 as follows; 0.24 m of river based exfiltration, 0.11 m of surface based exfiltration, and after deducting the river based infiltration, a total exfiltration of 0.34 m occurs between 1/8/2000 and

31/7/2001 on an area of 8205.25 km². A total exfiltration value of 0.29 m is observed for the year 1995, however, the observed impact of the flood of 2001 was much greater. It should be noted that Fig. 5.72 represents only the simulated values and the actual value in 2001 might have been greater than 0.34 m. This brings to mind that there could be a high volume of water stored in the unsaturated zone and this volume is released only when the water table approaches the surface. To represent this phenomenon several modifications in the conceptual model can be made, particularly, in the unsaturated model (NONSAT). A feedback from MODCOU to NONSAT can be established and as the water table rises the number of reservoirs representing the unsaturated thickness can be decreased. In addition, the volume of water in the submerged reservoirs can be directly added to the groundwater. By this way, the abrupt increase in the piezometric head which was observed during the flood event can be better demonstrated by the model. Moreover, the effect of long-lasting rainfall can be observed within a shorter time as the unsaturated depth will get smaller.

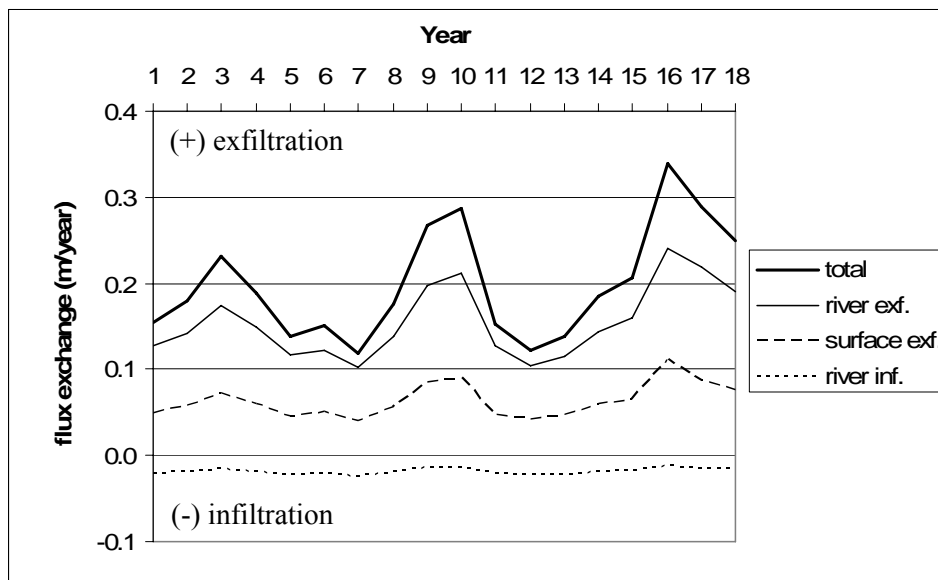


FIG. 5.72 Flux exchange between the surface and the aquifer in the period 1/8/1985-31/7/2003.

In Fig. B. 1, the piezometric head hydrographs are illustrated. The problem explained above can also be recognized in the hydrographs of wells 358x216, 463x036, 465x007, 474x011, 486x015, 632x023, 633x132, 636x020 and 803x003. The abrupt rise in year 2001 can be observed. In addition, at 334x029 a difference of 32 m is observed which is thought to be a perched aquifer. While at 616x023 and 624x085 the situation is reversed, despite all the calibration the simulated values stayed above the observations, this can be

due to an error caused by the resolution of DEM, such that, the actual elevation of these points may be less than those supplied in DEM. On the other hand, 238x037, 327x062, 332x036, 335x005, 444x008, 444x048, 464x013, 471x010, 487x015, 636x020, 637x093, 638x116, 813x043 are some of the wells in which the dynamics of groundwater were successfully represented. The statistical criteria concerning all the 50 wells used are given in Table B. 1.

5.7. Sensitivity Analysis

Sensitivity analysis is used to evaluate the effect of parameter uncertainty on model results (Anderson and Woessner 1992). In such an analysis the sensitivity of the results to variations in parameter values, grid size, and boundary conditions is tested. According to Hill (1998), the use of sensitivity analyses is a guideline for evaluating potential new data, such as the degree to which new data might improve model calibration. Johnson (2007) presents a study on sensitivity analyses to guide field data collection.

During the calibration of the model, several sensitivity analyses were performed regarding the discharge coefficient (Cd) controlling stream depletion (Fig. 5.56) and storage constant (τ) of the unsaturated model (Fig. 5.61-Fig. 5.63). At this stage, parameters controlling groundwater flow were examined. Initially, sensitivity of the model to variations in transmissivity (T) and specific yield (S_y) was tested. At each model run, only one parameter value is changed. Transmissivity and specific yield values of the whole domain were increased by 10, 25 and 50%. Therefore, the model was run 6 times for exactly the same period of 18 years. The effects of variations in transmissivity and specific yield on the average root mean squared error ($RMSE$) are illustrated in Fig. 5.73, and those on the average groundwater level change in Fig. 5.74. Average $RMSE$ values were calculated by taking the average of 50 $RMSE$ values corresponding to piezometric head fits used throughout the modeling process. Similarly, average groundwater level changes were calculated by using the average of 50 simulated heads each of which is averaged over 18 years. As can be seen in these figures, the model is much more sensitive to transmissivity than specific yield. Average $RMSE$ is linearly increasing for transmissivity while it remains almost constant for specific yield. On the other hand, the average groundwater level changes parabolically with increasing transmissivity, whereas it is slightly influenced by the specific yield.

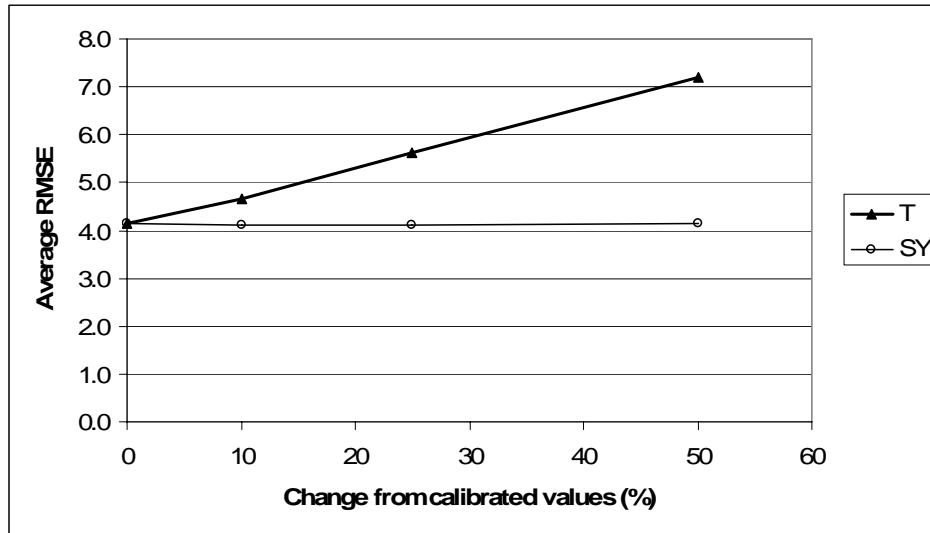


FIG. 5.73 Effect of transmissivity and specific yield change on the average root mean squared error obtained by using 50 head observation points.

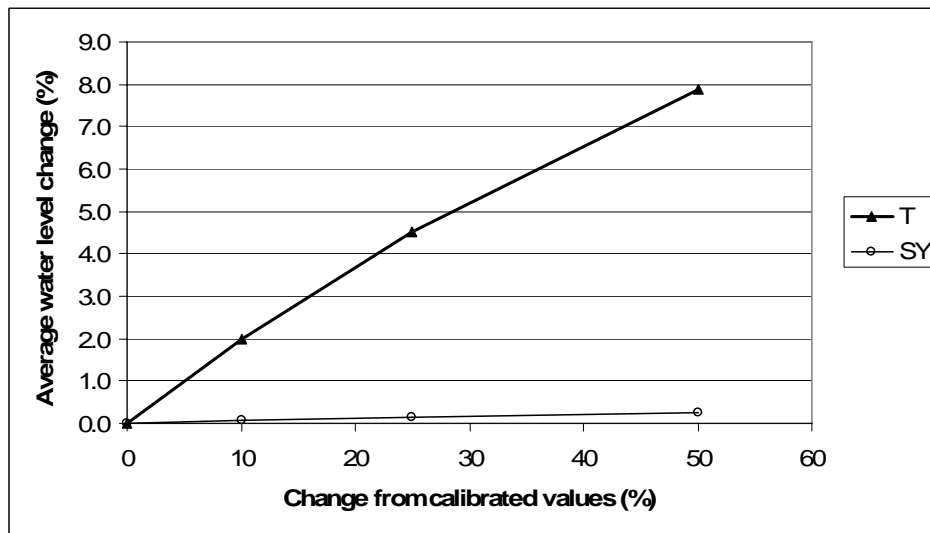


FIG. 5.74 Effect of transmissivity and specific yield change on the average groundwater level change obtained by using 50 head observation points.

Another sensitivity analysis was performed to observe the effect streambed conductance (C_{riv}) on the flux exchange between the surface and the aquifer. Similarly, the value of streambed conductance was increased by 10, 25 and 50%. The result is depicted in Fig. 5.75. To obtain this figure, the flux exchange values corresponding to the period 1/1/2001-31/12/2001 were used. The most sensitive value is the infiltration in river cells for C_{riv} is a controlling parameter as described in relation (3.42). The exfiltration in surface cells is slightly affected by the value of streambed conductance whereas exfiltration in river cells is almost not affected. In addition, the values of average *RMSE*

of piezometric heads and average groundwater level remains nearly unchanged for variations in streambed conductance. When the overall effect of infiltration in river cells is considered as already shown in Fig. 5.72, it can be concluded that streambed conductance does not have a significant effect on the flow.

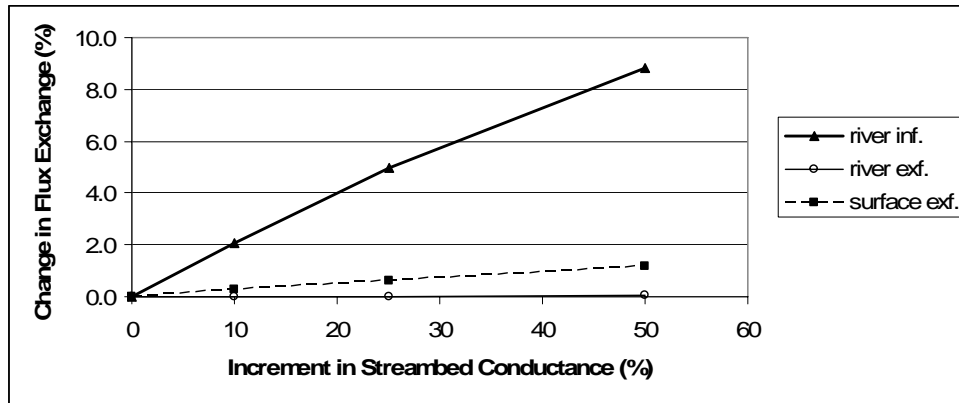


FIG. 5.75 The effect of streambed conductance on flux exchange.

As a result, the most important parameter concerning the groundwater flow is found to be transmissivity. For future model calibration, more field measurements for transmissivity can be performed.

The next analysis was made to assess the impact of groundwater level on the flood of 2001. The model was run for two times in the period 1/8/2000-31/7/2001 using the piezometric levels of 1/8/1998 and 1/8/1999 as initial conditions. As a result, the run with the values of 1/8/1998 yielded a slightly lower flood peak; however, similar consequences would occur for there was not a significant reduction in the maximum flowrate values. The reason is that the difference between the calibrated and the tested flowrate closes rapidly and towards the end of the simulation period this difference becomes negligible. The flowrate values related to this analysis are presented in Table 5.7.

TABLE 5.7 The flowrate values concerning the test simulations with initial piezometric levels of 1/8/1999 and 1/8/1998.

flowrate	Q_{\min} (m ³ /s)	Q_{\max} (m ³ /s)	Q_{avg} (m ³ /s)
observed	26.90	104.00	59.16
calibrated	27.51	104.75	54.71
test (1999)	18.81	101.36	52.97
test (1998)	15.62	97.23	51.07

It can be concluded that the flood in year 2001 does not depend only on the level of groundwater table. The volume of water contained in the unsaturated zone and the intensity of rainfall should also be considered to be the causes of the flood.

CHAPTER 6

CONCLUSIONS

6.1. Summary

In present study, hydrogeological modeling of the Somme river basin situated in the north of France was made with special emphasis on the stream-aquifer interaction. The modeling was based on the coupled model developed at Ecole des Mines de Paris. GIS tools were incorporated during all the stages of modeling process as both preparation of input data and visualization of the results of simulations.

Initially the process began with extracting spatial information on the basin by using Digital Elevation Model (DEM) analysis. Based on the raster image of topography having a pixel size of 125 m, this analysis consisted of finding flow directions, accumulated drainage areas, deriving the stream network, subcatchment partitioning and basin delineation. These analyses were carried out using the program HYDRODEM.

After acquiring the necessary spatial data, the surface grid was generated by using SIGMOD. SIGMOD generates a nested grid where refinement is made on the stream network and subcatchment boundaries in order to increase the accuracy of numerical solution. The most suitable grid to be used by the model was found by trial-and-error procedure. Several grids were generated according to different stream networks obtained by different threshold values for accumulated drainage areas. In addition, small subcatchments were merged to form bigger ones to avoid unnecessary refinement. The boundaries of the domain were extended to the closest natural boundaries; such as, rivers, in order to have prescribed head boundary conditions wherever possible. One other reason is that the aquifer of the Somme basin has important effects on the flow and to account for its vast extent, its limits could not be restricted to surface altitudes. After the surface grid, the aquifer grid was generated by SIGSOU exactly on the same spatial extent to enable surface-aquifer interaction at every point inside the basin. While

generating the aquifer grid, by a regrouping procedure the small sized cells on the surface grid were merged to obtain larger grid cells as surface topography was not very important for the aquifer grid, however, the same refinement was maintained beneath the river cells so as to keep the accuracy in stream-aquifer interaction. After generating the grids, a total of 71653 cells on the surface and 63226 cells on the aquifer were formed. The sizes of the cells were 125, 250, 500 and 1000 m.

The coupled model consists of 4 major modules, namely, MODSUR, NEWSAM, NONSAT and MODCOU. In order to run the surface model MODSUR, meteorological forcing, land use and soil type data were acquired. The necessary meteorological forcing was provided by Météo-France on a grid covering the whole basin area with square cells having a size of 8 km. The daily rainfall and potential evapotranspiration values were supplied for the period 1/8/1985-31/7/2003. Land use data was obtained from CORINE Land Cover database and soil type data from INRA database. Land use and soil type data were later superimposed in GIS environment in order to obtain production zones. MODSUR uses a production function which partitions the precipitation between surface runoff, infiltration and actual evapotranspiration according to these production zones. It calculates the volume of water infiltrating at every surface cell and the volume of water arriving at each river cell for every time step. Production function of MODSUR has a parameter set for each of the production zones. To find the optimum values of these parameters a calibration procedure was followed on the period 1/8/1995-31/7/2003. The effect of each parameter on the flow hydrograph of the Somme at Abbeville (5560 km²) was analyzed and described in detail. In the end of calibration, a validation was performed on the period 1/8/1985-31/7/1995. Statistical values for the fit were sufficiently successful, such that, the Nash-Sutcliffe coefficient was 0.93 for the calibration, 0.72 for the validation and 0.86 in overall period.

The next module used is NEWSAM which simulates only the groundwater flow. In present study, it was used in steady-state mode in order to obtain a piezometric head distribution to serve as an initial condition. The infiltration values computed for every time step are averaged in the steady-state mode. Initial data regarding the aquifer was supplied by BRGM. Hydraulic conductivities were defined on 5 different zones. The data provided by BRGM was on a different grid than the one used in the present study, therefore, data falling on missing portions were estimated in GIS environment depending on certain criteria such as surface topography. As the model utilizes transmissivity instead

of hydraulic conductivity, the values of hydraulic conductivity were multiplied by the average thickness of groundwater which was as well provided by BRGM. Different piezometric head distributions were obtained by NEWSAM with different transmissivity distributions.

The unsteady groundwater and surface flow simulations were carried out by MODCOU. It simulates surface and groundwater flows by taking into consideration the stream-aquifer interaction. As input it requires the daily surface runoff values arriving at each river cell (from MODSUR), the daily values of groundwater recharge (from NONSAT), an initial piezometric head distribution (from NEWSAM), transmissivity, specific yield, pumpage rate, maximum infiltration rate, and streambed conductance. As output, MODCOU gives daily flowrate values at locations of streamgauge stations and outlets of the rivers defined on the boundaries of the basin, daily piezometric head values in up to 50 locations inside the domain, and the piezometric head distribution inside the aquifer in the end of each year. A very elaborated calibration was performed and each step was described in detail. Initially, a transmissivity calibration was performed to a certain degree. A correspondence between the simulated and observed piezometric head values was sought. The results were both depicted as x-y traces and visualized in GIS environment. Next, a rough calibration of the specific yield values was carried out, such that, the lowest values were multiplied by 2 to observe the global effect of specific yield. In the following step, a topographic problem was discovered, such that, the sinks that almost always exist in a DEM were not filled. Along a streamline, there were increases in elevation from a cell to the cell at its downstream which caused interrupted exfiltration of groundwater on the surface. A code was written in FORTRAN to apply the 'fill' procedure to the DEM. The algorithm of this procedure is given in detail. After the execution of the code, a mean rise of 0.029 m was applied to the basin area. One other correction concerning the same problem was applied to the river cells. Because of the resolution of the DEM (125 m), river cells had higher elevations than their actual values and were not draining enough the groundwater. In order to partly compensate this situation, on each river branch the elevations of river cells above the average slope line were reduced to the elevation of it. A better correction could be made if exact elevations of several points on the stream network were known. Nevertheless, this correction had an enhancement on the exfiltration along the stream network. In the next step, the initial values of specific yield were re-assumed because in the second step, multiplying the lowest values by 2 was a very rough calibration although it had a positive effect.

Afterwards, specific yield values were calibrated regionally and in detail by considering all the piezometric head observations, and finally an improvement was observed in 43 out of 50 locations. In addition, the effects of specific yield on piezometric head fluctuations were analyzed. In the sixth step, transmissivity values were calibrated for the second and the last time. Goodness of fit was sought not only in piezometric heads but also in flow hydrographs. Especially in the subcatchments of the Avre and the Selle, major modifications were performed. The key issues regarding the calibration of transmissivity in a 2-dimensional flow system were analyzed carefully. Its differences from 1-dimensional flow are explained in detail. Consequently, improvements in 37 of the piezometric heads and in the flow hydrographs of the Nièvre, the Avre and the Selle were observed. In the last calibration step, the values of discharge coefficient were calibrated. It is a parameter controlling the rate of flow from a cell to another and also from a river segment to another. Its calibration positively influenced the flow hydrographs of the Avre, the Selle and the Hallue particularly in reducing the instantaneous peaks.

The simulation of flow in the unsaturated zone was performed by NONSAT. NONSAT computes the daily recharge of groundwater by using daily surface recharge that was initially calculated by MODSUR. In fact, it is an optional module that is run before MODCOU. However, its calibration was made after MODCOU, for this reason it was described lastly. In order to run NONSAT, two parameters have to be identified for every cell, namely, the number of reservoirs representing the unsaturated zone and their storage constants. The unsaturated zone, which is the difference between the surface and average groundwater head provided by BRGM, is divided into layers having a thickness of 5 m. Hence, for every 5 m of the unsaturated zone a reservoir was allocated to the cell, and this partitioning was not modified throughout the simulations. On the other hand, the storage constants, which control the emptying rate of these reservoirs, were subjected to calibration. Two different calibrations were performed. Initially, during MODSUR simulations three values of storage constant were tested for all the reservoirs in every cell; 1, 5 and 10 days. The value of 5 days gave the best result and used until the end of MODCOU simulations. In the end, a more detailed calibration was performed and different values were assigned to the reservoirs in each subcatchment. This second calibration improved all the flow hydrographs, especially in recession curves better fits were observed.

Validation of the model was made using the observed discharges at two other points on the Somme, namely, Hangest-Sur-Somme (4835 km²) and Peronne (1294 km²) which had not been used in any stage of the modeling process. Therefore, it was rather a rigorous testing of model performance. The Nash-Sutcliffe coefficients for the discharges on the Somme were; 0.87 at Abbeville (calibration), 0.84 at Hangest-Sur-Somme (validation) and 0.78 at Peronne (validation), which indicates that the coupled model used in present study demonstrates a successful performance. Further validation was made for the Nièvre, the Avre and the Hallue. For the Avre and the Hallue satisfactory results were obtained, however, for the Nièvre acceptable but not very satisfactory results were obtained. The flow is almost all the time underestimated. This can be due to inaccurate calibration of production function variables or improper division of production zones in that region as they were responsible for the satisfaction of water balance. A comparison of the model was made with another model named CaB and it was observed that the coupled model demonstrates better performance than CaB. The reason is that CaB is a surface model based on TOPMODEL which is intended to work for basins with shallow aquifers.

Further research was done concerning the flood of 2001. The total exfiltration depth on the surface in 2001 was compared with a satellite derived image representing the percent of surface flooded and as a result a satisfactory correspondence was observed. The same result was in addition compared with that of the model developed by BRGM called MARTHE. Similarities and differences were analyzed in detail.

In the end, sensitivity analyses were performed for three parameters, namely, transmissivity, specific yield and streambed conductance. It is found that, the most effective parameter on the groundwater flow is transmissivity and its priority was underlined for future field data collection.

6.2. Discussion

During the modeling process there were several problems encountered, some of which were resolved. These problems are explained in the following.

Selection of the DEM and its resolution are important steps that have to be taken carefully. In order to minimize the problem of shifting between the mapped stream network and that obtained by DEM analysis, a selection of DEM obtained from digitized

contour maps instead of satellite based images are strongly suggested as both vertical and horizontal displacement errors will be smaller. In addition, due to computational limitations a resolution of 125 m was selected which is reasonable for the surface topography, however, for the river cells it is considerably large especially for those in the upstream portion of the Somme and in the tributaries. Therefore, a finer resolution will definitely contribute to the accuracy of the numerical solution although it requires additional computation time. Moreover, the corrections regarding the DEM, which are the 'fill' procedure and the correction of river cell elevations, should be applied as early as possible in such a modeling.

Another issue arises from large number of parameters with respect to observations. This can lead to equifinality which means that there can be many different structures or parameter sets within the same model giving equally acceptable results or behavioral representation of the observed processes (Beven and Freer 2001). This problem can occur when a model is calibrated by two different users. In order to overcome this situation the number of observations concerning both the aquifer and the surface flow should be increased.

The next problem is related to the stream flow. Neither the coupled model nor MARTHE can satisfactorily simulate the discharge at the Nièvre. This can be due to various reasons such as insufficient calibration or error in obtaining the field data. Therefore, a study of this particular catchment is suggested.

Concerning the flow in unsaturated zone, NONSAT helped diminish the intense peaks in flow hydrographs. However, the thickness of the unsaturated zone was kept constant all the time which is not a very realistic assumption. In fact, when the piezometric head hydrographs are considered (see Appendix B), fluctuations up to 15 m are observed which corresponds to 3 reservoirs in NONSAT. Therefore, NONSAT should be developed to simulate correctly the saturation-unsaturation process due to water table movement. A solution can be found by establishing a feedback from MODCOU to NONSAT and as the water table fluctuates the number of reservoirs representing the unsaturated thickness can be modified.

A final remark can be made regarding the aquifer. The specific properties of the chalk aquifer such as fissures and dual porosity were not taken into consideration in this model, nevertheless, good results were obtained for the discharges and piezometric heads.

6.3. Conclusion

In this thesis, many contributions to the coupled model were made. Initially, the grid generators SIGMOD and SIGSOU were improved. In SIGMOD, transfer time calculation and refinement of the grid on subcatchment boundaries were corrected. A subroutine was written in FORTRAN to merge small subcatchments. In SIGSOU, proper functioning was ensured by using a small test basin and all the criteria for regrouping of the cells in a grid were tested on this basin. Concerning the DEM analysis, a 'fill' algorithm was developed and written in FORTRAN. This procedure scans a DEM and finds the sinks that hinder a flow line and raises the elevations of cells inside the sink up to the tip elevation. A widespread application area can be found for this procedure. Another important contribution is the correction procedure implemented for the elevations of river cells which scans every single reach in the stream network and reduces the elevations of the cells falling above the straight line connecting the upstream and downstream points of the reach to the elevation of the line. It is a flexible program which can be of use to many models. Especially when exact elevations of several locations on the stream network are known, it can be employed to reduce the error caused by the resolution of the DEM. In addition, the coupled model was modified to output the exfiltration depths. The visualization of this data can be useful in flood risk assessment. In addition to these, the calibration of all the elements of the coupled model was described in detail. Especially, the calibration procedure concerning the satisfaction of water balance and simulation of the piezometric surface can serve as a guide to researchers in future application of the same model to other basins.

All in all, a sophisticated modeling was performed. In river basins such as the Somme, which are strongly influenced by groundwater, many models particularly those based on TOPMODEL fail to represent the actual phenomenon because TOPMODEL assumes a shallow aquifer. In this research, very satisfactory results for the stream flows were obtained. The groundwater behavior and its effect on the surface flow and the flood of 2001 are well represented. The advantage of the model used is that it simulates groundwater and surface flows simultaneously and takes into account the stream-aquifer

interaction in every time step. The diversity of parameters controlling the flow such as production zones, streambed conductance, and discharge coefficient demonstrates the flexibility of the model. The advantage of being composed of several independent modules, namely, MODSUR, NEWSAM, NONSAT and MODCOU enables the user intervention and eases the calibration of the model. Incorporating the advanced technology of Geographic Information Systems (GIS) in all the stages made easier to visualize, prepare and interpret spatial data and opened another perspective in the modeling process.

6.4. Perspective

The outcome of this research will be used by the research project REXHYSS which aims at estimating the impact of climate change on water resources and hydrology of the Somme and the Seine river basins. REXHYSS is a part of the GICC (Gestion et Impact du Changement Climatique) program which is funded by MEDAD (Ministère de l'écologie, du développement et de l'aménagement durables). The climate effects on the low and high flows and droughts will be determined using classical frequency analyses. Flood risk assessment will be performed so as to determine probable damages that can be caused to infrastructures, transportation or energy production. In addition, agricultural effects on the water resources of the basins will be considered, such as, irrigation demand, crop production and nitrate pollution.

The current results will also be integrated to the project SIM-FRANCE. The Safran-Isba-MODCOU system is a hydrological model run every day to calculate the water and energy budget for the whole France. Soil moisture, temperature and snow depth are simulated by Safran. The stream flow is simulated at over 400 streamgauge stations. For the time being, the aquifers of the Garonne, the Rhône and the Seine basin are taken into consideration. After the addition of the Somme, better results for the north of France are expected.

REFERENCES

Anderson, M.P. and Woessner, W.W. (1992). *Applied groundwater modelling: simulation of flow and advective transport*. Academic Press, California.

Amraoui, N., Golaz, C., Mardhel, V., Négrel, Ph., Petit, V., Pinault, J.L. and Pointet, T. (2002). *Simulation par modèle des hautes eaux de la Somme*. BRGM/RP-51827-FR report, 184 p.

Aral, M. M. (1990). *Ground Water Modeling in Multilayer Aquifers: unsteady flow*. Lewis, Michigan.

Arc Hydro (2007). Arc Hydro Tools, ESRI. Available at: <http://support.esri.com/index.cfm?fa=downloads.dataModels.filteredGateway&dmid=15>
Last accessed: Jan 8, 2008.

ASCE, (1993). "Criteria for evaluation of watershed models." *J. Irrig. Drain. Engrg.*, ASCE, 119(3), 429-442.

Banque Hydro (2007). Banque nationale de données pour l'hydrométrie et l'hydrologie. *Ministry of Ecology and Sustainable Development*, France. Available at: <http://www.hydro.eaufrance.fr/>, last accessed: Jan 8, 2008.

Bear, J. (1972). *Dynamics of Fluids in Porous Media*. American Elsevier, New York.

Bear, J. and Verruijt, A. (1987). *Modeling Groundwater Flow and Pollution*. Reidel Publishing Co., Netherlands.

Bénédicte, A. (2002). *Fonctionnement hydrologique d'une zone humide : Conséquences sur son potentiel épurateur*. Mémoire, UPMC, UPS, EMP and ENGREF, France.

Besbes, M. (1978). "L'estimation des apports aux nappes souterraines. Un modèle regional d'infiltration efficace." Thesis, Université P. & M. Curie, France.

Beven, K. J. (2000). *Rainfall-runoff modeling: the primer*. John Wiley & Sons Ltd., New York.

Beven, K. and Freer, J. (2001). "Equifinality, data assimilation, and uncertainty estimation in mechanistic modelling of complex environmental systems using the GLUE methodology." *J. Hydrol.*, 249, 11-29.

Beven, K. and Kirkby, M. J. (1979). "A physically based variable contributing area model of basin hydrology." *Hydrol. Sci. Bull.*, 24(1), 43-69.

Beven, K. and Kirkby, M. J. (1993). *Channel network hydrology*. John Wiley & Sons Ltd., New York.

Bouwer, H. (1978). *Groundwater Hydrology*. McGraw-Hill, New York.

Bouwer, H., Back, J. T. and Oliver, J. M. (1999). "Predicting infiltration and groundwater mounds for artificial recharge." *J. Hydrol. Engrg.*, ASCE, 4(4), 350-357.

Carli, M. (2005). "Modélisation du bassin versant de la Somme à l'aide du modèle CaB." Thesis, UPMC-EMP-ENGREF, France.

Carré, B.A. (1961). "The determination of the optimum accelerating factor for successive over-relaxation." *Computer J.*, 4, 73.

Collectif (1996). *Corine land cover : une base de données géographiques d'occupation du sol*. IFEN, Agence Européenne pour l'Environnement.

Crampon N., Roux J. C. and Bracq P. (1993). "Hydrogéologie de la craie en France." *Hydrogéologie*, 2, 81-123.

Darcy, H. (1856). *Les Fontaines Publiques de la Ville de Dijon*. V. Dalmont, Paris.

Delleur, J. W. (1999). *The Handbook of Groundwater Engineering*. Springer, Germany.

Deneux, M., and P. Martin (2001). Rapport de la commission d'enquête sur les crues de la Somme, *Sénat*, 34, 606 pp.

Ducharne, A., Koster, R. D., Suarez, M., Stieglitz, M., and Kumar, P. (2000). "A catchment based approach to modeling land surface processes in a GCM - Part 2: Parameter estimation and model demonstration." *J. Geophys. Res.*, 105(D20), 24823-24838.

Durand, Y., Burn, E., Merindol, L., Guyomarc'h, G., Lessafre, B. and Martin, E. (1993). "A meteorological estimation of relevant parameters for snow models." *Annals of Glaciology*, 18, 65-71.

Girard, G., Morin, G. and Charbonneau, R. (1972). "Modèle précipitations-débits à discrétisation spatiale." Cahiers ORSTOM, série Hydrologie, 9(4), 35-52.

Golaz-Cavazzi, C. (1995). "Exploitation d'un modèle numérique de terrain pour l'aide à la mise en place d'un modèle hydrologique distributè." D.E.A., Ecole des Mines de Paris – Université Paris 6, Paris, France.

Golaz-Cavazzi, C. (1999). "Modélisation hydrologique à l'échelle régionale appliquée au bassin du Rhône." PhD Thesis, Ecole Nationale Supérieure des Mines de Paris, France.

Gomez, E. (2002). "Modélisation intégrée du transfert de nitrate à l'échelle régionale dans un système hydrologique. Application au bassin de la Seine." PhD Thesis, Ecole Nationale Supérieure des Mines de Paris, France.

Habets, F., Gascoin, S., Korkmaz, S., Thiéry, D., Zribi, M., Amraoui, N., Carli, M., Ducharne, A., Leblois, E., Ledoux, E., Martin, E., Noilhan, J., Ottlé, C. and Viennot, P. (2007). "Multi-model simulation of a major flood in the groundwater-fed basin of the Somme River (France)." *J. Geophys. Res.* [SUBMITTED].

Hantush, M. M., Harada, M., and Marino, M. A. (2002). "Hydraulics of stream flow routing with bank storage." *J. Hydrol. Eng.*, 7(1), 76-89.

Hill, M.C. (1998). Methods and guidelines for effective model calibration. USGS Water-Resources Investigations Report 98-4005. Reston, Virginia: USGS.

Hubert, P. (2001). La crue et les inondations de la vallée de la Somme de mars à mai 2001, report, *Cons. Gén. de la Somme*, Amiens, France.

Johnson, R. H. (2007). "Ground Water Flow Modeling with Sensitivity Analyses to Guide Field Data Collection in a Mountain Watershed." *Ground Water Monitoring & Remediation*, 27 (1), 75-83.

King D, Le Bas C, Jamagne, M and Daroussin, HR, J. (1995). *Base de données géographique des sols de France à l'échelle du 1/1000000. Notice générale d'utilisation.* Rapport technique, INRA. Service d'étude des sols et de la carte pédologique de France.

Korkmaz, S. and Önder, H. (2006). "Seepage from a Rectangular Ditch to the Groundwater Table." *J. Irrig. Drain. Engrg.*, ASCE, 132(3), 263-271.

Koster, R. D., Suarez, M., Ducharne, A., Stieglitz, M., and Kumar, P. (2000). "A catchment based approach to modeling land surface processes in a GCM - Part 1: Model structure." *J. Geophys. Res.*, 105(D20), 24809–24822.

Larkin, R. G., and Sharp, J. M. Jr. (1992). "On the relationship between river-basin geomorphology, aquifer hydraulics, and ground-water flow direction in alluvial aquifers." *Geol. Soc. Am. Bull.*, 104, 1608-1620.

Ledoux, E. (1980). "Modélisation intégrée des écoulements de surface et des écoulements souterrains sur un bassin hydrologique." PhD Thesis, ENSMP-UPMC, France.

Ledoux, E., Girard, G. and Villeneuve, J. P. (1984). "Proposition d'un modèle couplé pour la simulation conjointe des écoulements de surface et des écoulements souterrains sur un bassin hydrologique." *La Houille Blanche*, 1/2, 101-110.

Ledoux, E., Gomez, E., Monget, J.M., Viavattene, C., Viennot, P., Ducharne, A., Benoit, M., Mignolet, C., Schott, C. and Mary, B. (2007). "Agriculture and groundwater nitrate contamination in the Seine basin. The STICS–MODCOU modelling chain." *Science of the Total Environment*, Elsevier, 375, 33-47.

Lefrou, C. (2001). Mission d'expertise sur les crues d'avril 2001 du bassin de la Somme, report, *Ministry of Ecology and Sustainable Development*, France. Available at: http://www.ecologie.gouv.fr/article.php3?id_article=1034 , last accessed: Jan 8, 2008.

Levassor, A. and Ledoux, E. (1996). *Programme Newsam – Notice d'Utilisation*. Ecole des Mines de Paris, France.

Lewis, M.A., Jones, H.K., Macdonald, D.M.J., Price, M, Barker, J.A., Shearer, T.R., Wesselink, A.J., Evans, D.J. (1993). Groundwater storage in British aquifers: Chalk. R&D Note 169, National Rivers Authority, Bristol.

McDonald, M. G., and Harbaugh, A. W. (1988). "A Modular Three-Dimensional Finite Difference Ground-Water Flow Model." *U.S. Geological Survey Open-File Report*, 83-875.

McMaster, K. J. (2002). "Effects of digital elevation model resolution on derived stream network positions", *Water Resour. Res.*, 38(4), 1042.

Nash, J. E. (1959). "Systematic determination of unit hydrograph parameters." *J. Geophys. Res.*, 64(1).

Nash, J. E. and Sutcliffe, J. V. (1970). "River flow forecasting through conceptual models." *Journal of Hydrology*, 10, 282-290.

Négrel, Ph. and Petelet-Giraud, E. (2005). "Strontium isotopes as tracers of groundwater-induced floods: the Somme case study (France)." *Journal of Hydrology*, 305, 99–119.

O'Callaghan, J. F. and Mark, D. M. (1984). "The extraction of drainage networks from digital elevation data." *Computer Vision, Graphics and Image Processing*, 28, 323-344.

Önder, H. and Korkmaz, S. (2007). "Groundwater Mound Due to Constant Recharge from a Strip Basin." *J. Hydrol. Engrg., ASCE.*, 12(3), 237-245.

Pinault, J.L., Amraoui N., and Golaz C. (2005). "Groundwater-induced flooding in macropore-dominated hydrological system in the context of climate changes." *Water Resour. Res.*, 41, W05001, doi:10.1029/2004WR003169.

Pointet, T., Amroui, N., Golaz, C., Mardhel, V., Negrel, P., Pennequin, D., and Pinault, J.L. (2003). "La contribution des eaux souterraines aux crues exceptionnelles de la Somme en 2001: Observations, hypothèses, modélisation." *La Houille Blanche*, 6, 112-122.

PPRI (2004). Plan de Prévention des Risques d'Inondation sur la Vallée de la Somme et ses Affluents, report, *Prefecture of the Picardie Region, Prefecture of the Somme*. Available at: http://www.picardie.equipement.gouv.fr/article.php?id_article=99 , last accessed: Jan 8, 2008.

Price, M., Low, R.G., and McCann, C. (2000). "Mechanisms of water storage and flow in the unsaturated zone of the Chalk aquifer." *Journal of Hydrology*, 233, 54–71.

Quinn, P., Beven, K., and Culf, A. (1995). "The introduction of macroscale hydrological complexity into land surface-atmosphere transfer models and the effect on planetary boundary layer development." *Journal of Hydrology*, 166, 421-444.

Quintana-Segui, P., Le Moigne, P., Durand, Y., Martin, E., Habets, F., Baillon, M., Canellas, C., Franchisteguy, L., and Morel, S. (2007). "The SAFRAN atmospheric analysis : Description and validation." *J. Applied Meteorol. and Climatology*, [TO APPEAR].

Rushton, K. R. (2003). *Groundwater Hydrology: Conceptual and Computational Models*. Wiley, UK.

Sophocleous, M. (2002). "Interactions between groundwater and surface water: the state of the science." *Hydrogeology Journal*, 10, 52-67.

Stephens, D. B. (1996). *Vadose zone hydrology*. CRC Press-Lewis Publishers, Boca Raton.

Tarboton D. G. (1997). "A new method for the determination of flow directions and upslope areas in grid digital elevation models." *Water Resour. Res.*, 33, 309-319.

Thiéry, D. (1990). Logiciel MARTHE. Modélisation d'aquifère par un maillage rectangulaire en régime transitoire pour le calcul hydrodynamique des écoulements. Version 4.3, BRGM report 4S/EAU R32210 1990.

Thiéry, D. (1998). Modélisation couplée nappe-rivière-drain-précipitations avec le logiciel Marthe - version 5.7. Technical Report, BRGM DR/HGT.

Todd, D. K. and Mays, L. W. (2005). *Groundwater Hydrology*. Wiley, NJ.

Tóth, J. (1963). "A theoretical analysis of groundwater flow in small drainage basins." *J. Geophys. Res.*, 68, 4785-4812.

Trefethen, L. N. (1996). *Finite Difference and Spectral Methods for Ordinary and Partial Differential Equations*, unpublished text, available at: <http://web.comlab.ox.ac.uk/oucl/work/nick.trefethen/pdetext.html> , last accessed: Jan 8, 2008.

Varga, R. (1962). *Matrix Iterative Analysis*. Prentice-Hall, Englewood Cliffs, New Jersey.

Wilby, R.L. (Ed.) (1997). *Contemporary Hydrology: Towards Holistic Environmental Science*. Wiley, Chichester, UK, 354 pp.

Zribi, M., André, C., Ottlé, C., Guichaoua, M. and Habets, F. (2007). "Floods mapping based on ERS/SAR radar images over the SOMME French catchment." European Geosciences Union - General Assembly, Vienna, Austria, on April 16-20, 2007.

APPENDIX A

CALIBRATION OF MODSUR

A.1. Flow Hydrographs of the Tributaries of the Somme during Calibration

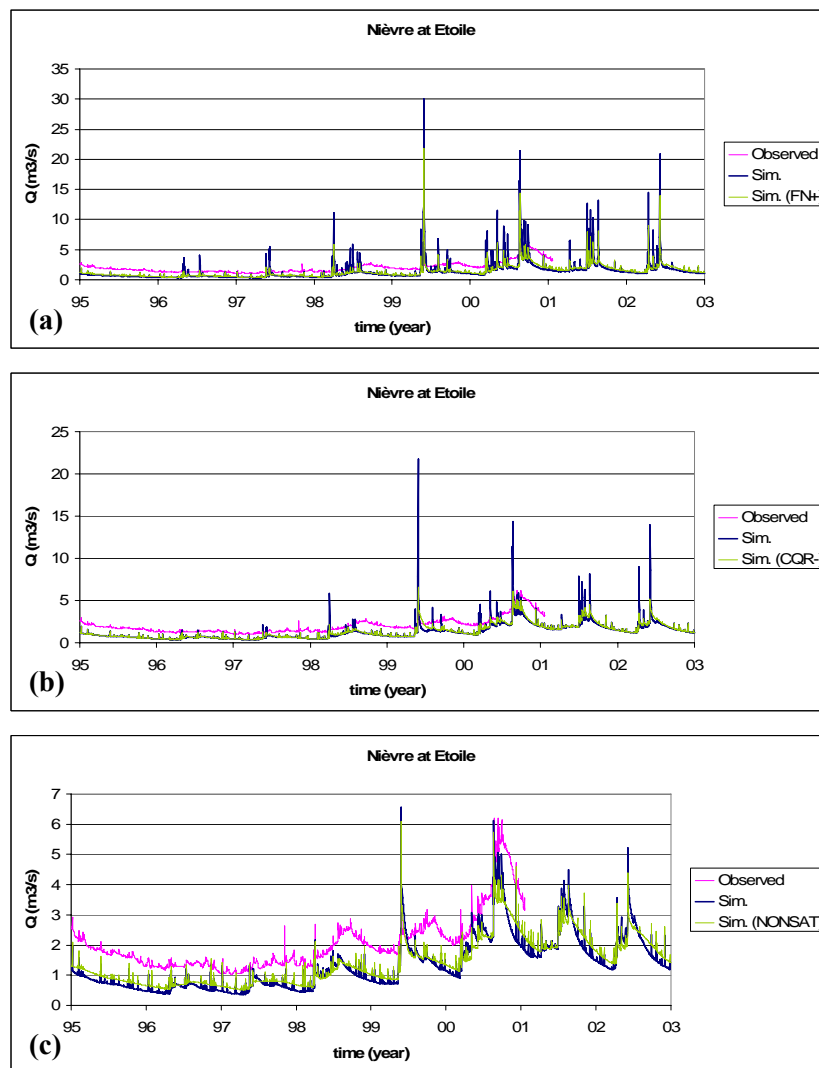


FIG. A. 1 The evolution of flow hydrograph of the Nièvre gauged at l'Etoile (269 km^2) during the calibration of MODSUR; **a)** increment of FN , **b)** decrement of C_{QR} , **c)** inclusion of NONSAT, **d)** calibration of parameters of Artificial Surfaces, **e)** calibration of parameters of Agricultural Zones.

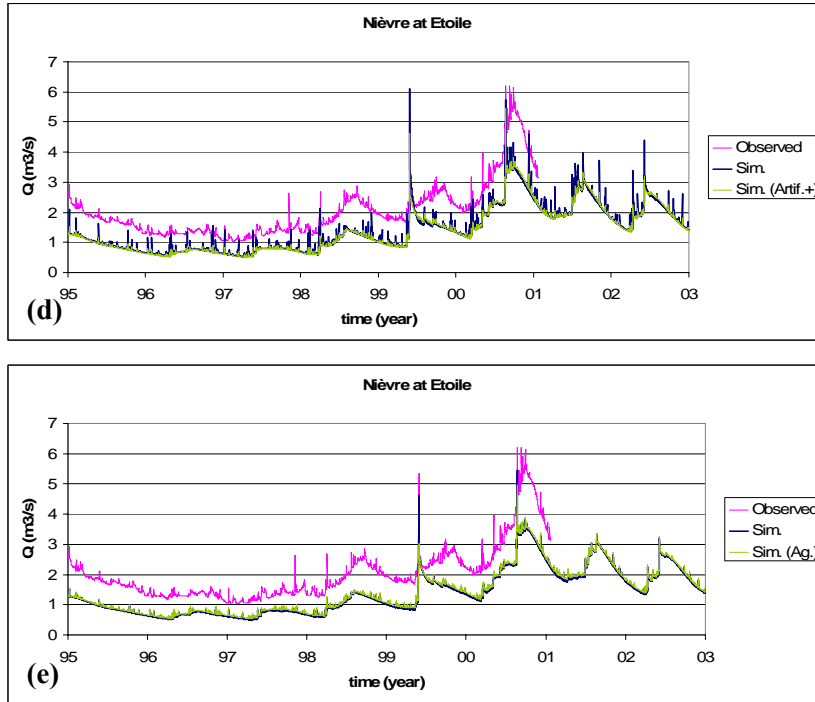


FIG. A. 1 (continued)

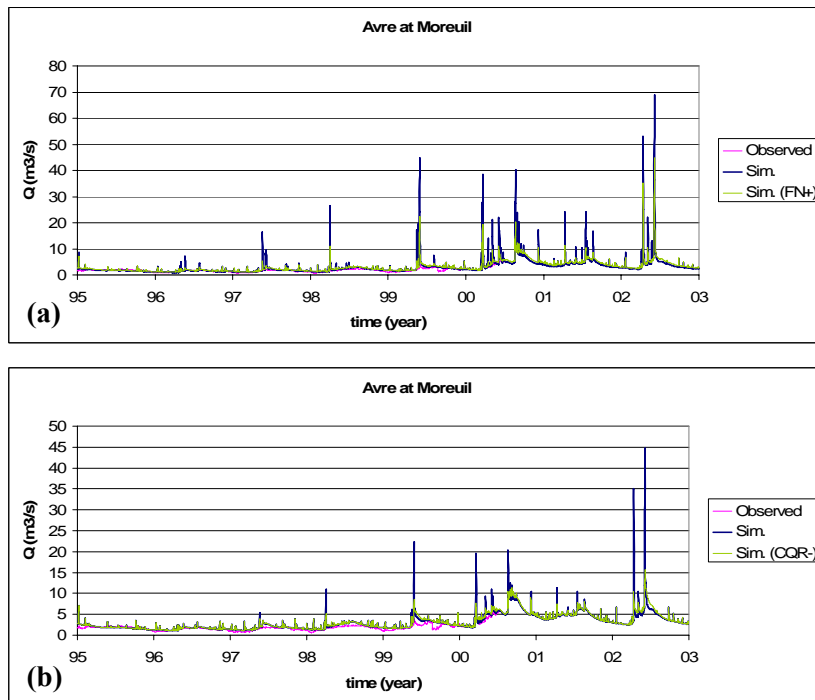


FIG. A. 2 The evolution of flow hydrograph of the Avre gauged at Moreuil (642 km²) during the calibration of MODSUR; **a**) increment of FN , **b**) decrement of C_{QR} , **c**) inclusion of NONSAT, **d**) calibration of parameters of Artificial Surfaces, **e**) calibration of parameters of Agricultural Zones.

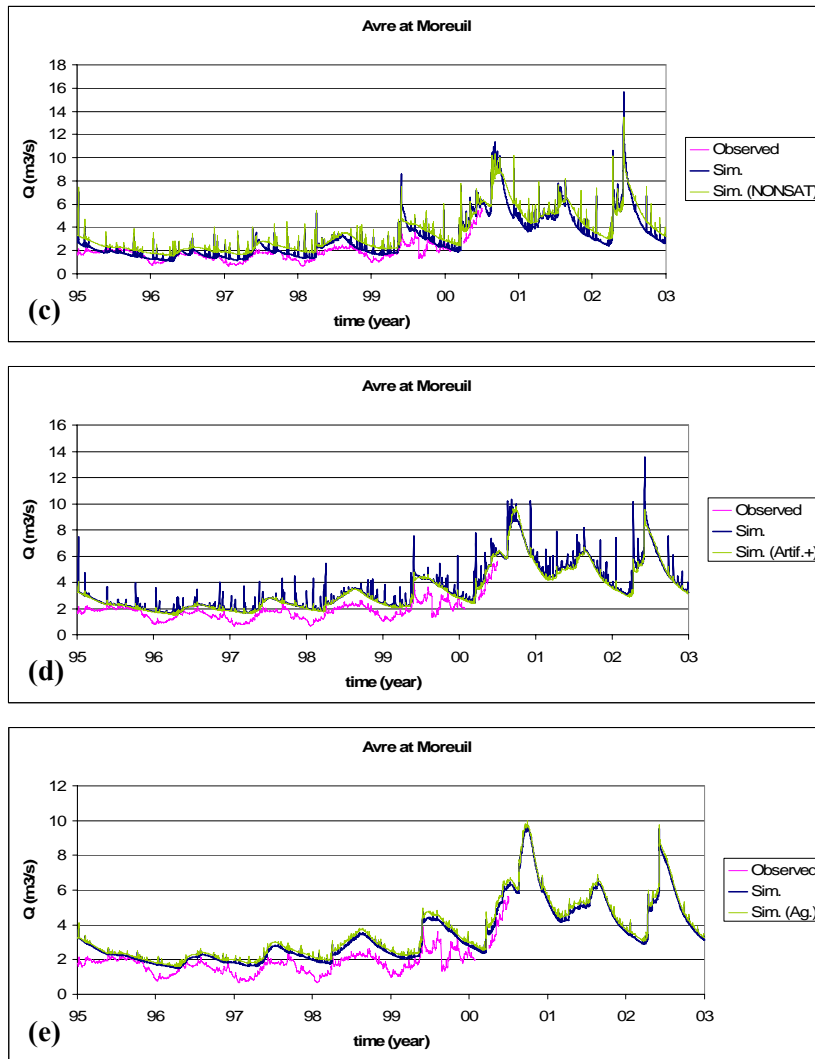


FIG. A. 2 (continued)

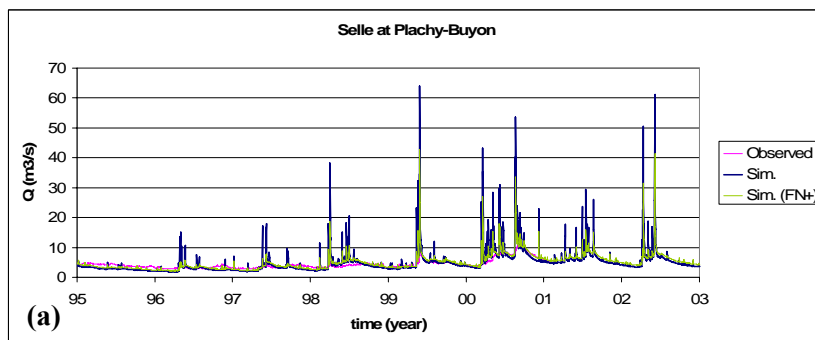


FIG. A. 3 The evolution of flow hydrograph of the Selle gauged at Plachy-Buyon (524 km^2) during the calibration of MODSUR; **a)** increment of FN , **b)** decrement of C_{QR} , **c)** inclusion of NONSAT, **d)** calibration of parameters of Artificial Surfaces, **e)** calibration of parameters of Agricultural Zones.

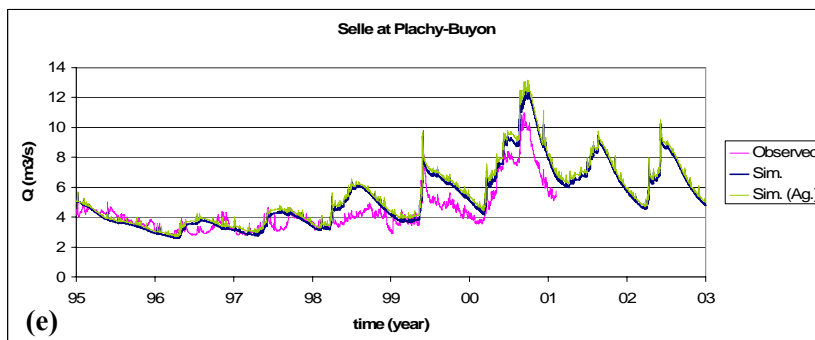
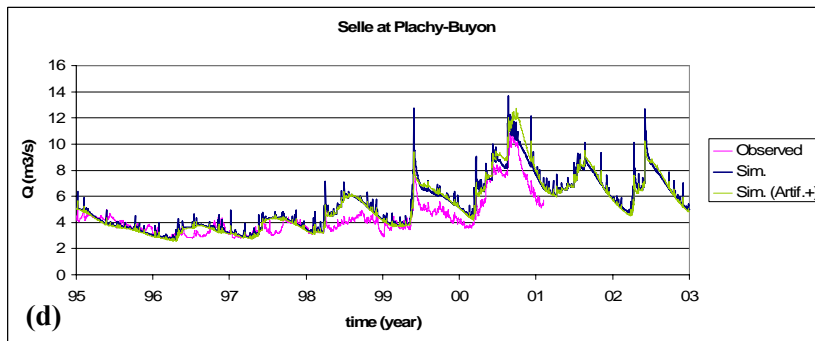
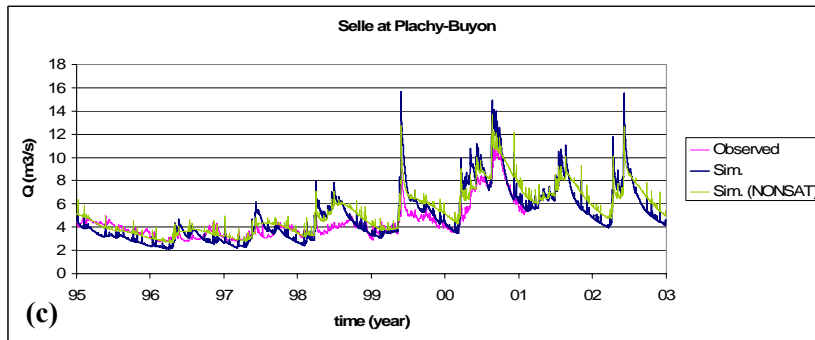
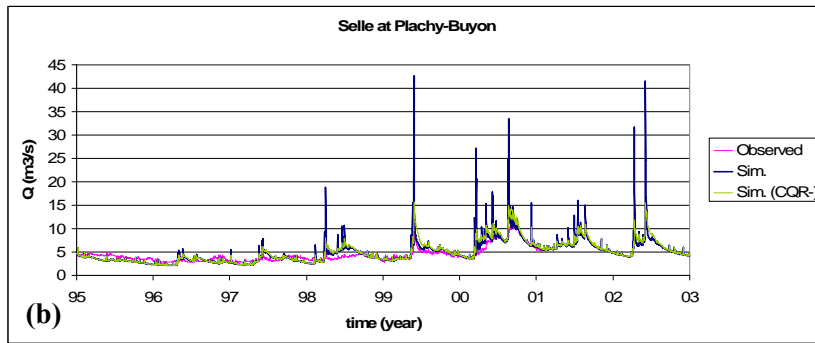


FIG. A. 3 (continued)

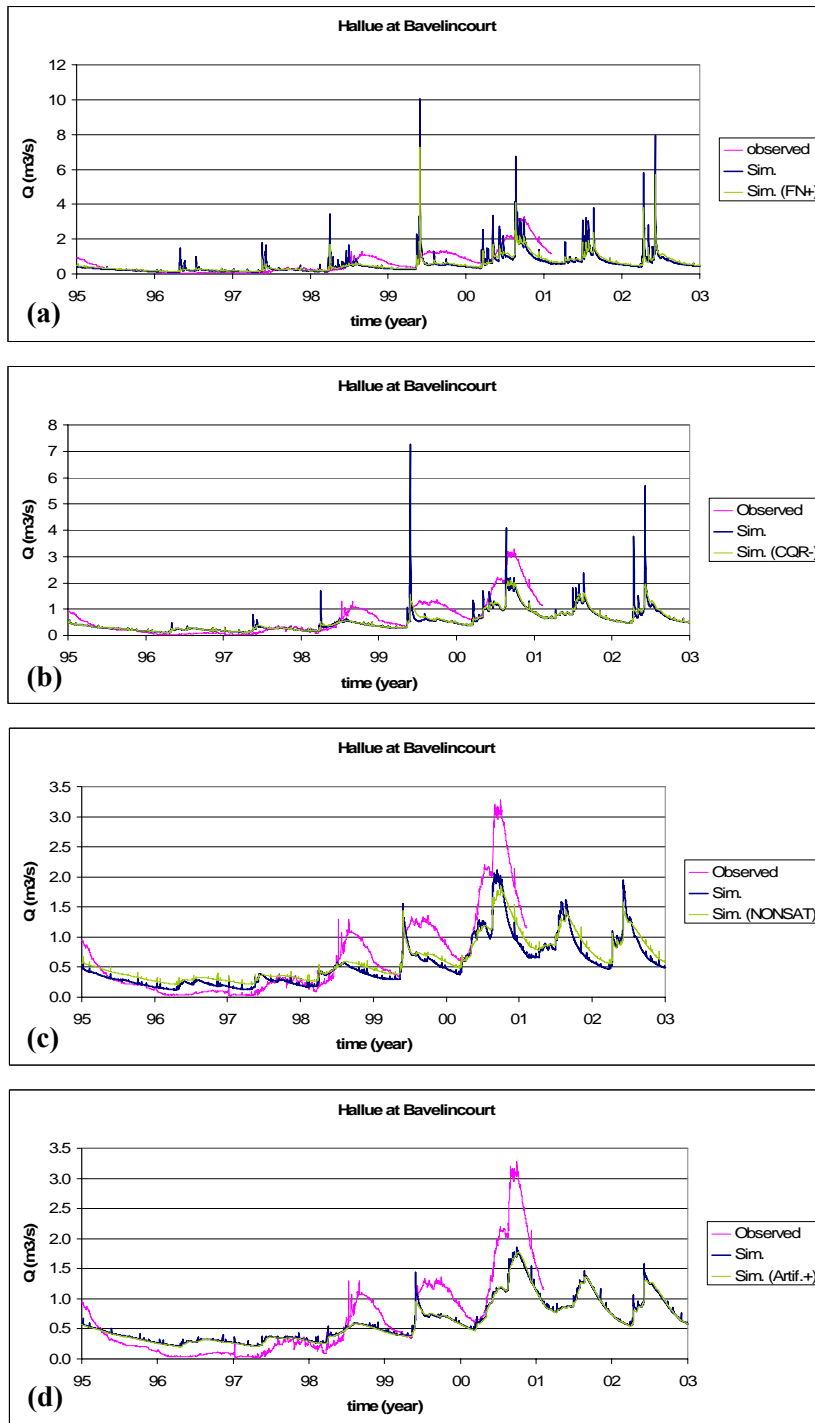


FIG. A. 4 The evolution of flow hydrograph of the Hallue gauged at Bavelincourt (115 km^2) during the calibration of MODSUR; **a**) increment of FN , **b**) decrement of C_{QR} , **c**) inclusion of NONSAT, **d**) calibration of parameters of Artificial Surfaces, **e**) calibration of parameters of Agricultural Zones.

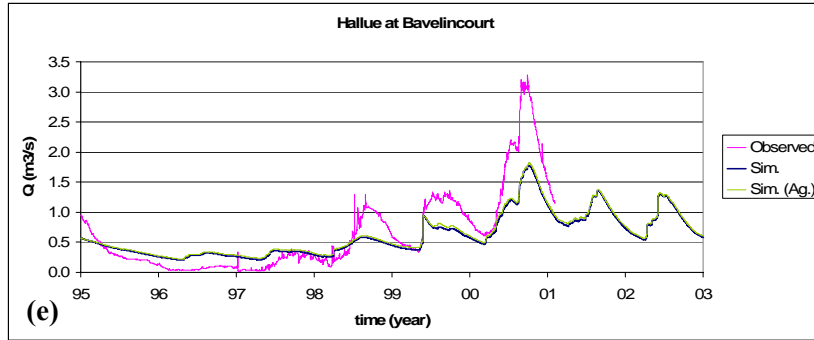


FIG. A. 4 (continued)

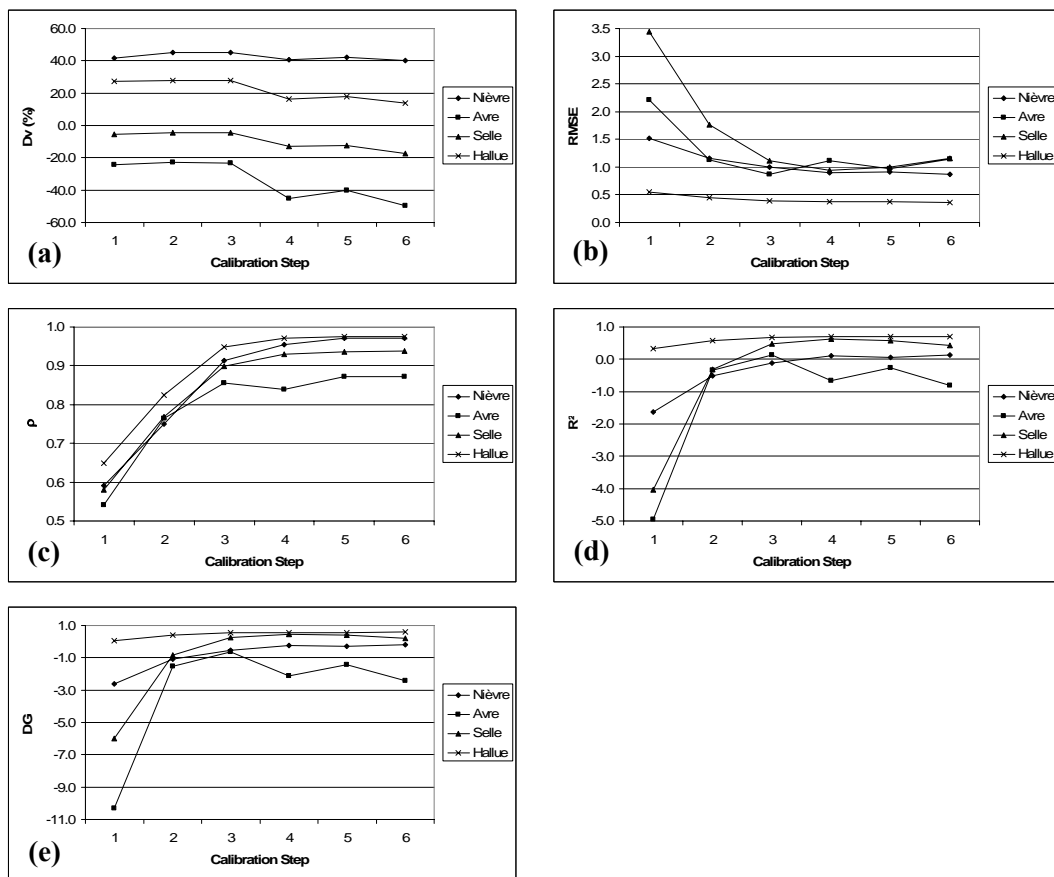


FIG. A. 5 Evolution of measures of error; **a)** Deviation of runoff volumes (D_v), **b)** Root mean squared error ($RMSE$), **c)** Correlation coefficient (ρ), **d)** Nash-Sutcliffe coefficient (R^2), **e)** Coefficient of gain from daily mean (DG).

A.2. Flow Hydrographs of the Tributaries of the Somme during Validation

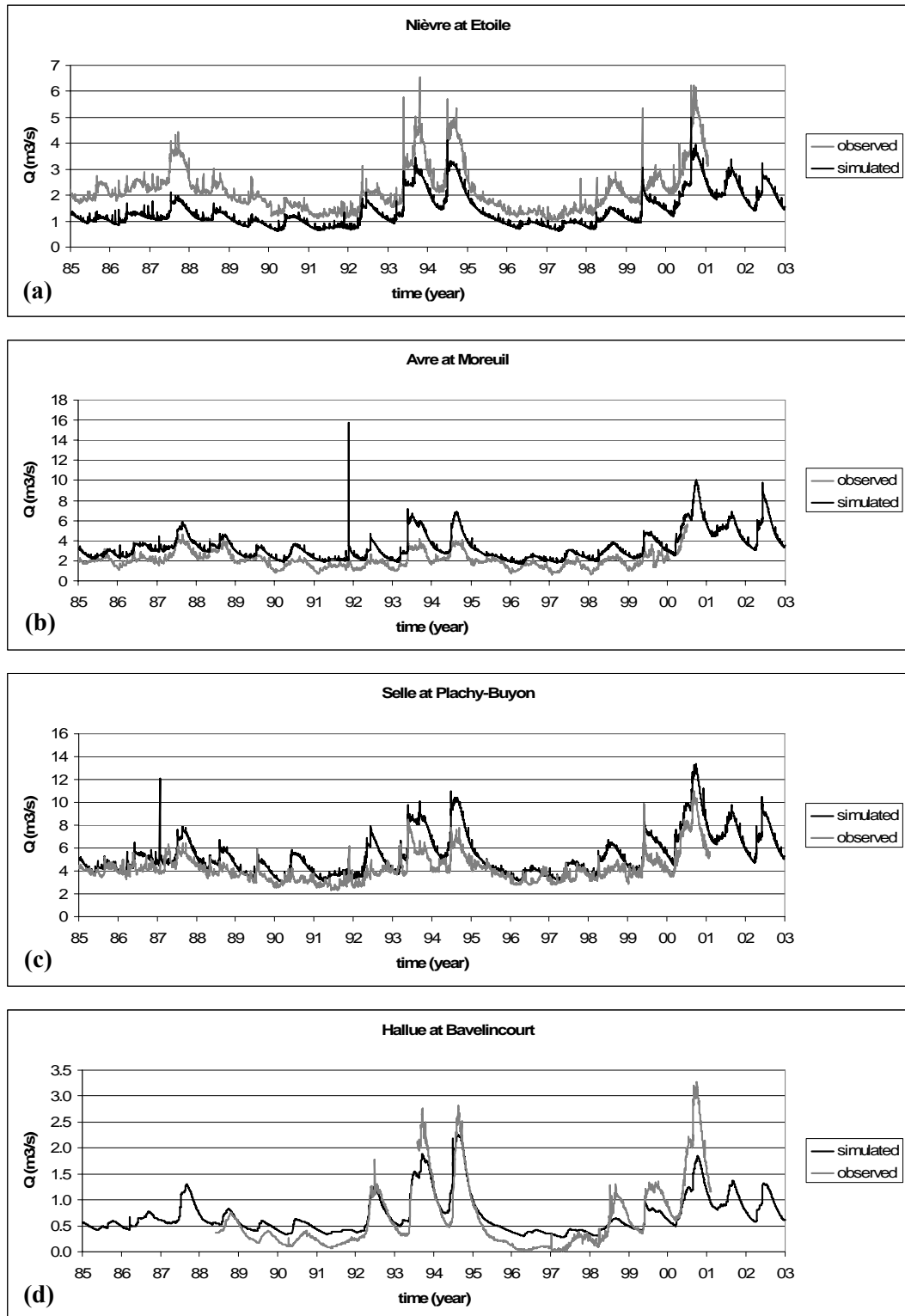


FIG. A. 6 The flow hydrographs of tributaries of the Somme after the validation of production function; **a)** the Nièvre, **b)** the Avre, **c)** the Selle, **d)** the Hallue.

APPENDIX B

PIEZOMETRIC HEADS

B.1. Hydrographs

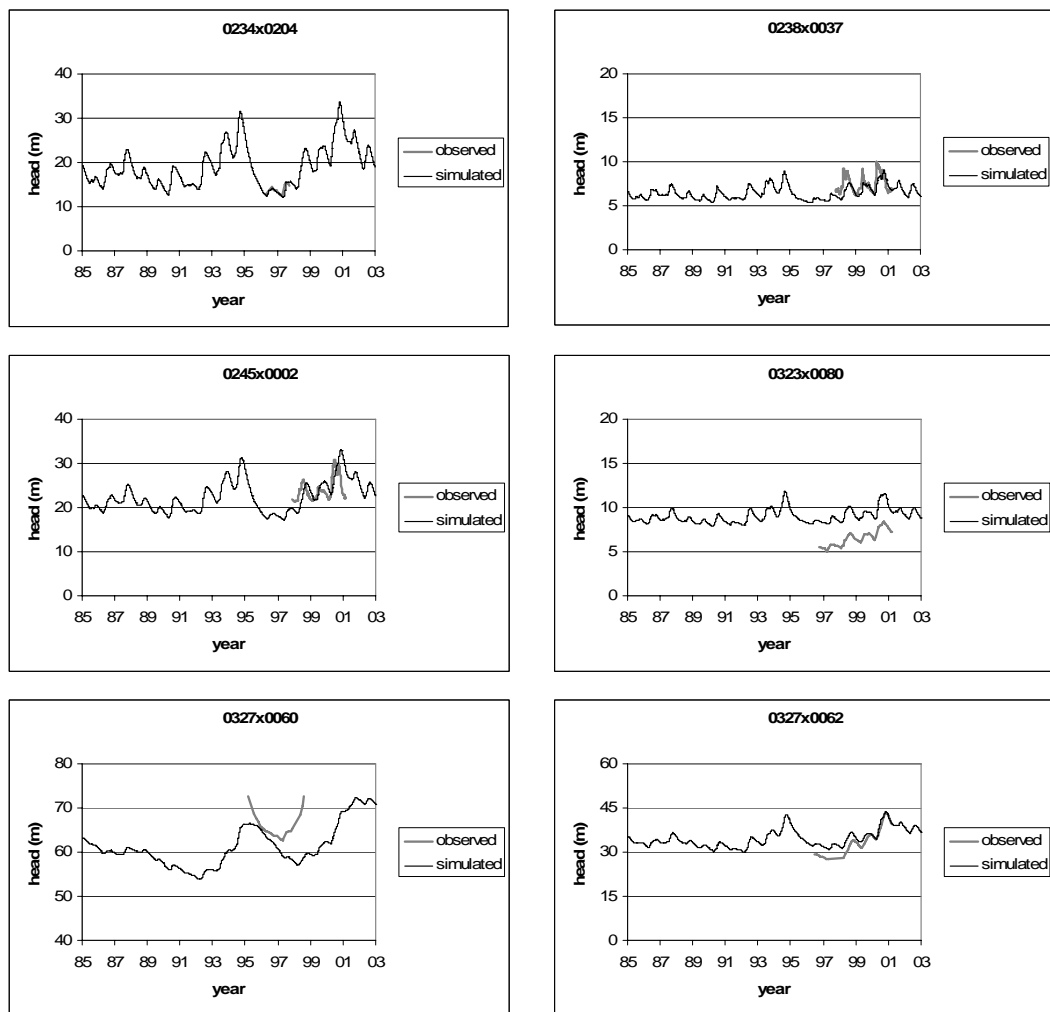


FIG. B. 1 Piezometric head hydrographs.

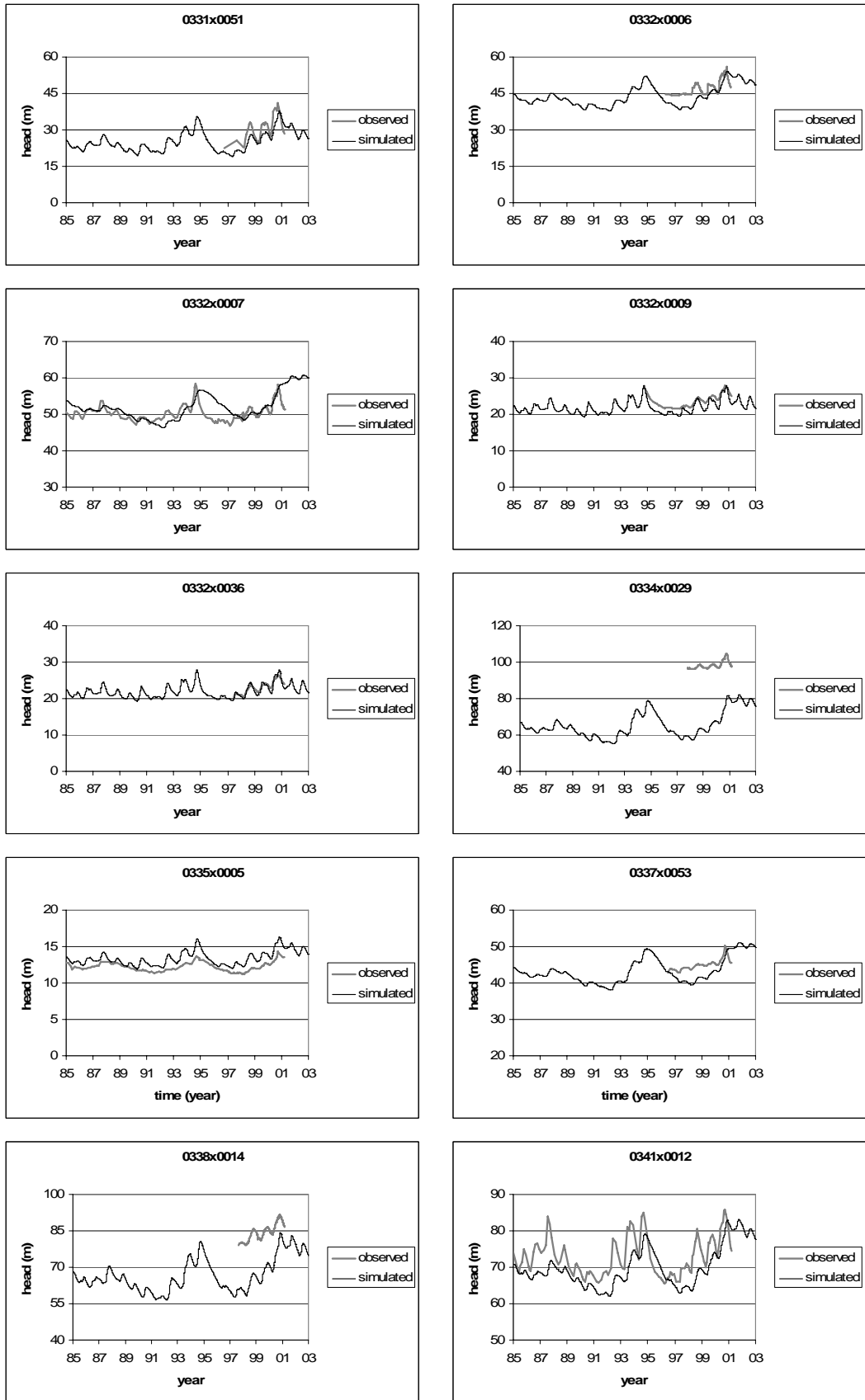


FIG. B. 1 (continued)

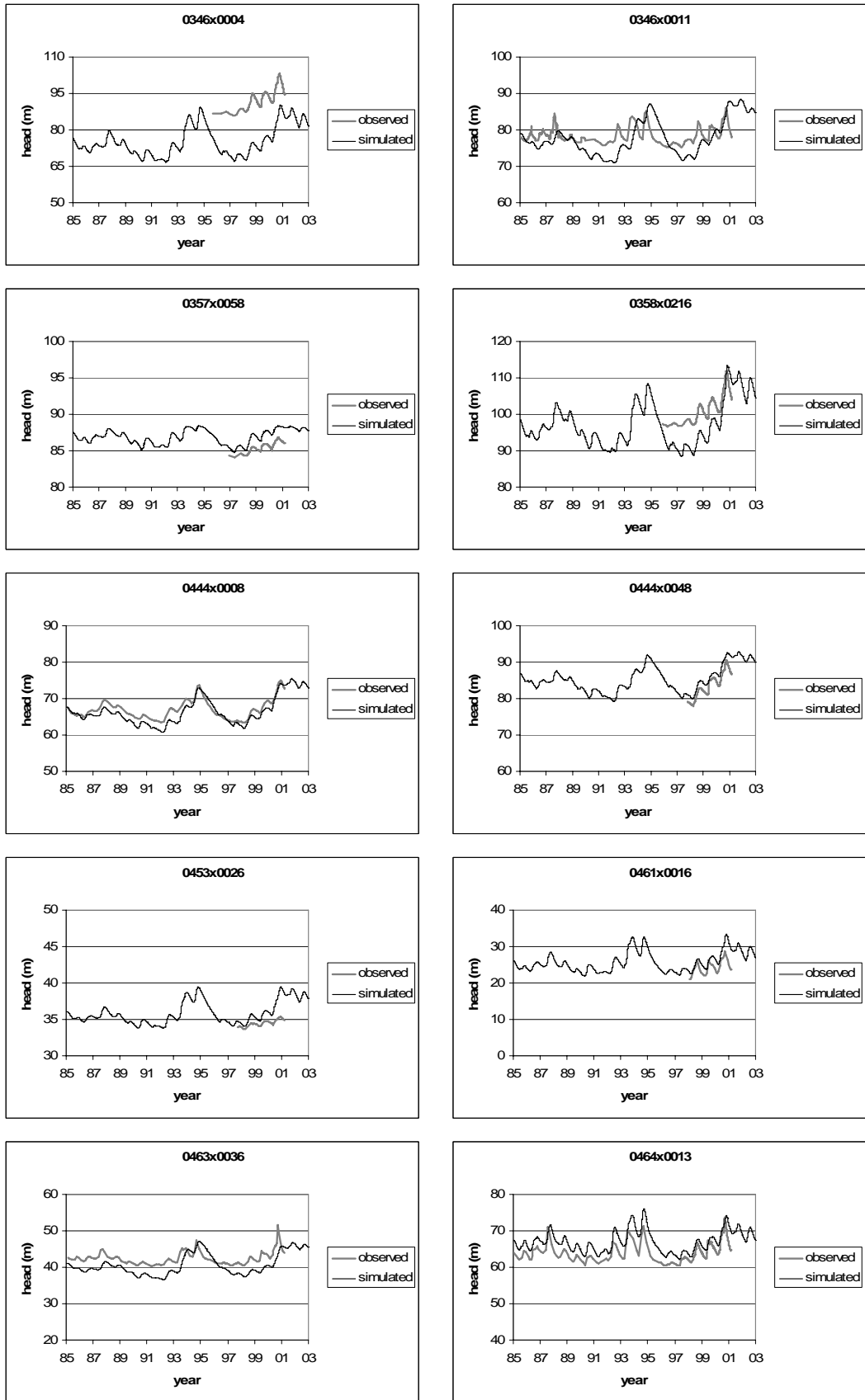


FIG. B. 1 (continued)

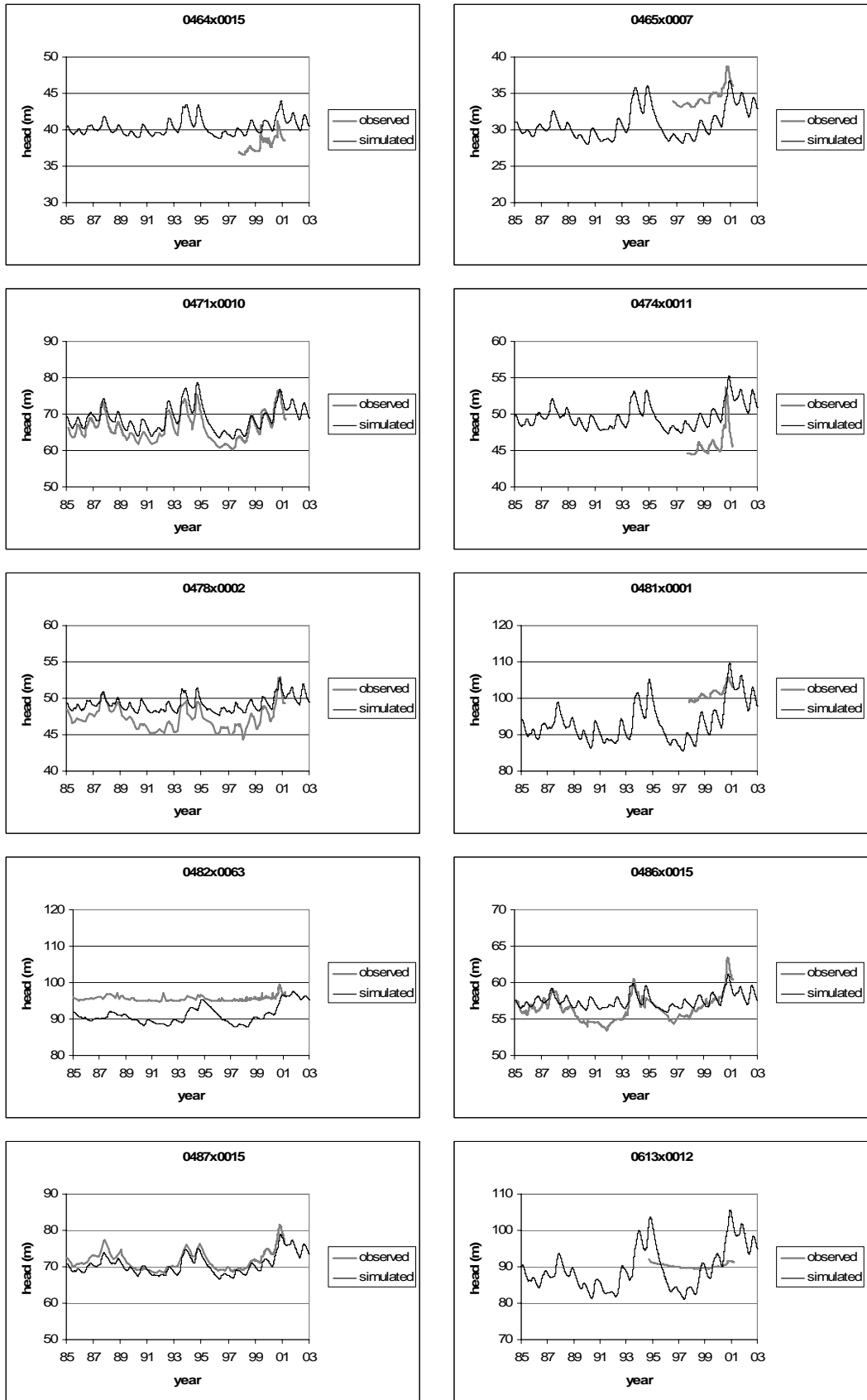


FIG. B. 1 (continued)

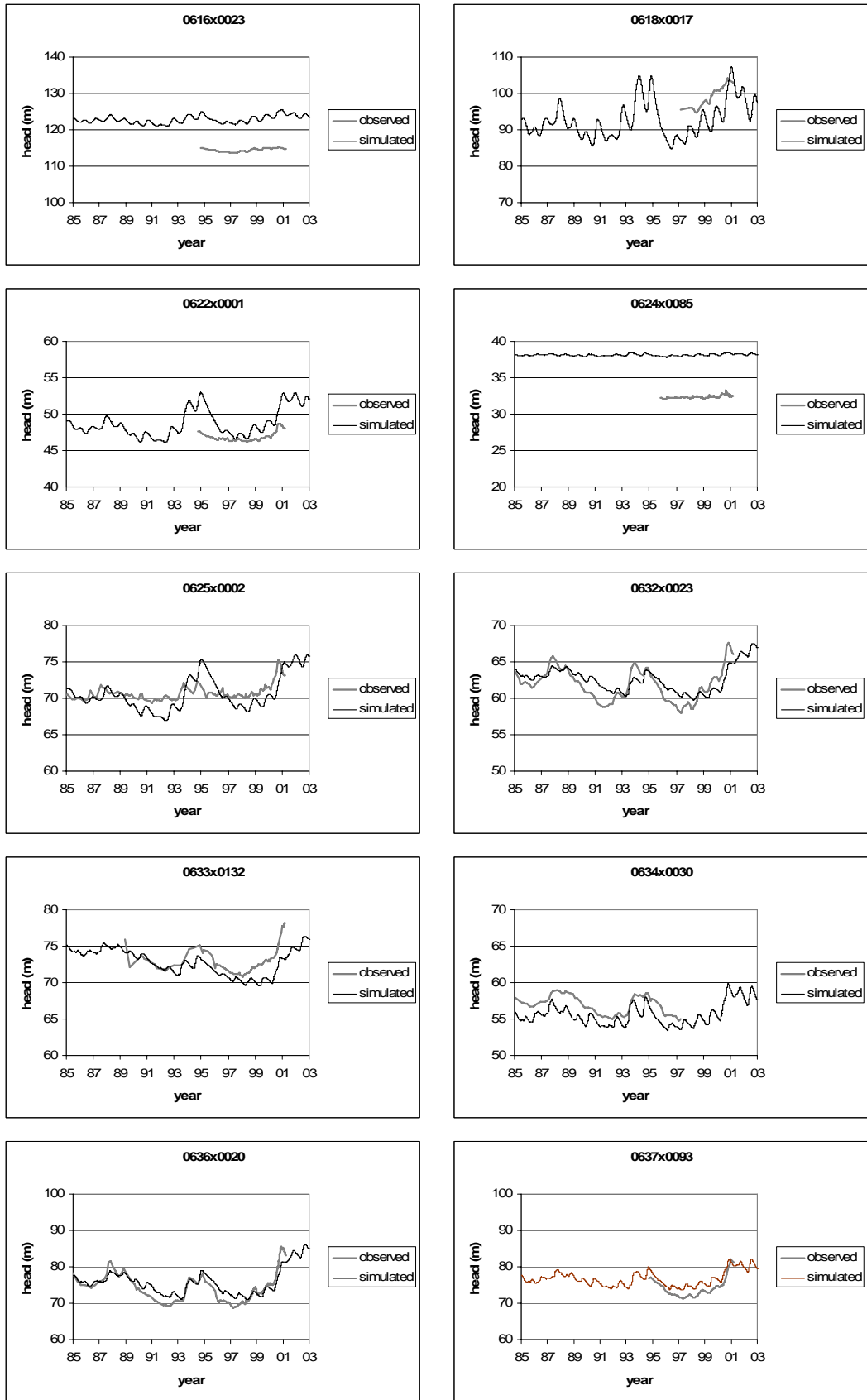


FIG. B. 1 (continued)

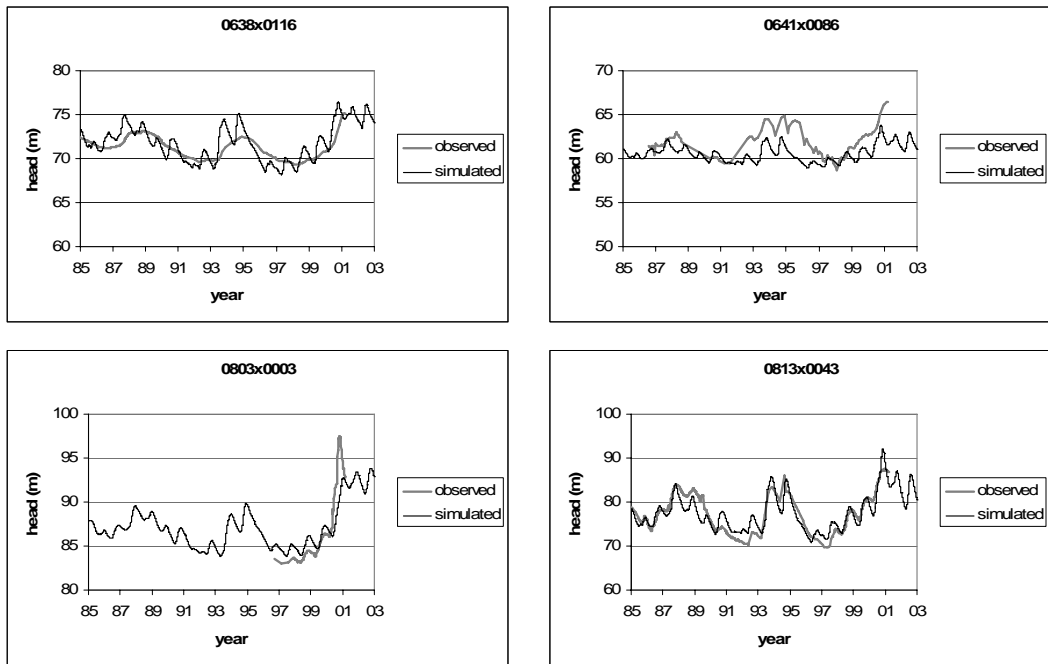


FIG. B. 1 (continued)

B.2. Error criteria

TABLE B. 1 Error criteria for piezometric heads.

No.	Well Id	AVG(obs)	AVG(sim)	Nash(R ²)	RMSE
1	234x204	13.84	13.69	0.76	0.49
2	238x037	7.52	7.01	0.07	0.96
3	245x002	24.08	24.71	-0.87	3.37
4	323x080	6.54	9.33	-8.98	2.79
5	327x060	65.63	61.92	-2.71	5.02
6	327x062	34.09	35.96	0.72	2.36
7	331x051	30.51	27.77	0.32	3.92
8	332x006	47.78	44.85	-0.89	4.08
9	332x007	51.02	51.74	0.05	2.43
10	332x009	23.63	22.18	0.15	1.61
11	332x036	23.08	22.90	0.77	0.78
12	334x029	98.31	66.26	-222.71	32.41
13	335x005	12.23	13.30	-2.25	1.21
14	337x053	44.98	42.63	-3.34	3.07
15	338x014	84.37	68.53	-21.10	16.26
16	341x012	72.85	68.99	-0.11	5.52
17	346x004	92.87	75.66	-15.18	17.41
18	346x011	78.31	76.81	-1.47	3.07
19	357x058	85.44	87.05	-4.38	1.64
20	358x216	101.71	96.70	-1.35	6.07
21	444x008	67.05	65.96	0.69	1.59
22	444x048	83.82	85.97	0.58	2.29
23	453x026	34.44	35.93	-16.64	1.83
24	461x016	24.32	26.74	-1.63	2.98
25	463x036	42.44	40.11	-1.72	2.96
26	464x013	64.57	66.93	0.11	2.75
27	464x015	38.03	40.80	-6.06	2.88
28	465x007	34.73	31.11	-5.79	3.77
29	471x010	68.03	69.60	0.75	2.19
30	474x011	46.06	50.05	-3.50	4.20
31	478x002	47.22	49.09	-0.59	2.05
32	481x001	101.44	95.27	-16.96	7.54
33	482x063	95.81	90.85	-34.23	5.24
34	486x015	56.54	57.53	0.24	1.60
35	487x015	72.64	70.80	0.58	2.08
36	613x012	90.12	90.45	-81.72	5.85
37	616x023	114.45	123.03	-301.66	8.55
38	618x017	99.21	94.41	-2.86	5.83
39	622x001	46.86	48.66	-11.35	2.22
40	624x085	32.40	38.16	-689.21	5.74
41	625x002	70.81	70.11	-1.27	1.64
42	632x023	61.70	62.03	0.57	1.49
43	633x132	72.88	71.30	-0.37	1.99
44	634x030	56.87	55.16	-1.28	1.85

TABLE B. 1 (continued)

No.	Well Id	AVG(obs)	AVG(sim)	Nash(R²)	RMSE
45	636x020	74.63	74.50	0.78	2.02
46	637x093	74.33	76.27	0.42	2.13
47	638x116	71.43	71.69	0.18	1.10
48	641x086	62.02	60.60	-0.34	1.90
49	803x003	87.50	86.91	0.66	2.59
50	813x043	77.52	77.31	0.79	2.10

APPENDIX C

STRUCTURE OF THE COUPLED MODEL

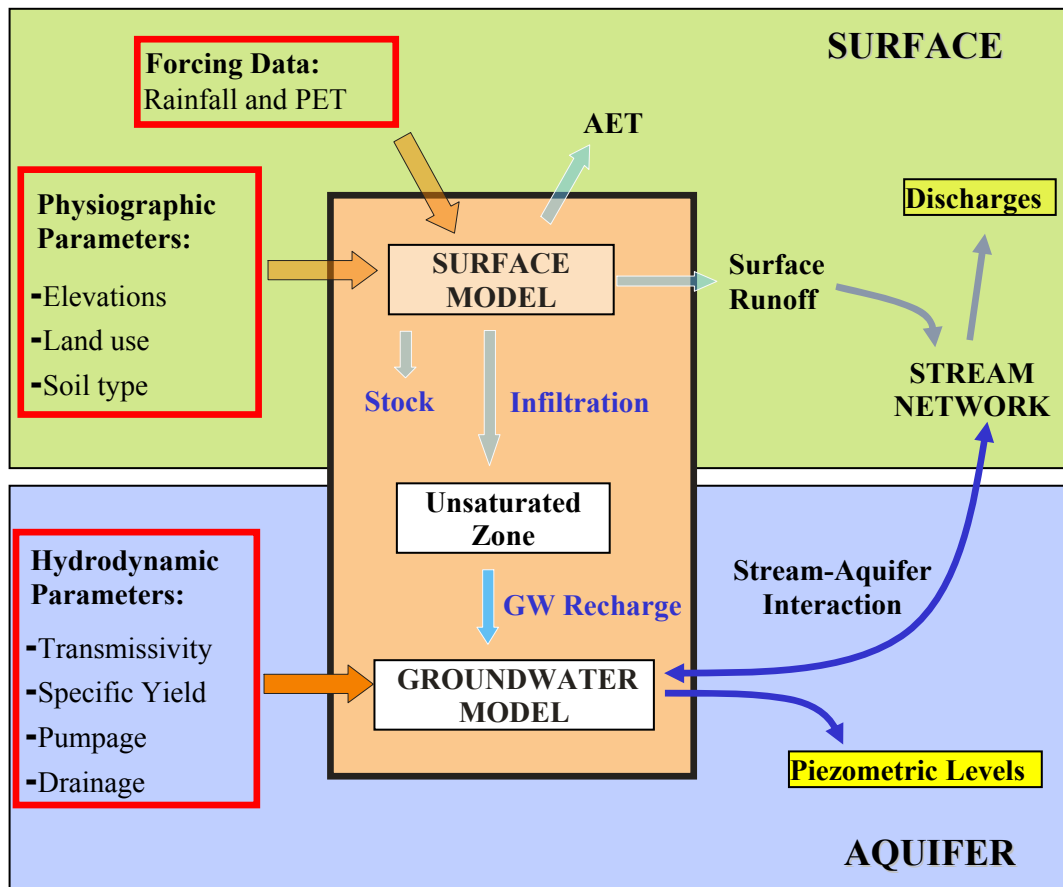


FIG. C. 1 Structure of the coupled model.

CURRICULUM VITAE

Name: Serdar KORKMAZ

Nationality: Turkish

Date of Birth: 29.11.1977

Place of Birth: Kırklareli, Turkey

e-mail: skorkmaz06@gmail.com

EDUCATION

- ***Joint Ph.D. in Civil Engineering and 'Hydrologie et Hydrogéologie'*** **2007**
Middle East Technical University, Ankara – Ecole des Mines de Paris
Dissertation: "Modeling of the Flood Regimes in Coupled Stream-Aquifer Systems"
- ***M.Sc. in Civil Engineering*** **2002**
Middle East Technical University, Ankara
Thesis: "Seepage from Detention Basins to Groundwater Table"
- ***B.S. in Civil Engineering*** **1999**
Middle East Technical University, Ankara

WORK EXPERIENCE

- ***Research Associate*** **8-12/2007**
Centre de Géosciences of Ecole des Mines de Paris
- ***Research Assistant*** **2001-2007**
Hydromechanics Laboratory, Civil Eng. Dept. of METU
- ***Project Engineer*** **1999-2000**
Baget Engineering, Consulting and Trade Co. Inc.

PUBLICATIONS

- Habets, F, Gascoin, S., **Korkmaz, S.**, Thiéry, D., Zribi, M., Amraoui, N., Carli, M., Ducharme, A., Leblois, E., Ledoux, E., Martin, E., Noilhan, J., Ottlé, C. and Viennot, P. (2007). "Multi-model simulation of a major flood in the groundwater-fed basin of the Somme River (France)." *J. Geophys. Res.* [SUBMITTED].

- Önder, H. and **Korkmaz, S.** (2007). “Groundwater Mound Due to Constant Recharge from a Strip Basin.” *J. Hydrol. Engrg.*, ASCE, 12(3), 237-245.
- **Korkmaz, S.** and Önder, H. (2006). “Seepage from a Rectangular Ditch to the Groundwater Table.” *J. Irrig. Drain. Engrg.*, ASCE, 132(3), 263-271.
- **Korkmaz, S.**, Ledoux E. and Önder, H., (2006). Hydrological Modeling with Improved Stream-Aquifer Interaction. *7th International Congress on Advances in Civil Engineering*, Istanbul.
- **Korkmaz, S.** and Önder, H., (2004). Steady Groundwater Flow Resulting from a Constant Recharge through a Strip Basin. *6th International Congress on Advances in Civil Engineering*, Istanbul.

LANGUAGES

- Turkish – native language
- English – fluent
- French – advanced (20 months of stay in France)